FRESHWATER RUNOFF FROM PACIFIC-DRAINING CONTINENTAL AND COASTAL BASINS IN PATAGONIA:
CHARACTERIZING REGIONAL INPUTS TO CHILEAN FJORDS ASSOCIATED WITH CHANGES IN LAND USE/COVER

BY
PAULO MORENO MEYNARD

Dissertation discussed in partial fulfillment of
the requirements for the Degree of

DOCTOR OF PHILOSOPHY

Marine Science and Technologies
curriculum in Science of the Marine Ecosystem,
Department of Earth, Environmental and Life Sciences, University of Genoa, Italy

October, 2023

Adviser(s):

Dr. Brian Reid – Center for Patagonian Ecosystem Investigation (CIEP)

Prof. Giorgio Bavestrello – Department of Earth, Environmental and Life Sciences, University of Genoa

External Reviewers:

Dr. Jorge León Muñoz – University Católica de la Santísima Concepción

Dr. Marcelo Somos-Valenzuela – Butamallin Research Center for Global Change, University of the Frontera

Examination Committee:

Prof. Marzia Bo – Department of Earth, Environmental and Life Sciences, University of Genoa

Prof. Marcelo Somos-Valenzuela – Butamallin Research Center for Global Change, University of the Frontera

Dr. Iñigo Irrárazabal – Center for Patagonian Ecosystem Investigation (CIEP)

Ph.D. program in *Marine Science and Technologies*

Curriculum in Science of the Marine Ecosystem

Cycle XXXV

Acknowledgements

The Ph.D. research was economically supported by the Center for Patagonian Ecosystem Investigation (CIEP), where most of the activities were performed. I thank the Marine Zoology Department, DISTAV, University of Genoa, for sharing the installations for finishing this research.

The landscape is changing
The landscape is crying
Thousands of acres of forest are dying
Carbon copies from the hills above the forest line
Acid streams are flowing ill across the countryside

'Cause I don't care if you're going nowhere
Just take good care of the world…

Can we be blamed for the security of ignorance?

'Cause I don't care if you're going nowhere
Just take good care of the world…

Extract from the song *"The Landscape is Changing"*, Depeche Mode, 1983

Index

List of Tables

List of Figures

INTRODUCTION

"Patagonia", the first thoughts or feelings when we read the word Patagonia is wild, isolated, and far away from everywhere. Few places in the world evoke similar sensations, e.g., Alaska, Greenland, Australia, Lapland, and Siberia. In effect, the colonization process in Patagonia has been recent, with a significant percentage of this territory still with a very low human footprint (Hansen et al., 2013; Potapov et al., 2017; Watson et al., 2018). In a specific study in the area, Astorga et al. (2021), through high-resolution satellite imagery, defined 66.000 km^2 of intact forested watersheds in west-southern Patagonia, corresponding to 49% of the whole mature forested watersheds area. Like Astorga et al. (2018; 2021) from a hydrographic perspective and the one established by Torres et al. (2014) from a marine point of view I defined west-southern Patagonia, the study area of this research, as every basin with freshwater discharges, directly or indirectly, to the Pacific Ocean, starting in the north with the Inner Sea of Chiloé (41°S) until Cape Horn (56°S) in the south (figure I.1).

West-southern Patagonia has remarkable characteristics such as the mightiest rivers in the western Andes, including Puelo, Yelcho, Palena, Aysén, Baker, and Pascua rivers, some of the largest lakes on the continent and the deepest and crystalline in the world, and the largest temperate icefields on the planet (Reid et al., 2021). Mountain ranges elevational extremes are lower than the northern Andes. There is no significant central valley; hence linear distances and fluvial courses from the source to the sea are relatively short, and overall stream gradients are relatively high. These characteristics of west-southern Patagonia produce a system of channels and fjords with an extended coastline, one of the most relevant worldwide (Kelso & Patterson, 2010; Schneider et al., 2014).

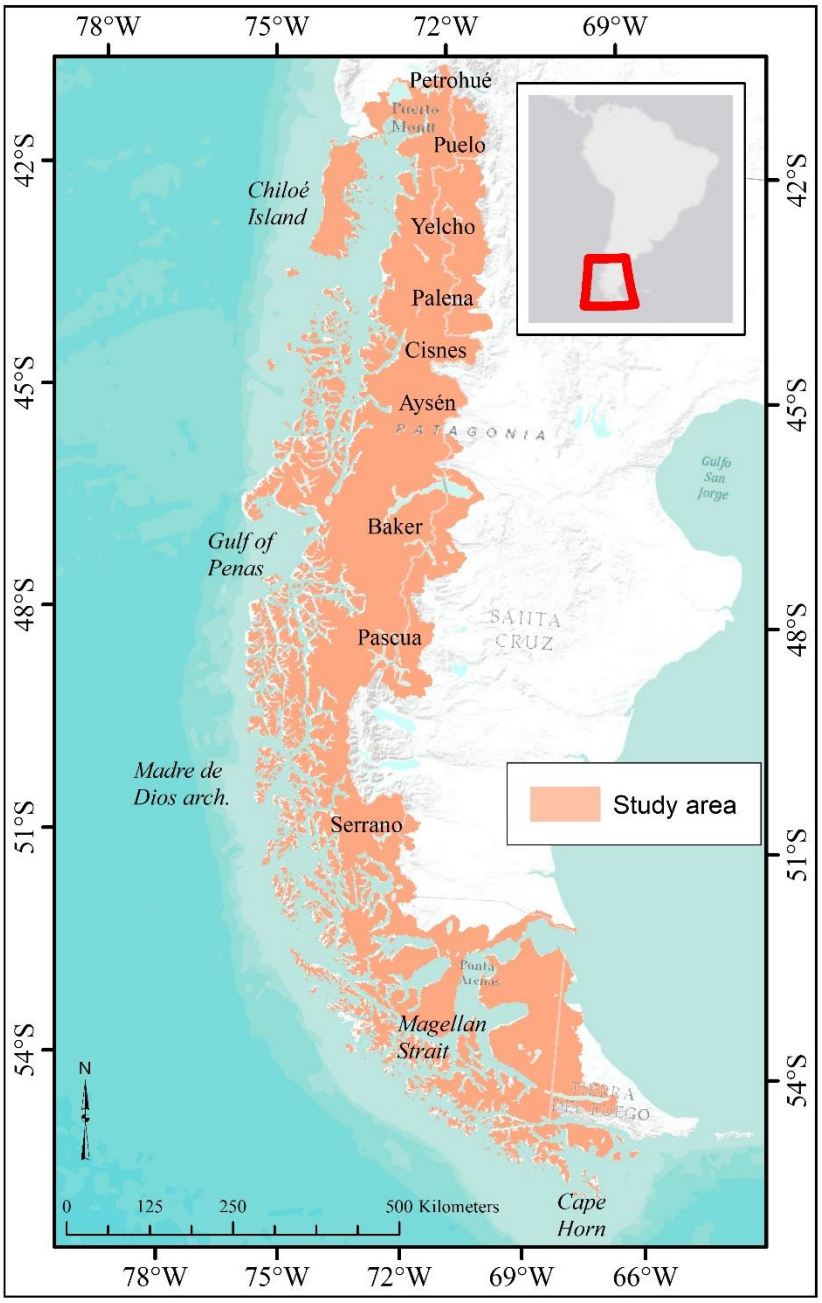

Figure I.1. *Identification of west-southern Patagonia showing every basin with freshwater discharge to the Pacific Ocean.*

The high amount of freshwater discharges in channels and fjords generates a brackish layer with a highly variable 5-10 m freshwater and a more uniform saltier lower layer (Calvete & Sobarzo, 2011; Schneider et al., 2014). This two-layer vertical structure produces effects, as expected, in salinity in the water column (Calvete & Sobarzo, 2011; Schneider et al., 2014), temperatures (Schneider et al., 2014), biogeochemistry and primary productivity (Torres et al.,

2020; 2023; Vandekerkhove et al., 2016), light availability (Amann et al., 2022; Vandekerkhove et al., 2020), and biological communities (Quiroga et al., 2016) of fjords and coastal ecosystems. However, in a vast territory as west-southern Patagonia, the freshwater discharges with their sediments and nutrients have an enormous variability, depending on factors such as precipitation and temperature, landforms, vegetation, soils, and related physical conditions and alterations from land use that may generate distinct water characteristics at the source. A conceptual model of how freshwater discharges from terrestrial ecosystems may affect physics and biology variables in fjords and channels is presented in figure I.2. A balance of resource loading (high DSi but low nutrients), light limitation, and internal cycling of nutrients will govern production as seen from a general sequence along the river delta to marine/estuarine gradient (left to right) (B. Reid, personal communication, February 2023).

Therefore, it is important to incorporate analyses of terrestrial and stream ecosystems to understand the different processes that occur in inner seas, fjords, and channels. However, a low percentage of marine studies in Patagonia incorporate variables from rivers, even more unusual about basins and land use/cover information. Some exceptions are the studies of Torres et al. (2014) that identified silicic acid concentrations as a function of precipitation rates, geology (granitic rocks), melting from glaciers and andosols area due to the density of volcanoes; Quiroga et al. (2016) (sediments and organic matter from terrestrial sources) and Amann et al. (2022) (sediment from glacierized watersheds) where marine studies looked beyond the marine system. However, most marine studies just mentioned the connections with terrestrial ecosystems and streams but with no measurement outside the fjords and channels.

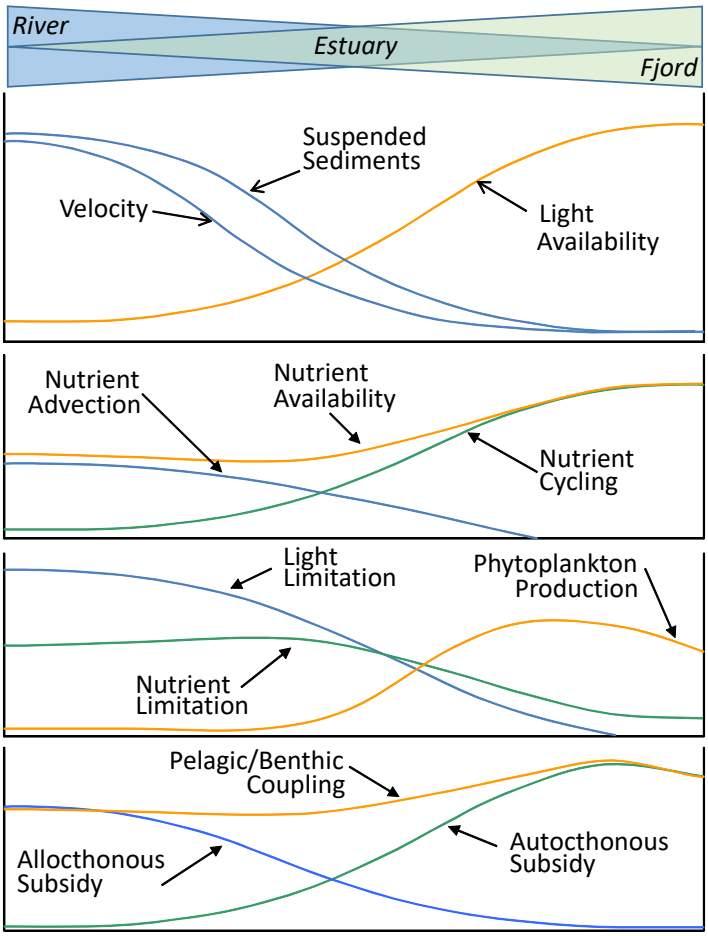

Figure I.2. *Conceptual one-dimensional model about several effects of riverine forcing in pelagic and benthic energy flow in the fjord. Image created by B. Reid.*

As was mentioned before, west-southern Patagonia is one of the host spots of wilderness on the planet (low human footprint) but, at the same time, has suffered severe land use/cover changes (LUC) and forest degradation by the colonization process mainly associated with the transformation of forests into grasslands for cattle raising through extensive forest fires (Veblen et al., 1996). However, the time, location, and magnitude of these impacts are not the same, with the northern part of the region (~41°S) being the earliest and most severe (Veblen et al., 1996). Instead, the Aysén region (~44° to 50° S) has an early colonization process of only ~120 years but with substantial effects, e.g., the three million hectares burnt between 1900 and 1950 or Aysén port unusable by sandbanks due to erosion (Bizama et al., 2011). Furthermore, the harvesting of ciprés de la guaitecas, a native cypress, has generated forest fires in the whole

islands zone, producing severe erosion due to the high precipitation rate (Mac-Clure, 1970; Veblen et al., 1996). From a terrestrial point of view, LUCs are a crucial human driver modifying flows and their characteristics.

The importance of freshwater discharges in inner seas, fjords, and channels in west-southern Patagonia is well known. However, magnitude discharges, type and concentration of nutrients, seasonal dynamics of these flows, and tendencies caused by climate change are still unknown. Additionality, runoff quantification in Patagonia is limited to a few main rivers with monitoring stations, mostly in the north section that is associated with continental basins. Besides, most of the archipelago area (44° to 56°), with a higher precipitation rate, does not count with any monitoring stations. Also, headwater watersheds are the most sensitive area of a stream (Máčka et al., 2023), but headstreams have been monitored with less intensity than the most attractive big rivers. Figure I.3 presents the general approach of this study focused on quantification of discharges but also attending to the effects of LUC, with bioindicators and hydrology signature. Additionally, to answer the questions about magnitude and characteristics of discharges, the methodology framework goes from terrestrial, with a basin perspective, passing by streams, to marine ecosystems.

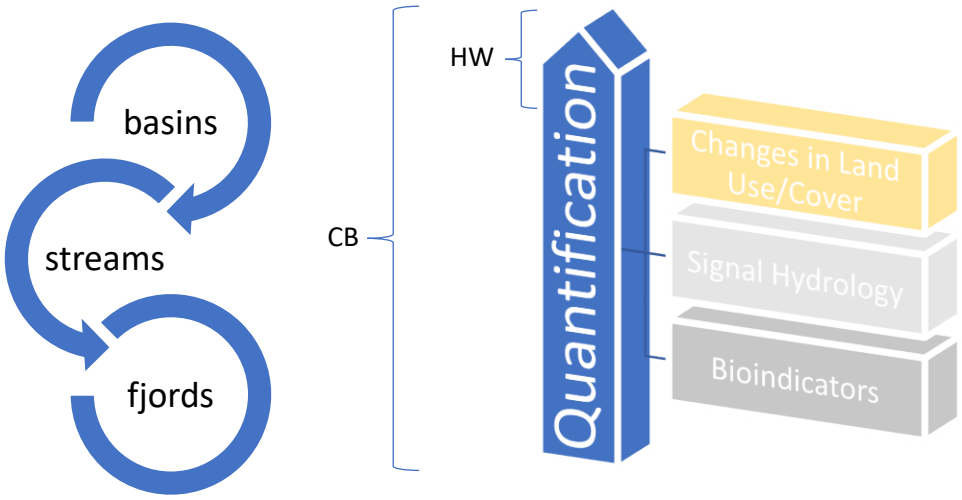

Figure I.3. *General approach used in this study. HW, Headwater streams; CB, Coastal basins.*

The aim of this research is focused on the quantification of freshwater coastal discharges in west-southern Patagonia and the identification of the effects of LUC in the runoff. Specific objectives are 1) to characterize the runoff from terrestrial basin based on climate, current land use/cover, geology and soils; 2) to identify those variables or factors that can be used as bioindicators of LUC impacts; and 3) to identify relations between hydrology indicators and LUC and climate variables. To address the objectives, two approaches were carried on; 1) macro-scale studies associated with the whole study area (see figure I.1) and regional researches based on coastal basins (CB), and 2) a micro-scale study in 12 headwater streams (HW), with a high monitoring intensity, located in the Aysén region.

The first study (chapter 1) is a research of coastal freshwater discharges in the whole study area, i.e., runoff from Pacific-draining continental and coastal basins in west-southern Patagonia (41-56° S; 315,740 km^2). The main objective was the volume estimation of discharges through the FLOW model developed by the Fisheries Development Institute (IFOP, http://www.ifop.cl) and based on the Variable Infiltration Capacity Model (VIC)(Hamman et al., 2018; Liang et al., 1994). FLOW has daily streamflow and snowmelt information between 1979 and 2018 from 31,220 basins. In addition, we analyzed these flows by considering various factors that impact the watershed, including soil, geology, land use/cover, and climate. This was done to provide a general understanding of nutrient concentration, as chemical monitoring stations were unavailable. Besides, an analysis of consequences in marine ecosystems was carried on with the information on the volume and runoff characteristics.

Chapter 2 is focused on the quantification of freshwater inputs in the inner fjord transect with sampling stations starting in the Magallanes Strait (Sta. 1; 53.7°S) until Madre de Dios Archipelago (Sta. 29; 50.5°S). Three primary sources were identified: direct precipitation to the fjord surface, surface runoff from coastal watersheds (liquid rainfall), and input from glacial

ablation. The time scale of freshwater inputs was based on annual integrated inputs of runoff or precipitation, or in the case of glacial inputs, the average long-term net loss in glacier mass within the estimated contributing areas. The results were applied on a regional study of natural freshwater pulses of allochthonous bioavailable forms of iron and silicon to the Patagonia archipelago's inner waters during the productive season's onset play a potentially significant role in modulating macronutrient dynamics (input vs. utilization) and influencing coastal phytoplankton assemblages (see appendix 2).

An intensive micro-scale study is presented in chapter 3, whose primary purpose was to analyze if hydrology indicators can identify the effects of LUC in paired headwater catchments with short temporal series of data for early detection. Additionally, we aim to determine if flow data aggregation hides response due to forcings that occur on an hour-scale through daily and sub-daily signature analyses. The selection of headwater catchments as freshwater monitoring units was due to streams of 0-2 order are formed might be assumed as ideally representative and sensitive to the two primary drivers of terrestrial landscapes: LUC and variability in climate forcing (including climate change). We developed observational research in 12 headwater catchments over five years to address the study objective along different hydrological regimes and land use/cover gradients. Flow data was obtained with pressure sensors in the catchment outlets, and watershed attributes were measured on the field thanks to a systematic inventory and remote sensing analysis. Finally, identifying effects in the headwater streams hydrology due to LUC in the temperate zone of the southern hemisphere is relevant in terms of methodology but also associated with observation points of monitoring and conservation activities based on the concept of climate observatory or Long-Term Socio-Ecological Network.

A regional study (45-47°S) is presented in appendix 3 identifying possible effects of LUC from a biologic perspective. The research discusses those environmental attributes of

headwater streams that influence the composition of aquatic macroinvertebrate communities. Freshwater ecosystems are uniquely structured at the landscape level with a hydrologic network that is directional and hierarchical, connecting terrestrial and marine ecosystems. At the origins of these networks, headwater catchments are perhaps the watershed's most vulnerable point. Furthermore, small streams are closely connected to land use change (especially forest cover) and climate/global change watershed-scale drivers, underscoring the importance of headwater streams to organisms and ecosystems downstream (Abell et al., 2007; Lowe & Likens, 2005). This study aimed to determine stream macroinvertebrate taxonomic and functional feeding group (FFG) composition in 53 forested headwater streams (0-3 order). Many catchment attributes were related to LUC processes, such as the percentage of forest and watershed with no impact. However, other variables were focused on the flow, such as stream velocity. The use of the macroinvertebrate community as a bioindicator of LUC and, therefore, as a predictor of the chemical and sediment composition of coastal freshwater discharges was also a secondary objective of this research. My participation in this research was associated with statistical analysis through exploratory Metric Multidimensional Scaling (MDS) and predictive Boosted Regression Trees (BRT) to identify the most significant environmental variables that explain the variation in taxonomic and FFG diversity.

Human impacts on the terrestrial landscape are not only related to LUC but to degradation. Appendix 4 involves the identification of bioindicators as in appendix 3 but related to degradation processes in evergreen forests in Patagonia (43-48°S). Forest degradation is a "human-induced loss of resilience which prevents natural recovery to the pre-disturbance state" (Jaboury Ghazoul et al., 2015). Forest structure changes and composition may alter soil properties and processes (Hudson & Alcántara-Ayala, 2006). They may deplete water sources or change the nutrient concentration, which can reduce the terrestrial and freshwater ecosystem functioning (Chazdon, 2008) or end in an ecosystem collapse (Bergstrom et al., 2021). The

process of forest degradation and deforestation is the second most significant producer of greenhouse gas emissions, just behind the burning of fossil fuels (van der Werf et al., 2009). However, forest degradation has been challenging to quantify, mainly because forest resilience and ecological thresholds must be quantitatively determined (Hirota et al., 2011; Scheffer, 2009). This study's objective was to determine critical factors that define a degraded forest, and that allows us to identify and quantify those areas with no change in their land use/cover (evergreen forest) but with a chemical and sediment component runoff more related to no-forest conditions. My contribution to this study was the determination of degradation predictors and their thresholds, indicating a severe loss of resilience. An unsupervised method, Non-Metric Dimensional Scaling (NMDS), was used to discover general relationships, and BRT, a machine learning technique, as a supervised approach for ecological process predictions.

LITERATURE CITED

Abell, R., Allan, J. D., & Lehner, B. (2007). Unlocking the potential of protected areas for freshwaters. *Biological Conservation*, *134*(1), 48-63.

Amann, B., Bertrand, S., Alvarez-Garreton, C., & Reid, B. (2022). Seasonal Variations in Fjord Sediment Grain Size: A Pre-requisite for Hydrological and Climate Reconstructions in Partially Glacierized Watersheds (Baker River, Patagonia). *Journal of Geophysical Research: Earth Surface*, *127*(2), e2021JF006391. https://doi.org/10.1029/2021JF006391

Astorga, A., Moreno, P., & Reid, B. (2018). Watersheds and Trees Fall Together: An Analysis of Intact Forested Watersheds in Southern Patagonia (41–56° S). *Forests*, *9*(7), 385. https://doi.org/10.3390/f9070385

Astorga, A., Reid, B., Moreno, P., & Rojas, P. (2021). Donde nacen los ríos: cuencas de bosques prístinos en la Patagonia occidental austral. In J. C. Castilla, J. J. Armesto, & M. J. Martínez-Harms (Eds.), *Conservación en la Patagonia chilena: evaluación del conocimiento, oportunidades y desafíos.* (pp. 167-198). Ediciones Universidad Católica.

Bergstrom, D. M., Wienecke, B. C., van den Hoff, J., Hughes, L., Lindenmayer, D. B., Ainsworth, T. D., Baker, C. M., Bland, L., Bowman, D. M. J. S., Brooks, S. T., Canadell, J. G., Constable, A. J., Dafforn, K. A., Depledge, M. H., Dickson, C. R., Duke, N. C., Helmstedt, K. J., Holz, A., Johnson, C. R., . . . Shaw, J. D. (2021). Combating ecosystem collapse from the tropics to the Antarctica. *Global Change Biology*, *27*(9), 1692-1703.

Bizama, G., Torrejón, F., Aguayo, M., Muñoz, M. D., Echeverría, C., & Urrutia, R. (2011). Pérdida y fragmentación del bosque nativo en la cuenca del río Aysén (Patagonia-Chile) durante el siglo XX. *Revista de Geografía Norte Grande*(49), 125-138.

Calvete, C., & Sobarzo, M. (2011). Quantification of the surface brackish water layer and frontal zones in southern Chilean fjords between Boca del Guafo (43°30′S) and Estero

Elefantes (46°30′S). *Continental Shelf Research*, *31*(3), 162-171. https://doi.org/10.1016/j.csr.2010.09.013

Chazdon, R. L. (2008). Beyond deforestation: restoring forests and ecosystem services on degraded lands. *Science*, *320*, 1458-1460.

Ghazoul, J., Burivalova, Z., Garcia-Ulloa, J., & King, L. A. (2015). Conceptualizing Forest Degradation. *Trends in Ecology & Evolution*, *30*(10), 622-632. https://doi.org/10.1016/j.tree.2015.08.001

Hamman, J. J., Nijssen, B., Bohn, T. J., Gergel, D. R., & Mao, Y. (2018). The Variable Infiltration Capacity model version 5 (VIC-5): Infrastructure improvements for new applications and reproducibility. *Geoscientific Model Development*, *11*(8), 3481-3496.

Hansen, M. C., Potapov, P. V., Moore, R., Hancher, M., Turubanova, S., Tyukavina, A., Thau, D., Stehman, S., Goetz, S., & Loveland, T. (2013). High-resolution global maps of 21st-century forest cover change. *science*, *342*(6160), 850-853. https://doi.org/10.1126/science.1244693

Hernández-Moreno, Á., Soto, D. P., Miranda, A., Holz, A., & Armenteras-Pascual, D. (2023). Forest landscape dynamics after large-scale fires in western Patagonia: evidencing surprising temperate forest recovery trends.

Hirota, M., Holmgren, M., Van Nes, E. H., & Scheffer, M. (2011). Global resilience of tropical forest and savanna to critical transitions. *Science*, *334*, 232-235.

Hudson, P. F., & Alcántara-Ayala, I. (2006). Ancient and modern perspectives on land degradation. *Catena*, *65*(1), 102-106.

Kelso, N. V., & Patterson, T. (2010). Introducing natural earth data-naturalearthdata. com. *Geographia Technica*, *5*(82-89), 25.

Liang, X., Lettenmaier, D. P., Wood, E. F., & Burges, S. J. (1994). A simple hydrologically based model of land surface water and energy fluxes for general circulation models. *Journal of Geophysical Research: Atmospheres*, *99*(D7), 14415-14428.

Lowe, W. H., & Likens, G. E. (2005). Moving headwater streams to the head of the class. *BioScience*, *55*(3), 196-197. https://doi.org/10.1641/0006-3568(2005)055[0196:MHSTTH]2.0.CO;2

Mac-Clure, R. (1970). *La Sobrevivencia de Chile, la Conservación de sus Recursos Renovables. 2nd ed.* Santiago, Chile: Ministerio de Agricultura

Máčka, Z., Galia, T., Škarpich, V., Michalková, M. Š., & Krejčí, L. (2023). A method for assessment of sediment supply and transport hazard and risk in headwater catchments for management purposes. *Environmental Earth Sciences*, *82*(1). https://doi.org/10.1007/s12665-022-10707-z

Potapov, P., Hansen, M. C., Laestadius, L., Turubanova, S., Yaroshenko, A., Thies, C., Smith, W., Zhuravleva, I., Komarova, A., & Minnemeyer, S. (2017). The last frontiers of wilderness: Tracking loss of intact forest landscapes from 2000 to 2013. *Sciences Advances*, *3*(1), e1600821. https://doi.org/10.1126/sciadv.1600821

Quiroga, E., Ortiz, P., González-Saldías, R., Reid, B., Tapia, F. J., Pérez-Santos, I., Rebolledo, L., Mansilla, R., Pineda, C., Cari, I., Salinas, N., Montiel, A., & Gerdes, D. (2016). Seasonal benthic patterns in a glacial Patagonian fjord: the role of suspended sediment and terrestrial organic matter. *Marine Ecology Progress Series*, *561*, 31-50. https://www.int-res.com/abstracts/meps/v561/p31-50/

Reid, B., Astorga, A., Madriz, I., & Correa, C. (2021). Estado del conocimiento y conservación de los ecosistemas dulceacuícolas de la Patagonia occidental austral. In J. C. Castilla, J. J. Armesto, & M. J. Martínez-Harms (Eds.), *Conservación en la Patagonia chilena: evaluación del conocimiento, oportunidades y desafíos*. Ediciones Universidad Católica.

Scheffer, M. (2009). *Critical transitions in nature and society*. Princeton University Press.

Schneider, W., Pérez-Santos, I., Ross, L., Bravo, L., Seguel, R., & Hernández, F. (2014). On the hydrography of Puyuhuapi Channel, Chilean Patagonia. *Progress in Oceanography*, *129*, 8-18. https://doi.org/10.1016/j.pocean.2014.03.007

Torres, R., ilva, N., Reid, B., & Frangopulos, M. (2014). Silicic acid enrichment of subantarctic surface water from continental inputs along the Patagonian archipelago interior sea (41–56°S). *Progress in Oceanography*, *129*, 50-61. https://doi.org/10.1016/j.pocean.2014.09.008

Torres, R., Reid, B., Frangópulos, M., Alarcón, E., Márquez, M., Häussermann, V., Försterra, G., Pizarro, G., Iriarte, J. L., & González, H. E. (2020). Freshwater runoff effects on the production of biogenic silicate and chlorophyll-a in western Patagonia archipelago (50–51°S). *Estuarine, Coastal and Shelf Science*, *241*, 106597. https://doi.org/10.1016/j.ecss.2020.106597

Torres, R., Reid, B., Pizarro, G., Frangópulos, M., Alarcón, E., Márquez, M., Díaz, F., Menschel, E., González, H. E., Moreno-Meynard, P., Montero, P., Pacheco, H., Pinto-Torres, M., Alarcón, C., Ibañez, R., & Hawkings, J. (2023). Iron and silicic acid addition effects on early Spring macronutrient drawdown and biogenic silica production of Patagonia estuarine waters. *Progress in Oceanography*, 102982. https://doi.org/10.1016/j.pocean.2023.102982

Van der Werf, G. R., Morton, D. C., DeFries, R. S., Olivier, J. G. J., Kasibhatla, P. S., Jackson, R. B., Collatz, G. J., & Randerson, J. T. (2009). CO2 emissions from forest loss. *Nature Geoscience*, *2*, 737-738.

Vandekerkhove, E., Bertrand, S., Crescenzi Lanna, E., Reid, B., & Pantoja, S. (2020). Modern sedimentary processes at the heads of Martínez Channel and Steffen Fjord, Chilean Patagonia. *Marine Geology*, *419*, 106076. https://doi.org/10.1016/j.margeo.2019.106076

Vandekerkhove, E., Bertrand, S., Reid, B., Bartels, A., & Charlier, B. (2016). Sources of dissolved silica to the fjords of northern Patagonia (44–48 S): the importance of volcanic ash soil distribution and weathering. *Earth Surface Processes and Landforms*, *41*(4), 499-512.

Veblen, T., Donoso, C., Kitzberger, T., & Rebertus, A. (1996). Ecology of southern Chilean and Argentinean Nothofagus forests. In T. Veblen, R. Hill, & J. Read (Eds.), *The ecology and biogeography of nothofagus forests* (pp. 293–353). Yale University Press.

Watson, J. E. M., Evans, T., Venter, O., Williams, B., Tulloch, A., Stewart, C., Thompson, I., Ray, J. C., Murray, K., Salazar, A., McAlpine, C., Potapov, P., Walston, J., Robinson, J. G., Painter, M., Wilkie, D., Filardi, C., Laurance, W. F., Houghton, R. A., . . . Lindenmayer, D. (2018). The exceptional value of intact forest ecosystems. *Nature Ecology and Evolution*, *2*(4), 599-610. https://doi.org/10.1038/s41559-018-0490-x

Chapter 1: Flow-weighted sourcing of freshwater runoff from Pacific-draining continental and coastal basins in Patagonia (41-56°S): characterizing regional inputs to Chilean fjords for the FLOW platform

Paulo Moreno-Meynard, Osvaldo Artal, Rodrigo Torres, Brian Reid

In preparation.

Abstract

Estimates of the global supply of dissolved and suspended materials to the ocean, in order to be relevant at either political or ecological scales, belie a finer-scale necessary for understanding specific terrestrial-marine interactions. This is especially true for continental runoff to the marine critical zone of inland fjords and channels, where mechanisms, drivers, and predictions need to be elaborated in the context of changing land use and shifting climate forcing. In fjords in west-southern Patagonia, runoff from small coastal and large continental basins (~310 x10^3 km^2), sourced from a diverse geography and wide climatic gradient (<150 – 6,000+ mm/y), correspond with a very low density of hydrological and water quality observations. Based on the recently developed regional runoff model (FLOW), we estimated the coastal freshwater discharges and characterized flow-weighted sourcing (cover type, land use change, glaciers/geology, and soil province) from 41º to 56º south latitude. An estimated 692 km^3/year (mean across 1979-2018), or 2% of worldwide total, also shows significant regional variation inn term of seasonality. Based on limited water quality observations and extrapolation from local studies, we demonstrate or propose general patterns of export for key continental resources, including a N-S gradient in declining input of silicic acid, increase input of glacial sediment ad iron, and potential shift in dissolved organic matter input sources from rainforest (potentially labile) to peatlands (refractory). We conclude with a general discussion of spatial consequences for marine ecosystem productivity and function, together with

recommendations for water quality observations, development of water quality standards for coupled river and marine ecosystems, of which the vast majority of this region is still within near-reference condition.

Keywords: west-southern Patagonia, coastal discharges, freshwater, inner seas, fjords, water quality, chemical composition runoff.

1.1 INTRODUCTION

Rivers are an important connection between terrestrial and marine ecosystems, with annual global coastal discharges estimated between 36 to 45 x 10^3 km^3 of fresh water together with an estimated 20 billion tons of particulate and dissolved solids (Milliman & Farnsworth, 2011; Oki & Kanae, 2006). These riverine forcings are crucial for salinity, allochthonous/autochthonous nutrient cycling, water temperature, and light availability, among other processes, in estuarine and coastal systems essential for human well-being ecosystem services (Millenium Ecosystems Assessment, 2005). However, these environments are strongly affected by human activities such as river contamination, erosion by land use changes, overharvesting, etc. (Milliman & Farnsworth, 2011; Pörtner et al., 2022). The proliferation of global estimates of specific resource export to marine systems is noteworthy: particulate C and N (Beusen et al., 2005), dissolved N (Bouwman et al., 2005; Dumont et al., 2005), P (Seitzinger et al., 2005), dissolved silica (DSi)(Beusen et al., 2009), and total alkalinity (AT)(Fry et al., 2015). Nevertheless, the most comprehensive global synthesis of riverine export, Milliman and Farnsworth (2011), highlights a data deficit in estimating basic suspended sediment export, noting that <5 rivers with reliable or comprehensive data are available for the western Andes.

According to these authors, potentially over 200 x10^6 t/year of suspended sediments and 20 x10^6 t/year of dissolved solids are exported from rivers in southern Chile, approximately the same order of magnitude of any regional basin in South America except for the Amazon, and among the highest globally in terms of specific yield. While the southern cone of South

America (including Patagonia) is the largest land mass in the southern oceans (> 30ºS, excluding Antarctica), almost none of this area is represented in the abovementioned global estimates of riverine export to marine systems (van der Struijk & Kroeze, 2010).

In a regional scale, west-southern Patagonia (41-56°S) has remarkable characteristics such as the mightiest rivers in the western Andes, including Puelo, Yelcho, Palena, Aysén, Baker, and Pascua rivers, some of the largest lakes on the continent and the deepest and crystalline in the world, and the largest temperate icefields on the planet (Reid et al., 2021). Mountain ranges elevational extremes are somewhat less than the northern Andes being lower in stature. There is no significant central valley, hence linear distances and/or fluvial courses from source to the sea are relatively short, and overall stream gradients relatively high. These characteristics of west-southern Patagonia produce a system of channels and fjords with an extended coastline, one the most relevant worldwide (Kelso & Patterson, 2010; Schneider et al., 2014).

The significant freshwater runoff affecting channels and fjords generates a highly variable 5-10 m freshwater-brackish lens overlying more uniform near-seawater salinity (Calvete & Sobarzo, 2011; Schneider et al., 2014). This vertical structure in water column salinity (Calvete & Sobarzo, 2011; Schneider et al., 2014), also corresponds with temperature and physical stability (Schneider et al., 2014), biogeochemistry (Torres et al., 2020; Vandekerkhove et al., 2016), light availability (Amann et al., 2022; Vandekerkhove et al., 2020), and productivity and structure of biological communities (Quiroga et al., 2016; Torres et al., 2021; 2023) of Patagonian fjords. The consequences of this interaction is amply illustrated by observations during an extreme drought in 2016, where relation between reduced freshwater input and water column stability to harmful algal blooms (HAB) has been suggested (León-Muñoz et al., 2018). While a general sense of the importance of freshwater inputs to marine systems is being developed, more precise estimates over spatially relevant distributions are lacking. Moreover, interpretations of cause and effect between continental and marine systems in Patagonia have

taken into account water quality only to a very limited extent (Torres et al., 2014), and causation sometimes proposed without evidence (see Torres et al., 2021; response to Vargas et al., 2018).

The quality and chemical composition of continental waters, the array of dissolved and suspended constituents that flow from land to sea, begins with the transformation of dilute precipitation inputs through processes of weathering, leaching and erosion. Land forms, vegetation, soils and corresponding physical conditions and alterations from land use may generate distinct water quality signatures at the source. Subsequently, the transformation of these initial sources may occur through physical, chemical and biological reactions, degradation and complexation, in transit over the continents, over short to long residence times. From these origins, continental waters may contribute a wide range of elements, complexes and diversity of dissolved organic compounds, exported by rivers to coastal areas, which may be simplified as the following generalized list: (1) macronutrients Nitrogen (N) and Phosphorous (P); (2) resources dissolved silica (DSi) and dissolved carbon (DOC – generalized in bulk terms although general comments on biological availability or lability are included); (3) trace nutrients such as dissolved iron (DFe); and (4) suspended sediments (predominantly mineral, with emphasis on glacial inputs). Macronutrients play a general role in primary productivity in ecosystems, whether terrestrial, freshwater or marine, the inorganic forms of N (NO_3^-, NO_2^-, NH_4^+) and P (PO_4^{+3}) being the most readily available for assimilation, while excessive loading (especially of N) may drive tipping points in marine ecosystems at large scales (Heinze et al., 2021; Voss et al., 2011). Concentration of macronutrient export to Chilean fjords is presumed to be minimal compared to internal marine cycling, although some exceptions may occur due to natural potentially climate driven pulses of N and P (B. Reid, unpubl.). However, the cumulative effect of terrestrial load has never been assessed, and there is a complete lack of time series data from major rivers that might enable such estimation. Dissolved silica is another important resource for marine ecosystems, as an essential resource

for diatom production, in turn the base for the coastal trophic systems: DSi is largely provided by river runoff in the Chilean fjords (Torres et al., 2014). Organic carbon exports to marine systems may provide energy to marine communities, in terms of particulate matter inputs to benthic communities (Quiroga et al., 2016; Quiroga et al., 2013), while dissolved carbon may contribute to microbial production, depending on a very wide range of species and lability. Dissolved iron stands out as an important but poorly characterized trace nutrient for diatom proliferations in Chilean fjords in early spring (Torres et al., 2020; 2023), and like DSi is sourced almost exclusively from river inputs, at concentrations 1-2 orders of magnitude greater than marine concentrations. Finally, suspended sediment inputs may simultaneously and heterogeneously supplement or inhibit marine productivity. Suspended sediments sourced from glacial meltwater or soil erosion, may on one hand form the substrate for marine benthic communities or attached microbial communities, often co-occurring with POM inputs (Quiroga et al., 2013) or potentially interacting with macronutrients (P) and trace elements (DFe), while on the other hand diminishing light availability for marine primary producers.

There is a general lack of knowledge on quantitative and/or spatially explicit freshwater coastal discharges in west-southern Patagonia. This is further underscored by data poor region in terms of water quality observations, lack of any time series or even seasonal characterization, or even a basic comprehension of how runoff sources are associated with specific terrestrial characteristics such as soils, geology, land use/cover, and climate. In the present study we will use the streamflow results simulated by the FLOW model (Reche et al., 2021). FLOW was developed by the Fisheries Development Institute (IFOP). Our general objective is to develop a refined regional and also spatially segregated estimate of continental runoff to the Patagonia fjords, together with spatially distributed estimates of runoff sourcing and potential implications on the export of key terrestrially derived, nutrients, energy and materials.

1.2 METHODS

1.2.1 Study area

The geographic definition of a territory such as Patagonia is always controversial due to its history, geopolitical interests, goals to commit, etc. However, our definition of west-southern Patagonia is by no means arbitrary, i.e., every basin with discharges, directly or indirectly, to the Pacific Ocean, starting in the north with the Inner Sea of Chiloé until Cape Horn in the south (figure 1.1). The study area is similar to the one by Astorga et al. (2018) from a hydrographic perspective and the one established by Torres et al. (2014). The inland territory starts from the Río Petrohué basin (discharged at 41.5°S, into the estuary of Reloncaví), following south with several trans-Andean catchments such as Puelo, Yelcho, Palena, Cisnes, Aysén, Baker, and Serrano basins. The insular area starts with the Chiloé island, following south with every archipelago until Cape horn (56°S). The site includes the political jurisdictions of some of the Los Lagos Region (Llanquihue, Palena, and Chiloé provinces), Aysén, and Magallanes Regions in Chile, and the Provinces of Chubut, Santa Cruz, and Tierra del Fuego in Argentina. Geomorphology, geology and soil characteristics, climate, land use/cover, and human activities influence the runoff in west-southern Patagonia. The geomorphology of this region, with a lower elevation of the Andes Mountains ranges and the lack of a central valley, compare to the northern part of Chile, translates into an extensive net of fjords, channels, and islands.

The regional geology is diverse, for example, on Chiloé island, sedimentary deposits from the Cenozoic, and metamorphic rocks from the Paleozoic are predominant. The latter, known as Chonos Formation, continues to the south in the archipelagos zone until the Taitao Peninsula. However, intrusive rocks, mainly Mesozoic granitoids, i.e., Patagonian Batholith, are presented at the same latitude in the continental area. This formation continues to the south until Cabo de Hornos, one of the most essential in the extreme south continent. Additionally, volcanic rock

complexes from the Mesozoic and Cenozoic times appear to the east of the Andes Mountain ranges. Moreover, the Paleozoic Easter Andes Metamorphic Complex occurs to the south of General Carrera Lake until the southern Patagonian Icefield (SPI). At the continent's end, sedimentary formations, and less importantly, volcanic, occurs associated with Mesozoic fluvial-glacial deposits. Finally, small formations of Holocene volcanic rocks are associated with Strato-volcanoes between 41-47°S, such as Osorno, Calbuco, Yates, Hornopirén, Michimahuida, Melimoyu, Hudson, etc. (SERNAGEOMIN, 2003; Vandekerkhove et al., 2016).

Volcanoes are associated with thicker andosols in the valleys and thinner eutric leptosols in steeper conditions, being predominant soils in the continental area until 47°S (Dijkshoorn et al., 2014; Stolpe, 2014). The composition of these soils is mainly tholeiitic, high-Al basalts to basaltic andesites, with the sporadic formation of andesites, dacites, and rhyolites (Vandekerkhove et al., 2016). Volcanic activity is permanent, with the last eruptions in 1991, 2008, and 2015 AD for Hudson, Chaitén, and Calbuco volcanoes, respectively. However, numerous volcanic registers have been obtained thanks to the tephra layers and sediment cores in lakes (Vandekerkhove et al., 2016). The Chonos Formation soils are mainly cambisols, with clay minerals and iron oxides. The archipelago soils southern to 47°S are thin, mainly leptosols with different origins due to parental material or vegetation presence. In the steppe, the predominant soils are podzols, cambisols, and phaeozems (Dijkshoorn et al., 2014).

Precipitations are strongly influenced by the humid southern Westerlies flow coming from the ocean and the topography of the Andes Mountain ranges. With a hyperhumid climate on the western side (5,000 to 10,000 mm/year) and a cold steppe climate due to rain shadow on the lee side of the Andes (< 300 mm/year), reaching one of the most severe rain ranges on the planet (Garreaud et al., 2013). The precipitation variability, intraseasonal and decadal scale, are provoked by the Southern Annular Mode (SAM) and the Pacific-South American (PSA)

patterns. The negative and positive SAM phases are associated with positive precipitation anomalies and dry conditions. The PSA patterns connect tropical disturbances with meridional territories in South America (Aceituno et al., 2021). An extreme dry event in 2016 was produced by one of the strongest warm-phase ENSO records (1950–2015) (Blunden and Arndt, 2017). The precipitation trends show a slight decrease of 2 mm/year in some stations in the Aysén region but a positive trend above 50 mm-decade in the Magallanes region (Castro and Gironás, 2021). Mean temperatures range by latitude from 10°C (41°S) to 5°C (55°S) with oscillations due to the altitudes of the Andes Mountain ranges. For example, the Patagonian Mountain range presents mean temperatures below zero degrees almost all year (Castro and Gironás, 2021).

The vegetation, as expected, is highly correlated with the climate in west-southern Patagonia with a west-east gradient (Luebert & Pliscoff, 2006). The hyper-humid climate produces an evergreen forest, mainly broadleaf but with some cypress patches (Donoso, 1993). These forests are present in Chiloé island, the archipelagos zone, and the western side of the Andes. Additionally, in less favorable conditions in the islands zone, moorland cover appears with shrubs, wetlands, and unweathered parent material. In colder situations associated with higher altitudes and to the eastern side of the Andes, deciduous *Nothofagus* forests appear. Finally, in the east of Patagonia, the dominant vegetation are gramineous due to the steppe's dry conditions (Luebert & Pliscoff, 2006).

The colonization process in Patagonia was associated with the transformation of forests into grasslands for cattle raising. The mechanism widely used for this transformation was extensive forest fires (Veblen et al., 1996). Additionally, forest harvesting, mining, forest plantations, urban habilitation, and roads are other human impacts of land use/cover changes. However, the time and magnitude of these impacts are not the same, with the northern part of the region (~41°S) being the earliest and most severe (Veblen et al., 1996). Instead, the Aysén region has

an early colonization process of only ~120 years but with substantial effects, e.g., Aysén port unusable by sandbanks due to erosion (Bizama et al., 2011). Furthermore, the harvesting of ciprés de la guaitecas, a native cypress, has generated forest fires in the whole islands zone, producing severe erosion due to the high precipitation rate (Mac-Clure, 1970; Veblen et al., 1996). However, these land use/cover changes in Patagonia due to their vast extension are not massive, e.g., Astorga et al. (2021) defined 66,000 km^2 (49% of mature forested watersheds) of intact forested watersheds between 41-56°S indicating the low rate of impacts in many areas of the region.

1.2.2 Land/sea zoning

The zoning is based on a marine perspective (Pickard & Stanton, 1980), including differences between inner seas, channel zones, and offshore coasts but with a basin point of view on the territory (figure 1.1 and table 1.1). First, Zone 1 comprises catchments related to the Inner Sea of Chiloé, including the Estuary of Reloncaví, with watersheds from inland and Chiloé island. The main basins in Zone 1 are Petrohué, Puelo, and Yelcho. Second, Zone 2 comprises Chiloé island catchments that discharge directly to the ocean, with the Pudeto, Chepu, and Huillinco basins as the most important. Third, Zone 3 corresponds with these catchments that discharge into the Aysén Sea, with their fjords and channels. The most critical basins in this zone are Palena, Cisnes, Aysén, and Exploradores. Forth, the island catchments flow directly to the ocean from Guaitecas until the Gulf of Penas corresponds to Zone 4. Fifth, Zone 5 comprises the catchments that discharge south of the Gulf of Penas until the north of the Madre de Dios archipelago (MDD). Baker and Pascua are the most extensive basins in Zone 5 and also is included the southern Patagonian Icefield (SPI). Sixth, Zone 6 corresponds to the catchments from MDD to the beginning of the Magellan Strait, with the Serrano basin as the most relevant inland basin. Finally, Zone 7 starts with the Strait of Magellan until Cape Horn. The total zoning is 310 $x10^3$ km^2 with 15° of latitude range (table 1.1), finding the most

important Chile's freshwater resources, in terms of rainfall, ice fields, among the world's largest, deepest and clearest lakes, together with significant rivers draining into one of the world's most extensive inland marine fjord systems (Reid et al., 2021).

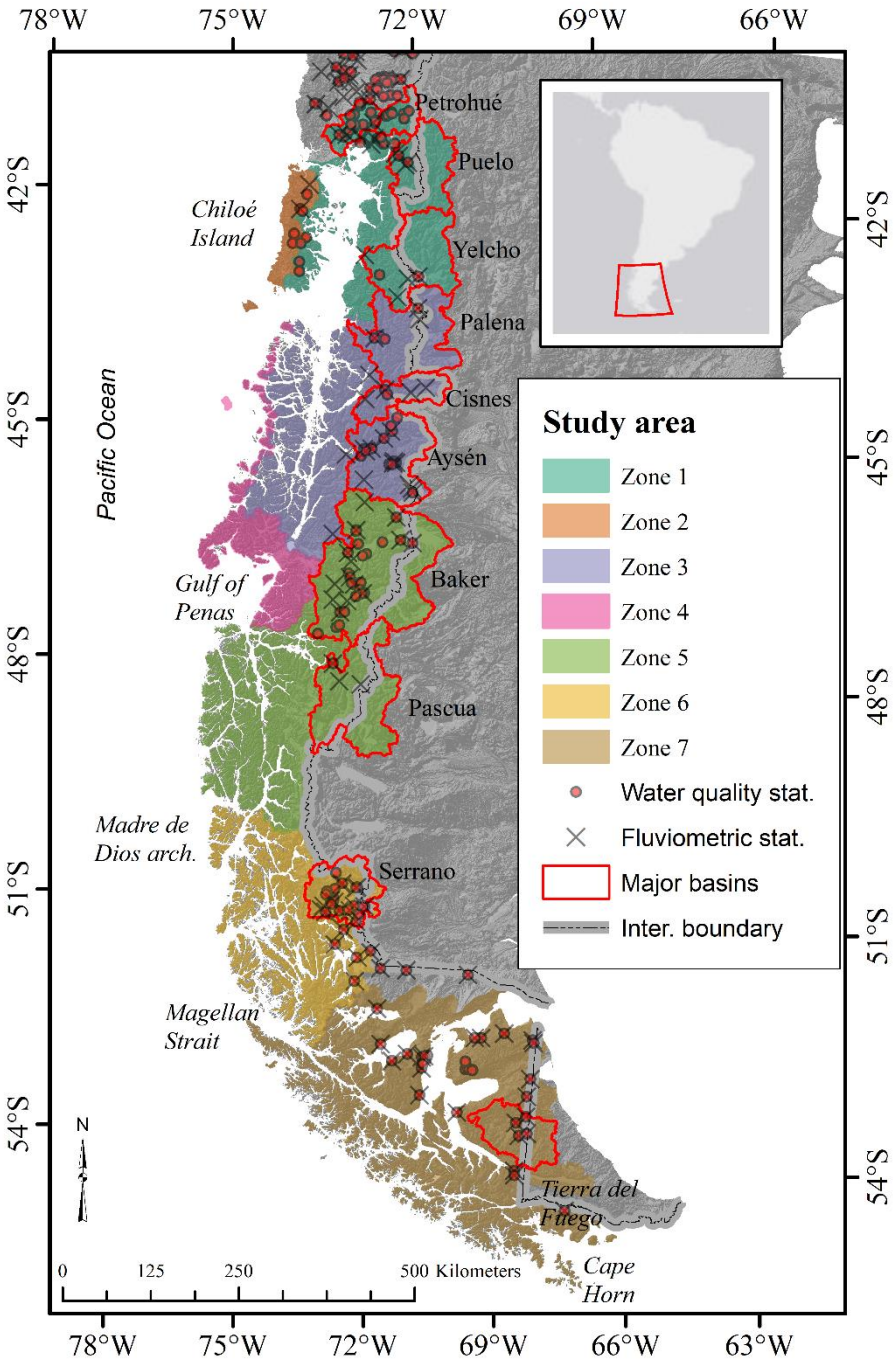

Figure 1.1. *West-southern Patagonia with proposed coastal watershed Zones 1-7, internal basin boundaries and major continental basins based on the hydrologic model FLOW.*

1.2.3 FLOW Model

FLOW is a web tool that allows exploring and visualizing the freshwater simulation results performed with the hydrological model VIC for southern Chile (https://chonos.ifop.cl/flow). VIC is a hydrological model that solves energy and water balance equations driven by atmospheric forcing, widely used by the scientific community. In Chile, it has been applied in climate change studies (Bozkurt et al., 2018; Demaria et al., 2013) and for water resources management (Fustos et al., 2022) and is currently being used for the new national water balance of the Chilean General Water Directorate (DGA). FLOW is also a part of a multicomponent oceanographic model and online platform CHONOS (Reche et al., 2021), in development for the Chilean Fjords, and is hence a first iteration of modeled runoff for the region: validation of hydrological outputs and extension to water chemistry exports are still needed.

FLOW has daily streamflow between 1979 and 2018, and snowmelt discharges from 31,220 basins in an area of 315,740 km^2. These basins are divided between those catchments from the VIC model or principals and those with a character of supplementary (no streams modeled) associated to the principals by a size factor (see table 1.1). In addition, it contains online information from 68 DGA fluviometric stations to compare simulated with observations data. VIC model uses as atmospheric forcing the daily gridded product of precipitation and temperature (maximum and minimum) of 0.05° spatial resolution from CR2MET (Boisier et al., 2018). Precipitation in CR2MET is obtained using transfer functions to convert precipitation, moisture fluxes, and other large-scale variables from ERA-Interim to regional precipitation raster. These transfer functions consider the local topography and are defined by a set of parameters calibrated with local precipitation observations. For temperature, in addition to local information (topography and temperature observations) and large-scale variables (ERA-Interim), surface temperature data estimated from satellite images (MODIS LST) are considered.

Table 1.1. Characterization of zones based on geography, climate land use/cover, and FLOW model distribution (number and area of sub-basins). Ranges are indicated in parentheses except for land use (% cover).

	Zone 1	*Zone 2*	*Zone 3*	*Zone 4*	*Zone 5*	*Zone 6*	*Zone 7*
Geography							
Area (km²)	40,683	5,754	57,857	14,265	77,591	37,161	77,638
Mean Elevation (m.a.s.l.)	746 (0–3332)	185 (0–854)	694 (0–3985)	392 (0–3376)	753 (0–3722)	382 (0–2821)	273 (0–2556)
Climate							
Annual Precip. (mm/year)	1,668 (473–3638)	2,208 (1456–2552)	1,679 (364–3102)	2,317 (1188–3788)	1,902 (128–6159)	2,058 (227–6869)	894 (251–3878)
Mean Monthly Temp. (°C)	7.8 (-3.7–12.1)	9.1 (6.2–10.9)	6.4 (-10.3–10.7)	6.8 (-7.4–9.3)	5.1 (-8.9–10.2)	5.3 (-6.9–7.8)	4.9 (-7.0–7.2)
Land Cover km² (%)							
Urban	106 (0.3%)	10 (0.2%)	23.9 (<0.1%)	0	5.7 (<0.1%)	5 (<0.1%)	42 (0.1%)
Forest/Shrub	27,439 (67.4%)	4,899 (85.1%)	38,101 (65.9%)	9,550 (66.9%)	28,155 (36.3%)	10,810 (29.1%)	30,318 (39.1%)
Moorland/ Wetland	586 (1.4)	169 (2.9)	1428 (2.5)	1,316 (9.2)	12,972 (16.7)	12,350 (33.2)	18,336 (23.6)
Snow/Glacier	3,691 (9.1)	0	5,508 (9.5)	2,297 (16.1)	15,323 (19.7)	3,886 (10.5)	6,498 (8.4)
Alpine	2,017 (5.0)	0	3,294 (5.7)	12 (0.1)	3,900 (5.0)	1,497 (4.0)	2,611 (3.4)
Pasture	2,594 (6.4)	486 (8.4)	2,662 (4.6)	0	268 (0.3)	115 (0.3)	4,592 (5.9)
Steppe	517 (1.3)	0	4,760 (8.2)	0	2,234 (2.9)	1,866 (5.0)	3,336 (4.3)
FLOW Distribution							
Model Catch. (count)	862	156	2,229	956	2,734	3,022	4,836
Mean Model Catch. (km²)	45.3 (1–11,513)	35.4 (1–1,056)	23,6 (1–13,162)	12.5 (1–1,735)	25,9 (1–27,666)	9.7 (1–7,768)	13,8 (1–7,203)
Secondary Catch. (count)	825	146	2,416	1,047	2,811	3,713	5,176
Mean Secondary Catch. (km²)	2.0 (0.1–18.7)	1.6 (0.1–9.4)	2,2 (0.1–31,4)	2.2 (0.1–32.2)	2,4 (0.1–32.2)	2.2 (0.1–29.1)	2.1 (0.1–28.3)
Fluviometric stations for calibr. (count)	13	2	20	0	10	11	9

Note: Mean elevation calculated from DEM ALOS-PALSAR 12.5 m (Rosenqvist et al., 2007); Climatic variables from WorldClim downscaled bioclimatic variables (Stephen E Fick & Robert J Hijmans, 2017); Land use/cover variables from Chilean national land use inventory maps (CONAF, 2016) and Argentinian national land use maps (IGN, 2013); FLOW model variables from https://chonos.ifop.cl/flow ; Model Catch., principal catchments with modeled streams; Secondary Catch., small watersheds with no modeled streams associated with neighbor principal catchments. Fluviometric stations for calibr., observational data used for calibration and validation of FLOW outputs.

Streamflow estimates were calculated using a "routing" (or transport) model that simulates the movement of water through the network of watercourses and rivers until it flows into the

sea (Lohmann et al., 2004). The routing model uses a hydrographic network generated from the 30-meter resolution Shuttle Radar Topography Missiom (SRTM) digital elevation model using TauDEM software. A value of 1 km^2 as the minimum contributing area was used, a value with sufficient detail to capture all relevant rivers, streams, and creeks for the purposes of FLOW model. Water transport from the grid cells of the VIC model to the outfall was modeled with a constant velocity of 1.8 m/s. It should be noted that the simulation results were relatively insensitive to the occupied velocity value since the vast majority of basins were relatively small, and the residence time in the river is generally less than 24 hours.

An essential aspect of the FLOW methodology was the treatment of glaciers in the VIC model. Glaciers, especially the Northern and Southern Patagonian Icefields, play an important role in the observed flow behavior in the study area. In several places, tidewater glaciers flow directly to the sea and constitute a significant source of freshwater. Unfortunately, the VIC model does not have a module to represent glaciers directly, so it was implemented and evaluated a degree-day estimation method (Schaefer et al., 2013; 2015).

To optimize the most critical parameters of the VIC model, 64 simulations were performed with different calibration parameters (METEODATA, 2020). The parameters considered were infiltration capacity, unit hydrograph, soil depth, max baseflow, and degree-day factor. The results of each simulation were compared with 68 DGA monitoring stations (METEODATA, 2020). The final simulation is the weighted average of the results of each simulation, where the weighting factors minimize the mean square error of the model.

The runoff was aggregated in each catchment identified in the model by season and year using the simulated database of the FLOW model. Additionally, these discharges were identified by the respective zone of analysis (see figure 1.1). Finally, the runoff flows were weighted with some attributes that affect their chemistry characteristics, such as soils, geology, climate, and land use/cover.

1.2.4 Flow-weighted sourcing of freshwater runoff

First, discharges weighted by geology attributes were calculated from Chilean and Argentinian digital geologic maps (SegemAR, 2021; SERNAGEOMIN, 2003). Second, in the case of the soils, flows were weighted using the Soil and Terrain database for Latin America and the Caribbean (SOTERLAC), version 2.0, with a scale of 1:5 million (Dijkshoorn et al., 2014). Third, land use/cover was obtained using the Chilean national land use inventory maps (CONAF, 2016) and Argentinian national land use maps (IGN, 2013), with some extra information to define moorlands/wetlands in the islands based on Luebert and Pliscoff (2006). Finally, climatic zones were determined with the WorldClim downscaled annual precipitation (Fick & Hijmans, 2017) with humid, intermediate, and dry classes ranging from >1200 mm, 1200-600 mm, and <600 mm, respectively. Differences in the annual amount of runoff by zone were identified by analyses of variance, with the Holm method for p-values adjustment for multiple comparisons. All statistical analyses were performed in R software (Core-Team, 2017).

1.2.5 Chemical information of rivers in Patagonia

A review of chemical characterizations for selected river observations in west-southern Patagonia that interpret the nutrients exported to marine ecosystems from the terrestrial areas was performed. The information was extracted from the Chilean General Water Directorate (DGA; https://snia.mop.gob.cl/BNAConsultas/reportes). Series on average with ten years of data between 2006 and 2015 were utilized. Annual chemical data ranges between 1 to 4 measurements.

1.3 RESULTS

1.3.1 Total and seasonal coastal freshwater runoff in west-southern Patagonia

The coastal runoff discharges in west-southern Patagonia was estimated by FLOW model at 692 km^3/year averaged over 40 years (95% CI [679.8,711.8]), corresponding to ~2% of world freshwater runoff estimated by Milliman and Farnsworth (2011). The zones in study had different discharge magnitudes due to catchment sizes and precipitation amounts (figure 1.2 and figure 1.3A). Zone 5 presented the highest runoff amount, with an average close to 200 km^3/year, with two big inland basins, Baker and Pascua, besides the runoff from the southern Patagonian Icefield (SPI) and the archipelago with the highest rate of precipitation. Another important discharge area was Zone 3, with ~150 km^3/year, incorporating the basins of Palena, Cisnes, and Aysén as the most crucial. The zones with significant influences of inland basins, Zones 1, 3, and 5, presented a higher dispersion in annual discharges. In contrast, those zones with stronger island influences, Zones 2, 4, 6, and 7, showed lower distribution between years. For example, Zone 2 presented values of discharges close to the median most of the time (flat violin shape in figure 1.2). Three Zones (1, 6, 7) presented similar mean values, but generally, the zones gave different annual runoff.

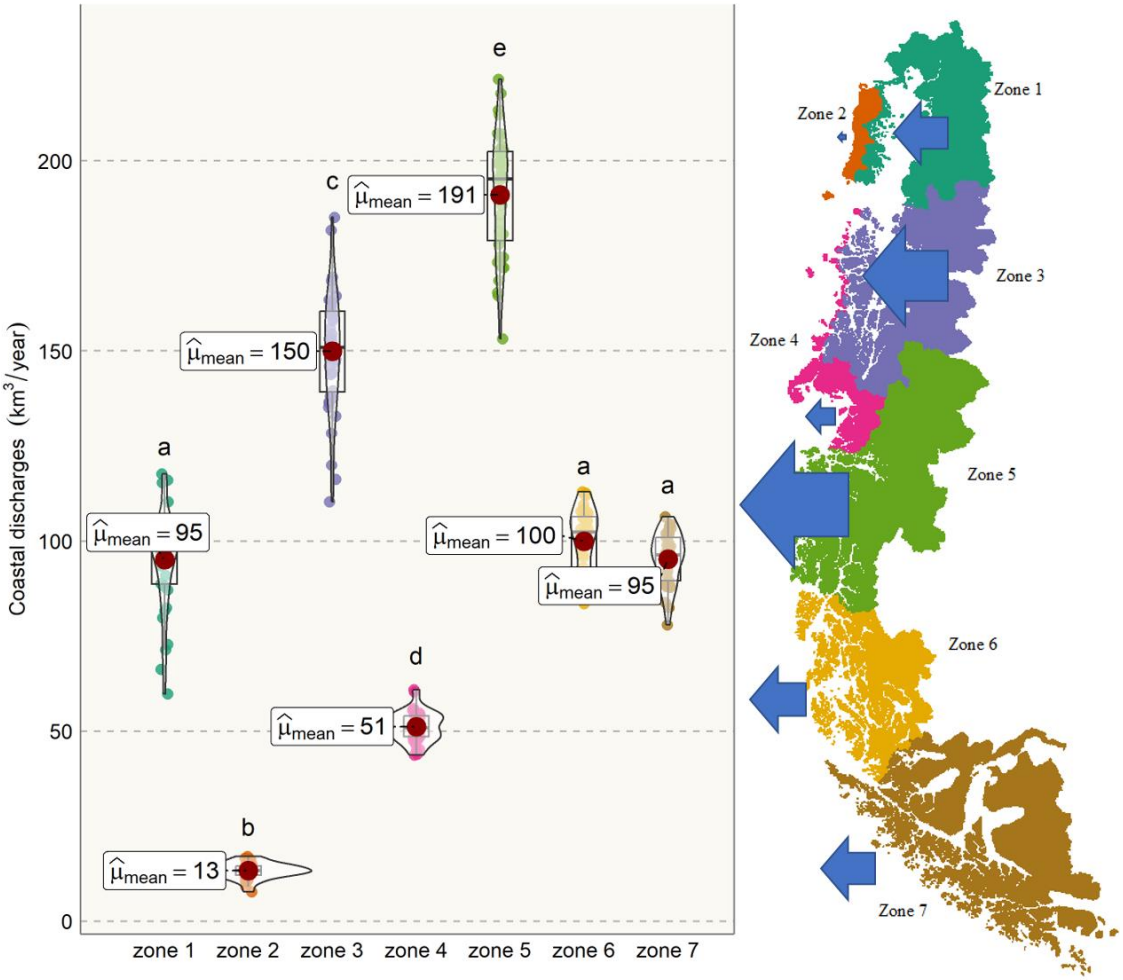

Figure 1.2. *Estimated annual discharge by Zone (mean based on 40 years: 1979 and 2018) using the FLOW Model.* Box-violin plots represent the freshwater runoff distributions. *Means and multiple pair-comparisons are shown (letters). Zoning is presented by easy spatial interpretation. Blue arrows represent annual coastal discharges.*

Seasonal discharges were calculated to have a closer view of the runoff characteristics in each zone (figure 1.3B). Despite Zone 5 with the highest discharges, in winter, its relative importance decreases and is surpassed by Zone 3. Probably, the latter is provoked by lower temperatures in winter for Zone 5, having most watersheds associated with snow- and glacier-feed regimes. The uniform behavior of intra-annual distributions in those zones associated with island catchments repeats at the season level. Zone 1 presented a similar amount of runoff from autumn to spring but decreased significantly in summer, generating a particular condition with lower freshwater influences in the Inner Sea of Chiloé. Thus, Zone 1 had a large proportion of rain-feed catchments where dry summers presented a notable decrease in coastal discharges.

The Sea of Aysén, composed mainly of channels and fjords, had an influence of runoff based on rain-feed basins, mainly with higher discharges between autumn and spring, having a decrease in summer. Finally, the austral zones, specifically 6 and 7, present higher coastal discharges associated with snow- and glacier-feed catchments in spring and summer.

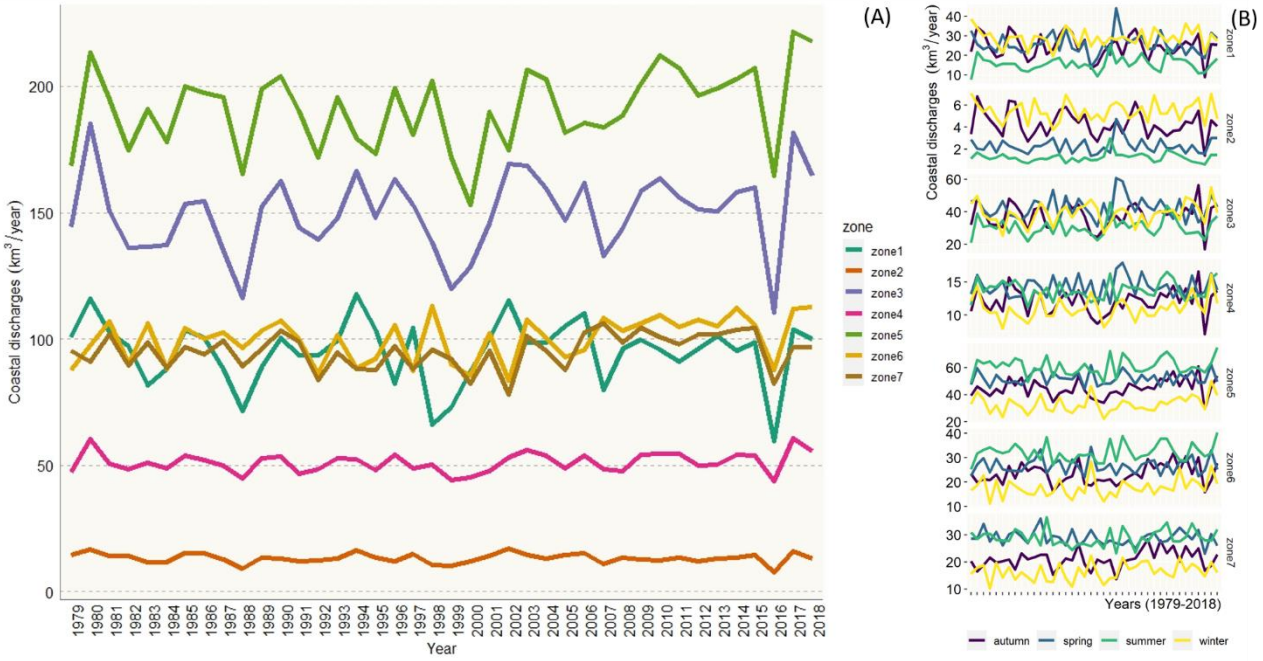

Figure 1.3. *Discharges between 1979 and 2018 (40 years) by Zone. (A) Distribution of coastal discharges. (B) Interannual variability of seasonal trends.*

1.3.2 Source characterization of freshwater runoff

Flows were weighted (percentage on each watershed) with some attributes that affect their chemistry characteristics, such as soils, geology, climate, and land use/cover (figure 1.4). The results show a high variability source characterization of freshwater discharges between zones. As expected, the higher amounts of runoff come from wet or hyper-humid climates, i.e., places with precipitation >1200 mm. However, Zone 5 had a crucial influence from a dry environment with rainfall <600 mm. Additionally, austral Zone 7 is dominated by flows from intermediate and dry areas. The zones associated with only coastal discharges directly to the ocean (Zones 2, 4) showed only runoff from hyper-humid climates.

In the case of flow-weighted from a geologic perspective, the runoff in each zone is influenced by crystalline rocks, mainly granitoids. However, basins with different geologic characteristics are in Zone 2, where the flows especially come from metamorphic and unconsolidated quaternary sediments. The sedimentary formations increase their importance to the south (Zone 5-7), associated with flat areas in the steppe. Something similar occurs with the influence of flows from glaciers, with Zone 5 influenced by the SPI. Associated with geology, the soils presented a strong influence from volcanic activities. Andosols are the most common soils in the study area's inland northern zone (Zones 1, 3). However, weathering regolith soils are principals in the oceanic and austral zones. Unconsolidated sediments from the Holocene are important in Zone 1 and 3. In the rest of the zones, their influence is low.

Forest is the primary land use/cover that influencing the runoff from Zone 1 to 5. Specifically, in the northern Zone (1-3), the importance of forests and shrubs on the discharges is crucial. However, moorlands and wetlands begin to influence the runoff from Zone 5 to the south, reaching the higher flows from these land use/covers. Alpine areas over the tree line are present in most zones due to Andes's topography. Pastures with fertilizers had a higher proportion in those most populated zones (1 to 3). Finally, urban areas had minor influences on the amount of runoff, but the impact on the discharge flows is critical due to the intensity of biochemistry changes.

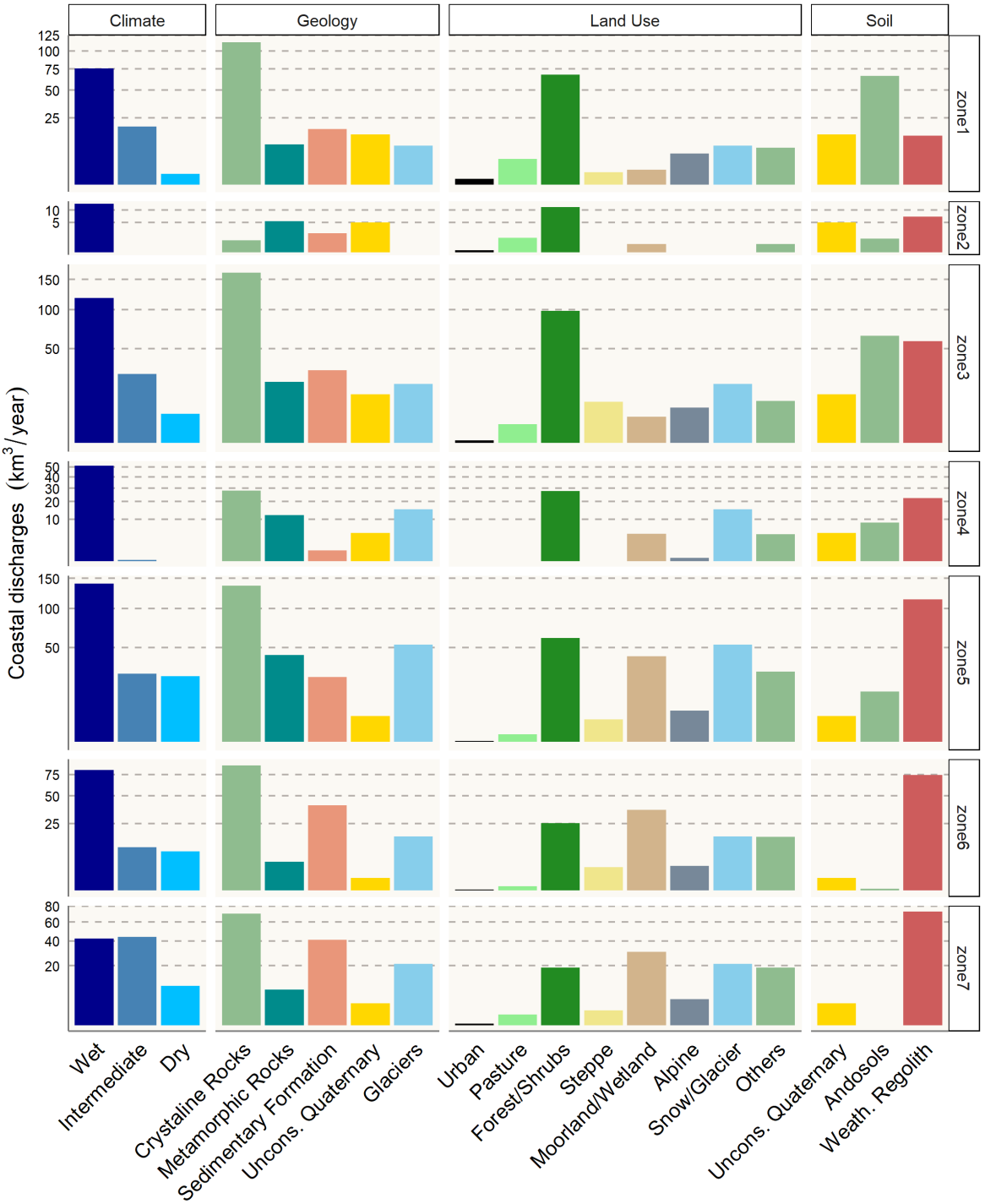

Figure 1.4. *Flow-weighted by climatic, geologic, land use/cover, and soil attributes. Wet, >1200 mm; Intermediate, <1200 mm but >600 mm; Dry, <600 mm. Uncons. Quaternary, geologic sediments from the Holocene; Weath. Regolith, weathered regolith. Square root scale in axis y.*

Table 1.2 presents some river observations in Patagonia that interpret the nutrients exported to marine ecosystems from the terrestrial areas. In general, Patagonian rivers are moderately to

highly dilute, low ionic strength systems, while in terms of water quality streams and rivers in the region very frequently falling into the highest level of "excepcional". Specific conductivity is usually less than 100 μS/cm for most volcanic formations, somewhat lower than 50 μS/cm for granitic catchments, and often in the range of 10-20 μS/cm for coastal catchments with high runoff coefficient. In areas transitioning to cold steppe such as many headwaters of major rivers, or from more arid climates (Punta Arenas or Tierra del Fuego) with high evaporation rates, specific conductivity may surpass 150 to 200 μS/cm. Suspended sediment concentration, largely unknown for most systems, nevertheless may be very significant in glacial meltwater rivers. Reliable values for pH, which is one of the most difficult parameters to measure in low ionic strength system, are hard to come by. In general, mildly basic systems (pH 7.5-8.5) are not unusual in arid pampas transitions and also the unusual limestone features of Madre de Dios archipelago (MDD), circum-neutral pH of 7 to 7.5 is common in the Andes Mountain ranges, while mildly acidic conditions pH 6-7 are typical of coastal catchments with high runoff. These patterns correspond with the distribution of alkalinity across rivers of different origin, generally in the range of 0.4-0.6 meq, 0.1-0.2 meq and <0.1 meq respectively (B. Reid, unpubl. data).

Major nutrients N and P are often close to detection limits. Concentrations of inorganic phosphorous in the range of 2-10 ug/L for $P\text{-}PO_4$ are typical, usually somewhat more elevated in streams of arid origin, while values <2 ug/L are common especially in granitic lithology, or glacial or snowmelt origin in the cordillera. Anomalously high $P\text{-}PO_4$ documented for some glacial rivers such as Rio de la Colonia (B. Reid, pers obs) may be due to geochemical processes in the northern Patagonian Icefield (NPI), described for other Andean streams with glacial origin (Chillrud et al., 1994). Total P may be an order of magnitude higher for systems with high solid load, including glacial rivers. Values of 10-40 ug/L for inorganic $N\text{-}NO_3$ nitrate nitrogen are also typical. Although limited information exists on dissolved organic carbon,

DOC is generally low in the cordillera (<0.5 mg/l) but higher in the coastal systems (>1-2 mg/l), and significantly higher (e.g., classified as dystrophic) where lakes or wetlands provide a significant contribution to streams, especially in coastal watersheds (>10 mg/l in Chiloé, J. Nimptsch U. Austral, pers. com.). Dissolved silica (DSi, silicic acid) is another important chemical species of regional significance. Silica concentration in major rivers appears to be highly related to depth and perhaps age of volcanic soils (Vandekerkhove et al., 2016).

Stream temperature is low for all systems, summer maximums of around 20 ºC may occur for larger rivers, but generally temperatures are less than 15 ºC. Much lower summer temperatures of 1-6 ºC are expected for glacial rivers. Outlets of major lakes may be thermally buffered in both summer and winter: the Baker River usually ranges between 6 and 12 ºC. Extremes of 1 ºC annual average temperatures are reported for moderate elevations in Río Róbalo, Isla Navarino (Contador et al., 2015), the authors also noting the extreme elevational gradient in thermal regime (decline in mean annual temperature by 1 ºC per 100 meters elevation) and thermal buffering (low annual range in temperature, with no extreme lows): the latter relieving the thermal limitations that might occur in equivalent northern latitudes. Perhaps more important from a biogeochemical or biological perspective (especially in the case of ectothermic organisms or organic matter breakdown) are the degree days, or accumulated temperature over the course of the year: although data exist, no estimates of accumulated temperature are currently available for the region. Corresponding with low nutrient conditions, low bio-available organic matter inputs, low temperatures and high reaeration rates in higher gradient mountain streams, dissolved oxygen concentrations are usually very close to saturation. Highly supersaturated dissolved oxygen (110-115%), approaching lethal levels for some aquatic organisms, are also not unusual below major falls in larger rivers (e.g., Río Baker and Río Ibañez).

1.4 DISCUSSION

1.4.1 Regional and global importance of runoff from west-southern Patagonia drainages

In addition to the extensive coastline, the influences of westerly winds with water from the Pacific Ocean evaporation and the barrier topography of the Andes Mountain range provoke a higher volume of precipitation. This aggrupation of factors generates a substantial amount of runoff where the FLOW model estimate, on average for 40 years, 692 km^3/year. This amount corresponds to 1.5 to 2% of world freshwater runoff (Milliman & Farnsworth, 2011; Oki & Kanae, 2006). Milliman and Farnsworth (2011) estimate a 79.3 km^3/year for west-southern Patagonia but with a base of five major rivers. The differences are explained because the FLOW model was built with an observational database and incorporated almost all the watersheds with discharges into the coast. Dávila et al. (2002) found higher runoff values ~876 km^3/year but with a larger area (35-55°S).

Table 1.2. Biochemical characterization of rivers in Patagonia by Zone based on minimum 10 years of observations (approximately 1-4 observations per year between 2006 a 2015; exceptions noted in text). River categories: C - coastal lowland; S snowmelt-cordilleran; L - lake discharge; G - glacier-fed; P – pampas-cold steppe; M – major basins. Near or direct coastal discharges shown in bold. n.d. no data; b.d. below detection.

ID	Zone	River	Basin [km^2]	Latitude	Longitude	C	S	L	G	P	M	Temp. [^oC] min/max	Cond. [µS/cm] *mean (SD)*	pH mean (SD)	Cl^- [mg/l] mean (SD)	SO_4^{2-} [mg/l] mean (SD)	Ca^{2+} [mg/l] mean (SD)	Fe_T [µg/l] mean (SD)	$N\text{-}NO_3^{2-}$ [µg/l] mean (SD)	$P\text{-}PO_4^-$ [µg/l] mean (SD)
1	1	**Cochamó**	249	41°29'14"	72°14'46"		X					4.4/12.5	32 (16)	6.93 (0.55)	1.3 (0.2)	3.8 (1.9)	4.4 (2.7)	102 (143)	17 (55)	4 (1)
2	1	**Chamiza**	686	41°29'15"	72°50'09"		X					4.2/21.1	54 (20)	6.95 (0.58)	4.7 (2.0)	2.8 (2.2)	4.3 (2.1)	644 (395)	96 (55)	14 (10)
3	1	**Puelo**	8650	41°38'39"	72°10'20"		X	X			X	6.7/15.1	41 (7)	7.09 (0.41)	2.1 (1.1)	2.8 (1.4)	5.3 (1.3)	397 (1.464)	45 (58)	8 (7)
4	1	Futaleufu	7280	43°10'43"	71°45'27"		X	X				6.1/13.7	48 (12)	7.18 (0.36)	2.4 (1.4)	2.8 (1.2)	6.9 (4.1)	146 (309)	35 (56)	11 (18)
5	1	**Yelcho**	9975	43°10'29"	72°26'18"		X	X			X	7.7/14.2	39 (5)	7.06 (0.57)	2.5 (1.0)	2.3 (1.5)	5.0 (1.5)	80 (69)	35 (55)	7 (14)
6	2	Puntra	97	42°09'57"	73°43'27"	X						4.5/18.4	52 (22)	6.79 (0.55)	5.4 (1.1)	2.0 (1.4)	3.1 (2.0)	449 (224)	150 (71)	22 (22)
7	2	Grande	203	42°21'12"	73°50'32"	X						3.0/14.4	27 (9)	6.45 (0.61)	4.7 (1.5)	1.7 (0.8)	1.4 (1.7)	216 (155)	52 (50)	9 (10)
8	2	Bravo	610	42°41'22"	73°56'22"	X						5.3/17.0	41 (10)	6.46 (0.53)	7.7 (1.6)	1.6 (0.8)	2.1 (2.4)	401 (108)	151 (50)	12 (27)
9	3	**Cisnes**	3155	44°42'05"	72°13'57"		X			X	X	1.7/18.0	32 (10)	7.25 (0.70)	1.7 (0.7)	1.9 (1.7)	3.7 (1.3)	298 (775)	40 (50)	9 (11)
10	3	Ñirehuao	1820	45°10'12"	72°08'35"					X		0.5/20.7	62 (17)	7.50 (0.63)	1.7 (0.9)	3.3 (1.7)	8.7 (5.8)	274 (232)	48 (55)	11 (10)
11	3	Coyhaique	633	45°34'02"	72°01'52"					X		0.8/22.8	65 (23)	7.37 (0.61)	2.0 (0.8)	2.8 (1.7)	7.3 (2.5)	468 (1270)	48 (46)	60 (60)
12	3	Oscuro	97	45°56'29"	71°42'31"					X		0.2/18.8	98 (37)	7.46 (0.65)	1.5 (0.8)	6.1 (3.9)	14.5 (6.6)	651 (1610)	44 (49)	25 (16)
13	3	Simpson	2632	45°33'09"	72°04'06"		X			X		1.0/20.8	83 (28)	7.47 (0.64)	2.0 (0.9)	4.0 (2.2)	9.9 (3.1)	601 (527)	71 (50)	37 (37)
14	3	Blanco	2965	45°25'57"	72°35'21"		X	X				4.1/17.4	27 (7)	7.34 (0.63)	1.7 (0.6)	1.7 (0.9)	2.7 (1.3)	229 (149)	49 (56)	9 (8)
15	3	**Aysén**	11428	45°24'27"	72°37'23"						X	3.7/16.5	39 (17)	7.33 (0.63)	1.8 (0.7)	2.0 (1.4)	4.1 (1.7)	346 (273)	64 (58)	19 (31)
16	5	Ibañez	2393	46°16'07"	71°59'20"		X					0.1/17.5	63 (24)	7.46 (0.65)	1.6 (0.7)	8.3 (2.8)	7.9 (4.8)	1653 (2801)	61 (77)	22 (20)
17	5	Murta	902	46°26'51"	72°43'09"		X					3.8/11.2	45 (14)	7.38 (0.61)	1.4 (0.5)	4.5 (1.1)	8.0 (2.0)	656 (773)	20 (12)	11 (12)
18	5	Engaño	302	46°27'28"	72°43'23"		X					2.4/12.2	17 (6)	7.45 (0.57)	1.6 (0.8)	1.6 (0.8)	2.2 (0.8)	635 (1566)	34 (47)	15 (26)
19	5	Tranquilo	76	46°37'20"	72°40'31"		X					4.0/16.1	76 (24)	7.54 (0.54)	1.5 (0.7)	2.0 (1.6)	13.7 (3.4)	396 (855)	55 (77)	12 (11)
20	5	Leones	21	46°44'15"	72°51'37"			X	X			2.4/12.2	29 (11)	7.43 (0.58)	1.5 (0.7)	2.4 (1.2)	5.5 (5.3)	2472 (1790)	52 (80)	17 (20)

21	5	Jeinimeni	1370	46°35'12"	71°40'11"	X		X	0.6/15.6	94 (30)	7.41 (0.80)	1.1 (0.3)	7.8 (3.7)	15.5 (6.5)	2642 (3992)	20 (14)	10 (8)
22	5	Nef	759	47°07'29"	72°46'40"		X		n.d.	29 (6)	7.17 (0.39)	2.9 (2.7)	n.d.	4.0 (1.3)	2569 (784)	n.d.	n.d.
23	5	Chacabuco	1394	47°06'54"	72°36'20"	X		X	0.9/16.6	97 (38)	7.48 (0.78)	2.0 (1.4)	11.0 (5.0)	18.9 (6.3)	1487 (2433)	25 (14)	11 (10)
24	5	El Salto	1244	47°17'45"	72°41'31"	X			1.5/14.4	46 (18)	7.40 (0.49)	1.1 (0.3)	3.4 (1.2)	7.7 (2.5)	615 (576)	20 (8)	9 (8)
25	5	Los Ñadis	989	47°29'43"	72°53'56"	X			1.9/10.6	49 (18)	7.37 (0.49)	1.3 (0.8)	4.4 (1.4)	8.0 (2.6)	857 (513)	22 (¡4)	9 (6)
26	5	Jaramillo	121	47°41'47"	73°02'46"	X			3.8/15.4	23 (6)	7.34 (0.75)	1.2 (0.3)	b.d.	4.4 (2.6)	84 (69)	32 (17)	4 (2)
27	5	**Baker**	21355	47°30'15"	72°58'48"	X	X	X	5.3/12.1	48 (16)	7.32 (0.55)	1.3 (0.6)	4.8 (1.3)	7.6 (1.8)	1633 (988)	18 (11)	12 (10)
28	6	**Serrano**	8096	51°20'13"	73°06'44"		X	X	1.4/9.2	52 (10)	7.59 (0.48)	2.7 (1.9)	6.7 (1.6)	7.3 (1.9)	1248 (1901)	61 (61)	10 (8)
29	7	**Side**	876	52°46'05"	69°17'03"			X	0.1/14.5	254 (35)	7.90 (0.37)	32.6 (3.5)	12.8 (6.5)	20.5 (5.7)	753 (365)	186 (69)	120 (96)
30	7	**Oro**	542	52°51'11"	69°53'59"			X	0.0/12.7	153 (23)	7.66 (0.28)	17.4 (3.8)	7.2 (3.4)	14.4 (4.1)	1080 (533)	94 (37)	21 (8)
31	7	**Róbalo**	21	54°56'55"	67°38'25"	X			0.0/11.1	85 (21)	7.63 (0.41)	6.7 (2.8)	10.7 (4.2)	11.1 (3.5)	87 (24)	72 (41)	6 (7)

Note: Source. Chilean General Water Directorate (DGA). https://snia.mop.gob.cl/BNAConsultas/reportes. ID. station DGA codes: 1. 10461000-5; 2. 10432001-5; 3. 10520001-3; 4. 10702002-0; 5. 10711001-1; 6. 10904004-5; 7. 10904001-0; 8. 10906003-8; 9. 11144001-8; 10. 11302001-6; 11. 11316001-2; 12. 11310002-8; 13. 11317003-4; 14. 11337001-7; 15. 11342001-4; 16. 11505001-K; 17. 11514001-9; 18. 11514002-7; 19. 11022001-4; 20. 11516001-K; 21. 11520002-K; 22. 11533002-0; 23. 11535001-3; 24. 11539002-3; 25. 11544000-4; 26. 11548000-6; 27. 11545000-K; 28. 12289001-5; 29. 12802001-2; 30. 12806001-4; 31. 12930001-9. Stations showed here are a subset (20%) of quality water stations in study area. Basin area based on hydrography model of Astorga et al. (2018).

The coastline length of a territory is difficult to estimate because of the coastline paradox associated with a spatial scale fractal behavior, e.g., Chile has 6,435 and 78,563 km of coastline, according to TWF (CIA, 2000) and WRI (WRI, 2000), respectively. However, it is possible to compare the coastline of different territories using the same source of information. For example, west-southern Patagonia (41-56ºS) has an extensive coastline of 27.2 $x10^3$ km, corresponding to 34% of South America (79.7 x 10^3 km) using the same database (Natural-Earth, 2022). The importance of this coastline increases when we observed the "coast/area ratio" with 87.5 m/km^2 in west-southern Patagonia versus 0.004 m/km^2 in South America or 59.7 m/km^2 of Chile (Natural-Earth, 2022). In addition, terrestrial exports of freshwater to marine zones below the 40° south latitude (excluding Antarctica) are mainly concentrated in Patagonia. Specifically, the west-southern basins in Patagonia, with 310 $x10^3$ km^2, are the most significant landmass drained directly with the Pacific Ocean.

The principal freshwater discharges were those from Zone 5, where the Baker/Pascua complex is the most considerable point input south of the Parana basin, with 53.6 km^3/year (Reid et al., 2021). Besides, Puelo, Yelcho, Palena, and Aysén basins are between the Chiles' ten largest rivers. A significant difference between the latter and the major rivers in the southeast Pacific is that the firsts discharge freshwater to interior seas rather than offshore coasts. In summary, the west-southern Patagonia discharge to internal seas, fjords, and channels approximately 631 km^3/year (excluding watersheds with flows directly to the ocean, Zone 2 and 4). Thus, the topography, precipitation, magnitude of runoff, global location, and characteristics of the interior marine ecosystem bring international importance to the coastal discharges in west-southern Patagonia.

1.4.2 Spatial and Temporal Volume Runoff Variability

Runoff timing and seasonality will result in varied continental forcing of marine systems depending on the region. In general, interannual hydrologic variability is much more evident in Zones with the most extensive continental basins (Zones 1,3,5), while coastal systems (Zones 2, 4) have the slightest variation across years. This would be expected to have consequences regarding freshwater influence and density stratification: inland marine areas linked to continental systems are potentially more susceptible to drought influences on both physical stratification and the water quality of inputs. Seasonal variability is also distinct across coastal vs. continental zones, with much less variability in coastal systems across seasons. Summer discharges are lower in the northern area (Zones 1 and 2) compared with the rest of the seasons, mainly associated with rain-feed basins with less precipitation in summer. However, this behavior changes to the south, where certain homogeneity between seasons exists in the central part (Zones 3, 4). Even summer discharges are the most important in the year for the south area (Zones 5-7). The latter is explained by a much more homogeneous distribution of precipitation year around and the incorporations of basins with mixed and snow-feed regimens. The oceanic watersheds of Chiloé (Zone 2) present the most extended period with small discharges between spring and summer. From Zone 4 to 7, southern zones, winter is the season with less runoff. Zone 5 (Baker/Pascua complex) has the most significant coastal freshwater season discharges, except by Zone 3, in winter, with the highest runoff.

Precipitation interannual variability is marked mainly by the Pacific-South American phenomenon known as El Niño/Southern Oscillation (ENSO), in its warm phase, generates dry anomalies in Patagonia with a reduction of runoff in summer and autumn (Garreaud et al., 2013). This effect is notorious from Zone 1 to 4, but the behavior of the trend in the south part, associated

with archipelagos, is more regular without extreme falls of coastal discharges. This runoff homogeneity year/season in Zones 5 to 7 is also influenced by the Southern Annular Mode (SAM). The flow model estimated a record (for 40 years) of minimal coastal discharges in the autumn of 2016 (Zones 1-4), interpreting the extreme ENSO event of that year (Blunden & Arndt, 2017; León-Muñoz et al., 2018).

In summary, seasonal and climate phenomenon pattern affects coastal discharges, provoking changes in surface brackish water in thickness as on area extension (Calvete & Sobarzo, 2011; Castillo et al., 2016; León-Muñoz et al., 2018; Schneider et al., 2014), intense harmful algal blooms in occurrence and persistence (HABs) (León-Muñoz et al., 2018; Mardones et al., 2023), water temperature (Calvete & Sobarzo, 2011; Mardones et al., 2023), aquiculture production (Lara et al., 2016; Mardones et al., 2023), sediments (Amann et al., 2022; Quiroga et al., 2016), nutrients (Jacob et al., 2014; Quiroga et al., 2016; Torres et al., 2014; 2020; 2023), Chlorophyll (Jacob et al., 2014; Lara et al., 2016; Torres et al., 2020), salinity (Dávila et al., 2002), primary production (Montero et al., 2011; 2017; Torres et al., 2014), among others factors. Next, we will discuss how the runoff variability, forced by climate variables, is increased with different chemical characteristics due to land use/cover, geology, soils, and dry conditions.

1.4.3 Spatial distribution of freshwater runoff sourcing

As was discussed before, the magnitude of coastal freshwater discharges is large, but at the same time, the variability across Zones is enormous, not only in yearly volume but also seasonal. In addition, other sources of high spatial variability affect the runoff. For example, climate, geology, land use, and soils differed significantly in the Zones. These factors have been identified as the primary sources of water quality and chemical characteristics (Torres et al., 2014; Torres et al., 2023; Vandekerkhove et al., 2016).

The region's northern half, Zones 1 to 4, presented weighted flows associated with hyper-humid climate, crystalline rocks as geologic basements, mainly Andosols soils due to volcanic activity, and forest as the most common land use. However, Zone 2 has some particularities as a different geologic characteristic and the loss of importance of volcanic soils. On the other hand, in the southern region, Zones 5 to 7, although the hyper-humid conditions are predominant, flows from areas with less precipitation start to have a higher preponderance. Also, streams are more related to wetlands and moorlands ecosystems than forest stands, melting from glaciers starting a have a significant discharge in some fjords and channels, and the influence of Andosols decreases towards the south until it disappears in zone 7, to be replaced by soils of sedimentary origin.

Although both climate and land use drivers of water quality are expected to change, initial trends and rates are still unclear (Falvey & Garreaud, 2009). Global models predict a drying climate northward, more humid trends toward the south (Garreaud et al., 2013) although the rate and precise location of this transition, in the complex mountain geography of Patagonia, has not been evaluated adequately with regional climate modeling. Other studies report changes in precipitation (Boisier et al., 2018b; León-Muñoz et al., 2018; Aguayo et al., 2021), runoff of some rivers (León-Muñoz et al., 2018; León-Muñoz et al., 2021), snow (Schaefer et al., 2015; Pérez et al., 2018; Aguayo et al., 2021), etc.

A shift in runoff dominance from fall to spring, a potential consequence of declining annual runoff, and seasonally declining fall rains together with only a somewhat less significant declining snowpack, has been observed for the Puelo basin (Zone 1; 41°S). Here the potential decline in DOM input suggested by Leon-Munoz et al. (2021) may be offset by change in organic matter quality (unknown) nutrient and weathering inputs (potentially reduced load from declining discharge together with slightly reduced weathering rates). These potential trends, however based

on a relatively more complete baseline, are still highly speculative. More insight, based on smaller scale monitoring nested within the basin, and multifactor experimentation (climate vs. land use) would be required to develop reasonable insight into future runoff conditions for this basin. Elsewhere, increased land use intensity, urbanization, agricultural development and contamination, is expected to significantly increase the risk of macronutrient inputs, especially for Zones 1,3 and 5, having higher potential population density and access to transportation systems.

1.4.4 Interpretation of spatial patterns in runoff water quality

Existing synthesis of water quality in streams and rivers at a regional or broader scale (Vega et al., 2018) notes only a few general trends applicable to the study region (e.g., 40-55°S), such as pH slightly increasing from circumneutral, and electrical conductivity (an indicator of dissolved salts increasing from nearly trace levels to ranges of 100-500 uS/cm starting from the Serrano basin (52°S). However, parameters relevant to terrestrial fjord linkages are either not discussed, unavailable, or of limited quality (nutrient levels ceased to be reported in 2010).

Macronutrient concentration in continental waters and precipitation inputs of Patagonia may be significantly lower than global averages (Diaz et al., 2007; Pedrozo et al., 1993) , at least for more rigorously studied systems in Argentina. Nitrate in pacific (Chilean) forested headwater streams are among the lowest observed worldwide, together with unusual fractionation favoring organic forms, e.g., DON>>N-NH_4>N-NO_3 (Perakis & Hedin, 2002). Natural sources of phosphate may be constrained by the high sorption capacity of volcanic soils which dominate the region (Besoain et al., 1995), hence limited to local effects of geology outside of recent volcanic provinces, such as southern watersheds of the XII region (table 1.2), drier climatic zones downwind of concentrated tephra rain, or both. Low inorganic nitrogen in continental waters may also be limited by P limitation, in turn acting as a threshold for N fixation (e.g., << ug/l P-PO_4), as presumed for many

Patagonian lakes (Diaz et al., 2007). In general, where cropland may be proportional to N export and increased urbanization is generally related to N/P export (Kalff, 2002), the continental runoff in the study area may provide insignificant contributions of inorganic macronutrients broadly across the fjord regions, but only while urbanization and agricultural inputs (e.g., fertilizers) remain at very low intensity or limited importance. More subtle spatial patterns of N and P export might be estimated for the region based on potentially comparable coefficients and land use classes for New Zealand developed by Snelder et al. (2018). However, a similar analysis would be limited, as most (if not all) of the available data for Patagonia would not likely meet the criteria established by these authors.

Dissolved silica concentrations in Patagonia, which are substantially higher than global means (Pedrozo & Chillrud, 1998), may range from moderate levels compared to major weathering cations via regolith or glacial weathering (DSi:K^++Ca^{2+}-Cl^- ~1:1 ratio), to two-fold higher levels sourced from the weathering of volcanic glass (2:1 ratio). Additionally, DSi levels may be substantially greater as a function of depth of tephra soil horizons (Vandekerkhove et al., 2016), potentially another 2-fold higher for recently deposited material (e.g., ash plume of the 1991 Hudson eruption; B. Reid unpubl. data). Limited local observations on dissolved carbon concentrations are generally higher but more seasonally variable for the deciduous forest zone, and lower but proportional to flow (positive Q:C relationship) for humid zones. We also expect that lability of DOC would be greater for pulsed forest inputs such as leaf fall and lower for dissolved organic matter linked to soil erosion or wetland inputs, especially for cold rainy regions dominated by peatland vegetation. Dissolved iron may be variably and unpredictably sourced by weathering and local geology, however we also expect that higher DFe (principally ferric/Fe^{3+}, although equilibrium with mineral and organic complexes and oxyhydroxides are unknown) may be in

balance or otherwise correlate with high suspended solids (SS) load, especially glacial, as suggested by Serrano and Nef Rivers in table 1.2. Loading of DFe may also be enhanced by reduced conditions, such as groundwater inputs in general or those related to recently glaciated areas and peatlands. Finally, major drivers of SS concentration in Patagonian rivers include seasonal glacial meltwater and snowmelt, and spoil erosion from dry climate during peak annual flows or extreme precipitation events.

1.4.5 Extrapolation to potential geographic patterns of continental runoff to Patagonia fjords

While table 1.2 presents a general summary of water quality parameters for selected Patagonian rivers, some limitations in terms of regional runoff characterization are evident. Except for major basins, about 37% of the land area, information is limited for all but very few smaller direct coastal drainages (figure 1.1). Moreover, larger basins represent the summation of a wide range of sources. For example, the variability among monitoring stations in the Aysén basin (table 1.2: 10-15) or Baker basin (table 1.2: 16-27) compared to the main river is very evident, and presumably, the water quality at the final discharge point of the major rivers is a weighted sum of these sources, with their relative overlapping season patterns (figure 1.3) together with whatever reactions or processes that may occur in transport. On this latter point, the abundance of mid-catchment lakes is a principal factor (Reid & Astorga, 2023), contributing to the loss of sediments, uptake of nutrients, in some cases uptake of DSi (more productive systems), and loss of DOC via photo-oxidation. Apart from this general caveat, equally limited by complexity as a minimal frequency and selectivity (i.e., DSi or DOM not analyzed) of time series water quality observations of these systems, some regional or geographic patterns in potential runoff water quality may be proposed.

Based on the conceptual model depicted in the introduction (Figure I.2), which elucidates the various impacts of riverine forcing on fjord ecosystems, the investigation conducted in this study enabled the characterization and quantification of coastal discharges. Additionally, incorporating information from a limited number of chemical monitoring stations, it became feasible to identify distinct latitudinal patterns about nutrients and suspended solids, which are closely associated with marine productivity (figure 1.5). This integrated scientific approach provides valuable insights into the interplay between river inputs and coastal dynamics, shedding light on the intricate relationships and processes that govern fjord ecosystems. For example, the northern half of the region, dominated by volcanic andosols, is expected to have consistently higher levels of DSi in river export (Zones 1,3,5). Exceptions are due to the leeward side of the volcanic sources (Zones 2, 4) and dilution by other sources slow DSi, such as meltwater (Zone 4). A maximum focused load of DSi might be expected for large continental basins in these zones, where high discharge coincides with moderate to high concentrations (Yelcho, Palena, and Puelo rivers). Arid zones with concentrated weathering products, including DSi (parts of Zone 7), might also be expected to have significant yet diffuse loadings. Evidence for this pattern is obvious from the DSi index proposed by Torres et al. (2014), where the molar ratio of DSi to N approaches an intercept (i.e., riverine end member) that, in turn, declines southward. Conversely, iron loading may be more predominant in southern regions (Zones 5-7) due to increased glacial inputs and/or arid zone concentration – this is notable from the north-south trends in table 1.2. Suspended sediments are similarly expected to increase southward (Zones 5-7), except seasonal inputs during fall rains or spring snowmelt of more northern cordilleran basins.

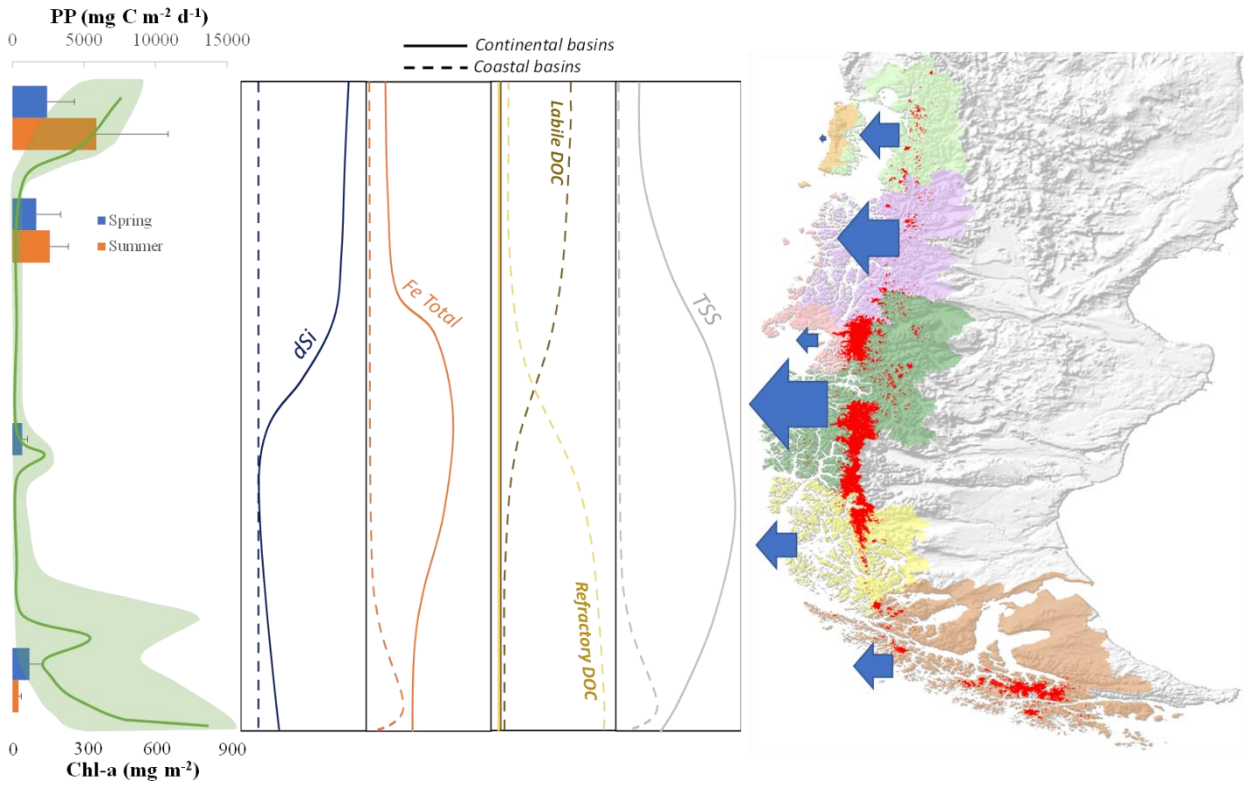

Figure 1.5. *Latitudinal model of the potential link between regional flow magnitude from continental runoff, patterns in runoff quality, and corresponding patterns in marine productivity. Left panel shows estimate of primary productivity (data from Aracena et al 2011) and Chlorophyl A (redrawn from Cuevas et al 2019). Middle panel shown general latitudinal trends in concentration for significant subsidies/drivers of marine systems for both coastal and continental sources (e.g. Table 1.2;). Note that macronutrient inputs (N, P) from runoff are presumed negligible. Right panel shows regional runoff inputs, with size of arrows proportional to annual flow magnitude (Figure 1.2); Glaciers/Ice Fields shown in red.*

In terms of climate and interaction with vegetation, the following generalization is proposed: for humid coastal region characterized by extremely low weathering inputs yet significant temperate zone vegetation that has received low levels of intervention (Zones 2,4), we expect extremely low macronutrient inputs, and moderate to high DOC inputs of relatively labile quality (leaching of forests litter). Meanwhile, colder humid regions dominated by peatlands (Zones 6-7) may have variable to high DOC loads of a more refractory quality (e.g., humic substances sourced from *Sphagnum* bogs). Finally, in terms of macronutrients, levels of inorganic N and P are

expected to be naturally very low throughout, however, this baseline may be affected by urban and agricultural development – this is expected from Zone 3, with two of three of the largest urban centers, and moderate agricultural activity concentrated in the Aysén basin (moderately elevated levels of inorganic N and P have been observed here based on recent monitoring of Patagonia major rivers: B. Reid, unpubl. data).

1.4.6 Consequences in marine ecosystems based on current patterns and expected change in runoff

Macronutrient-rich oceanic subantarctic water that floods Patagonia channels and fjords have conspicuously low DSi and DFe concentrations. The scarcity of these elements in the deep mixed oceanic water column (which reduces phytoplankton exposure to light) limits diatoms' capacity to rapidly use available macronutrients (C, N, P) and to dominate phytoplankton assemblage. Differently, the dilution of subantarctic oceanic water with continental waters of Patagonia enhances the water column stratification constraining the turbulent layer closer to the surface and thus improving the phytoplankton light regimen. More light, together with the enrichment in Si and Fe, has been suggested to be key factors promoting diatoms blooms during the beginning of the productive season. The persistence of that diatom proliferation also depends on Si availability (under low DSi supply the bloom of diatom is short-lived), among others factors. Latitudinal gradients of runoff and its solute composition could not only play a role in modulating the triggering but also the persistence of diatom proliferation in Patagonian coastal waters (Aracena et al., 2011; Cuevas et al., 2019).

The shift from diatom-dominated phytoplankton assemblage to other functional groups can determine critical aspects of the marine food web and its functioning, including ecosystem services disruptions (e.g., Si deficit could enhance the probability of the occurrence of dinoflagellate toxic

blooms, which preclude the human consumption of a wide variety of seafood resources). Besides the timing and spatial variability of coastal ocean freshening per se, the quantity and proportions of runoff´s bioactive solutes are expected to modulate the phytoplankton community dynamic (Torres et al., 2021).

Latitudinal variation in Si discharges from the continent (associated with volcanic ash, see andosol distribution in figure 1.4) are consistent in Si-Macronutrients ratios along Patagonia coastal waters with maximum Si/N ratios in northern Patagonia and minimum Si/N ratio values in coastal waters of Austral Patagonia (Torres et al., 2014). This pattern, in turn, coincided with more frequent warming reports of toxic dinoflagellate proliferations in southern Patagonia compared with Norther Patagonia (Torres et al., 2020). The Si deficit in south Patagonia, where the continental runoff has lower content of Si, could result in a short-lived diatom bloom and an early shift to other functional groups' dominance (dinoflagellates).

Dry summer patterns could reduce Si inputs to coastal waters, even when, in this warmest period, the snow and ice melting is at maximum. While Si concentrations from melted ice water are low even when these waters are often slit-rich, large Si concentrations are often associated with large hydrographic basins with volcanic soils located in the northern portion of Patagonia, where a maximum reduction in the runoff has been recorded. Dry summer-autumn years imply not only lower DSi inputs but also clear ski (high irradiance), which could promote bloomings of non-silicious phytoplankton, the same of them capable of producing toxins. Certainly, understanding the effects of timing and net discharges of bioactive terrestrial solutes to the coastal ocean is a necessary step to assess the overall effect of changes in the hydrological cycle in Patagonia.

1.4.7 Guidelines for policy and management in west-southern Patagonia

The present work addressed the need to interconnect different ecosystems, such as marine, freshwater, and terrestrial, where most of the time are studied as closed systems. For example, studies related to terrestrial and marine ecosystems are dispersed and without of integrate analysis producing inefficient conservation programs (Castilla et al., 2021). From a watershed perspective, everything happening in the terrestrial affects the streams from headwater until coastal discharges, producing diverse consequences in fjords and channels of west-southern Patagonia. On the other hand, a considerable volume/chemistry variability in the seasonal and annual freshwater flows due to climate, geology, soils, dry conditions, and land use/cover was identified. Both interconnections of ecosystems and an adequate spatial scale due to actual variability must be the bases for a conservation policy and management of west-southern Patagonia.

The possibility of an integrative management vision for terrestrial, freshwater, and marine ecosystems is an excellent opportunity to bring west-south Patagonia a new development model, avoiding extractive activities without state planning. The base for conserving these land/sea connections is the extensive area of national parks, national reserves, and other conservation lands in Chile and Argentina (trans-Andes basins). These protected areas are an enormous opportunity for effective long-term conservation with holistic planning of watersheds, streams, and inner seas but with public financial support for real conservation. Additionally, the protection must not be framed only in public lands but also in private areas, some still within near-reference conditions. Finally, the estate must impulse regional planning with practical applicability in the territory, not only with recommendations to the private sector.

At the same time, a conservation program needs a monitoring plan to address baseline and identify changes in flows and water quality due to human and climate forcing. Currently, west-

southern Patagonia has a scarcity of measurement stations, even more if we focus on the coastal catchment outlet and the archipelago zone (see figure 1.1). Thus, the extrapolation of a hydrology model, such as FLOW, generates significant uncertainties due to the lack of observational data (see number of calibration stations in table 1.1). However, Olivares (2022), found an excellent performance of the FLOW model in three basins in Patagonia (Nash-Sutcliffe coefficient ~0.81) but with smoothing outputs by the model, masking the high flows. Thus, Olivares indicates that the FLOW model slightly sub estimates the observational discharges. In summary, the uncertainties of the FLOW model are associated with shorter time scales, i.e., monthly and daily, due to the acceleration of the melting snow process. However, the modeled data at an annual and seasonal level performs satisfactorily (METEODATA, 2020).

Finally, better information about coastal discharges in Patagonia will be possible with an intensive net of permanent flow sampling. Mainly covering those isolated areas with no data. Sub-daily estimations are not included in the FLOW model but could be an excellent upgrade in the future, even incorporating real-time flow forecasting. The platform's next steps must also focus on future climate scenarios and the main water quality characteristics associated with land use/cover, geology, dry conditions, and soils. These upgrades will help create more realistic fjord scenarios in a global change era.

1.5 CONCLUSIONS

West-southern Patagonia, with its extensive coastline, inner seas, archipelagos, glaciers, lakes, fjords, and channels, is one of the most critical land/sea ecosystems on a global scale. In addition, the high rate of precipitation and the short distances of fluvial courses from the source to the sea generates a significant coastal discharge of freshwater runoff. The importance of these freshwater flows into marine ecosystems provokes the well-known vertical stratification of the water column.

Our study estimates by modeled data a coastal discharge close to the 2% global, with no other significant continental landmass comparable in these southern latitudes. Besides, we exposed a considerable volume/chemistry variability in the seasonal and annual freshwater flows due to climate, geology, soils, dry conditions, and land use/cover in the different zones of this study. In order to comprehend the impact of bioactive terrestrial solutes' timing and net discharges on primary productivity and/or toxic dinoflagellate blooms in coastal oceans, it is crucial to study and monitor the effects of this variability's physics and chemicals in local marine ecosystems. It is imperative to prioritize validating hydrological models with more observational data, increase water quality monitoring, and develop secondary or water quality standards for coupled river and marine ecosystems in this region with a near-reference condition.

1.6 ACKNOWLEDGEMENTS

FLOW was funded through the Subsecretary of Fisheries and Aquaculture and the Ministry of Economy, Development, and Tourism of the Chilean Government. We thank the entire group of IFOP in Putemún-Castro and Meteodata for its valuable help in the development and web support of FLOW. P.M.M. thanks the financial support of Programa Regional ANID R20F0002 (PATSER).

1.7 LITERATURE CITED

Aceituno, P., Boisier, J. P., Garreaud, R., Rondanelli, R., & Rutllant, J. A. (2021). Climate and Weather in Chile. In B. Fernández & J. Gironás (Eds.), *Water Resources of Chile* (pp. 7-29). Springer International Publishing. https://doi.org/10.1007/978-3-030-56901-3_2

Aguayo, R., León-Muñoz, J., Garreaud, R., & Montecinos, A. (2021). Hydrological droughts in the southern Andes (40–45°S) from an ensemble experiment using CMIP5 and CMIP6 models. *Scientific Reports*, *11*(1), 5530. https://doi.org/10.1038/s41598-021-84807-4

Amann, B., Bertrand, S., Alvarez-Garreton, C., & Reid, B. (2022). Seasonal Variations in Fjord Sediment Grain Size: A Pre-requisite for Hydrological and Climate Reconstructions in Partially Glacierized Watersheds (Baker River, Patagonia). *Journal of Geophysical Research: Earth Surface*, *127*(2), e2021JF006391. https://doi.org/10.1029/2021JF006391

Aracena, C., Lange, C. B., Luis Iriarte, J., Rebolledo, L., & Pantoja, S. (2011). Latitudinal patterns of export production recorded in surface sediments of the Chilean Patagonian fjords (41–55°S) as a response to water column productivity. Continental Shelf Research, 31(3), 340-355. https://doi.org/10.1016/j.csr.2010.08.008

Astorga, A., Moreno, P., & Reid, B. (2018). Watersheds and Trees Fall Together: An Analysis of Intact Forested Watersheds in Southern Patagonia (41–56° S). *Forests*, *9*(7), 385. https://doi.org/10.3390/f9070385

Astorga, A., Reid, B., Moreno, P., & Rojas, P. (2021). Donde nacen los ríos: cuencas de bosques prístinos en la Patagonia occidental austral. In J. C. Castilla, J. J. Armesto, & M. J. Martínez-Harms (Eds.), *Conservación en la Patagonia chilena: evaluación del conocimiento, oportunidades y desafíos.* (pp. 167-198). Ediciones Universidad Católica.

Besoain, E., Ruiz, R., & Hepp, C. (1995). La erupción del Volcán Hudson, XI Región, y sus consecuencias para la agricultura. *Agricultura Técnica*, *55*(3-4), 204-219.

Beusen, A., Bouwman, A., Dürr, H., Dekkers, A., & Hartmann, J. (2009). Global patterns of dissolved silica export to the coastal zone: Results from a spatially explicit global model. *Global Biogeochemical Cycles*, *23*(4).

Beusen, A., Dekkers, A., Bouwman, A., Ludwig, W., & Harrison, J. (2005). Estimation of global river transport of sediments and associated particulate C, N, and P. *Global Biogeochemical Cycles*, *19*(4).

Bizama, G., Torrejón, F., Aguayo, M., Muñoz, M. D., Echeverría, C., & Urrutia, R. (2011). Pérdida y fragmentación del bosque nativo en la cuenca del río Aysén (Patagonia-Chile) durante el siglo XX. *Revista de Geografía Norte Grande*(49), 125-138.

Blunden, J., & Arndt, D. S. (2017). State of the Climate in 2016. *Bulletin of the American Meteorological Society*, *98*(8), Si-S280. https://doi.org/10.1175/2017BAMSStateoftheClimate.1

Boisier, J. P., Alvarez-Garretón, C., Cepeda, J., Osses, A., Vásquez, N., & Rondanelli, R. (2018). *CR2MET: A high-resolution precipitation and temperature dataset for hydroclimatic research in Chile* https://ui.adsabs.harvard.edu/abs/2018EGUGA..2019739B

Bouwman, A. F., Van Drecht, G., Knoop, J. M., Beusen, A. H. W., & Meinardi, C. R. (2005). Exploring changes in river nitrogen export to the world's oceans. *Global Biogeochemical Cycles*, *19*(1). https://doi.org/10.1029/2004gb002314

Bozkurt, D., Rojas, M., Boisier, J. P., & Valdivieso, J. (2018). Projected hydroclimate changes over Andean basins in central Chile from downscaled CMIP5 models under the low and high emission scenarios. *Climatic Change*, *150*(3), 131-147.

Calvete, C., & Sobarzo, M. (2011). Quantification of the surface brackish water layer and frontal zones in southern Chilean fjords between Boca del Guafo (43°30′S) and Estero Elefantes (46°30′S). *Continental Shelf Research*, *31*(3), 162-171. https://doi.org/10.1016/j.csr.2010.09.013

Castilla, J. C., Armesto, J. J., & Martínez-Harms, M. J. (2021). Conservación en la Patagonia Chilena: Evaluación del conocimiento, oportunidades y desafíos. Ediciones UC.

Castillo, M. I., Cifuentes, U., Pizarro, O., Djurfeldt, L., & Caceres, M. (2016). Seasonal hydrography and surface outflow in a fjord with a deep sill: the Reloncaví fjord, Chile. *Ocean Science*, *12*(2), 533-544. https://doi.org/10.5194/os-12-533-2016

Castro, L., & Gironás, J. (2021). Precipitation, Temperature and Evaporation. In B. Fernández & J. Gironás (Eds.), Water Resources of Chile (pp. 31-60). Springer International Publishing. https://doi.org/10.1007/978-3-030-56901-3_3

Chillrud, S., Pedrozo, F., Temporetti, P., Planas, H., & Froelich, P. (1994). Chemical weathering of phosphate and germanium in glacial meltwater streams: effects of subglacial pyrite oxidation. *Limnology and Oceanography*, *39*(5), 1130-1140.

CIA, C. I. A. (2000). The World Factbook 1998. *Reference Reviews*, *14*(2), 44-44. https://doi.org/10.1108/rr.2000.14.2.44.101

CONAF. (2016). *Catastro de uso de suelo y vegetación*. Retrieved 02 october 2017 from http://www.ide.cl/descarga/capas/item/catastros-de-uso-de-suelo-y-vegetacion.html

Contador, T., Kennedy, J. H., Rozzi, R., & Villarroel, J. O. (2015). Sharp altitudinal gradients in Magellanic Sub-Antarctic streams: patterns along a fluvial system in the Cape Horn Biosphere Reserve (55 S). *Polar Biology*, *38*(11), 1853-1866. https://doi.org/10.1007/s00300-015-1746-4

Core-Team. (2017). *R: A language and environment for statistical computing*. In R Foundation for Statistical Computing. http://www.R-project.org

Cuevas, L. A., Tapia, F. J., Iriarte, J. L., González, H. E., Silva, N., & Vargas, C. A. (2019). Interplay between freshwater discharge and oceanic waters modulates phytoplankton size-structure in fjords and channel systems of the Chilean Patagonia. *Progress in Oceanography*, *173*, 103-113. https://doi.org/10.1016/j.pocean.2019.02.012

Dávila, P. M., Figueroa, D., & Müller, E. (2002). Freshwater input into the coastal ocean and its relation with the salinity distribution off austral Chile (35–55°S). *Continental Shelf Research*, *22*(3), 521-534. https://doi.org/10.1016/S0278-4343(01)00072-3

Demaria, E., Maurer, E. P., Thrasher, B., Vicuña, S., & Meza, F. J. (2013). Climate change impacts on an alpine watershed in Chile: Do new model projections change the story? *Journal of Hydrology*, *502*, 128-138.

Diaz, M., Pedrozo, F., Reynolds, C., & Temporetti, P. (2007). Chemical composition and the nitrogen-regulated trophic state of Patagonian lakes. *Limnologica-Ecology and Management of Inland Waters*, *37*(1), 17-27.

Dijkshoorn, J., Huting, J., & Tempel, P. (2014). *Soil and Terrain Database for Latin America and the Caribbean (version 2.0)-scale 1: 5 million (SOTERLAC)*.

Donoso, C. (1993). Bosques templados de Chile y Argentina: variación, estructura y dinámica.

Dumont, E., Harrison, J. A., Kroeze, C., Bakker, E. J., & Seitzinger, S. P. (2005). Global distribution and sources of dissolved inorganic nitrogen export to the coastal zone: Results from a spatially explicit, global model. *Global Biogeochemical Cycles*, *19*(4). https://doi.org/10.1029/2005GB002488

Falvey, M., & Garreaud, R. D. (2009). Regional cooling in a warming world: Recent temperature trends in the southeast Pacific and along the west coast of subtropical South America (1979–2006). *Journal of Geophysical Research: Atmospheres*, *114*(D4).

Fick, S. E., & Hijmans, R. J. (2017). WorldClim 2: new 1-km spatial resolution climate surfaces for global land areas. *International Journal of Climatology*, *37*(12), 4302-4315. https://doi.org/10.1002/joc.5086

Fry, C. H., Tyrrell, T., Hain, M. P., Bates, N. R., & Achterberg, E. P. (2015). Analysis of global surface ocean alkalinity to determine controlling processes. *Marine Chemistry*, *174*, 46-57.

Fustos, I., Abarca-del-Río, R., Artal, O., Alvial, F., & Sepúlveda, H. (2022). Impact on discharge modelling using different spatial and temporal resolution scenarios in South of Chile. *Journal of South American Earth Sciences*, *115*, 103727.

Garreaud, R., Lopez, P., Minvielle, M., & Rojas, M. (2013). Large-Scale Control on the Patagonian Climate. *Journal of climate*, *26*(1), 215-230. https://doi.org/10.1175/JCLI-D-12-00001.1

Heinze, C., Blenckner, T., Martins, H., Rusiecka, D., Döscher, R., Gehlen, M., Gruber, N., Holland, E., Hov, Ø., Joos, F., Matthews, J. B. R., Rødven, R., & Wilson, S. (2021). The quiet crossing of ocean tipping points. *Proceedings of the National Academy of Sciences*, *118*(9), e2008478118. https://doi.org/10.1073/pnas.2008478118

IGN. (2013). *Cobertura del Suelo*. Retrieved 2 october 2017 from http://www.ign.gob.ar/NuestrasActividades/InformacionGeoespacial/CapasSIG

Jacob, B. G., Tapia, F. J., Daneri, G., Iriarte, J. L., Montero, P., Sobarzo, M., & Quiñones, R. A. (2014). Springtime size-fractionated primary production across hydrographic and PAR-light gradients in Chilean Patagonia (41–50°S). *Progress in Oceanography*, *129*, 75-84. https://doi.org/10.1016/j.pocean.2014.08.003

Kalff, J. (2002). *Limnology, Inland Water Ecosystems 1st ed.* Prentice.

Kelso, N. V., & Patterson, T. (2010). Introducing natural earth data-naturalearthdata. com. *Geographia Technica*, *5*(82-89), 25.

Lara, C., Saldías, G. S., Tapia, F. J., Iriarte, J. L., & Broitman, B. R. (2016). Interannual variability in temporal patterns of Chlorophyll–a and their potential influence on the supply of mussel larvae to inner waters in northern Patagonia (41–44°S). *Journal of Marine Systems*, *155*, 11-18. https://doi.org/10.1016/j.jmarsys.2015.10.010

León-Muñoz, J., Aguayo, R., Marcé, R., Catalán, N., Woelfl, S., Nimptsch, J., Arismendi, I., Contreras, C., Soto, D., & Miranda, A. (2021). Climate and Land Cover Trends Affecting Freshwater Inputs to a Fjord in Northwestern Patagonia. *Frontiers in Marine Science*, *8*. https://doi.org/10.3389/fmars.2021.628454

León-Muñoz, J., Urbina, M. A., Garreaud, R., & Iriarte, J. L. (2018). Hydroclimatic conditions trigger record harmful algal bloom in western Patagonia (summer 2016). *Scientific Reports*, *8*(1), 1330. https://doi.org/10.1038/s41598-018-19461-4

Lohmann, D., Mitchell, K. E., Houser, P. R., Wood, E. F., Schaake, J. C., Robock, A., Cosgrove, B. A., Sheffield, J., Duan, Q., & Luo, L. (2004). Streamflow and water balance intercomparisons of four land surface models in the North American Land Data Assimilation System project. *Journal of Geophysical Research: Atmospheres*, *109*(D7).

Luebert, F., & Pliscoff, P. (2006). *Sinopsis bioclimática y vegetacional de Chile*. Editorial Universitaria.

Mac-Clure, R. (1970). *La Sobrevivencia de Chile, la Conservación de sus Recursos Renovables. 2nd ed.* Santiago, Chile: Ministerio de Agricultura

Mardones, J. I., Paredes-Mella, J., Flores-Leñero, A., Yarimizu, K., Godoy, M., Artal, O., Corredor-Acosta, A., Marcus, L., Cascales, E., Pablo Espinoza, J., Norambuena, L., Garreaud, R. D., González, H. E., & Iriarte, J. L. (2023). Extreme harmful algal blooms, climate change, and potential risk of eutrophication in Patagonian fjords: Insights from an exceptional Heterosigma akashiwo fish-killing event. *Progress in Oceanography*, *210*, 102921. https://doi.org/10.1016/j.pocean.2022.102921

METEODATA. (2020). Construcción de un Modelo Hidrológico para la Estimación de Caudales de Agua Dulce en las Regiones X-XI-XII, Etapa I. Informe final.

Millenium Ecosystems Assessment. (2005). *Ecosystems and Human Well-Being: Synthesis*. Island Press.

Milliman, J. D., & Farnsworth, K. (2011). *River Discharge to the Coastal Ocean – A Global Synthesis*. https://doi.org/10.1017/CBO9780511781247

Montero, P., Daneri, G., González, H. E., Iriarte, J. L., Tapia, F. J., Lizárraga, L., Sanchez, N., & Pizarro, O. (2011). Seasonal variability of primary production in a fjord ecosystem of the Chilean Patagonia: Implications for the transfer of carbon within pelagic food webs. *Continental Shelf Research*, *31*(3), 202-215. https://doi.org/10.1016/j.csr.2010.09.003

Montero, P., Daneri, G., Tapia, F., Iriarte, J. L., & Crawford, D. (2017). Diatom blooms and primary production in a channel ecosystem of central Patagonia. *Latin american journal of aquatic research*, *45*(5), 999-1016.

Natural-Earth. (2022). *Ocean Coastline, including major islands v. 4.1.0*.

Oki, T., & Kanae, S. (2006). Global hydrological cycles and world water resources. *science*, *313*(5790), 1068-1072.

Olivares, J. (2022). *Variabilidad e incerteza de la herramienta FLOW (IFOP): Ríos de la Patagonia modelados con VIC* Universidad de Concepción]. Concepción, Chile.

Pedrozo, F., & Chillrud, S. (1998). Relative water fluxes and silicate weathering from the tributaries of a small glaciated watershed in the Southern Patagonian Andes (Upper manso watershed, Argentina). *Internationale Vereinigung für theoretische und angewandte Limnologie: Verhandlungen*, *26*(3), 935-939.

Pedrozo, F., Chillrud, S., Temporetti, P., & Diaz, M. (1993). Chemical composition and nutrient limitation in rivers and lakes of northern Patagonian Andes (39.5°-42° S; 71° W) (Rep. Argentina). *SIL Proceedings, 1922-2010*, *25*(1), 207-214. https://doi.org/10.1080/03680770.1992.11900093

Perakis, S. S., & Hedin, L. O. (2002). Nitrogen loss from unpolluted South American forests mainly via dissolved organic compounds. *Nature*, *415*(6870), 416. https://doi.org/10.1038/415416a

Pérez, T., Mattar, C., & Fuster, R. (2018). Decrease in Snow Cover over the Aysén River Catchment in Patagonia, Chile. *Water*, *10*(5).

Pickard, G. L., & Stanton, B. R. (1980). Pacific Fjords - A Review of Their Water Characteristics. In H. J. Freeland, D. M. Farmer, & C. D. Levings (Eds.), *Fjord Oceanography* (pp. 1-51). Springer US. https://doi.org/10.1007/978-1-4613-3105-6_1

Pörtner, H.-O., Roberts, D. C., Adams, H., Adler, C., Aldunce, P., Ali, E., Begum, R. A., Betts, R., Kerr, R. B., & Biesbroek, R. (2022). Climate change 2022: Impacts, adaptation and vulnerability. *IPCC Sixth Assessment Report*.

Quiroga, E., Ortiz, P., González-Saldías, R., Reid, B., Tapia, F. J., Pérez-Santos, I., Rebolledo, L., Mansilla, R., Pineda, C., Cari, I., Salinas, N., Montiel, A., & Gerdes, D. (2016). Seasonal benthic patterns in a glacial Patagonian fjord: the role of suspended sediment and terrestrial organic matter. *Marine Ecology Progress Series*, *561*, 31-50. https://www.int-res.com/abstracts/meps/v561/p31-50/

Quiroga, E., Ortiz, P., Reid, B., & Gerdes, D. (2013). Classification of the ecological quality of the Aysen and Baker Fjords (Patagonia, Chile) using biotic indices. *Marine Pollution Bulletin*, *68*(1), 117-126. https://doi.org/10.1016/j.marpolbul.2012.11.041

Reche, P., Artal, O., Pinilla, E., Ruiz, C., Venegas, O., Arriagada, A., & Falvey, M. (2021). CHONOS: Oceanographic information website for Chilean Patagonia. *Ocean & Coastal Management*, *208*, 105634. https://doi.org/10.1016/j.ocecoaman.2021.105634

Reid, B., & Astorga, A. (2023). Landscape Disturbance and Ecosystem Function of Pacific Patagonia Rivers. In *Rivers of Southern Chile and Patagonia: Context, Cascade Process, Geomorphic Evolution and Risk Management* (pp. 13-33). Springer.

Reid, B., Astorga, A., Madriz, I., & Correa, C. (2021). Estado del conocimiento y conservación de los ecosistemas dulceacuícolas de la Patagonia occidental austral. In J. C. Castilla, J. J. Armesto, & M. J. Martínez-Harms (Eds.), *Conservación en la Patagonia chilena: evaluación del conocimiento, oportunidades y desafíos.* Ediciones Universidad Católica.

Rosenqvist, A., Shimada, M., Ito, N., & Watanabe, M. (2007). ALOS PALSAR: A Pathfinder Mission for Global-Scale Monitoring of the Environment. *IEEE Transactions on Geoscience and Remote Sensing*, *45*(11), 3307-3316. https://doi.org/10.1109/TGRS.2007.901027

Schaefer, M., Machguth, H., Falvey, M., & Casassa, G. (2013). Modeling past and future surface mass balance of the Northern Patagonia Icefield. *Journal of Geophysical Research: Earth Surface*, *118*(2), 571-588.

Schaefer, M., Machguth, H., Falvey, M., Casassa, G., & Rignot, E. (2015). Quantifying mass balance processes on the Southern Patagonia Icefield. *The Cryosphere*, *9*(1), 25-35.

Schneider, W., Pérez-Santos, I., Ross, L., Bravo, L., Seguel, R., & Hernández, F. (2014). On the hydrography of Puyuhuapi Channel, Chilean Patagonia. *Progress in Oceanography*, *129*, 8-18. https://doi.org/https://doi.org/10.1016/j.pocean.2014.03.007

SegemAR. (2021). *Mapa Geológico de Bicontinental de la República Argentina, escala 1:5.000.000*.

Seitzinger, S., Harrison, J., Dumont, E., Beusen, A. H., & Bouwman, A. (2005). Sources and delivery of carbon, nitrogen, and phosphorus to the coastal zone: An overview of Global Nutrient Export from Watersheds (NEWS) models and their application. *Global Biogeochemical Cycles*, *19*(4).

SERNAGEOMIN. (2003). *Mapa geologico de Chile version digital, scale 1/1.000.000.*

Snelder, T. H., Larned, S. T., & McDowell, R. W. (2018). Anthropogenic increases of catchment nitrogen and phosphorus loads in New Zealand. *New Zealand Journal of Marine and Freshwater Research*, *52*(3), 336-361. https://doi.org/10.1080/00288330.2017.1393758

Stolpe, N. B. (2014). Clasificación de suelos de valles productivos de la Región de Aysén. In C. Hepp & N. B. Stolpe (Eds.), *Caracterización y propiedades de los suelos de la Patagonia occidental (Aysén)* (Vol. 298, pp. 53-76). INIA.

Torres, R., Alarcón, E., & Reid, B. (2021). Simultaneous CO 2 and O 2 Supersaturation in Waters of Southern Patagonia? The Importance of Evaluating Overall Carbonate System Parameters Uncertainty and External Consistency. A Comment to Vargas et al., 2018. *Journal of Geophysical Research: Biogeosciences*, *126*. https://doi.org/10.1029/2019JG005523

Torres, R., Silva, N., Reid, B., & Frangopulos, M. (2014). Silicic acid enrichment of subantarctic surface water from continental inputs along the Patagonian archipelago interior sea (41–56°S). *Progress in Oceanography*, *129*, 50-61. https://doi.org/10.1016/j.pocean.2014.09.008

Torres, R., Reid, B., Frangópulos, M., Alarcón, E., Márquez, M., Häussermann, V., Försterra, G., Pizarro, G., Iriarte, J. L., & González, H. E. (2020). Freshwater runoff effects on the production of biogenic silicate and chlorophyll-a in western Patagonia archipelago (50–51°S). *Estuarine, Coastal and Shelf Science*, *241*, 106597. https://doi.org/10.1016/j.ecss.2020.106597

Torres, R., Reid, B., Pizarro, G., Frangópulos, M., Alarcón, E., Márquez, M., Díaz, F., Menschel, E., González, H. E., Moreno-Meynard, P., Montero, P., Pacheco, H., Pinto-Torres, M., Alarcón, C., Ibañez, R., & Hawkings, J. (2023). Iron and silicic acid addition effects on early Spring macronutrient drawdown and biogenic silica production of Patagonia estuarine waters. *Progress in Oceanography*, 102982. https://doi.org/10.1016/j.pocean.2023.102982

Van der Struijk, L. F., & Kroeze, C. (2010). Future trends in nutrient export to the coastal waters of South America: Implications for occurrence of eutrophication. *Global Biogeochemical Cycles*, *24*(4). https://doi.org/10.1029/2009GB003572

Vandekerkhove, E., Bertrand, S., Crescenzi Lanna, E., Reid, B., & Pantoja, S. (2020). Modern sedimentary processes at the heads of Martínez Channel and Steffen Fjord, Chilean Patagonia. *Marine Geology*, *419*, 106076. https://doi.org/10.1016/j.margeo.2019.106076

Vandekerkhove, E., Bertrand, S., Reid, B., Bartels, A., & Charlier, B. (2016). Sources of dissolved silica to the fjords of northern Patagonia (44–48 S): the importance of volcanic ash soil distribution and weathering. *Earth Surface Processes and Landforms*, *41*(4), 499-512.

Vargas, C. A., Cuevas, L. A., Silva, N., González, H. E., De Pol-Holz, R., & Narváez, D. A. (2018). Influence of Glacier Melting and River Discharges on the Nutrient Distribution and DIC Recycling in the Southern Chilean Patagonia. *Journal of Geophysical Research: Biogeosciences*, *123*(1), 256-270. https://doi.org/10.1002/2017JG003907

Veblen, T., Donoso, C., Kitzberger, T., & Rebertus, A. (1996). Ecology of southern Chilean and Argentinean Nothofagus forests. In T. Veblen, R. Hill, & J. Read (Eds.), *The ecology and biogeography of nothofagus forests* (pp. 293–353). Yale University Press.

Vega, A. S., Lizama, K., & Pastén, P. A. (2018). Water quality: trends and challenges. *Water policy in Chile*, 25-51.

Voss, M., Baker, A., Bange, H. W., Conley, D., Deutsch, B., Engel, A., Heiskanen, A.-S., Jickells, T., Lancelot, C., & McQuatters-Gollop, A. (2011). Nitrogen processes in coastal and marine ecosystems. In. Cambridge University Press.

WRI, W. R. I. (2000). *Marine Jurisdictions: Coastline length*.

Chapter 2: Calculating the Freshwater Inputs for an Inner Fjord Transect.

Extracted from "Iron and silicic acid addition effects on early Spring macronutrient drawdown and biogenic silica production of Patagonia estuarine waters". Progress in Oceanography, 102982, doi: 10.1016/j.pocean.2023.102982 (Appendix A2)

2.1 STUDY AREA

Hyper humid subantarctic fjords and continental reservoirs of freshwater (including ice fields and peatlands) result in high levels of freshwater discharge year-round, particularly during the warm summer period associated with snow and glacier melting as is observed in the largest hydrographic basin of the study area (Rio Serrano basin, figure 2.1).

Freshwater discharge varied spatially depending on hydrographic basin configuration, latitudinal and longitudinal gradients in precipitation associated with westerlies, with maximum levels (up to 7-10 m y^{-1}) at the western boundary of the archipelago where hydrographic basins are small (e.g., near 50°S) contrasting with large hydrographic basin at the continental side. The continental inputs include different freshwater discharge sources (glacier runoff and non-glacier runoff fed by direct precipitation) that flow into coastal waters, likely influencing the dissolved and particulate material loads of freshwaters (Pryer et al., 2019 ; 2020).

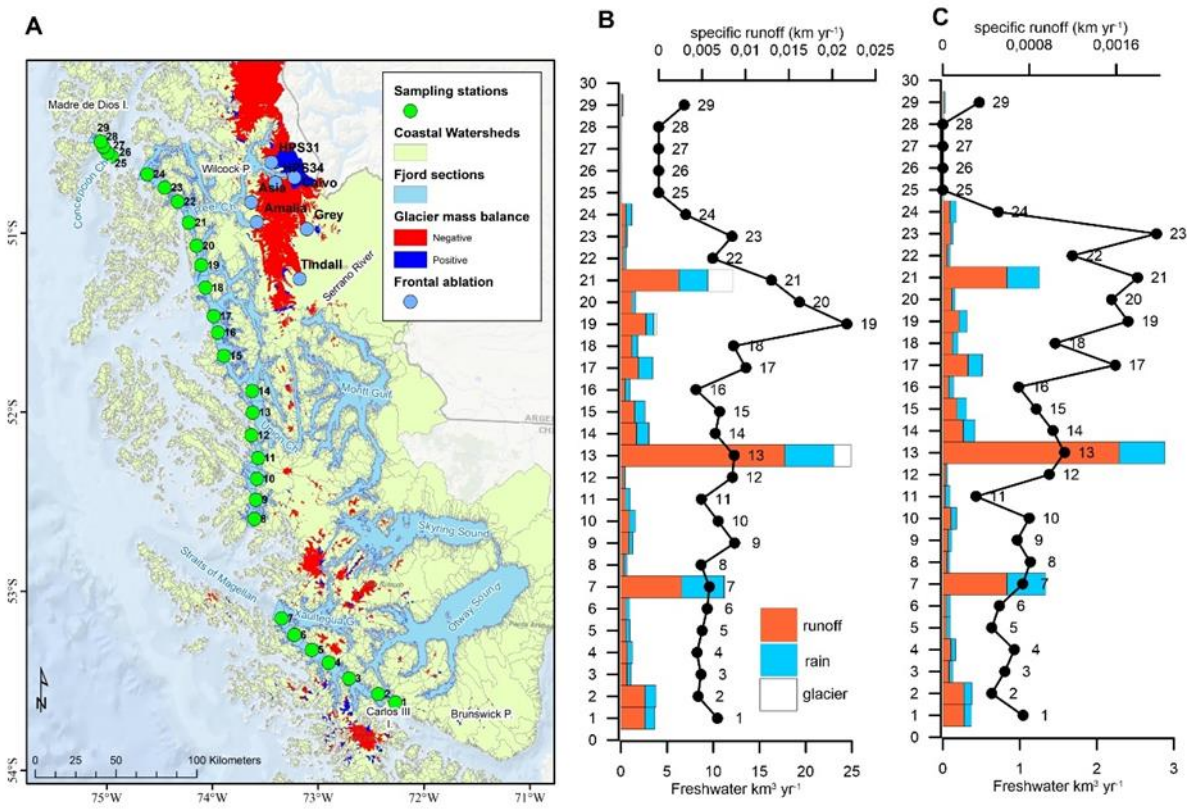

Figure 2.1. *Surface water sampling stations and estimation of freshwater inputs linked to transect stations. Left panel shows stations along the coastal transect of fjords and channels spanning 3 degrees. Also shown are coastal watersheds providing runoff from adjacent terrestrial sources, together with glacial inputs indicated by areas of receding glaciers, and net changes in ice field thickness. Central panel summarized mean annual freshwater volume input near sampling stations and respective sources along the transect, based on calculation shown in supl. table A.1. Right panel summarized freshwater input near the stations during August and September 2017 and respective sources along the transect.*

The transect of marine interior fjord waters starts in the Magellan Strait, running from Peninsula Brunswick near the mouth of Otway sound (Sta. 1; 53.7°S) to the mouth of Xaultegua Gulf (Sta. 7; 53.1°S), where the transect is interrupted by western ocean exposure, resuming in interior waters near Isla Renourd (Sta. 8; 52.6°S) and continuing until Madre de Dios Archipelago (Sta. 29; 50.5°S). The transect is therefore characterized by constrained inland marine waters in close contact with innumerable small to medium point sources of continental runoff, areas of concentrated high-volume runoff where interior canals connect with the large Rio Serrano basin (Stations 12-13, near the western mouth of Union Channel), and areas of glacial input from the

Darwin Range (Stations 1-2) and the Southern Patagonia Icefields (Stations 17-22). In addition to runoff generated from continental basins and glacial meltwater, direct precipitation is expected to contribute a significant percentage of dilute freshwater input along the transect, which is characterized by a precipitation gradient ranging from 2.000 to 7.000 mm/year. Surface lithology along this transect is diverse (Torres et al., 2014), as is vegetation cover (Luebert & Pliscoff, 2006) and potentials soils (virtually uncharacterized, but likely ranging from volcanic Andosols, Entisols in recently deglaciated areas, and abundant Histosols corresponding with extensive wetlands). The corresponding quality of freshwater inputs, in terms of nutrients and other solutes is also expected to be diverse but remains poorly unknown.

2.2 CALCULATION OF FRESHWATER COASTAL DISCHARGES

Freshwater inputs to inner fiords and channels, geographically segmented along transect stations 1-7 and 8-29 (figure 2.1) were estimated for three distinct sources: direct precipitation to fjord surface, surface runoff from coastal watersheds (liquid precipitation), and input from glacial ablation. Time scale of freshwater inputs was based on annual integrated inputs of runoff or precipitation, or in the case of glacial inputs, the average long-term net loss in glacier mass within the estimated contributing areas.

Lateral boundaries between fjord segments were spaced equidistant from respective stations (marine sampling points), running roughly perpendicular to surrounding land features, or extending an equal distance from the penultimate segment in the case of start/end points or gaps in the transect (stations 1, 7, 8 and 24). A conservative 1 km buffer was applied for near ocean transect points (stations 25-28. Inner and outer segment boundaries conformed to land features, or defined by linear segments across channels between land masses that were connected with outer fjord waters (in some cases this linear boundary was shared by 2 stations, see below). The inner

boundary for fjord segments 7, 13 and 21 included more extensive inland marine waters in between sampling stations and contributing catchments. Respective areas of fjord segments (table 2.1) ranged from 100 to 740 km^2.

Direct annual precipitation was based on a regional database of quality-controlled, downscaled long-term regional precipitation observations PatagoniaMet v. 1.0 (Aguayo et al. 2021; cell size 0.04977° x 0.04985°), which was re-interpolated (bilinear; final cell size 0.0003°. Integrated annual contribution of direct precipitation inputs (km^3/year) to transect segments was calculated over the previous year (Oct 2016-Sept 2017)

Terrestrial runoff was calculated via an empirically generated rainfall/runoff coefficient, generally between 0.7 and 0.9 for the study area, derived from the Chilean National Water Balance (MOP 1987), precipitation for each downscaled pixel (PatagoniaMet 1.0) integrated over watersheds modeled based on a 90m SRTM (CGIAR-CSI version 4.1, Jarvis et al. 2008) using ArcHydro tools for ArcGIS (ESRI 2011), described in detail in Astorga et al. (2018). Watersheds whose drainage points intersected the respective fjord segments were used to calculate integrated runoff across all inputs. Pixels that were the limits of glacial coverage (Randoph Glacier Initiative; RGI Consortium 2017) were excluded from runoff estimation. Direct runoff for non-stream generating remnants falling below the stream generation criteria (50 pixels, smallest watersheds approximately 0.4 km^2), were identified as the difference between the DEM land masses, fjords and mapped watersheds, and runoff calculation for these areas was also included for respective fjord segments.

Input from glacial melt-water contributes runoff based on times scales much greater than the annual runoff estimates calculated above. We estimated an annual average runoff contribution

from glacial masses within the contributing watershed boundaries based on two recent estimates of corresponding mass losses at the decadal scale (2000-2019): (1) aerial changes in the glacial front (Minowa et al 2020; blue circles in figure 2.1), and (2) negative changes in thickness of the ice sheet (Dussaillant et al 2019; red polygons in figure 2.1). Annual increments of these mass losses, assuming linear changes, included inputs from glacier HPS31, Calvo, HPS34, Asia, Amalia, Tindall y Grey. Conversion of solid (ice volume) to liquid water equivalents was based on Hock (2010).

A summary of transect stations, area of fjord segments and runoff contribution from the three sources and the total runoff volume (km^3/year) is shown in table 2.1. An estimate of specific runoff volume to fjord segments was approximated by dividing total runoff by segment area (km^2), a reported as m/year. We consider the specific value as a general index of the depth of the freshwater lens and/or halocline. The true values for any given fjord segment are likely to vary depending on advection and mixing with adjacent waters (including adjacent segments) or connectivity to open marine sources, and this index of specific runoff would clearly vary widely over spatial and temporal scales that would require much more complex physical process modeling (Reche et al 2021; https://chonos.ifop.cl/flow).

Table 2.1 Freshwater runoff estimates for transect stations and fjord segments.

Station #	**Segment Area** [x100 km^2]	**Direct Precipitation** [km^3/y]	**Terrestrial Runoff** [km^3/y]	**Glacial Input** [km^3/y]	**Total Freshwater Input** [km^3/y]	**Specific Freshwater Input** [m/y]
1	2.4	1.064	2.612	0.015	3.691	9.38
2	2.2	1.165	2.621	0.015	3.800	7.37
3	1.9	0.421	0.672	0.001	1.094	7.91
4	2.1	0.540	0.695	0.010	1.245	7.88
5	1.1	0.429	0.531	0.006	0.966	9.10
6	1.1	0.429	0.509	0.000	0.938	10.30
7	3.1	4.577	6.577	0.118	11.271	12.69
8	2.1	0.298	0.334	0.000	0.633	9.27

9	2.4	0.424	0.852	0.001	1.278	13.10
10	1.7	0.637	0.911	0.001	1.548	11.64
11	1.0	0.505	0.504	0.000	1.010	9.88
12	1.7	0.176	0.301	0.000	0.477	13.44
13	7.4	5.298	17.743	1.863	24.903	12.20
14	2.2	1.315	1.695	0.020	3.030	11.66
15	1.5	1.100	1.495	0.000	2.595	12.18
16	1.4	0.531	0.473	0.000	1.004	9.14
17	2.0	1.553	1.906	0.004	3.463	18.95
18	3.7	0.617	1.206	0.111	1.934	15.00
19	5.5	0.838	2.727	0.260	3.825	30.95
20	2.8	0.339	1.222	0.000	1.560	20.74
21	4.5	3.121	6.285	2.712	12.118	25.89
22	2.9	0.235	0.303	0.000	0.538	11.05
23	3.2	0.240	0.430	0.000	0.670	13.17
24	1.1	0.605	0.555	0.000	1.161	6.49
25	n.a.	0.017	0.000	0.000	0.017	5.32
26	n.a.	0.017	0.000	0.000	0.017	5.32
27	n.a.	0.017	0.000	0.000	0.017	5.32
28	n.a.	0.017	0.000	0.000	0.017	5.32
29	1.1	0.098	0.121	0.000	0.219	5.37

2.3 COMPARISON BETWEEN THE EMPIRICAL MODEL (this study) WITH FLOW MODEL (chapter 1)

We compared results to a similar effort to estimate freshwater inputs to Chilean fjords by the Instituto de Fomento Pesquero (IFOP, CHONOS http://chonos.ifop.cl/flow/) based on a robust model of watershed runoff (Variable Infiltration Capacity, VIC, which considers vegetation cover and general assumptions on soil types) presented in chapter 1. However, the precipitation inputs of FLOW model not subject to the level of quality control as for PatagoniaMet, and whose output does not coincide with the study period (figure 2.2). Results based on 5 watersheds representing the range of catchment area and climate, show that the two approaches scale consistently (R^2 = 0.9973; $p<0.001$) however the approach used here suggested up to 30% lower runoff ($y = 0.6885x + 0.0809$).

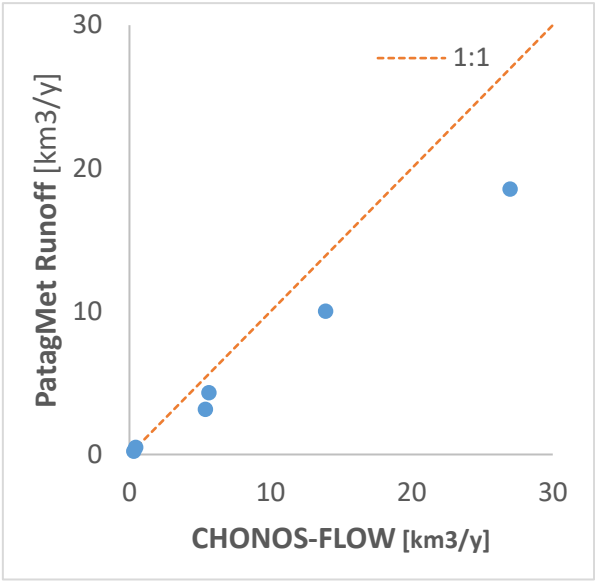

Figure 2.2. *Comparison of runoff from PatagoniaMet 1.0 versus CHONOS-Flow estimate for select watersheds.*

The disparities between the empiric model employed in this study and a more comprehensive model like VIC could be substantial. However, comparing both models yielded similar values, accentuating the differences in larger river basins. As mentioned in Chapter 1, both models suffer from a lack of high-quality observational fluviometric data for calibration and validation purposes. Consequently, identifying the superior model becomes even more challenging, notably when the archipelago area lacks any fluviometric stations (see figure 1.1) and exhibits significant discrepancies in precipitation raster inputs. To enhance flow modeling, it may be advantageous to incorporate a regional precipitation raster, such as the Patagonia Met dataset, into a more intricate and hydrologically comprehensive model like VIC, as employed in the FLOW study (chapter 1). Furthermore, prioritizing a more accurate estimation of the effects of solid precipitation on discharge becomes crucial, especially considering climate change projections indicating reduced snowfall and accelerated glacier melting rates.

In conclusion, obtaining improved information regarding coastal discharges in Patagonia necessitates the establishment of an extensive network for permanent flow sampling, particularly in isolated areas lacking data. While the FLOW model does not currently incorporate sub-daily estimations, integrating them in the future would be a valuable enhancement, potentially enabling real-time flow forecasting. By implementing these upgrades, more realistic fjord scenarios can be developed to address the challenges posed by global climate change.

2.4 LITERATURE CITED

Aguayo, R., León, J., Aguayo, M., Jacques, M. & Fernández, A. (2021). PatagoniaMet v1.0: A multi-institutional effort for an open database in Western Patagonia. (disponible en línea en www.rebrand.ly/pmet en septiembre 2021)

Astorga, A., Moreno, P. C., & Reid, B. (2018). Watersheds and trees fall together: an analysis of intact forested watersheds in southern Patagonia (41–56° S). *Forests*, *9*(7), 385.

Ministerio de Obras Públicas (MOP). (1987). Balance hídrico de chile. Dirección General de Aguas: Santiago, Chile.

Dussaillant, I., Berthier, E., Brun, F., Masiokas, M., Hugonnet, R., Favier, V., ... & Ruiz, L. (2019). Two decades of glacier mass loss along the Andes. *Nature Geoscience,12*(10), 802-808.

ESRI Arc hydro tools overview, ESRI Water Resources Team, Environmental Systems Research Institute: Redlands, CA, 2011.

Hock, R. (2010). Glacier Mass Balance. Summer school in Glaciology. Geophysical Institute, University of Alaska, Fairbanks. Available online on https://glaciers.gi.alaska.edu/sites/default/files/mccarthy/Notes_massbal_Hock.pdf

Minowa, M., Schaefer, M., Sugiyama, S., Sakakibara, D., & Skvarca, P. (2021). Frontal ablation and mass loss of the Patagonian icefields. *Earth and Planetary Science Letters,561*, 116811.

Reche, P., Artal, O., Pinilla, E., Ruiz, C., Venegas, O., Arriagada, A., & Falvey, M. (2021). CHONOS: Oceanographic information website for Chilean Patagonia. *Ocean & Coastal Management, 208,* 105634.

RGI Consortium (2017). Randolph Glacier Inventory – A Dataset of Global Glacier Outlines: Version 6.0: Technical Report, Global Land Ice Measurements from Space, Colorado, USA. Digital Media. DOI: https://doi.org/10.7265/N5-RGI-60

Chapter 3: Early detection of anthropogenic impacts on headstreams in Patagonia through hydrological signatures metrics

Paulo Moreno-Meynard, Rodrigo Aguayo, Luis Uribe, Anna Astorga, Brian Reid

In preparation.

Abstract

Watersheds integrate vegetation, soils, geology, hydrology, and climate, being a fundamental concept for the management and conservation of the earth's critical zone. Watersheds as fundamental ecosystem units, as has been proposed, would in practice depend on questions of scale, context, and available resources for monitoring. Small watersheds where streams of 0-2 order are formed might be assumed as ideally representative and sensitive to the two major drivers of terrestrial landscapes: changes in land use/soils and variability in climate forcing (including climate change). Conversely, one of the challenges in watershed studies is the highly dynamic stream ecosystem, specifically hydrology and water chemistry, and the corresponding dependence on longer-term and/or high-frequency observations in order to characterize patterns and responses. We evaluated small watersheds as potential ecosystem units based on a network of small headwater basins and their streams (2-5 km^2; 0-1 order) in western Chilean Patagonia: 12 basins in four groups along a strong climatic gradient (precipitation 700-2000 mm/year), each group consisting of three land use grades (intact, moderate and high level of intervention). We analyzed 2-6 years of high-frequency discharge observations based on two systems of hydrologic indicators, testing for their utility in discerning physical watersheds condition defined by vegetation, soils, and basin geomorphology. We found that event dynamics, with sub-daily indicators, presented higher predictive power than seasonal dynamics, with daily indicators, to detect the effects of land use

changes on streamflow with short-time datasets. In detail, sub-daily indicators were important to address changes in flows due to evapotranspiration, being most critical in water-limited ecosystems. As expected, climate variables were crucial for predicting the magnitude, timing, and pulse of high, low, and base flows in seasonal dynamics. However, some catchment attributes associated with changes in land use/soils such as the cover of pastures, bare land, riparian zone with forest, and mature forest with dense canopy were good predictors of many hydrology indicators. This methodology allows understanding some correlations and brings useful information for building specific hypotheses to study in the future.

Keywords: Hydrology indicators; Patagonia; headstream; catchment; land use/cover changes; short-time scale.

3.1 INTRODUCTION

Streams have been widely studied because they are essential in many aspects, such as agriculture, navigation, energy production, recreation, floods, the water cycle, etc. (Millenium Ecosystems Assessment, 2005). The watershed is the ideal geographic area to analyze streams, integrating factors such as soils, geology, geomorphology, vegetation, hydrology, climate, and human activities. The watershed ecosystem is crucial as a management and conservation unit but also depends on questions of scale, context, and available resources for monitoring (Whittemore & Ice, 2007). In a vulnerability context, headwater watersheds (HW) are the most sensitive area of a stream net where, e.g., land use/cover changes or contamination are evident downstream (Máčka et al., 2023). However, despite their importance, headstreams have been studied with less intensity than the most attractive big rivers, e.g., Amazon, Mississippi, Nile, Yangtze, Danube, Volga, and Ganges (Milliman & Farnsworth, 2011).

HWs are extremely sensitive to the two major drivers of terrestrial landscapes: changes in land use/cover (LUC) and climate variability. Several studies have described the effects of human activities on streams where land use changes (LUC) have been critical to river hydrology and erosion of sediments (Becerra-Rodas et al., 2019; Desmit et al., 2018; Donoso et al., 2014; Frêne et al., 2021; Lara et al., 2021; León-Muñoz et al., 2021; Little et al., 2009; Miranda et al., 2017). On the other side, climate variability, especially, in precipitation (Ryberg Karen et al., 2014; Wang & Alimohammadi, 2012) and temperature (Chen et al., 2007) instantly affects the runoff response. In a regional context, another source of climate variability in Patagonia are the anomalies such as El Niño-Southern Oscillation (ENSO) and Southern Annular Mode (SAM) with strong influences on the rain and temperatures (Aceituno et al., 2021; Aguayo, 2021; Boisier et al., 2018; Garreaud et al., 2013; Reche et al., 2021). The precipitation trends show a slight decrease of 2 mm/year in some stations in the Aysén region but a positive trend above 5 mm/year in the Magallanes region (Castro & Gironás, 2021). Temperatures change trends in Patagonia are not uniform, not only decreasing (-0.04 to 0 °C) in minimal temperatures for steppe climates but also increasing (0.01 to 0.05°C) in oceanic climates (Castro & Gironás, 2021).

Rivers are the primary connection between terrestrial and marine ecosystems, with annual global estimated coastal discharges between 36×10^3 km^3 of freshwater and an estimated 20 billion tons of total sediments (Milliman & Farnsworth, 2011). These riverine forcings are crucial for salinity, allochthonous/autochthonous nutrient cycling, water temperature, and light availability, among other processes, in estuarine and coastal systems essential for human well-being ecosystem services (Millenium Ecosystems Assessment, 2005). The quality and chemical composition of continental waters, the array of dissolved and suspended constituents that flow from land to sea, begins with the transformation of dilute precipitation inputs through processes of weathering,

leaching, and erosion (Milliman & Farnsworth, 2011). Land forms, vegetation, soils, and corresponding physical conditions and alterations from land use may generate distinct water quality signatures at the source. In summary, the concept of watershed, especially HW as a vulnerable ecosystem, is the fundamental unit that can integrate the conditions and forcings of the land and water.

Once stablished HW importance, how it is possible observe or monitor the changes in the ecosystem due to LUC and climate?. From a hydrology point of view, the signals of a stream are as a medical exam about the health of the system. Several approaches exist for identifying alteration in streams, such as water yield (Donoso et al., 2014; León-Muñoz et al., 2021; Little et al., 2009), chemistry and nutrient export (Becerra-Rodas et al., 2019; León-Muñoz et al., 2021; Little et al., 2008; Oyarzun et al., 1998; Perakis & Hedin, 2002), remote sensing (Hernandez et al., 2022), sediment and water quality (Amann et al., 2022; Frêne et al., 2021), biodiversity indicators (Astorga et al., 2022; Tolod et al., 2022), hydrological analysis (Donoso et al., 2014; Hernandez et al., 2022; Ma et al., 2014; Pizarro et al., 2022), among others. One popular methodology to identify impacts in a river has been the analysis of hydrology signatures (McMillan, 2021), which correspond to quantitative metrics or indices that describe statistical or dynamical properties of hydrologic data series. The metrics are categorized into five ecologically important features of flow regimes: magnitude, timing, frequency, duration, and rate of change. Richter et al. (1996; 1997) developed 33 indicators of hydrology alteration (IHAs) and 34 environmental flow components (EFCs) associated with specific metrics of high, low, and base flows. However, a problem with the selection of indicators, that translate the signature of a stream, is the selection of an optimal temporal scale. The majority of indicators are based on daily flow measurement but

some process as high rate of evaporation due to loss of vegetation cover could have an effect in some few hours during the day (Dierauer et al., 2017; Frêne et al., 2021; Richter et al., 1996).

In western Patagonia (~41° to 55°S), headstreams have a higher relevance due to their fragmented geography, where rain is discharged into fjords from the mountains in a few hours (Abell et al., 2008; León-Muñoz et al., 2021; Reid et al., 2021). For example, to quantify the importance of small streams, in the Aysén basin (~46°S; 12,300 km^2), there are 15,200 km of headstreams but only 1100 km are rivers (Surface hydrography dataset, digitized from 1970s series topographic maps, Dirección General de Aguas). In addition, the differences in climate are abrupt, e.g., in a few kilometers, the precipitation ranges from >6000 to 500 mm/year (Astorga et al., 2021; Castro & Gironás, 2021). Regard, LUC status west-southern Patagonia supports extensive areas of forested headwaters, where recent mapping suggest 66,000 km^2 (49% of total forested watersheds) of intact forested watersheds (IFWs) from 41° and 56°S, extending across several forested biomes (Astorga et al., 2018; 2021). The conservation of IFWs in Patagonia reach a global importance because they are the largest extensions of intact temperate forests in the southern hemisphere (Astorga et al., 2018). At the same time, intense recent (ca. 100 years) land use pressure has led to heavy impacts from fires and clearing, including severe erosion and complete conversion to pasture, especially at lower elevations (Hernández-Moreno et al., 2023). The proximity of these two extremes in land use, often characterizing adjacent catchments, presents a unique opportunity to understand how these LUC relate to hydrology, soil and water chemistry, and stream ecosystem processes across a wide range of climate regime.

The main problem in Patagonia is the lack of long series of hydrologic data, even worse, when we focused in HW associated with alpine areas, many of them with serious accessibility problems. At the same time, these HW could be the most responsive unit in the stream net due to capacity to

identify specific forcings such as LUC. The main objective of this study is to identify relations between hydrology indicators and LUC and climate variables, with short-time scale data, through exploratory and predictive statistics that allows builds specific hypotheses to test in future researches. To address this objective, we developed an observational study in 12 headwater catchments over five years, along different hydrological regimes and land use/cover gradient. Flow data was obtained with pressure sensors in the catchment outlets, and watershed attributes were measured on field thanks to a systematic inventory and remote sensing analysis. In the present study, we hypothesize that hydrology indicators can identify the effects of LUC in paired headwater-catchments with short temporal series of data for early detection. Additionally, we aim to determine if flow data aggregation hides response due to forcings that occur on an hour-scale through daily and sub-daily signature analyses. Finally, the identification of effects in the HW hydrology due to LUC in the temperate zone of the southern hemisphere is relevant in terms of methodology but also associated with observation points of monitoring and conservation activities based on the concept of climate observatory or Long-Term Socio-Ecological Network.

3.2 METHODS

3.2.1 Study area

Twelve headwater catchments in the Andes Mountain range in the Aisén region, Chilean Patagonia, were selected to represent the climatic and land use gradient, ranging between latitudes 46-47°S, in the Aysén and Baker river basins. This area is characterized by a range of climates and corresponding forest cover transitions east to west, from cold steppe (BSk'c) associated with *Nothofagus antarctica* through boreal or sub-antartic (Dfk'c) with a majority presence of *N. pumilio* and finishing in a humid temperate climate (Cfk'n) where species such as *N. nitida, N. betuloides, N. dombeyi, Drimys winteri,* and *Laureliopsis philippiana* are the most common species

(Donoso, 1993; Silva et al., 1999). The soil origins are associated with vulcanism (andosols) with major deep in the valleys. Volcanic activity is continuous in the time with recent eruptions but with ancient registers found from tephra layers and sediment cores in lakes (Stolpe, 2014; Vandekerkhove et al., 2016). The catchments were distributed in four sites, Coyhaique Alto, Trapananda, Portales, and Carrera (figure 3.1), with deciduous *Nothofagus* forests as the most common land cover. In each site, three similar-sized or paired catchments were selected across a land use gradient; from streams with nearly pristine forested catchments (Ref) and two impacted catchments with different levels of LUC (Imp1 and Imp2) with present-day and historical impacts of fire and cattle farming (Veblen et al., 1996). Additionally, the site´s hydrological regimes varied from nival to pluvial in a continuum from east to west. Specifically, the Coyhaique Alto site has a nival regime, the Trapananda site presented a mixed regime but mainly nival, the Carrera site also has a mixed regime but mainly pluvial, and the Portales site has a pluvial regime (figure 3.2). Besides, flow duration curves (FDC) of 8 catchments are shown (figure 3.3) to identify patrons or/and differences between sites and degree of impacts. Overall, the reference catchments showed more discharge than the corresponding impacted ones, using the flow duration curves (FDC). For example, the flows in reference catchments were notorious higher in Trapananda and Carrera sites, indifferently of the magnitude, i.e., high or low flows. Imp1 catchments (Trapananda and Carrera sites) have high percentages of second-growth forests, prairies, and bare land coverages. In the Portales site, the discharge of the reference catchment was slightly higher 85% of the time compared to the impacted. On the contrary, the Coyhaique Alto site is a water-limited ecosystem, especially in summer. The impacted catchment presented higher low-flows 60% of the time but lowered magnitudes in high-flows.

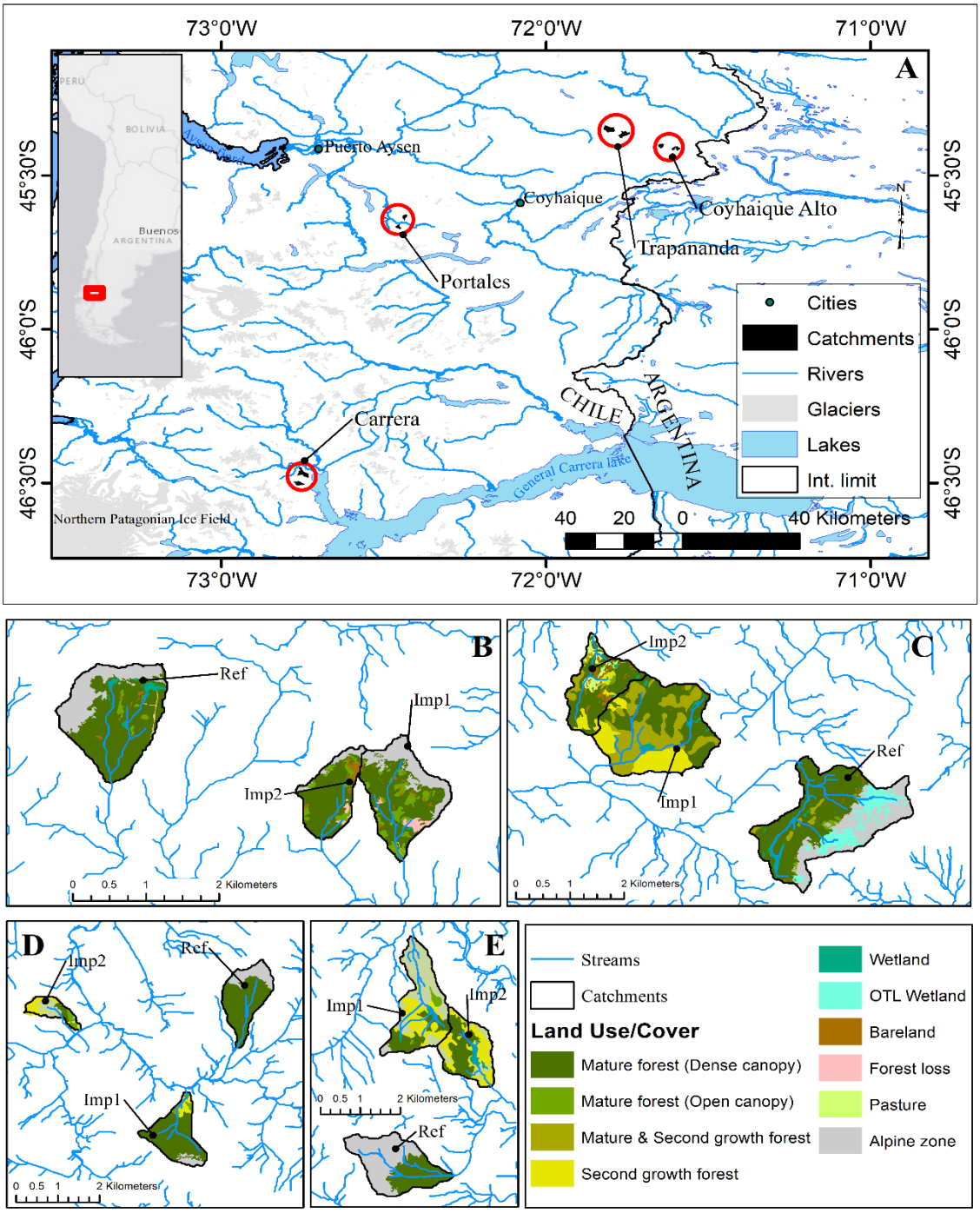

Figure 3.1. *A. Location of study area and the four sites (red circle). B. Land use/cover of the Coyhaique Alto site. C. Land use/cover of the Trapananda site. D. Land use/cover of the Portales site. E. Land use/cover of the Carrera site. Ref, catchment of reference; Imp1 e Imp2, catchments with impacts. OT, over treeline.*

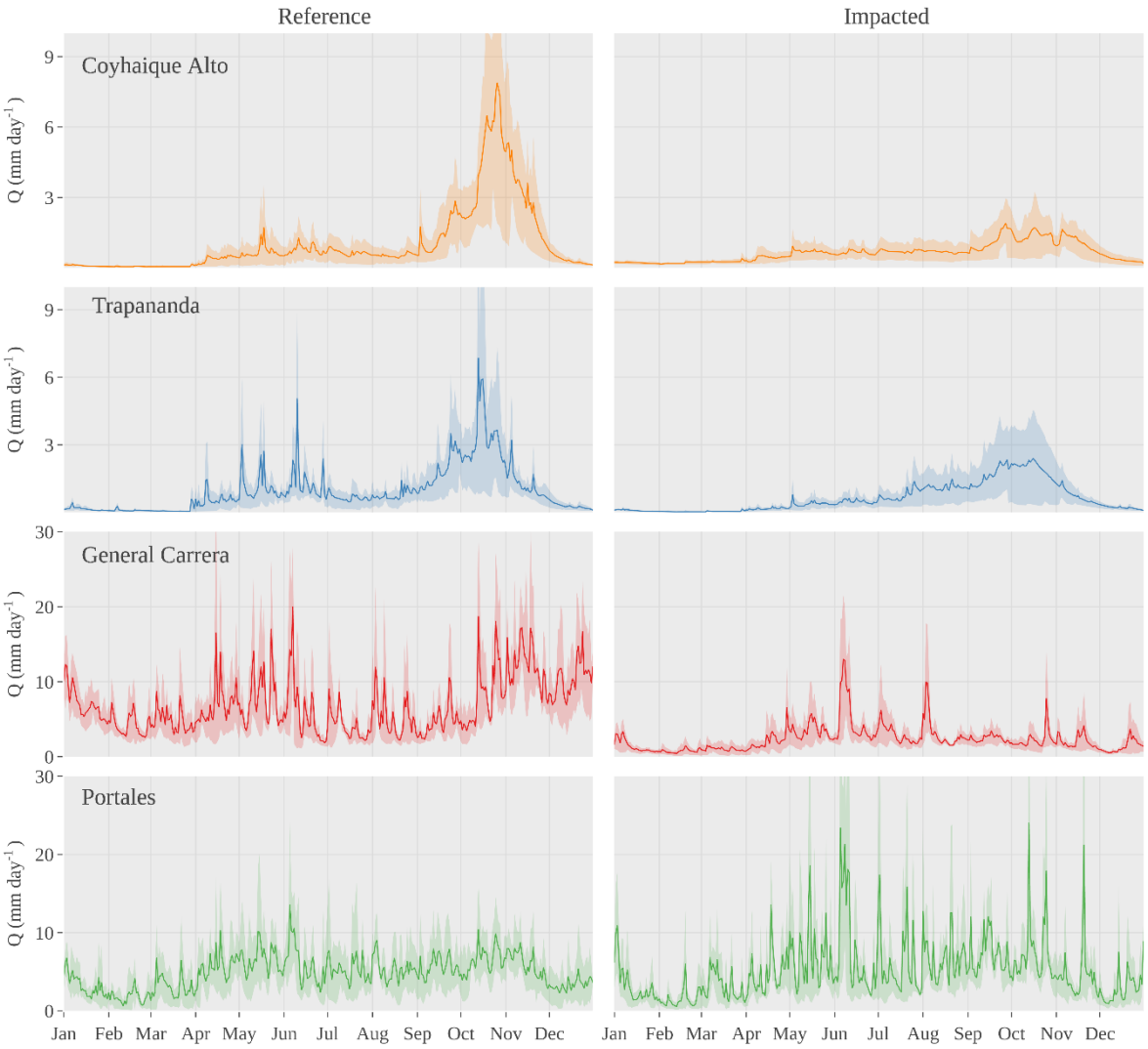

Figure 3.2. *Daily discharge data (in mm day-1) for the four sites (eight catchments). The left panel indicates the references catchments (Ref), while the right panel indicates the impacted catchments (Imp1). Only catchments with five years of discharge data were considered in this figure. The shaded area corresponds to the 15th and 85th percentiles.*

The headwater catchments were built using the DEM ALOS-PALSAR 12.5 m (Rosenqvist et al., 2007) and the local stream drainage network from Chilean General Water Directorate (DGA) using Arc Hydro 10.2 for ArcGIS 10.8 software (ESRI, 2011).

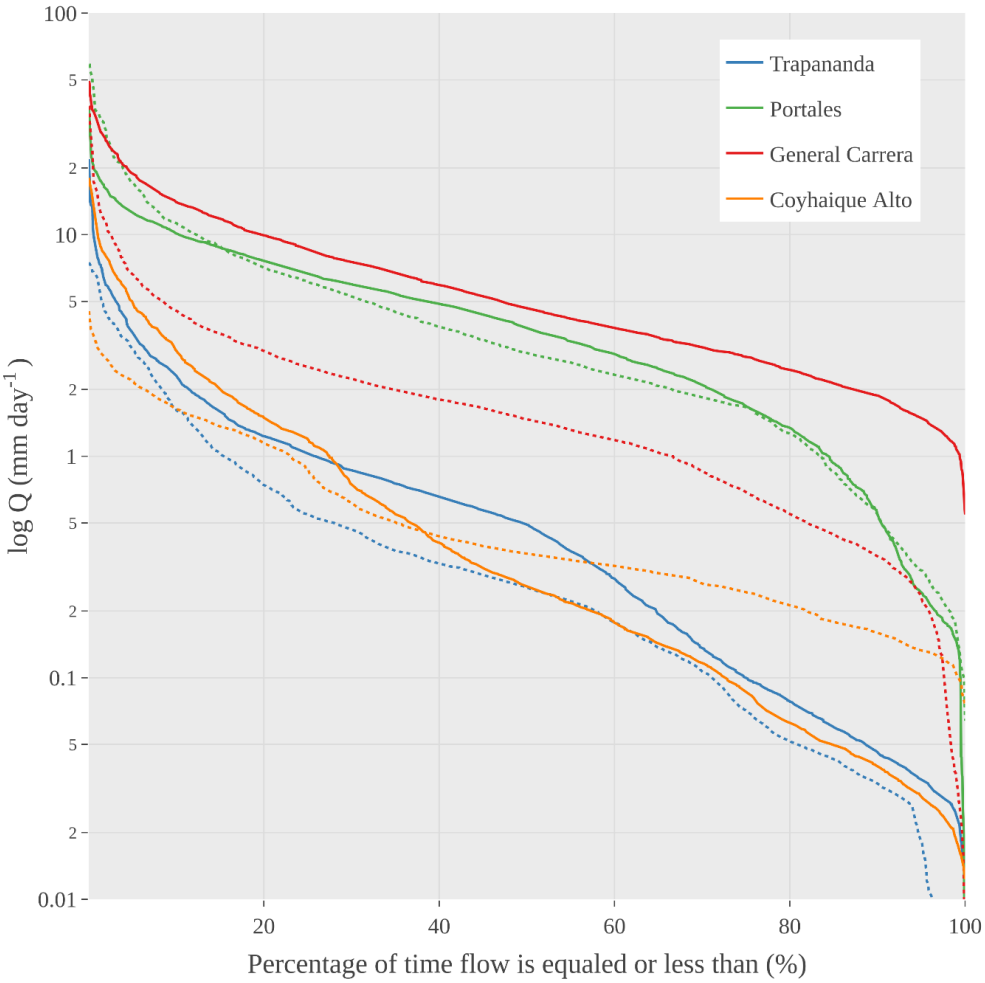

Figure 3.3. *Flow duration curve for the eight catchments (in log scale). The dotted line corresponds to the impacted catchments of each site. Only watersheds with five years of discharge data were considered in this figure (Ref and Imp1).*

3.2.2 Analysis strategy

The main objective, as was proposed in introduction, is to identify watershed processes between LUC and effects in the hydrology signature for the 12 headwater catchments in study. The strategy of analysis is to incorporate the maxima information available with no preconception hypothesis. In a hydrological point of view, we aggregated flow data in daily and sub-daily temporal scale to analyze both type of information. In other hand, we included available information from the watershed such as climate, soil, land use/cover, topography, and biology

indicators as predictors of the hydrology signature. Specifically, biology indicators as aquatic macroinvertebrates and vascular flora were included not as forcing factors but as possible connection with results of appendix 3 and 4, about LUC and these specific bioindicators. A subset of predictors (watershed attributes) was selected to avoid a high correlation between them that provokes a misleading prediction's meaning. In the same way, a subset of responses (hydrology indicators) was identified to decrease the initial high number of them. Finally, to identify watershed processes, exploratory (PCA) and predictive analyses (Random Forests and ANOVA) were done (Addor et al., 2018). Based on the results of both daily and sub-daily indicators, specific hypotheses have been formulated for future research. A schematic diagram of the strategy analysis is presented in figure 3.4.

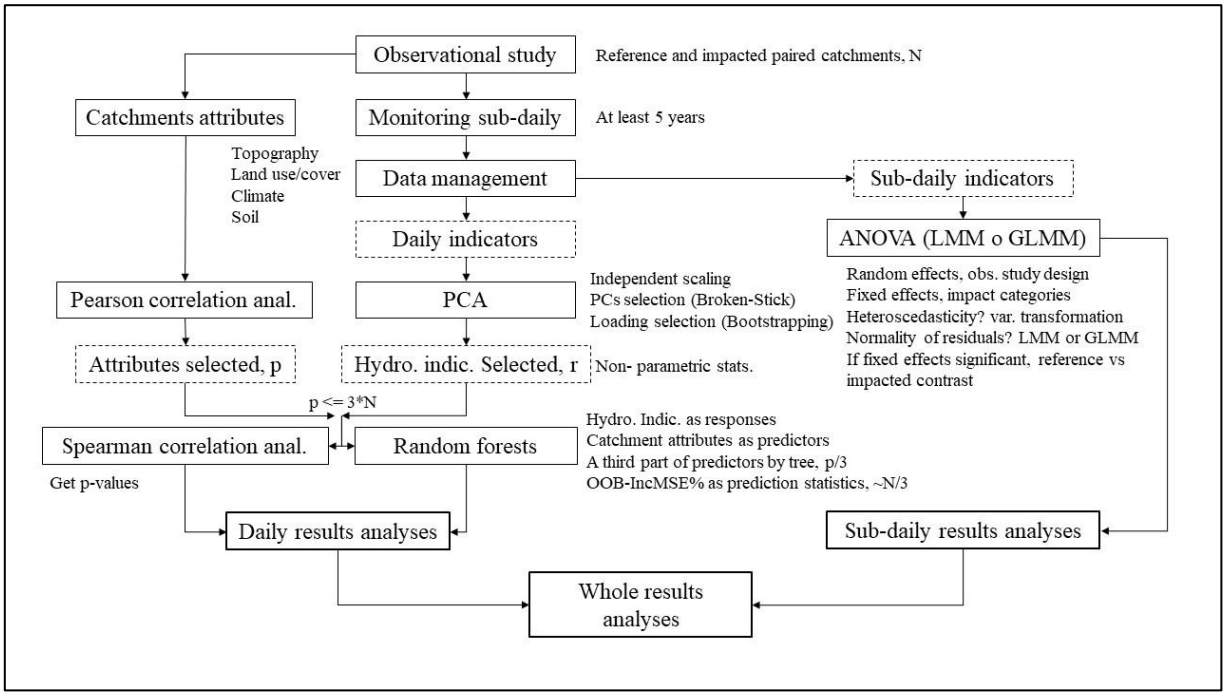

Figure 3.4. *Methodology diagram for early detection identification of impacts in the hydrology signature of headstreams.*

3.2.3 Hydrological signature

3.2.3.1 Stream data

A HOBO U20L-04 water level logger set to record water pressure and temperature every 10 min was installed in each of the 12 catchment outlets (see figure 3.1). The logger was installed in a stable section of the stream inside a galvanized tube with the sensor hanging and touching the bottom of the channel. Additionally, a barometric pressure compensation logger was installed in each site. From the 12 catchments, 8 have had loggers since 2016 (all the reference (Ref) and impacted 1 (Imp1)). In 2020, to increase the range of variability in the land use impacts, four additional catchments (Imp2) were included and their loggers installed with the same methods. For this analysis, the data vectors end mid-March 2022.

On average, the data was downloaded from HOBO sensors every 45 days. Also, during each visit we measured flow using a Flow Tracker Handheld Acoustic Doppler Velocimeter or a Swoffer 3000 Current Velocity Meter-Flowmeter, taking at least 15 measurements at 60% depth in the cross-channel transect. The pressure and temperature vectors were joined, with an exhaustive revision, checking information gaps, problems with time information between consecutive measurements, data errors from sensor manipulation in the downloading process, among others. Finally, the data was averaged every 30 min to avoid outliers (field logger set at 10 min). Calculations of water level and simple rating curves were done following the methodology of Water-Resources Investigations (Sauer, 2002). The supplementary material presents thirty-minute flow curves of the 12 catchments.

3.2.3.2 Seasonal dynamics with daily indicators

One procedure to identify the impacts of alterations on the seasonal dynamic of streams has been daily hydrology indicators (McMillan, 2021; Olden & Poff, 2003; 1998; Richter et al., 1996;

1997). The analysis of seasonal dynamics was based on two set of daily metrics (table S.3.1-S.3.2). The first set corresponded to the metrics proposed by Richter et al. (IHA) (Richter et al., 1996), which are classified into: magnitude, duration, timing, frequency and duration of pulses (Richter et al., 1996). The second set proposed by Dierauer (2017), known as Environmental Flow Components (EFC), are specific daily indicators of high, low, and base flows.

The hydrological year was defined from March to February due to the annual cycle of precipitation in this area. The metrics (median) were calculated for five years of data in eight catchments (Ref and Imp1, mean series length = 90,000) and two years for the rest (Imp2, mean series length = 35,000). The daily values of each catchment were normalized by their area, i.e., the unit is mm/day. The hydrological metrics proposed by Richter et al. (1996) were calculated by the IHA Software developed by the The Nature Conservancy (TNC, 2009), while the EFC parameters were calculated by the Flowscreen package (Dierauer et al., 2017) developed in R.

Several studies have identified similarities between hydrology indicator schemes, generating methodologies to select those with no correlation, avoiding multicollinearity with strange responses and reducing the number of indicators (Chen et al., 2010; 2018; Olden & Poff, 2003; Pyron & Neumann, 2008). First step in the selection of indicators was the unification of the same indexes from both schemes, e.g., "Annual minima, 7-day means (IHA)" with "Mean annual minimum 7-day flow (EFC)". Second, a scale-independent Principal Component Analysis (PCA) was performed to identified those essential indicators (Cheng et al., 2018; Olden & Poff, 2003; Pyron & Neumann, 2008). Some specific characteristics of PCA are featured below. A scaling was performed by dividing each metric by its mean because they are in different units. The covariance matrix instead of the correlation matrix was used to build the PCA. This method leads to PCs, which are scale independent while retaining the observed variability (Dharmawardena et al., 2017). The Broken-Stick technique was performed to select the number of PCs most important that

explain the variability (MacArthur, 1957; Olden & Poff, 2003). Besides, a bootstrapping with 1,000 repetitions was done to identify the significance of the factor loadings (Peres-Neto et al., 2003). Finally, the selection was sequential, where first, each scheme was done independently, and second, the best indicators of both groups together were identified.

3.2.3.3 Event dynamics with sub-daily indicators

Considering the size of the catchments (< 400 ha), we used to a standardized approach to detect the intensity, timing, and frequency of sub-daily flow fluctuations. For this purpose, we used an automatic event detection algorithm to analyze hydrographs and detect hydropeaking events implemented in the hydropeak package for R (Greimel et al., 2016). The implemented event-based algorithm detects flow fluctuations corresponding to increase events (IC) and decrease events (DC). For each event, a set of parameters related to the fluctuation intensity is calculated: maximum flow fluctuation rate (MAFR), mean flow fluctuation rate (MEFR), amplitude (AMP) which is the difference between maximum flow and minimum flow (Qmax – Qmin), and flow ratio (RATIO, Qmax/Qmin). In this approach, we used a temporal resolution of 30 minutes between 2020 to 2022 as common period for the 12 catchments.

3.2.4 Catchment attributes

Attributes of the 12 catchments were obtained and classified in topography, land use/cover, soil, bioindicators, and climate, where the specific variables are shown in supplementary material (table S.3.3). First, topographic attributes were elaborated using the DEM ALOS-PALSAR 12.5 m (Rosenqvist et al., 2007). The variables were area, slope, and elevation (maximum, minimum, mean, median, and range). Second, the land use/cover was classified by photointerpretation using the base map image of ArcGIS 10.8 (ESRI, 2016). The coverage was recorded as both an area and

percentage. Additionally, a riparian zone of 50 m from the stream was defined, with percentages of each land use/cover.

To obtain soil chemical attributes and soil loss variables, a systematic inventory (grid of 500x500 m) with 91 cluster plots was planned to cover the 12 catchments. However, due to accessibility, some points were eliminated, leaving a total of 81 cluster plots. The soil sample was obtained in each cluster by mixing three subsamples separated by 50 m. Each subsample was obtained by a depth composite mix of 0-30 cm. Soil samples were chilled and transported to the closest soil laboratory for analysis (Instituto de Investigaciones Agropecuarias Tamel Aike). The chemical variables obtained in laboratory were pH, nitrogenous, phosphorus, potassium, sulfur, organic matter, calcium, magnesium, potassium, sodium, aluminum, effective cation-exchange capacity, and aluminum saturation percentage. Attributes of soil loss were obtained using the same systematic inventory, with depth measurements of leaf litter, litter, organic (H0), and mineral (HA) horizon. In addition, as soil loss proxy, the depth of the bare roots of every tree with a distance less than to 12.62 m (500 m^2) from the location of each soil subsample was measured.

In appendix 3, the aquatic macroinvertebrate community was defined mainly by a climatic gradient and different land use/covers. Besides, in appendix 4, one of the most important predictors to define if an evergreen forest was degraded was the number (>5) of exotic species of vascular flora. Interpreting these results, we incorporated two variables as possible bioindicators related with climate and LUC such as richness of macroinvertebrates and vascular flora. Richness of vascular plants was obtained based on at least twelve flora plots of 1 m^2 located in each cluster plots from the systematic inventory. The richness of freshwater macroinvertebrates was measured by a specific inventory carry-on spring in each stream. Specifically, four-minute kick-net samples (mesh size 0.3 mm), consisting of eight 30-s subsamples, were obtained. Macroinvertebrate

samples were preserved in 70% ethanol. Identification was made following the methodology of Astorga et al. (2022).

Finally, the last set of watershed attributes were related with climate variables such as precipitation, snow, potential evapotranspiration (PET), seasonality index (SI), and aridity index (AI). The mean annual precipitation and air temperature were calculated from PMET-sim v1.0 (Aguayo, 2021), a gridded product (0.05°) developed for Western Patagonia (1980-2020) based on a compilation of hydrometeorological observed data and ERA5 (Hersbach et al., 2020). Considering that size of the catchments is lower than the grid size, the temperature was downscaled to a resolution of 0.001° (~100m) using a constant lapse rate of -0.0065°C/km. The potential evapotranspiration was calculated using the Hargreaves-Samani equation (McMahon et al., 2013) based on the minimum and maximum downscaled temperature. The solid fraction of precipitation was calculated from days when the mean daily temperature (average between the maximum and minimum temperature) was equal to or less than 0°C. The seasonality of the precipitation was calculated using the SI derived by Walsh and Lawler (1981). The AI was created with the ratio of precipitation over potential evapotranspiration (Zomer et al., 2022). All the climatic indexes were calculated using data from 1990-2020.

The complete list of attributes was analyzed to avoid multicollinearity provoking a misleading prediction result, identifying only those with the lowest Pearson correlations ($-0.8<\rho<0.8$).

3.2.5 Influence of catchment attributes into hydrological signatures

3.2.5.1 Seasonal dynamics analyses

A hydrological signature of a stream brings some information about the watershed processes and how the catchment attributes affect the flows. Thus, to associate the characteristics of a catchment with the daily indicators, exploratory analyses through correlation and predictive

analyses using random forests were performed (Addor et al., 2018; Gareth James et al., 2013). Non-parametric statistics were performed using the median in each hydrology series to avoid problems with data normality (Cheng et al., 2018; Olden & Poff, 2003). Therefore, the Spearman correlation index was used as a rank-based measure of association for non-parametric statistics as the median. Like Addor et al. (2018), we perform random forests, a machine-learning algorithm, to predict hydrological signatures using the catchment attributes. Each random forest was composed of 1,000 bagged trees for evaluation. Additionally, a sample of predictors close to p/3 was selected in each tree, where p is the total number of predictors (Addor et al., 2018). We used the out-of-bag (OOB) increment in mean square error (IncMSE%) as error estimation statistics, where, on average, each bagged tree makes use of around two-thirds of the observations (Gareth James et al., 2013). The resulting OOB error is a valid estimate of the test error, similar to a leave-one-out cross-validation error since the response for each catchment is predicted by trees that were not fit using that observation (Gareth James et al., 2013). The IncMSE% is translated as the relative influence of each catchment attribute on the hydrology signature. Thus, it was possible to determine which predictors are better than others (Addor et al., 2018).

3.2.5.2 Event dynamics analyses

In the case of sub-daily indicators linear mixed models (LMM-ANOVA) were realized for those continuous responses as MAFR, MEFR, and AMP with a log transformation, where assumptions of normality are accomplished. However, RATIO and DUR responses were fitted with generalized linear mixed models (GLMM-ANOVA), using Gaussian and Poisson distributions, respectively, and logarithm as link function. For each model, the fixed effect was LUC (impact) associated with catchments Ref, Imp1, and Imp2. The random effects were site, year, and month in a nested structure. Random slopes were applied to the site. Contrasts between

the REF as control and both impacted catchments (Imp1 and Imp2) were made. Linear model assumptions were checked before analyses.

The statistical analyses were performed totally in the software R (Core-Team, 2017) using several libraries, such as “nmle” (LMM), “lme4” (GLMM), “emmeans” (contrast), “vegan” (PCA), “corrplot” (correlations), and “randomForest” (random forest).

3.3 RESULTS

3.3.1 Daily indicators with the lowest correlation

As was mentioned in the methods, a step to reduce the high number of daily indicators was the selection of those with less correlation. The initial number of indicators (51) was calculated by hydrology year in each catchment (table S.3.4 to S.3.8). After the PCA procedure, 41 hydrology indicators were selected. The high proportion of selected indicators shows us the independency and no correlation due to the orthogonality of principal components (figure 3.5). Most indicators are related to the first axis, which explains 59% of the variability due to the magnitude of flows. However, another source of variability is associated with the number of days of high and low pulses. Specifically, sites such as Coyhaique Alto and Trapananda present long periods in summer with low pulses but, at the same time, many days in spring with high pulses due to snow melting.

The list of daily indicators selected for seasonal dynamics is presented in table 3.1. Every monthly magnitude indicator was selected less than October. Also, many magnitude and duration of annual extreme water conditions indicators from IHA and EFC were incorporated, such as "annual minima, 1-3-7-10-30-90 day mean", "annual maxima, 1-3-7-30-90 day mean", "Q10", "Q25", "Q80", "Q90", "day of year 25% annual flow ", "days duration between 25% and 75% annual flow". Besides, the majority of indexes related to base flow were selected as "mean daily discharge", "annual baseflow volume", "annual mean baseflow ", "annual maximum baseflow",

"annual minimum baseflow", "mean annual baseflow index", and "duration between 25% and 75% baseflow volume". Hydrologic signatures associated with pulses in water condition changes were important, such as "number of low pulses", "number of high pulses", "rise rate", "fall rate", "median duration of low pulses (days)", and "median duration of high pulses (days)".

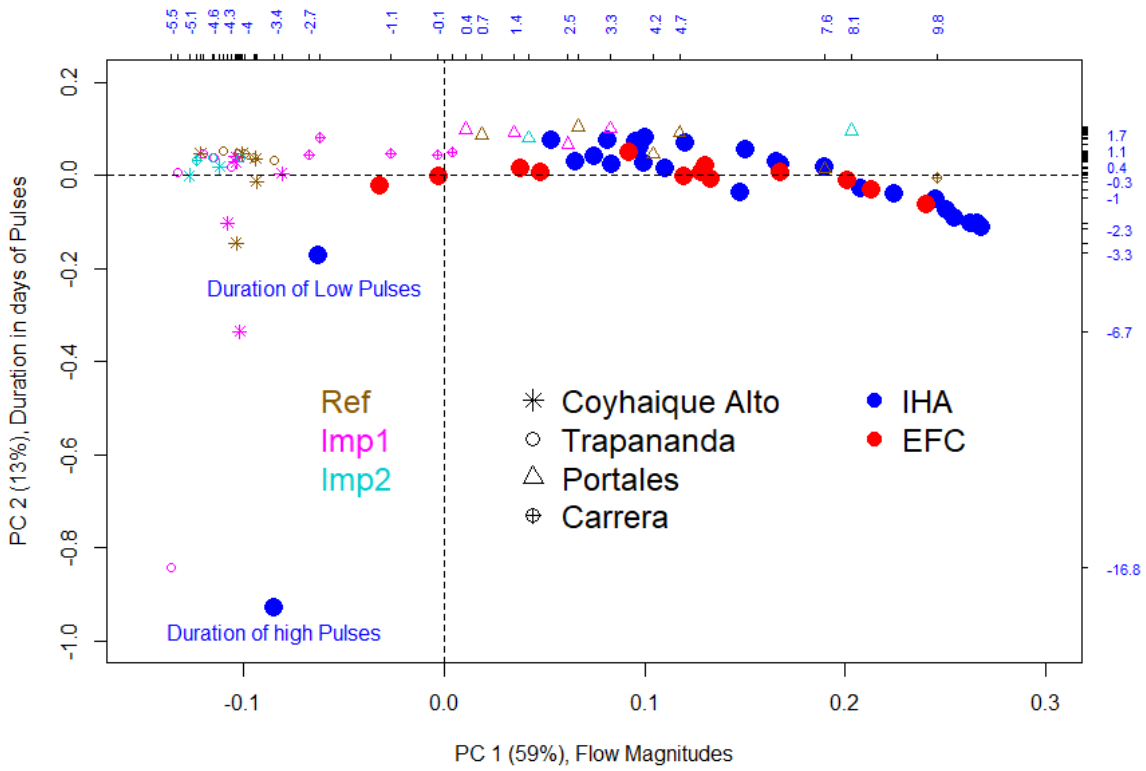

Figure 3.5. *Two main components of PCA for the 12 catchments in each hydrologic year. Selected hydrology indicators from IHA and EFC schemes are shown.*

Table 3.1. Seasonal selected metrics calculated for the 12 catchments.

Category	Metrics and description	Units
Magnitude of monthly water conditions (n = 11)	Median value for each calendar month, except for October	$m^3 s^{-1}$
Magnitude and duration of annual extreme water conditions (n = 17)	Annual minima, 1-day mean (1.day.min)	$m^3 s^{-1}$
	Annual minima, 3-day means (3.day.min)	$m^3 s^{-1}$
	Annual minima, 7-day means (7.day.min)	$m^3 s^{-1}$
	Annual minima, 10-day means (10.day.min)	$m^3 s^{-1}$
	Annual minima, 30-day means (30.day.min)	$m^3 s^{-1}$
	Annual minima, 90-day means (90.day.min)	$m^3 s^{-1}$
	Annual maxima, 1-day mean (1.day.max)	$m^3 s^{-1}$
	Annual maxima, 3-day means (3.day.max)	$m^3 s^{-1}$
	Annual maxima, 7-day means (7.day.max)	$m^3 s^{-1}$
	Annual maxima, 30-day means (30.day.max)	$m^3 s^{-1}$
	Annual maxima, 90-day means (90.day.max)	$m^3 s^{-1}$
	10% flow quantile (Q10)	$m^3 s^{-1}$
	25% flow quantile (Q25)	$m^3 s^{-1}$
	80% flow quantile (Q80)	$m^3 s^{-1}$
	90% flow quantile (Q90)	$m^3 s^{-1}$
	Day of Year 25% Annual Flow (Day.25%.Q)	Julian date
	Duration between 25% and 75 % annual flow (25%.75%.Q.duration)	days
Base flow (n = 7)	Mean daily discharge (Mean.daily)	$m^3 s^{-1}$
	Annual baseflow volume (Baseflow.volume)	$m^3 s^{-1}$
	Annual mean baseflow (Mean.baseflow)	$m^3 s^{-1}$
	Annual maximum baseflow (Maximun.baseflow)	$m^3 s^{-1}$
	Annual minimum baseflow (Minimun.baseflow)	$m^3 s^{-1}$
	Mean annual baseflow index (baseflow.Index)	unitless
	Duration between 25% and 75 % annual baseflow (25%.75%.BF.duration)	days
Frequency, rate and duration of high and low pulses (n = 6)	Number of low pulses within each water year (Low.pulse.number)	Events (n)
	Median duration of low pulses (Low.pulse.duration)	days
	Number of high pulses within each water year (High.pulse.number)	Events (n)
	Median duration of high pulses (High.pulse.duration)	days
	Rise rates: Median of all positive differences between consecutive values (Rise.rate)	$m^3 s^{-1}$
	Fall rates: Median of all negative differences between consecutive values (Fall.rate)	$m^3 s^{-1}$

3.3.2 Selected catchment attributes

A total of 29 from 57 attributes were selected to avoid multicollinearity and misleading results interpretation, rule of thumb of $-0.8<\rho<0.8$ (table 3.2). The attributes categorization is land

use/cover area (3), land use/cover proportion (5), land use/cover riparian proportion (2), soil (11), richness (2), topography (4), and climatic (2) (figure S.3.1). Some of the selected attributes are related to anthropogenic impacts (see table S.3.3), such as mineral and organic soil horizon, litter, depth of bare roots, percentage of prairies in the catchment, second-growth forest, forest in the riparian zone, barelands, stands with a mosaic of second-growth and mature forest, and mature forest with open canopy.

Table 3.2. Selected catchment attributes.

Category	**Metrics and description**	**Units**
Land use/cover (n=10)	Pastures	% catchment
	Second Growth Forest (SG_Forest)	Ha
	Riparian Alpine Zone (Rip_Alpine)	% riparian zone
	Mature Forest, dense canopy (Mature_Forest_DC)	Ha
	Mature Forest, open canopy (Mature_Forest_OC)	Ha
	Bareland	% catchment
	Mature & Second Growth Forest (Mature_SG_Forest)	% catchment
	Riparian Forest (Rip_Forest)	% riparian zone
	Wetland	% catchment
	Over Treeline Wetland (OT_Wetland)	% catchment
Soil (n=11)	Depth mineral soil (HA)	cm
	Depth organic soil (H0)	cm
	Depth litter (Litter)	cm
	Depth bare roots (Bare_Roots)	cm
	Potasium (K)	ppm
	Nitrogen (N)	ppm
	Sodium (Na)	cmol (+) / kg
	Sulfur (S)	ppm
	Phosphorus (P)	ppm
	Effective cation-exchange capacity (CICE)	
	Organic matter (OM)	%
Richness (n=2)	Macroinvertebrate (Macro_Inv)	count
	Vascular_Flora	count
Topography (n=4)	Range_Elevation (Range_Elev)	m
	Slope	%
	Max_Elevation (Max_Elev)	m a.s.l.
	Area	ha
Climatic (n=2)	Precipitation	mm/year
	Solid fraction precipitation (Snow)	mm/year

3.3.3 Influences of catchment attributes into seasonal dynamics of hydrologic indicators

Predictive analysis was done to determine the most important attributes (table 3.2) that condition each daily indicator (table 3.3). In detail, a Random Forest model (RF) was built for each daily hydrology indicator. Additionally, a Spearman correlation was elaborated to identify the correlation direction of those attributes most important in each RF.

3.3.3.1 Exploratory analysis of seasonal dynamics through Spearman correlation

The Spearman correlation between catchment attributes and hydrology indicators showed relevant exploratory results (figure S.3.2). First, climate attribute as precipitation positively affects the flows in winter (July to September), as expected, and also in summer (January and February). Besides, the annual precipitation affects the positive pulses (High.pulse.number and Rise.rate) and anticipates the day of the year with 25% flow (Day.25%.Q). Additionality, the solid fraction of precipitation (Snow) positively influences the November caudal and the high flows (Q80 and Q90), showing the effects of nival freshet. Thus, snow provides information on those catchments with a nival regime, while annual precipitation is related to rain-fed catchments.

Second, in the case of land use/cover attributes, the duration of high pulses is longer in those catchments with more area of mature forest with open canopy (Mature_Forest_OC) than those with more canopy cover (Mature_Forest_DC). Furthermore, the catchments with a higher proportion of bare land (Bareland) have more significant negative differences between consecutive daily values (Fall.rate), which is related to a decrease in the number of high pulses (High.pulse.number) and rises (Rise.rate). On the other hand, a high proportion of bare land delays the day where it is discharged the quarter of annual caudal (Day.25%.Q).

Regarding soil attributes, two elements have a massive correlation with hydrology indicators (figure S.3.2). The first is sulfur (S), where high values of this element were significant with higher

values of the hydrological signature. Otherwise, phosphorus (P) has a negative relation with most indicators. In detail, catchments with higher concentrations of P were related to lower flows in summer (January and February). However, these higher concentrations of P were positively significant with the day of the year with 25% flow (Day.25%.Q), bringing forward the date and producing the opposite effect of sulfur. Besides, the catchments with fewer concentrations of P had a lower number of high pulses (High.pulse.number) and rises (Rise.rate); instead, these catchments had a higher rate of falls (Fall.rate). The litter depth (Litter) negatively correlated with some hydrologic signals associated with low flows (1.day.min, 10.day.min, Q10, and Minimum.baseflow). On the other hand, the bare-roots depth (Bare_Roots) positively correlated with most indicators associated with the magnitude of monthly water conditions. Also, these catchments presented higher values of low flow indicators (3- 7- 10- 30- and 90.day.min, Q10, and Q25). The effective cation-exchange capacity (CICE) was negatively correlated with the monthly stream flows of March, April, and November. Also, higher values de CICE were related to lower extreme condition values (90.day.min, Q25, Q80, Q90, and 25%.75%.Q.duration) and with a reduction of low pulse numbers (Low.pulse.number).

Topographic attributes presented diverse effects on correlations (figure S.3.2). First, those catchments with a higher mean slope (Slope) had lower values in indicators associated with high flow conditions (1- 3- 7- 30- and 90.day.max and Q90) and with the base flow (Mean.daily, Baseflow.volume, Mean.baseflow, and Maximum.baseflow). Second, the catchments with higher elevation ranges (Range_Elev) showed a positive correlation with some monthly flow indicators (April, July, August, September, January, and February), with low extreme condition indicators (30- and 90.day.min, Q10, and Q25), with more flat hydrology cycles (25%.75%.Q- and BF.duration), and with the number of high pulses and rises (High.pulse.number and Rise.rate). Otherwise, higher values of range elevation were negatively correlated to the date with the 25% of

total flow (Day.25%.Q), with the baseflow index, the duration in days of low (Low.pulse.duration) and high pulses (High.pulse.duration), and with the falls (Fall.rate). Finally, the maximum elevation (Max_Elev) and the size of the catchments (Area) had no important correlation with the hydrological signature. The flow normalization by the catchment size could be the reason for the no correlation with the area, which translates into the possibility of comparing all the basins. Notably, none of the two richness attributes (Vascular_Flora and Macro_Inv) were significantly correlated to the hydrological signature. Thus, implies that these bioindicators could be not work very well as predictors of watershed processes.

3.3.3.2 Predictive analysis of seasonal dynamics through Random Forests models

The global results of the Random Forests models (RF) showed a lower explanation of the hydrological signature. Still, some specific attributes had a highlighted performance (warmest colors), while others depreciated the models (colder colors) (figure 3.6). Each column in figure 3.6 represents the results of one random forest model composed of 1000 trees, where the catchment attributes are the predictors, and each hydrology indicator is the response. As expected, the first cluster of predictors (Cl. 1) included the annual precipitation (Precipitation) being one of the most important predictors of the hydrological signature (warmer colors), explaining monthly responses (April to September) and extreme conditions (high and low), and some base flow signals. Besides, in almost every hydrological indicator, the high predictive performance of phosphorus in the soil (P) could be strongly related to Andosol diagenesis, a regional characteristic of the 12 catchments.

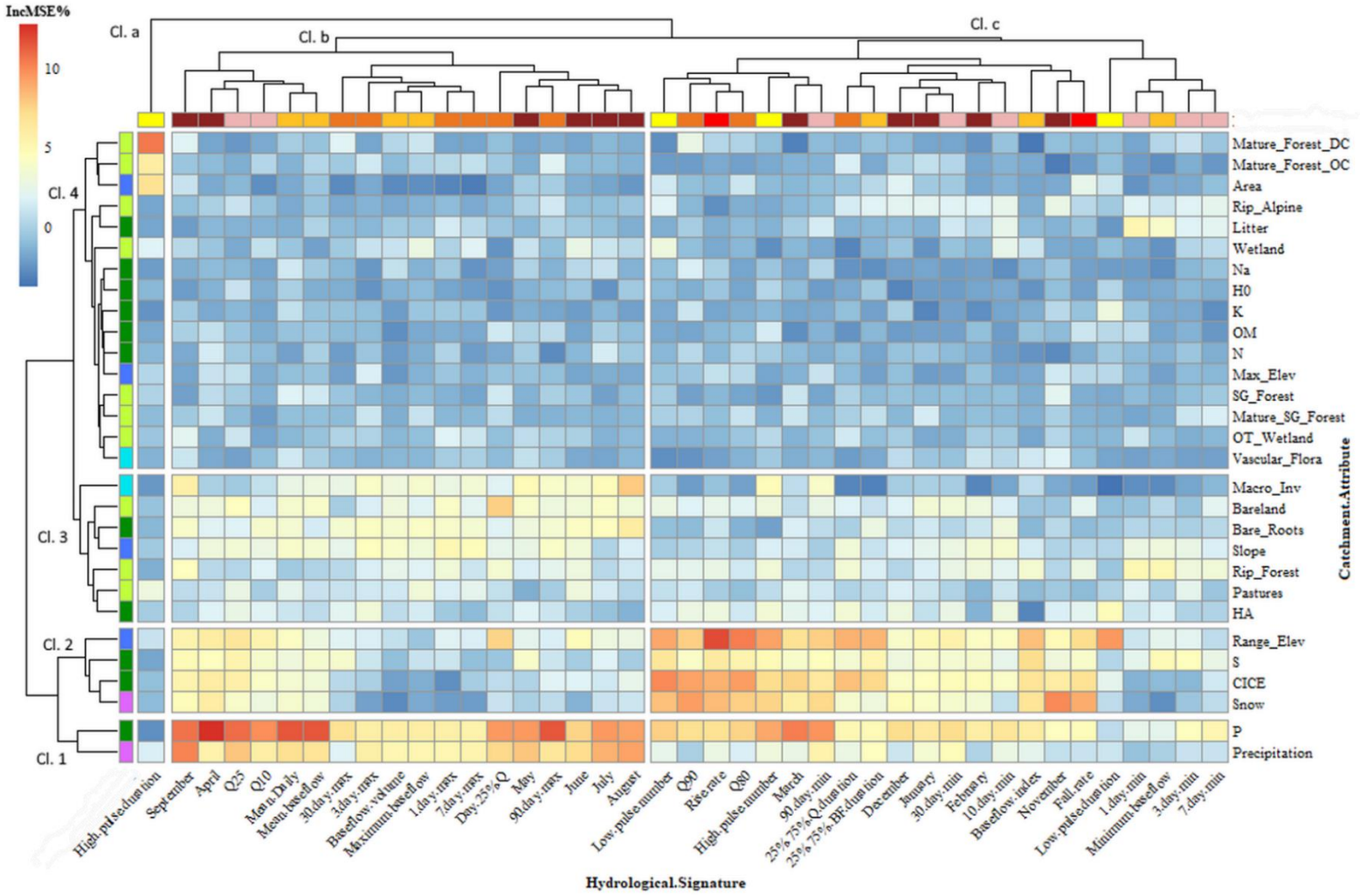

Figure 3.6. *Random forest predictive results with hydrological signatures as responses and catchment attributes as predictors. The influence of each attribute is measured using the "percentage of increase mean square error" (IncMSE%). Cold colors indicate a negative or null impact of predictors. Warm colors show an essential effect of predictors. More details about the variables are shown in the methods.*

The second cluster in performance prediction (Cl. 2) was composed of solid precipitation (Snow), the effective cation-exchange capacity (CICE), sulfur (S), and the range of elevation (Range_Elev) (figure 3.6). This group of attributes predicts very well the spring and summer months (September to April), those responses related to the number of pulses (Low- and High.pulse.number), rates (Rise- and Fall.rate), extreme flow quantiles (Q10, Q25, Q80, and Q90), several indicators associated with flowing duration curve (25%.75%.Q- BF.duration, 10- 30- and 90.day.min), and also with base flow signal (Mean.Daily- and baseflow, and Baselow.index). In summary, the first cluster of attributes (Cl. 1) could explain those catchments with a pluvial regime, and the second group of predictors (Cl. 2) is associated with nival regimes.

In addition to the first two environmental clusters, a third group of attributes (Cl. 3) related to land use-cover, soil, topography, and richness categories was significant in several random forest models. The percentage of bare lands (Bareland) was a relevant attribute with monthly caudal, specifically between April to February, also with the first quarter of flow (Q25 and Day.25%.Q), some base flow indicators (Mean.Daily- and baseflow), and with high flows signals (1- 7- and 90.day.max). Following land use/cover attributes, the forest percentage in the riparian zone (Rip_Forest) was associated with better predictions in low flows (1- 3- 7- 10- and 30.day.min, February, and Minimum.baseflow) being one of the best predictors for this kind of signals with a negative direction (see figure S.3.2). The bare-roots depth (Bare_Roots) was a good predictor (positively) of caudal for winter months (April to September), high flows (1- 3- 7- 30- and 90.day.max), and base flow signals (Mean.Daily, Baseflow.volume, and Maximum.baseflow). Furthermore, another soil attribute, mineral soil depth (HA), was necessary for the pulse and rate indicators (High.pulse.number, Low.pulse.duration, and Rise.rate). The slope was an essential predictor (negatively, see figure S.3.2) for some hydrology indicators distributed in almost every category. Macroinvertebrate richness was a fair predictor for caudal in winter's months (May to

September), high flows (1- 3- 7- and 90.day.max), and base flow indicators (Mean.Daily, Mean.baseflow, Baseflow.volume, and Maximum.baseflow). The remaining attributes (Cl. 4) had a low capacity to predict the hydrologic signature except for Litter associated with low flows (1.day.min and Minimum.baseflow).

On the other hand, clusters for the responses, i.e., the hydrology indicators, were identified. A group was related to conditions associated with a pluvial regime (Cl. b). Also, some signals had a relation with a nival regime (Cl. c), but there was an individual signal with no association, the duration of high pulses (High.pulse.duration; Cl. a) (figure 3.6). The latter indicator was predicted by three attributes associated with the superficies of mature forests with open and dense canopy coverage (Mature_Forest_OC and Mature_Forest_DC) and the size of the catchment (Area).

3.3.3.3 Predictive analysis of event dynamics using sub-daily signals

Sub-daily indices produce a much-reduced list, hence correlation among hydrologic indicators was not deemed necessary (See figure 3.4). The amplitude (AMP) of the reference catchments was higher than the impacted catchments (IMP1 and IMP2) in all the sited. For example, the amplitude of the reference catchment in the General Carrera site was an order of magnitude higher than the impacted catchments. Similarly, the maximum flow fluctuation rate (MAFR) and the mean flow fluctuation rate (MEFR) showed the same pattern, where the reference catchment presented higher values. Finally, the flow ratio (RATIO) gave notorious differences for those Imp1 catchments (figure 3.7).

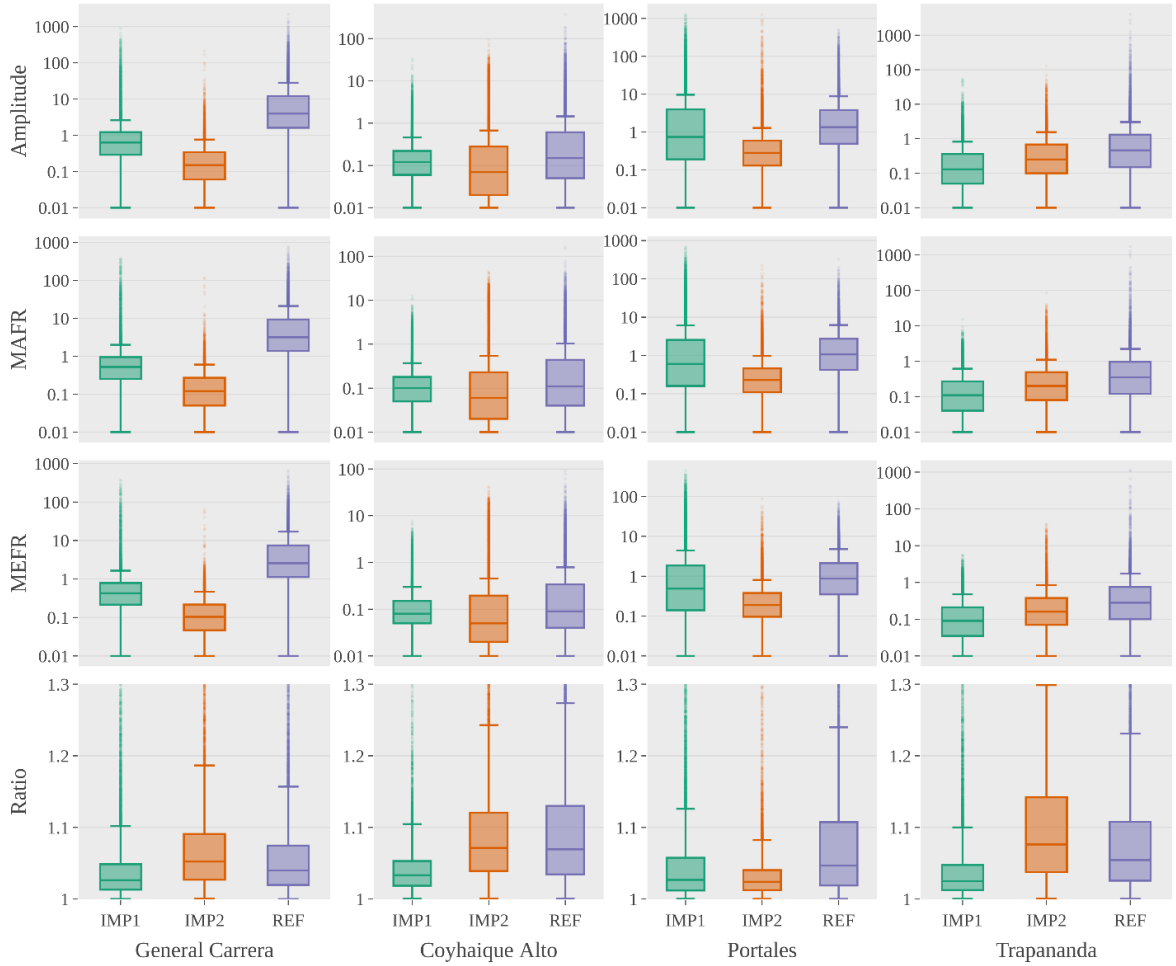

Figure 3.7. *Characterization of sub-daily flow fluctuations for all the catchments during the hydrological years 2020-2022. The variables analyzed were maximum flow fluctuation rate (MAFR), mean flow fluctuation rate (MEFR), amplitude (AMP), and flow ratio (RATIO). The y-axis is in log-scale except for the ratio.*

Because every site presents differences in climate (precipitation and temperatures), geomorphology, soil, etc., the LMM and GLMM have a nested structure that allows comparing the treatment in each site. Here the treatment is an observational analysis of a gradient of LUC (Ref to Imp). In every model, significant fixed effects of impacts were relevant for the sub-daily responses. Besides, almost every contrast between the control catchment (Ref) and the catchments with more human activities (Imp1 and Imp2) was significant (table 3.3). In particular, the duration

of sub-daily flow fluctuations (DUR) showed higher differences between the reference and the impacted catchments.

Table 3.3. Probabilistic statistics, log-likelihood (logLik), and contrast of fixed-effects results from the linear mixed models (LMM) and generalized linear mixed-effects (GLMM) models calculated for maximum flow fluctuation rate (MAFR), mean flow fluctuation rate (MEFR), amplitude (AMP), flow ratio (RATIO), and duration (DUR), as responses.

Response	*AIC*	*BIC*	*logLik*	*Contrast*	*p-value*	
MAFR	1393487	1393619	-696731	Imp1 - Ref	0.039	*
				Imp2 - Ref	0.028	*
MEFR	1352846	1352978	-676411	Imp1 - Ref	0.041	*
				Imp2 - Ref	0.035	*
AMP	1484671	1484803	-742323	Imp1 - Ref	0.035	*
				Imp2 - Ref	0.020	*
RATIO	2414245	2414322	-1207116	Imp1 - Ref	<0.001	***
				Imp2 - Ref	0.080	
DUR	1439390	1439456	-719690	Imp1 - Ref	<0.001	***
				Imp2 - Ref	<0.001	***

Note: AIC, Akaike information criterion; BIC, Bayesian information criterion; logLik, log-likelihood; MAFR, maximum flow fluctuation rate; MEFR, mean flow fluctuation rate; AMP, amplitude of flow fluctuations; RATIO, flow RATIO; DUR, duration of flow fluctuations.

3.4 DISCUSSION

3.4.1 Hydrology signature as a characterization of watershed processes

Richter et al. (1996) presented the indicators of hydrology alteration (IHA) as assessing the degree of change attributable to human influence within an ecosystem. However, the IHAs and EFC (Richter et al., 1997) can also read natural differences between rivers as watershed processes (McMillan, 2021). Thanks to the RF, the grouping responses showed two clusters of indicators that translate to rain-fed and snow-fed catchments (figure 3.6). First, the rain-fed catchments were associated with higher annual precipitation, especially in winter (April to September). Additionally, low flow indicators (Q10, Q25, and Day.25%.Q) with more significant magnitudes were clustered (Cl. b, in figure 3.6) to pluvial catchments. For example, catchments with high

annual precipitation brought the day forward for the first 25% of the flow. Second, every indicator associated with high flows (1- 3- 7- 30 -90.day.max) was grouped with rain-fed rivers. Finally, base flow indicators with more significant amounts were related to pluvial catchments.

On the other hand, another critical attribute of the RF was the solid fraction of precipitation (Snow). The cluster of indicators related to snow-fed rivers (Cl. c, in figure 3.6). However, snow and total precipitation better represented the hydrology regime. These snow-fed rivers were associated with lower monthly flows in summer (December to March). Additionality, a higher annual solid precipitation predicts higher flows for November, indicating the effect of melting snow. Likewise, every indicator associated with low flows (1- 3- 7- 10- 30- 90.day.min, baseflow.index, minimum.baseflow) was grouped with nival catchments. The snow-fed catchments had lower elevation ranges, explaining this attribute's importance in defining a hydrological regime. The peak of snow melting generated a less flat flow curve, with fewer days for the center of flow volume (25%.75%.Q.duration and 25%.75%.BF.duration), indicators highly correlated with narrower elevation ranges. Lower values of pulses and rate indicators were associated with snow-fed rivers, specifically with less annual rain and catchments with lower values of elevation ranges.

Thus, it is possible to identify associations of hydrology indicators with different fed regimes. But, how we can detect changes in watershed processes product of LUC?. McMillan (2021) presented that climate descriptors have a higher predictive power, while catchment attributes provide little predictive power for hydrology signature. Our results, showed a similar patron where precipitation and snow were the most crucial predictors in RF for almost every hydrology indicator (figure 3.6). In addition, some topographic attributes, such as range of elevation and slope, were important in the prediction. These attributes are related directly to site conditions, thus with climate, that divides two different ecosystems, deciduous forests in the east and evergreen forests

in the west. On the other hand, chemical soil predictors such as phosphorous, sulfur, and CICE were strong but possibly interpreted different and unique processes associated with Andosols diagenesis. However, some attributes related to LUC showed a superior predictive power, such as depth of mineral soil (HA), percentage of pastures in the catchment (Pastures), percentage of forest inside of riparian zone (Rip_Forests), depth of bare roots (Bare_Roots), percentage of bare lands (Bareland), and hectares of mature forest with open- and dense canopy (Mature_Forest_OC and Mature_Forest_DC). HA, Bare_Roots, and Bareland are predictors associated directly with soil loss (erosion process), thus, less water storage capacity. However, the effect's causation is unclear because, for example, bare roots depth is more correlated with precipitation (climate signal) than a LUC effect in Imp1 or Imp2 catchments (table S.3.3 and figure S.3.2).

On the other hand, mature forests with open- and dense canopies were essential in the number of days of high pulses (High.pulse.duration, see figure 3.6). Therefore, these predictors could explain evapotranspiration (ET) effects. Furthermore, these predictors present higher differences between references and impacted catchments (table S.3.3). In summary, the possibility of finding causations of LUC in seasonal dynamics was weak. Still, some specific hydrology indicators associated with ET could indicate that the temporal analysis scale is lower.

Following the idea of shorter temporal scale, the event dynamics analyses (sub-daily scale) were satisfactory for detecting differences between reference catchments and impacted ones (table 3.3). These impacted catchments showed lower daily fluctuations (AMP, MAFR, MEFR, and RATIO; figure 3.7). AMP of the diel fluctuations, which is higher in the reference than the impacted watersheds (figure 3.7), is consistent with the interpretation that the diel flow amplitude (Qmax – Qmin) is a measure of evapotranspiration, and the reference watersheds have more forest, which evapotranspire more than other land cover types.

Assuming the same precipitation in each site (table S.3.3) and a similar groundwater flow, the differences in runoff are related to evaporation, transpiration and soil water storage (eq. 1) (Asbjornsen et al., 2011).

$$PP = ET + R + S + D; \text{ where } ET = I + E + T \quad (1)$$

where "PP" is precipitation, "ET" is evapotranspiration, "R" is runoff, "S" is the soil water storage, "D" is the groundwater flow, "I" is the vegetation canopy interception, "E" is the soil evaporation, and "T" is plant transpiration. The references catchments have a higher transpiration and interception as was mentioned before but at the same time have a higher rate of water storage. Instead, impacted catchments had more erosion with less volume soil, thus lower storage capacity. Impacted catchments had less vegetation implying less interception and transpiration. Hence, the only variable to reduce flow fluctuations in impacted catchments is evaporation provoked by the exposition of soils with no coverage due to anthropogenic impacts, such as forest fires, clear cutting, and cattle breeding.

The latter is confirmed by the flow duration curves (FDC) of 8 catchments (figure 3.3). Overall, the reference catchments showed more discharge than the corresponding impacted ones, explained by lower evaporation rates. For example, the flows in reference catchments were notorious higher in Trapananda and Carrera sites, indifferently of the magnitude, i.e., high or low flows. Imp1 catchments (Trapananda and Carrera sites) have high percentages of second-growth forests, pastures, and bare land coverages. In the Portales site, the discharge of the reference catchment was slightly higher 85% of the time compared to the impacted. The similarity between FDCs in Portales must be because, in high-rainfall regions, E represents a much smaller fraction of PP (Asbjornsen et al., 2011). On the contrary, the Coyhaique Alto site is a water-limited ecosystem, especially in summer. The impacted catchment presented higher low-flows 60% of the time but

lowered magnitudes in high-flows. Hence, in those months with enough rain or snow melting, high evaporation was the cause of lower runoff in the impacted catchment. Conversely, under drier conditions, vegetation interception and transpiration were crucial factors provoking that the reference catchment, with more forest coverage, had a lower water yield.

As expected, higher amplitudes of daily fluctuation (AMP) in reference catchments were associated with longer rise or fall pulse duration time (DUR). Thus, evaporation not only smooths flow peaks but also shortens the duration of the fluctuations. As a result, duration is a good indicator to identify changes in the sub-daily hydrology due to anthropogenic impacts.

Therefore, it is possible to conclude that both seasonal and event dynamics approaches are sensitive to the effects of impacts in headstreams for early detection (short time series). However, elaborating the hypotheses and specific analyses must focus on shorter temporal scales and comparing climate with particular land use, for example, a high percentage of alpine zones in evergreen ecosystems.

3.4.2 Identification of hypotheses for specific effect of LUC in hydrology signals

After determining which catchment attributes have a high correlation or are good predictors, with some hydrology indicators are necessary to define possible causalities with specific hypotheses. Therefore, to identify the effects of LUC on hydrology signature, it is not required to include biogeochemical variables, such as sulfur, phosphorus, or cation exchange capacity, or ecological variables, such as vascular or macroinvertebrates richness, as explanatory variables for hydrology because they cannot be causes of streamflow quantity and timing. However, these variables could cover other kinds of hypotheses, e.g., biogeochemical cycles in Andosols soils or the development of bioindicators as monitoring of degradation processes in the watersheds.

The hypotheses for futures researches could be grouped by time scale, i.e., annual time scale, dry season, wet season, and event dynamics. In an annual time scale the hypotheses could be related with the annual runoff ratio (Q/P), specifically if is positively affected to 1) the percentage of non-forest cover, basal area, or canopy coverage, incorporating sub-hypotheses about interception, evaporation and transpiration; 2) the percentage of alpine zone, allowing questions about correlation with solid precipitation and if bare rock does not store water; 3) the percentage of wetland area, studying if type of land use transmit most incoming precipitation; 4) the percentage with flat zones (slope) associated with better condition for harvesting, among others.

In the case of dry season, the hypotheses could be focused with dry season flow (Q10), low flow duration, or dry months runoff ratio (Q_d/P_d), i.e., from December to March, positively related to 1) precipitation in previous 6-9 months, observing if the water is stored in soil and subsoil; 2) solid precipitation in previous 6-9 months, studying if water is stored in snowpacks and released during snowmelt or after; 3) the percentage of forest cover or basal area, where forest infiltration enhance storage for the dry season; 4) the percentage of alpine zone, associated with an enhanced of snow accumulation and delayed melt, contributing to subsurface storage and dry-season release of water; 5) the percentage of wetland area, studying how is capable this land use to sustain dry season streamflow; 6) the litter depth, because litter may enhance infiltration and subsurface moisture storage, which contributes to dry season low flows. Similar hypotheses could be studied for wet season streamflow.

The results for event dynamics showed marked differences between impacted and reference catchments. However, it is necessary to develop specific studies to understand the causes of these significant differences. For example, to test directly how the amplitude (AMP) of the diel flow, exclusively on sunny days, which may be a measure of evapotranspiration, is related to the percentage of type of forest (deciduous versus evergreen), forest cover, forest cover with open

canopy, or basal area. Besides, it is possible to use sub-daily indicators known as phases incorporating flows and temperatures to address how land use/cover percentages affect evapotranspiration. Finally, hypotheses can be focused on the peaks recession shape (McMillan, 2021) to identify the causation between impacts and evapotranspiration, soil water storage, and runoff.

3.4.3 How to define a safe operating space in watersheds through an early detection impacts on headstream

Long time series for headstream with a sub-daily time interval are scarce. Commonly, decades series are associated with big rivers on records done by governmental institutions. Besides, these registers are daily with no option to observe immediate changes due to high-intensity precipitation. The problem with short-time flow series is the difficulty of eliminating climate variability in the hydrology signature when the goal is to detect alteration by human impacts. A method to avoid misinterpreting anthropogenic impacts due to climate anomalies is not to use parametric statistics as the mean. Instead, the median, a non-parametric statistic, is a better estimate of the central tendency when the number of observations is reduced. Also, to identify, as random effects or/and blocking structure, the other sources of variability associated with climate anomalies are recommended.

The framework of this methodology is associated with headstreams where the impacts are on the catchments, especially LUC, but not in the stream as a dam. Also, these are catchments with no or shallow effects, close to the impacted ones. Headstream monitoring is essential because these small rivers not only represent a high percentage of a hydrologic network but also are fragile ecosystems (Máčka et al., 2023). However, reaching the highlands is not simple, provoking fewer monitoring sites with short temporal scales. Therefore, the studies on headwater catchments have

fewer monitoring sites than those with big rivers. As a result, several statistical analyses are impossible because they need more locations than parameters, e.g., multivariate analysis, linear models, boosted regression trees, etc. However, an excellent alternative is the random forest model, where it is possible to have the advantages of bagging. Besides, it is possible to assume the out-of-bag as a prediction error because, with small datasets, it is impossible to divide the sites for training and testing. In addition, random forests allow selecting a subset of parameters in each decision tree, facilitating the possibility of working with fewer sites.

In the best scenario, our study has six years of monitoring but only five hydrology years. The latter provokes a series with seasonal dynamics of five registers, one value by hydrologic year. Thus, a year anomaly greatly influences the central tendency statistic, even if it is the median. Additionally, a reduced number of sites forces to decrease in the number of attributes in the random forest models. Hence, the dynamic event analysis (with sub-daily indicators) is preferable with fewer sites and shorter temporal scales. However, in this study, some daily indicators still showed a good correlation with attributes associated with LUC.

The selection of hydrology indicator schemes, daily and sub-daily, is flexible and depends on the objectives of each research. For example, Richter et al. (1996) identified a battery of daily hydrology indicators (IHA) associated with magnitude, time, duration, frequency, pulse, and rates. Also, develop daily indicators related to the type of flows called environmental flow components (EFCs) (Richter et al., 1997). These indicators require long time series over 20 years and even more but with accuracy to evaluate changes in the frequency and intensity of events which may have a disproportionate effect on ecosystems as the Pulse Shunt Concept (Raymond et al., 2016) and also risks to human communities. Furthermore, sub-daily indicators are associated with rise and fall during the day, incorporating frequency, magnitude, duration, and rates, among other characteristics (Bejarano et al., 2020; Bevelhimer et al., 2015; Dierauer et al., 2017; Greimel et al.,

2016). The sub-daily indicators seem to be very sensitive, i.e., to minute scale, but the state of monitoring often uses sample frequencies between 1 to 2 hours with a loss of information.

The connection between impacts and hydrology signatures must incorporate those catchment attributes that define a watershed as impacted. In other words, it is preferable to work with characteristics of the catchment than a categorization as impacted or reference. The watershed characteristics bring specific information associated with possible impacts but also related to climate, topography, soils, etc. (Addor et al., 2018). Therefore, our methodology as exploratory analysis is feasible for early detection that starts with including a significant number of attributes. Second, a selection of them must be made to avoid multicollinearity. A rule of thumb is select attributes with low correlation and fewer than triple the sites. Additionally, also is necessary to identify those hydrology indicators that better explain the variability in each area and with a relation to the response that wants to study.

The methodology employed in this study serves as a crucial tool for watershed classification based on their hydrological signature, particularly in areas where the impacts of land use change (LUC) are minimal. For instance, watersheds characterized by sparse vegetation or the presence of snow exhibit specific outputs as indicated by their respective indicators. Conversely, watersheds with lower elevations are primarily influenced by rain, which manifests in unique hydrology indicator characteristics. Thus, employing a supervised classification approach utilizing hydrological indicators identified through this study's methodology becomes essential for basin management and planning, using threshold values or specific criteria to avoid intuitive decision-making. The limited influence of LUC in the Patagonia region enables detailed planning, as it possesses considerable conservation potential and opportunities for restoration where human activities have had minimal impact on the hydrological behavior of streams.

3.5 CONCLUSIONS

The hydrologic signature is highly influenced by climate descriptor as precipitation and snow, while catchment characteristics provide little predictive power. However, hydrology indicators for seasonal dynamics, i.e., daily indicators, in headwater catchments showed relatively good performance in identifying some relations between LUC and flows. But, an early prediction for short-term datasets, in our study with five hydrologic years, is still insufficient. With LUCs more recent and extensive, some flow signals could probably be more marked.

One of the essential effects of LUC is the changes in evapotranspiration on watersheds affecting the flows. The hydrology indicators associated with event dynamics, i.e., sub-daily indicators, showed a high performance in detecting the difference between impacted and reference watersheds. Thus, to see changes in streams with few monitoring years, sub-daily indicators were much more sensitive.

The methodology of this study allows for finding a strong correlation and predictive power between catchment attributes and hydrology signatures. However, some correlations are not associated with causation, e.g., biogeochemical variables do not cause effects in streamflow magnitude, pulse, and timing. But these findings could be the base for new hypotheses on watershed processes and water quality.

The application of a supervised classification approach utilizing hydrological indicators identified through the methodology of this study emerges as a crucial necessity for effective basin management and planning. By incorporating the identified hydrological indicators into the classification process, stakeholders can enhance their understanding of the basin's hydrological characteristics and make well-informed decisions that promote sustainable water management and optimize resource allocation within the basin.

Future work must be included the water quality characteristics, typically shown as flow dependence of concentration (Q:C, power function effect of dilution, production, or neutrality). Results based on hydrology versus watershed attributes suggest some potentially unexplored applications of water quality dynamics with daily or sub-daily hydrologic indicators.

3.6 ACKNOWLEDGEMENTS

We thank the members of field measurements team, especially to Yall Asenie, Daniela Bertens, Roberto Naranjo, Rodrigo and Omar Mancilla. This research was primarily funded by FONDECYT 11140495, additional support was granted by the Chilean Fondo de Investigación de Bosque Nativo (FIBN 033/2019), Laboratorio Ecoclimático (ANID R17A10002) and PATSER (ANID R20F0002).

3.7 LITERATURE CITED

Abell, R., Thieme, M. L., Revenga, C., Bryer, M., Kottelat, M., Bogutskaya, N., Coad, B., Mandrak, N., Balderas, S. C., Bussing, W., Stiassny, M. L. J., Skelton, P., Allen, G. R., Unmack, P., Naseka, A., Ng, R., Sindorf, N., Robertson, J., Armijo, E., . . . Petry, P. (2008). Freshwater Ecoregions of the World: A New Map of Biogeographic Units for Freshwater Biodiversity Conservation. *BioScience*, *58*(5), 403-414. https://doi.org/10.1641/b580507

Aceituno, P., Boisier, J. P., Garreaud, R., Rondanelli, R., & Rutllant, J. A. (2021). Climate and Weather in Chile. In B. Fernández & J. Gironás (Eds.), *Water Resources of Chile* (pp. 7-29). Springer International Publishing. https://doi.org/10.1007/978-3-030-56901-3_2

Addor, N., Nearing, G., Prieto, C., Newman, A. J., Le Vine, N., & Clark, M. P. (2018). A Ranking of Hydrological Signatures Based on Their Predictability in Space. *Water Resources Research*, *54*(11), 8792-8812. https://doi.org/10.1029/2018WR022606

Aguayo, R., León-Muñoz, J., Garreaud, R., & Montecinos, A. (2021). Hydrological droughts in the southern Andes (40–45°S) from an ensemble experiment using CMIP5 and CMIP6 models. *Scientific Reports*, *11*(1), 5530. https://doi.org/10.1038/s41598-021-84807-4

Aguayo, R., León-Muñoz, J., Aguayo, M., Baez-Villanueva, O., Fernandez, A. Zambrano-Bigiarini, M., and Jacques-Coper, M. (2021). PatagoniaMet v1.0: A multi-institutional effort for an open hydrometeorological dataset in Western Patagonia (40-56ºS). *In review*.

Amann, B., Bertrand, S., Alvarez-Garreton, C., & Reid, B. (2022). Seasonal Variations in Fjord Sediment Grain Size: A Pre-requisite for Hydrological and Climate Reconstructions in Partially Glacierized Watersheds (Baker River, Patagonia). *Journal of Geophysical Research: Earth Surface*, *127*(2), e2021JF006391. https://doi.org/10.1029/2021JF006391

Asbjornsen, H., Goldsmith, G. R., Alvarado-Barrientos, M. S., Rebel, K., Van Osch, F. P., Rietkerk, M., Chen, J., Gotsch, S., Tobón, C., Geissert, D. R., Gómez-Tagle, A., Vache, K., & Dawson, T. E. (2011). Ecohydrological advances and applications in plant–water relations research: a review. *Journal of Plant Ecology*, *4*(1-2), 3-22. https://doi.org/10.1093/jpe/rtr005

Astorga, A., Moreno, P., & Reid, B. (2018). Watersheds and Trees Fall Together: An Analysis of Intact Forested Watersheds in Southern Patagonia (41–56° S). *Forests*, *9*(7), 385. https://doi.org/10.3390/f9070385

Astorga, A., Reid, B., Moreno, P., & Rojas, P. (2021). Donde nacen los ríos: cuencas de bosques prístinos en la Patagonia occidental austral. In J. C. Castilla, J. J. Armesto, & M. J. Martínez-Harms (Eds.), *Conservación en la Patagonia chilena: evaluación del conocimiento, oportunidades y desafíos.* (pp. 167-198). Ediciones Universidad Católica.

Astorga, A., Reid, B., Uribe, L., Moreno-Meynard, P., Fierro, P., Madriz, I., & Death, R. G. (2022). Macroinvertebrate community composition and richness along extreme gradients: The role of local, catchment, and climatic variables in Patagonian headwater streams. *Freshwater Biology*, *67*(3), 445-460. https://doi.org/10.1111/fwb.13853

Becerra-Rodas, C., Little, C., Lara, A., Sandoval, J., Osorio, S., & Nimptsch, J. (2019). The Role of Streamside Native Forests on Dissolved Organic Matter in Forested and Agricultural Watersheds in Northwestern Patagonia. *Forests*, *10*(7), 595. https://doi.org/10.3390/f10070595

Bejarano, M. D., García-Palacios, J. H., Sordo-Ward, A., Garrote, L., & Nilsson, C. (2020). A new tool for assessing environmental impacts of altering short-term flow and water level regimes. *Water*, *12*(10), 2913. https://doi.org/10.3390/w12102913

Bevelhimer, M. S., McManamay, R. A., & O'Connor, B. (2015). Characterizing Sub-Daily Flow Regimes: Implications of Hydrologic Resolution on Ecohydrology Studies. *River Research and Applications*, *31*(7), 867-879. https://doi.org/10.1002/rra.2781

Boisier, J. P., Alvarez-Garretón, C., Cepeda, J., Osses, A., Vásquez, N., & Rondanelli, R. (2018). *CR2MET: A high-resolution precipitation and temperature dataset for hydroclimatic research in Chile* https://ui.adsabs.harvard.edu/abs/2018EGUGA..2019739B

Castro, L., & Gironás, J. (2021). Precipitation, Temperature and Evaporation. In B. Fernández & J. Gironás (Eds.), *Water Resources of Chile* (pp. 31-60). Springer International Publishing. https://doi.org/10.1007/978-3-030-56901-3_3

Chen, H., Guo, S., Xu, C.-y., & Singh, V. P. (2007). Historical temporal trends of hydro-climatic variables and runoff response to climate variability and their relevance in water resource management in the Hanjiang basin. *Journal of Hydrology*, *344*(3), 171-184. https://doi.org/10.1016/j.jhydrol.2007.06.034

Chen, Y. D., Yang, T., Xu, C.-Y., Zhang, Q., Chen, X., & Hao, Z.-C. (2010). Hydrologic alteration along the Middle and Upper East River (Dongjiang) basin, South China: a visually enhanced mining on the results of RVA method. *Stochastic Environmental Research and Risk Assessment*, *24*(1), 9-18. https://doi.org/10.1007/s00477-008-0294-7

Cheng, J., Xu, L., Wang, X., Jiang, J., & You, H. (2018). Assessment of hydrologic alteration induced by the Three Gorges Dam in Dongting Lake, China. *River Research and Applications*, *34*(7), 686-696. https://doi.org/10.1002/rra.3297

Desmit, X., Thieu, V., Billen, G., Campuzano, F., Dulière, V., Garnier, J., Lassaletta, L., Ménesguen, A., Neves, R., Pinto, L., Silvestre, M., Sobrinho, J. L., & Lacroix, G. (2018). Reducing marine eutrophication may require a paradigmatic change. *Science of The Total Environment*, *635*, 1444-1466. https://doi.org/10.1016/j.scitotenv.2018.04.181

Dharmawardena, P., Thattil, R. O., & Samita, S. (2017). Scale independent principal component analysis and factor analysis with preserved inherent variability of the indicators. *American Journal of Theoretical and Applied Statistics*, *6*(2), 90-94.

Dierauer, J. R., Whitfield, P. H., & Allen, D. M. (2017). Assessing the suitability of hydrometric data for trend analysis: The 'FlowScreen' package for R. *Canadian Water Resources*

Journal / Revue canadienne des ressources hydriques, *42*(3), 269-275. https://doi.org/10.1080/07011784.2017.1290553

Donoso, C. (1993). Bosques templados de Chile y Argentina: variación, estructura y dinámica.

Donoso, P. J., Frêne, C., Flores, M., Moorman, M. C., Oyarzún, C. E., & Zavaleta, J. C. (2014). Balancing water supply and old-growth forest conservation in the lowlands of south-central Chile through adaptive co-management. *Landscape ecology*, *29*(2), 245-260. https://doi.org/10.1007/s10980-013-9969-7

ESRI. (2011). *Arc Hydro Tools Overview*. In ESRI Water Resources Team, Environmental Systems Research Institute.

ESRI. (2016). *ArcGIS Desktop: Release 10*. In Environmental Systems Research Institute.

Frêne, C., Armesto, J. J., Véliz, F., Alfaro, F. D., & Weathers, K. C. (2021). High-frequency monitoring of hydrological and biogeochemical fluxes in forested catchments of southern Chile. *Hydrological Processes*, *35*(5), e14175. https://doi.org/10.1002/hyp.14175

Garreaud, R., Lopez, P., Minvielle, M., & Rojas, M. (2013). Large-scale control on the Patagonian climate. *Journal of climate*, *26*(1), 215-230.

Greimel, F., Zeiringer, B., Höller, N., Grün, B., Godina, R., & Schmutz, S. (2016). A method to detect and characterize sub-daily flow fluctuations. *Hydrological Processes*, *30*(13), 2063-2078. https://doi.org/10.1002/hyp.10773

Hernández-Moreno, Á., Soto, D. P., Miranda, A., Holz, A., & Armenteras-Pascual, D. (2023). Forest landscape dynamics after large-scale fires in western Patagonia: evidencing surprising temperate forest recovery trends.

Hernandez, D., Mendoza, P. A., Boisier, J. P., & Ricchetti, F. (2022). Hydrologic Sensitivities and ENSO Variability Across Hydrological Regimes in Central Chile (28°–41°S). *Water Resources Research*, *58*(9), e2021WR031860. https://doi.org/10.1029/2021WR031860

James, G., Witten, D., Hastie, T., & Tibshirani, R. (2013). *An introduction to statistical learning* (Vol. 112). Springer.

Lara, A., Jones, J., Little, C., & Vergara, N. (2021). Streamflow response to native forest restoration in former Eucalyptus plantations in south central Chile. *Hydrological Processes*, *35*(8), e14270. https://doi.org/10.1002/hyp.14270

León-Muñoz, J., Aguayo, R., Marcé, R., Catalán, N., Woelfl, S., Nimptsch, J., Arismendi, I., Contreras, C., Soto, D., & Miranda, A. (2021). Climate and Land Cover Trends Affecting Freshwater Inputs to a Fjord in Northwestern Patagonia. *Frontiers in Marine Science*, *8*. https://doi.org/10.3389/fmars.2021.628454

Little, C., Lara, A., McPhee, J., & Urrutia, R. (2009). Revealing the impact of forest exotic plantations on water yield in large scale watersheds in South-Central Chile. *Journal of Hydrology*, *374*(1), 162-170. https://doi.org/10.1016/j.jhydrol.2009.06.011

Little, C., Soto, D., Lara, A., & Cuevas, J. G. (2008). Nitrogen exports at multiple-scales in a southern Chilean watershed (Patagonian Lakes district). *Biogeochemistry*, *87*(3), 297-309. https://doi.org/10.1007/s10533-008-9185-8

Ma, Z. Z., Wang, Z. J., Xia, T., Gippel, C. J., & Speed, R. (2014). Hydrograph-Based Hydrologic Alteration Assessment and Its Application to the Yellow River. *Journal of environmental informatics*, *23*(1). https://doi.org/10.3808/jei.201400252

MacArthur, R. H. (1957). On the relative abundance of bird species. *Proceedings of the National Academy of Sciences*, *43*(3), 293-295. https://doi.org/10.1073/pnas.43.3.293

Máčka, Z., Galia, T., Škarpich, V., Michalková, M. Š., & Krejčí, L. (2023). A method for assessment of sediment supply and transport hazard and risk in headwater catchments for

management purposes. *Environmental Earth Sciences*, *82*(1). https://doi.org/10.1007/s12665-022-10707-z

McMahon, T. A., Peel, M. C., Lowe, L., Srikanthan, R., & McVicar, T. R. (2013). Estimating actual, potential, reference crop and pan evaporation using standard meteorological data: a pragmatic synthesis. *Hydrology and Earth System Sciences 17*(4), 1331-1363. https://doi.org/10.5194/hess-17-1331-2013

McMillan, H. K. (2021). A review of hydrologic signatures and their applications. *WIREs Water*, *8*(1), e1499. https://doi.org/10.1002/wat2.1499

Millenium Ecosystems Assessment. (2005). *Ecosystems and Human Well-Being: Synthesis*. Island Press.

Milliman, J. D., & Farnsworth, K. (2011). *River Discharge to the Coastal Ocean – A Global Synthesis*. https://doi.org/10.1017/CBO9780511781247

Miranda, A., Altamirano, A., Cayuela, L., Lara, A., & González, M. (2017). Native forest loss in the Chilean biodiversity hotspot: revealing the evidence. *Regional Environmental Change*, *17*(1), 285-297. https://doi.org/10.1007/s10113-016-1010-7

Olden, J. D., & Poff, N. L. (2003). Redundancy and the choice of hydrologic indices for characterizing streamflow regimes. *River Research and Applications*, *19*(2), 101-121. https://doi.org/10.1002/rra.700

Oyarzun, C. E., Godoy, R., & Sepulveda, A. (1998). Water and nutrient fluxes in a cool temperate rainforest at the Cordillera de la Costa in southern Chile. *Hydrological Processes*, *12*(7), 1067-1077.

Perakis, S. S., & Hedin, L. O. (2002). Nitrogen loss from unpolluted South American forests mainly via dissolved organic compounds. *Nature*, *415*(6870), 416. https://doi.org/10.1038/415416a

Peres-Neto, P. R., Jackson, D. A., & Somers, K. M. (2003). Giving meaningful interpretation to ordination axes: assessing loading significance in principal component analysis. *Ecology*, *84*(9), 2347-2363. https://doi.org/10.1890/00-0634

Pizarro, R., García-Chevesich, P., Balocchi, F., Pino, J., Ibáñez, A., Sangüesa, C., Vallejos, C., Mendoza, R., Ingram, B., & Sharp, J. O. (2022). Comparative analysis of annual and monthly peakflow tendencies, considering two periods in north-central Chile Análisis comparativo de la tendencia de los caudales punta anuales y mensuales, para dos períodos en Chile. *Tecnología y ciencias del agua*,. https://doi.org/10.24850/j-tyca-13-5-3

Pyron, M., & Neumann, K. (2008). Hydrologic alterations in the Wabash River watershed, USA. *River Research and Applications*, *24*(8), 1175-1184. https://doi.org/10.1002/rra.1155

Raymond, P. A., Saiers, J. E., & Sobczak, W. V. (2016). Hydrological and biogeochemical controls on watershed dissolved organic matter transport: pulse-shunt concept. *Ecology*, *97*(1), 5-16. https://doi.org/10.1890/14-1684.1

Reche, P., Artal, O., Pinilla, E., Ruiz, C., Venegas, O., Arriagada, A., & Falvey, M. (2021). CHONOS: Oceanographic information website for Chilean Patagonia. *Ocean & Coastal Management*, *208*, 105634. https://doi.org/10.1016/j.ocecoaman.2021.105634

Reid, B., Astorga, A., Madriz, I., & Correa, C. (2021). Estado del conocimiento y conservación de los ecosistemas dulceacuícolas de la Patagonia occidental austral. In J. C. Castilla, J. J. Armesto, & M. J. Martínez-Harms (Eds.), *Conservación en la Patagonia chilena: evaluación del conocimiento, oportunidades y desafíos.* Ediciones Universidad Católica.

Richter, B. D., Baumgartner, J. V., Braun, D. P., & Powell, J. (1998). A spatial assessment of hydrologic alteration within a river network. *Regulated Rivers: Research & Management*

14(4), 329-340 https://doi.org/10.1002/(SICI)1099-1646(199807/08)14:4<329::AID-RRR505>3.0.CO;2-E

Richter, B. D., Baumgartner, J. V., Powell, J., & Braun, D. P. (1996). A Method for Assessing Hydrologic Alteration within Ecosystems. *Conservation Biology*, *10*(4), 1163-1174. https://doi.org/10.1046/j.1523-1739.1996.10041163.x

Richter, B. D., Baumgartner, J. V., Wigington, R., & Braun, D. (1997). How much water does a river need? *Freshwater Biology*, *37*(1), 231-249. https://doi.org/10.1046/j.1365-2427.1997.00153.x

Rosenqvist, A., Shimada, M., Ito, N., & Watanabe, M. (2007). ALOS PALSAR: A Pathfinder Mission for Global-Scale Monitoring of the Environment. *IEEE Transactions on Geoscience and Remote Sensing*, *45*(11), 3307-3316. https://doi.org/10.1109/TGRS.2007.901027

Ryberg Karen, R., Lin, W., & Vecchia Aldo, V. (2014). Impact of Climate Variability on Runoff in the North-Central United States. *Journal of Hydrologic Engineering*, *19*(1), 148-158. https://doi.org/10.1061/(ASCE)HE.1943-5584.0000775

Sauer, V. B. (2002). *Standards for the Analysis and Processing of Surface-Water Data and Information Using Electronic Methods* [Report](2001-4044). (Water-Resources Investigations Report, Issue. U. S. G. Survey. http://pubs.er.usgs.gov/publication/wri20014044

Silva, F., Ahumada, M., & Cerda, J. (1999). Guías de condición para los pastizales de la ecorregión templada intermedia de Aysén. *Subdepartamento de Divulgación Técnica, Servicio Agrícola y Ganadero*.

Stolpe, N. B. (2014). Clasificación de suelos de valles productivos de la Región de Aysén. In C. Hepp & N. B. Stolpe (Eds.), *Caracterización y propiedades de los suelos de la Patagonia occidental (Aysén)* (Vol. 298, pp. 53-76). INIA.

TNC. (2009). *Indicators of Hydrologic Alteration Version 7.1. User's Manual.* https://www.conservationgateway.org/Documents/IHAV7.pdf

Tolod, J. R., Negishi, J. N., Ishiyama, N., Alam, M. K., Rahman, M. A. T. M. T., Pongsivapai, P., Gao, Y., Sueyoshi, M., & Nakamura, F. (2022). Catchment geology preconditions spatio-temporal heterogeneity of ecosystem functioning in forested headwater streams. *Hydrobiologia*, *849*(19), 4307-4324. https://doi.org/10.1007/s10750-022-04992-9

Vandekerkhove, E., Bertrand, S., Reid, B., Bartels, A., & Charlier, B. (2016). Sources of dissolved silica to the fjords of northern Patagonia (44–48 S): the importance of volcanic ash soil distribution and weathering. *Earth Surface Processes and Landforms*, *41*(4), 499-512.

Veblen, T., Donoso, C., Kitzberger, T., & Rebertus, A. (1996). Ecology of southern Chilean and Argentinean Nothofagus forests. In T. Veblen, R. Hill, & J. Read (Eds.), *The ecology and biogeography of nothofagus forests* (pp. 293–353). Yale University Press.

Walsh, R. P. D., & Lawler, D. M. (1981). Rainfall seasonality: description, spatial patterns and change through time *Weather*, *36*(7), 201-208. https://doi.org/10.1002/j.1477-8696.1981.tb05400.x

Wang, D., & Alimohammadi, N. (2012). Responses of annual runoff, evaporation, and storage change to climate variability at the watershed scale. *Water Resources Research*, *48*(5). https://doi.org/10.1029/2011WR011444

Whittemore, R., & Ice, G. (2007). Models for evaluating water quality and BMP effectiveness at the watershed scale. *Water and Energy Abstracts*, *17*(2).

Zomer, R. J., Xu, J., & Trabucco, A. (2022). Version 3 of the Global Aridity Index and Potential Evapotranspiration Database. *Scientific data*, *9*(1), 409. https://doi.org/10.1038/s41597-022-01493-1

3.8 SUPPLEMENTARY MATERIAL

Table S.3.1. Seasonal metrics calculated for the 12 catchments.

Metrics	Category	Metrics and description	Units
Indicators of Hydrologic Alteration (IHA) proposed by Ritcher et al. (1996)	Magnitude of monthly water conditions (n = 12)	Median value for each calendar month	$m^3 s^{-1}$
	Magnitude and duration of annual extreme water conditions (n = 12)	Annual minima, 1-day mean	$m^3 s^{-1}$
		Annual minima, 3-day means	$m^3 s^{-1}$
		Annual minima, 7-day means	$m^3 s^{-1}$
		Annual minima, 30-day means	$m^3 s^{-1}$
		Annual minima, 90-day means	$m^3 s^{-1}$
		Annual maxima, 1-day mean	$m^3 s^{-1}$
		Annual maxima, 3-day means	$m^3 s^{-1}$
		Annual maxima, 7-day means	$m^3 s^{-1}$
		Annual maxima, 30-day means	$m^3 s^{-1}$
		Annual maxima, 90-day means	$m^3 s^{-1}$
		Number of zero-flow days	days
		Base flow index: 7-day minimum flow/mean flow for year	$m^3 s^{-1}$
	Timing of annual extreme water conditions (n = 2)	Julian date of each annual 1-day maximum	Julian date
		Julian date of each annual 1-day minimum	Julian date
	Frequency and duration of high and low pulses (n = 4)	Number of low pulses within each water year	Events (n)
		Median duration of low pulses	days
		Number of high pulses within each water year	Events (n)
		Mean or median duration of high pulses	days
	Rate and frequency of water condition changes (n = 3)	Rise rates: Median of all positive differences between consecutive values	$m^3 s^{-1}$
		Fall rates: Median of all negative differences between consecutive values	$m^3 s^{-1}$
		Hydrologic reversals	Events (n)

Note: Number of zero-flow days index was not was used.

Table S.3.2. Seasonal metrics calculated for the 12 catchments.

Metrics	Category	Metrics and description	Units
Environmental Flows Components (EFC) metrics proposed by Dierauer et al. (2017)	High flow	Annual maximum value	$m^3 s^{-1}$
		Julian date of each annual 1-day maximum	Julian date
		Peaks over threshold	Events (n)
		Inter-event duration	days
		80% flow quantile (Q80)	$m^3 s^{-1}$
		90% flow quantile (Q90)	$m^3 s^{-1}$
		Day of Year 25% Annual Flow	Julian date
		Center of Volume	Julian date
		Day of Year 75% Annual Flow	Julian date
		Duration between 25% and 75 % annual flow	days
	Low flow	10% flow quantile (Q10)	$m^3 s^{-1}$
		25% flow quantile (Q25)	$m^3 s^{-1}$
		Annual minimum flow	$m^3 s^{-1}$
		Mean annual minimum 7-day flow	$m^3 s^{-1}$
		Mean annual minimum 10-day flow	$m^3 s^{-1}$
	Base flow	Mean daily discharge	$m^3 s^{-1}$
		Annual baseflow volume	$m^3 s^{-1}$
		Annual mean baseflow	$m^3 s^{-1}$
		Annual maximum baseflow	$m^3 s^{-1}$
		Annual minimum baseflow	$m^3 s^{-1}$
		Mean annual baseflow index	unitless
		Day of year 25% baseflow volume	Julian date
		Center of volume baseflow	Julian date
		Day of year 75% baseflow volume	Julian date
		Duration between 25% and 75% baseflow volume	days

Note: Drought indexes from Dierauer et al. (2017) were not used because not presence of drought season found.

Table S.3.3. Topography, land use/cover, soil, richness, and climatic catchments attributes.

Site		*Coyhaique Alto*			*Trapananda*			*Portales*			*Carrera*		
Impact	Unit	Ref	Imp1	Imp2	Ref	Imp1	Imp2	Ref	Imp1	Imp2	Ref	Imp1	Imp2
Topography													
Area	ha	173.1	124.8	71.5	371.5	328.6	134.7	151.0	142.5	51.3	256.4	278.1	185.2
Max_Elevation	m a.s.l.	1390	1356	1355	1459	1285	1215	1332	1219	527	1553	1272	901
Min_Elevation	m a.s.l.	1061	1028	1055	1091	940	797	278	201	175	552	325	444
Mean_Elevation	m a.s.l.	1231.3	1233.1	1200.1	1275.4	1069.6	1032.9	849.3	783.7	329.4	1120.4	697	609.4
Median_Elevation	m a.s.l.	1236.3	1241	1204.7	1290.2	1061.3	1023.7	851.5	808.1	315.6	1160.8	667.9	587.8
Slope	%	168.3	200	177.9	284.1	195.2	278.4	169	104.7	105.4	91.3	70.8	124.8
Range_Elevation	m	329	328	300	368	345	418	1054	1018	352	1001	947	457
Land use/cover													
Mature Forest (Dense canopy)	ha (% catchment)	114.0 (65.9)	63.9 (51.2)	49.5 (69.3)	191.3 (51.5)	126.8 (38.6)	78.9 (58.6)	114.4 (75.7)	111.1 (78.0)	6.8 (13.3)	98.5 (38.4)	54.7 (19.7)	73.0 (39.4)
Mature Forest (Open canopy)	ha (% catchment)	3.3 (1.9)	17.6 (14.1)	8.9 (12.5)	5.3 (1.4)	0.0 (0.0)	1.4 (1.0)	0.0 (0.0)	6.5 (4.6)	6.4 (12.4)	0.0 (0.0)	8.1 (2.9)	0.0 (0.0)
Mature & Second Growth Forest	ha (% catchment)	0.0 (0.0)	0.0 (0.0)	0.0 (0.0)	8.3 (2.2)	124.6 (37.9)	11.2 (8.3)	0.0 (0.0)	2.0 (1.4)	0.0 (0.0)	0.0 (0.0)	0.0 (0.0)	0.0 (0.0)
Second Growth Forest	h ha (% catchment)	0.0 (0.0)	0.0 (0.0)	0.0 (0.0)	0.0 (0.0)	67.7 (20.6)	13.8 (10.2)	0.0 (0.0)	8.5 (5.9)	15.5 (30.2)	0.0 (0.0)	66.1 (23.8)	77.6 (41.9)
Wetland	ha (% catchment)	6.0 (3.5)	0.4 (0.3)	0.1 (0.1)	11.7 (3.1)	7.6 (2.3)	1.3 (1.0)	0.0 (0.0)	0.3 (0.2)	0.0 (0.0)	1.8 (0.7)	6.6 (2.4)	10.3 (5.5)
Over Treeline Wetland	ha (% catchment)	0.0 (0.0)	0.0 (0.0)	0.0 (0.0)	57.4 (15.5)	0.0 (0.0)	0.0 (0.0)	0.4 (0.3)	0.4 (0.3)	0.0 (0.0)	0.0 (0.0)	0.0 (0.0)	0.0 (0.0)
Bareland	ha (% catchment)	1.4 (0.8)	8.1 (6.5)	6.4 (9.0)	2.4 (0.6)	1.9 (0.6)	12.7 (9.4)	0.0 (0.0)	0.0 (0.0)	0.0 (0.0)	0.1 (0.0)	0.0 (0.0)	0.0 (0.0)
Pastures	ha (% catchment)	0.0 (0.0)	0.0 (0.0)	0.0 (0.0)	0.0 (0.0)	0.0 (0.0)	15.4 (11.5)	0.0 (0.0)	1.7 (1.2)	22.6 (44.1)	0.0 (0.0)	136.7 (49.1)	24.4 (13.2)
Alpine Zone	ha (% catchment)	48.4 (28.0)	34.8 (27.9)	6.5 (9.1)	95.2 (25.6)	0.0 (0.0)	0.0 (0.0)	36.2 (24.0)	12.0 (8.4)	0.0 (0.0)	156.0 (60.8)	5.9 (2.1)	0.0 (0.0)
Riparian zone													
Forest	% riparian zone	91.5	88.6	91.4	70.1	90.9	73.5	99.8	96.2	59.8	58.5	38.0	66.1

Wetland	% riparian zone	7.3	1.1	0.5	29.6	7.8	0.9	0.0	0.9	0.0	3.0	8.3	24.9
Bareland	% riparian zone	1.1	8.7	8.1	0.4	1.3	6.0	0.0	0.0	0.0	0.0	0.0	0.0
Pasture	% riparian zone	0.0	0.0	0.0	0.0	0.0	19.5	0.0	2.9	40.2	0.0	53.7	9.1
Alpine Zone	% riparian zone	0.1	1.6	0.0	0.0	0.0	0.0	0.2	0.0	0.0	38.4	0.0	0.0
Soil													
pH		6.3	6.4	6.3	6.3	6.1	6.4	5.3	5.4	5.4	5.4	5.5	5.2
N	ppm	5.8	8.7	12.4	8.4	14.5	8.5	20.3	8.5	218.8	10.8	25.5	58.5
P	ppm	23.9	21.1	66.3	20.5	54.4	36.6	5.0	4.2	7.3	6.8	12.5	12.9
K	ppm	167.1	194.4	221.4	134.2	262.9	222.9	226.0	156.4	353.4	128.8	187.3	257.8
S	ppm	5.8	5.2	7.5	6.1	5.6	1.9	7.9	8.6	6.5	14.1	10.6	5.6
Organic matter	%	10.0	11.0	17.1	14.8	26.8	14.1	35.8	21.2	42.7	17.3	31.6	38.3
Ca	cmol (+) / kg	4.4	5.4	7.7	4.9	12.4	9.2	2.6	1.2	10.9	0.6	2.9	7.3
Mg	cmol (+) / kg	1.3	1.7	1.8	1.2	3.2	2.0	1.0	0.6	2.3	0.3	0.7	1.5
K	cmol (+) / kg	0.4	0.4	0.5	0.3	0.6	0.5	0.3	0.3	0.8	0.3	0.4	0.6
Na	cmol (+) / kg	0.1	0.1	0.1	0.1	0.1	0.1	0.1	0.1	0.2	0.1	0.2	0.2
Al	cmol (+) / kg	0.1	0.0	0.0	0.0	0.1	0.0	0.4	0.8	0.1	1.1	0.8	0.7
CICE		6.2	7.6	10.1	6.6	16.4	11.8	4.4	3.1	14.2	2.4	5.0	10.4
SAT Al	%	1.8	0.4	0.4	0.7	0.3	0.3	8.9	26.7	0.5	41.1	16.3	11.2
Leaf_Litter	cm	1.3	0.7	1.8	1.1	2.4	1.1	2.0	1.0	0.8	1.0	1.0	2.2
Litter	cm	1.2	0.6	2.5	1.2	2.1	0.9	2.0	1.2	1.2	1.2	1.2	2.3
Organic soil (H0)	cm	6.3	7.6	4.2	4.8	8.3	3.3	26.9	3.0	14.3	7.1	9.0	20.2
Mineral soil (HA)	cm	>30	29.2	>30	26.5	>30	26.8	>30	19.7	>30	23.1	28.7	28.1
Depth_bare_roots	cm	7.1	13.0	5.5	6.7	10.4	10.1	16.2	21.8	23.7	10.4	9.0	8.9
Richness													
Macroinvertebrate	count	23	24	17	25	20	22	40	36	38	19	28	30
Vascular_Flora	count	25	16	4	31	19	26	24	12	29	12	24	23
Climatic													
Precipitation	mm/year	716.0	675.0	687.0	741.0	825.0	863.0	2458.0	2463.0	2666.0	2229.0	2283.0	2189.0

Seasonality Index (SI)	unitless	0.4	0.4	0.3	0.3	0.3	0.3	0.3	0.3	0.2	0.3	0.3	0.3
Annual mean temperature	° Celsius	4.4	4.1	4.4	4.1	5.1	5.5	4.4	5.5	7.2	3.0	5.7	7.4
solid fraction precipitation	mm/year	292.0	281.0	275.0	281.0	208.0	219.0	676.0	569.0	127.0	941.0	256.0	123.0
PETl	mm/year	735.0	757.0	758.0	710.0	751.0	768.0	699.0	730.0	794.0	649.0	728.0	767.0
AI	unitless	1.0	0.9	0.9	1.0	1.1	1.1	3.5	3.4	3.4	3.4	3.1	2.9

Table S.3.4. Indicators of Hydrologic Alteration (IHA). Magnitude of monthly water conditions (mm/s).

Basin	*Year*	*March*	*April*	*May*	*June*	*July*	*August*	*September*	*October*	*November*	*December*	*January*	*February*
CoyAlto Ref	2017	1.67	14.51	21.48	15.09	26.22	18.12	17.79	53.07	29.44	5.86	0.88	0.59
CoyAlto Ref	2018	0.63	2.40	3.63	4.02	2.80	2.71	35.43	50.70	58.32	2.77	0.68	0.37
CoyAlto Ref	2019	0.44	1.78	1.72	6.03	6.22	3.26	3.08	54.21	46.55	4.73	1.00	0.76
CoyAlto Ref	2020	0.56	0.74	8.10	10.50	3.47	3.13	5.54	82.56	35.46	2.79	0.58	0.30
CoyAlto Ref	2021	0.32	0.63	0.86	1.45	1.03	1.50	4.74	24.06	4.89	0.75	0.30	0.19
CoyAlto Imp1	2017	5.15	10.97	21.02	14.57	20.97	23.66	23.06	32.73	30.87	10.80	1.60	1.48
CoyAlto Imp1	2018	2.81	4.13	5.60	6.17	7.05	5.83	16.95	13.92	16.54	4.82	2.72	2.32
CoyAlto Imp1	2019	2.78	3.54	3.74	4.30	3.99	3.97	3.48	15.08	12.60	1.66	1.97	1.93
CoyAlto Imp1	2020	1.94	2.08	5.44	7.25	3.97	3.42	6.61	22.17	6.39	1.48	2.97	1.61
CoyAlto Imp1	2021	2.01	2.42	3.89	3.45	3.56	3.25	4.67	4.76	4.26	1.60	1.51	1.77
CoyAlto Imp2	2020	0.69	0.49	4.26	9.91	4.34	2.26	6.67	54.95	24.23	5.81	0.42	0.31
CoyAlto Imp2	2021	0.63	0.72	1.25	0.83	2.30	1.48	7.30	10.14	6.44	0.94	0.11	0.12
Trapa Ref	2017	0.96	9.19	18.35	11.69	16.32	13.71	10.60	64.57	32.60	4.15	1.03	0.54
Trapa Ref	2018	0.69	10.06	10.70	9.48	6.89	10.87	39.49	39.14	23.34	5.05	1.02	0.43
Trapa Ref	2019	0.41	1.24	3.82	9.91	7.96	7.69	6.98	30.12	12.36	4.39	1.70	1.43
Trapa Ref	2020	0.65	1.12	10.62	9.88	2.28	2.97	6.51	42.37	10.64	2.41	1.16	0.56
Trapa Ref	2021	0.50	0.74	1.37	6.45	5.92	7.32	17.06	11.35	5.07	1.23	0.36	0.25
Trapa Imp1	2017	0.55	2.83	11.38	11.01	22.67	40.42	31.38	75.94	16.99	3.59	0.50	0.36
Trapa Imp1	2018	0.61	2.49	3.02	3.80	3.96	7.98	35.76	29.74	21.33	12.92	4.37	0.35
Trapa Imp1	2019	0.52	1.10	1.65	3.49	3.66	5.81	8.62	15.00	7.04	3.22	1.33	0.85
Trapa Imp1	2020	0.55	1.12	2.82	4.13	2.77	3.75	7.41	22.15	8.27	2.66	0.86	0.09
Trapa Imp1	2021	0.09	0.38	1.18	2.46	2.97	3.91	5.83	5.37	4.06	1.15	0.22	0.00
Trapa Imp2	2020	1.64	1.52	2.78	7.29	4.45	6.40	8.69	16.13	7.39	3.42	2.13	1.13
Trapa Imp2	2021	0.83	0.73	0.80	6.54	4.18	2.94	4.04	3.29	2.66	1.86	1.01	1.08
Port Ref	2017	21.24	32.05	75.23	47.25	74.17	62.40	61.13	89.27	69.27	61.97	27.93	21.16
Port Ref	2018	64.13	104.77	58.97	43.44	36.23	63.55	114.77	120.07	95.30	29.97	29.65	7.21
Port Ref	2019	11.64	34.94	29.15	60.56	50.89	32.97	27.83	34.66	79.07	58.72	21.39	40.05
Port Ref	2020	23.12	60.59	127.81	56.37	5.29	32.46	42.19	68.08	65.95	22.51	52.64	2.88
Port Ref	2021	2.65	53.09	47.81	39.62	101.06	50.75	77.62	57.87	43.69	3.39	5.47	2.45
Port Imp1	2017	26.95	31.00	38.60	28.40	45.42	34.25	34.25	54.66	21.96	16.57	11.47	11.13
Port Imp1	2018	36.36	62.00	19.01	19.96	22.35	35.90	81.50	61.13	44.54	7.91	4.06	1.88

Port Imp1	2020	0.74	30.64	82.27	71.25	18.96	89.58	99.82	89.43	64.56	29.36	33.02	3.53
Port Imp1	2021	5.28	28.43	30.82	38.86	93.37	50.95	66.13	40.87	17.14	2.88	7.39	3.07
Port Imp2	2020	11.46	36.45	152.85	121.04	43.04	88.67	42.88	30.67	22.62	24.32	22.45	10.32
Port Imp2	2021	9.21	18.17	45.03	79.97	89.45	63.05	32.53	18.54	14.18	6.41	7.28	5.47
Carr Ref	2017	29.39	29.39	29.39	29.39	29.39	29.39	53.63	108.70	138.81	220.87	114.32	56.67
Carr Ref	2018	88.11	108.58	50.82	29.40	18.12	34.23	40.45	53.04	137.72	113.81	75.98	42.75
Carr Ref	2019	39.20	74.30	60.61	53.51	43.37	41.15	26.11	50.04	153.09	150.08	77.11	47.15
Carr Ref	2020	33.17	38.69	99.61	53.47	28.89	21.60	30.46	56.40	128.28	106.75	73.87	32.82
Carr Ref	2021	23.30	52.19	41.07	33.93	42.79	22.41	36.51	67.28	80.31	42.79	30.31	17.01
Carr Imp1	2017	18.28	15.64	57.58	35.22	50.31	35.80	29.00	31.97	17.73	7.17	12.13	4.08
Carr Imp1	2018	22.63	41.10	23.17	26.17	19.17	21.76	40.28	20.11	18.50	6.84	8.91	2.83
Carr Imp1	2019	4.80	14.82	28.99	38.52	26.34	28.42	18.97	9.89	31.14	22.26	9.36	10.99
Carr Imp1	2020	3.43	5.65	36.61	44.38	11.64	20.87	24.80	20.19	7.13	4.19	4.93	0.55
Carr Imp1	2021	0.71	5.64	13.29	21.03	41.97	22.56	16.70	9.09	12.48	6.31	6.61	5.15
Carr Imp2	2020						0.62	2.72	3.20	1.39	2.10	2.28	1.33
Carr Imp2	2021	1.03	2.27	3.00	1.57	7.09	5.37	4.33	3.32	0.05	0.30	0.94	0.60

Table S.3.5. Indicators of Hydrologic Alteration (IHA). Magnitude and duration of annual extreme water conditions (mm/s).

Basin	Year	1-day min	3-day min	7-day min	30-day min	90-day min	1-day max	3-day max	7-day max	30-day max	90-day max	Base flow
CoyAlto Ref	2017	0.49	0.50	0.51	0.60	2.80	85.94	80.32	70.47	55.84	35.09	0.03
CoyAlto Ref	2018	0.34	0.35	0.35	0.38	1.69	196.62	182.41	135.26	82.90	50.79	0.02
CoyAlto Ref	2019	0.35	0.36	0.42	0.46	1.25	208.82	186.14	181.90	104.55	57.02	0.03
CoyAlto Ref	2020	0.24	0.24	0.26	0.30	1.39	162.19	149.87	119.85	94.59	41.59	0.02
CoyAlto Ref	2021	0.14	0.15	0.16	0.22	0.47	51.68	40.86	31.79	24.71	12.66	0.04
CoyAlto Imp1	2017	0.96	0.99	1.05	1.26	4.80	52.29	48.44	43.95	36.59	29.72	0.06
CoyAlto Imp1	2018	2.08	2.11	2.20	2.33	3.36	21.78	20.65	19.84	17.33	15.70	0.30
CoyAlto Imp1	2019	1.16	1.18	1.28	1.69	2.04	31.66	29.94	26.42	17.54	12.38	0.24
CoyAlto Imp1	2020	0.88	0.89	0.94	1.45	2.04	34.65	32.34	28.80	23.12	13.38	0.16
CoyAlto Imp1	2021	1.28	1.31	1.34	1.44	1.79	10.09	7.97	7.79	6.01	4.99	0.41
CoyAlto Imp2	2020	0.26	0.26	0.28	0.32	2.26	97.47	87.19	85.21	73.04	33.21	0.03
CoyAlto Imp2	2021	0.09	0.07	0.10	0.11	0.39	17.21	16.98	16.02	11.54	8.69	0.03
Trapa Ref	2017	0.38	0.38	0.39	0.55	2.28	192.45	170.49	135.20	79.62	44.36	0.02
Trapa Ref	2018	0.31	0.33	0.36	0.46	2.27	110.84	76.36	62.72	47.13	38.30	0.02

Trapa Ref	2019	0.27	0.30	0.33	0.41	2.21	121.74	96.33	77.33	44.01	22.57	0.04
Trapa Ref	2020	0.44	0.45	0.48	0.58	1.45	169.28	150.03	117.36	58.06	27.24	0.05
Trapa Ref	2021	0.15	0.17	0.17	0.28	0.65	254.15	121.31	71.76	23.68	13.09	0.03
Trapa Imp1	2017	0.30	0.31	0.34	0.37	1.62	86.71	84.58	82.64	72.38	49.28	0.02
Trapa Imp1	2018	0.30	0.31	0.33	0.37	2.17	48.97	46.54	42.85	36.92	28.39	0.03
Trapa Imp1	2019	0.32	0.33	0.45	0.54	1.24	20.87	19.50	18.86	16.60	11.37	0.10
Trapa Imp1	2020	0.00	0.00	0.00	0.13	1.21	30.77	29.91	27.82	22.63	13.55	0.00
Trapa Imp1	2021	0.00	0.00	0.00	0.07	0.51	12.25	8.36	7.73	5.90	5.37	0.00
Trapa Imp2	2020	0.83	0.88	0.95	1.12	2.18	89.67	68.35	50.63	23.73	13.29	0.16
Trapa Imp2	2021	0.54	0.59	0.64	0.70	0.79	15.65	14.49	11.82	7.05	4.60	0.26
Port Ref	2017	6.89	8.02	9.67	18.72	44.66	237.88	202.05	158.15	107.55	87.22	0.15
Port Ref	2018	0.07	0.69	1.01	9.17	28.09	258.87	199.93	151.13	136.23	116.75	0.01
Port Ref	2019	0.05	3.08	5.36	16.04	35.84	384.77	178.28	121.59	87.42	65.97	0.11
Port Ref	2020	0.13	0.28	2.00	5.08	27.57	426.36	273.25	195.03	141.32	97.42	0.04
Port Ref	2021	1.59	1.76	1.88	5.68	12.46	240.60	173.25	155.96	96.36	82.58	0.04
Port Imp1	2017	2.67	2.74	4.01	10.98	31.72	542.86	266.48	202.04	94.00	78.13	0.08
Port Imp1	2018	0.89	0.86	1.02	1.88	5.17	597.68	355.21	203.79	106.42	93.93	0.02
Port Imp1	2020	0.74	0.74	0.74	5.07	35.63	676.80	472.87	377.54	191.37	111.62	0.01
Port Imp1	2021	1.03	1.14	1.23	3.69	10.71	632.01	450.47	277.43	140.68	112.11	0.02
Port Imp2	2020	7.74	7.83	8.34	11.57	20.96	2047.58	1537.44	1148.21	472.89	223.87	0.02
Port Imp2	2021	3.57	3.93	4.25	5.74	6.98	1339.90	668.29	510.73	195.98	139.00	0.02
Carr Ref	2017	22.82	23.46	26.08	28.62	29.14	558.52	326.53	283.63	227.66	175.75	0.34
Carr Ref	2018	11.00	13.21	15.08	24.30	40.21	499.63	356.88	289.91	173.80	138.93	0.17
Carr Ref	2019	21.93	22.49	23.19	32.58	49.53	457.51	318.69	282.34	178.40	144.62	0.26
Carr Ref	2020	12.86	13.99	15.61	20.61	28.41	482.08	363.12	250.44	160.34	118.76	0.22
Carr Ref	2021	13.36	13.96	14.75	17.74	34.83	572.18	394.71	302.74	137.80	89.24	0.25
Carr Imp1	2017	2.55	2.48	2.90	4.46	12.03	289.24	171.54	149.53	84.04	62.72	0.09
Carr Imp1	2018	1.46	1.47	1.61	3.24	7.33	141.51	125.65	98.28	54.09	36.21	0.06
Carr Imp1	2019	1.93	2.71	3.58	6.03	19.03	328.08	277.77	159.64	66.17	51.50	0.12
Carr Imp1	2020	0.07	0.08	0.16	0.95	3.86	439.10	399.90	285.50	119.36	55.96	0.01
Carr Imp1	2021	0.19	0.26	0.35	1.24	6.43	370.05	220.41	151.94	66.57	47.15	0.02
Carr Imp2	2020	0.35					7.41	6.47	5.81	3.67	2.74	0.31
Carr Imp2	2021	0.02	0.02	0.03	0.07	0.54	35.40	20.18	14.83	9.27	6.49	0.01

Table S.3.6. Indicators of Hydrologic Alteration (IHA). Timing of annual extreme water conditions, Frequency and duration of high and low pulses, and Rate and frequency of water condition changes

Basin	*Year*	*Date min*	*Date max*	*Lo pulse #*	*Lo pulse L*	*Hi pulse #*	*Hi pulse L*	*Rise rate*	*Fall rate*	*Reversals*
CoyAlto Ref	2017	55	291	1	65	10	10	1.79	-0.84	125
CoyAlto Ref	2018	48	302	2	31.5	2	45	0.78	-0.34	124
CoyAlto Ref	2019	63	300	4	25	3	3	0.29	-0.38	133
CoyAlto Ref	2020	48	292	3	6	8	3	0.45	-0.56	188
CoyAlto Ref	2021	42	298	10	6	3	1	0.19	-0.16	154
CoyAlto Imp1	2017	33	290	1	68	5	3	0.36	-0.64	149
CoyAlto Imp1	2018	35	248	3	8	1	88	0.11	-0.28	131
CoyAlto Imp1	2019	365	273	5	28	2	31.5	0.12	-0.15	141
CoyAlto Imp1	2020	363	291	5	5	3	4	0.15	-0.13	126
CoyAlto Imp1	2021	363	160	8	7.5	0		0.12	-0.13	170
CoyAlto Imp2	2020	89	287	3	29	5	5	0.14	-0.16	148
CoyAlto Imp2	2021	16	303	6	3.5	4	12	0.04	-0.07	149
Trapa Ref	2017	58	290	2	48.5	17	3	4.45	-4.21	152
Trapa Ref	2018	55	288	2	30	14	2	3.03	-2.52	148
Trapa Ref	2019	95	269	6	6	8	2.5	1.84	-1.59	145
Trapa Ref	2020	89	290	3	3	5	3	1.32	-1.65	172
Trapa Ref	2021	45	163	8	8.5	11	2	0.92	-0.79	172
Trapa Imp1	2017	36	291	1	72	1	207	2.30	-1.59	122
Trapa Imp1	2018	48	267	2	23.5	3	5	1.33	-0.91	108
Trapa Imp1	2019	61	273	6	8	6	2	0.70	-0.56	133
Trapa Imp1	2020	48	291	3	6	3	1	0.86	-0.53	142
Trapa Imp1	2021	66	164	1	73	2	1	0.33	-0.29	122
Trapa Imp2	2020	41	296	4	1.5	9	3	0.43	-0.45	183
Trapa Imp2	2021	364	165	6	7.5	3	2	0.18	-0.16	184
Port Ref	2017	37	204	9	6	31	2	18.51	-17.18	162
Port Ref	2018	48	110	14	3	30	3	23.69	-18.15	168
Port Ref	2019	61	66	22	3	28	2	23.95	-11.84	147
Port Ref	2020	65	157	22	3	30	1	20.42	-17.18	170
Port Ref	2021	45	163	17	4	28	2.5	18.32	-14.25	164

Port Imp1	2017	37	161	14	4	30	2	12.63	-7.51	153
Port Imp1	2018	59	326	14	4.5	29	2	20.10	-6.73	129
Port Imp1	2020	61	136	7	3	29	3	18.96	-14.71	157
Port Imp1	2021	359	185	13	7	25	3	19.64	-7.75	146
Port Imp2	2020	57	157	1	30	8	9	2.80	-1.01	117
Port Imp2	2021	363	300	7	11	8	7	1.72	-0.59	132
Carr Ref	2017	253	360	1	8	12	4	20.11	-48.63	64
Carr Ref	2018	204	110	18	3	32	2	35.45	-31.37	158
Carr Ref	2019	255	107	8	2.5	27	2	40.73	-22.00	134
Carr Ref	2020	232	157	14	3	24	2.5	13.10	-23.95	140
Carr Ref	2021	236	300	22	4	27	1	24.24	-18.90	154
Carr Imp1	2017	59	121	5	15	13	4	8.66	-3.14	96
Carr Imp1	2018	46	326	8	3	15	5	8.30	-7.03	127
Carr Imp1	2019	61	217	8	3.5	20	2.5	9.91	-5.63	123
Carr Imp1	2020	47	157	11	11	10	2.5	5.17	-3.18	128
Carr Imp1	2021	65	300	10	6	8	7	4.80	-2.71	120
Carr Imp2	2020	227	262	1	1	10	2.5	0.28	-0.42	93
Carr Imp2	2021	323	186	2	28.5	15	2	0.55	-0.47	168

Table S.3.7. Environmental Flows Components. High and low flows (mm/s and days).

Basin	*Year*	*Q80*	*Q90*	*25 % Annual Flow*	*Center of Volume*	*75 % Annual Flow*	*25% - 75% Annual Flow Duration*	*Q10*	*Q25*	*Mean Annual Minimum Flow*	*10-day*
CoyAlto Ref	2017	25.26	36.24	125	199	236	111	0.73	3.77	0.53	
CoyAlto Ref	2018	27.13	49.41	207	238	254	47	0.52	1.34	0.35	
CoyAlto Ref	2019	16.82	49.45	221	237	253	32	0.58	1.17	0.42	
CoyAlto Ref	2020	12.82	33.55	208	233	250	42	0.47	0.72	0.27	
CoyAlto Ref	2021	4.03	13.86	208	227	239	31	0.28	0.42	0.17	
CoyAlto Imp1	2017	26.79	32.10	137	199	237	100	3.59	10.07	1.18	
CoyAlto Imp1	2018	14.25	16.98	159	210	255	96	2.49	4.70	2.24	
CoyAlto Imp1	2019	7.44	14.10	164	220	253	89	1.81	2.56	1.37	
CoyAlto Imp1	2020	7.78	15.89	143	217	237	94	1.66	2.01	1.00	
CoyAlto Imp1	2021	4.42	4.85	125	193	242	117	1.54	2.04	1.35	

CoyAlto Imp2	2020	8.21	17.53	215	238	251	36	0.24	0.49	0.21
CoyAlto Imp2	2021	4.14	6.23	191	222	246	55	0.08	0.41	0.07
Trapa Ref	2017	22.53	51.17	119	205	235	116	0.69	2.46	0.44
Trapa Ref	2018	23.78	36.27	130	203	241	111	0.59	1.80	0.38
Trapa Ref	2019	11.63	21.09	139	221	244	105	0.62	2.04	0.33
Trapa Ref	2020	12.31	27.06	104	227	236	132	0.60	1.22	0.50
Trapa Ref	2021	9.64	15.01	104	168	217	113	0.35	0.63	0.19
Trapa Imp1	2017	36.46	51.22	154	202	230	76	0.42	2.17	0.34
Trapa Imp1	2018	8.04	26.54	160	209	238	69	0.38	1.15	0.33
Trapa Imp1	2019	8.08	10.97	169	214	242	73	0.56	1.26	0.45
Trapa Imp1	2020	6.41	14.41	175	225	243	68	0.43	0.92	0.00
Trapa Imp1	2021	4.83	5.68	142	195	236	94	0.08	0.37	0.00
Trapa Imp2	2020	8.78	10.24	145	219	237	92	1.38	1.80	1.04
Trapa Imp2	2021	3.76	4.54	118	180	238	120	0.72	0.90	0.64
Port Ref	2017	90.42	117.16	101	175	250	149	15.61	32.08	10.60
Port Ref	2018	115.54	140.77	81	181	239	158	14.70	29.65	2.37
Port Ref	2019	72.25	94.54	106	201	275	169	9.30	18.94	6.11
Port Ref	2020	85.10	107.83	75	148	246	171	3.56	16.05	2.16
Port Ref	2021	89.40	114.16	100	156	223	123	2.45	8.81	2.03
Port Imp1	2017	59.21	103.28	82	142	205	123	8.74	20.64	7.39
Port Imp1	2018	86.96	126.03	108	188	229	121	8.48	19.48	8.56
Port Imp1	2020	110.85	160.97	85	157	223	138	12.00	22.57	2.79
Port Imp1	2021	76.33	132.22	100	141	200	100	3.14	6.87	1.43
Port Imp2	2020	18.85	32.56	80	101	163	83	16.36	23.06	9.55
Port Imp2	2021	13.40	25.16	101	131	183	82	6.08	8.73	4.44
Carr Ref	2017	141.52	186.75	81	232	279	198	22.11	38.34	10.70
Carr Ref	2018	133.08	193.04	58	228	279	221	22.08	31.87	16.41
Carr Ref	2019	120.73	174.40	91	245	290	199	30.42	38.61	23.27
Carr Ref	2020	114.49	154.79	87	232	285	198	20.86	32.33	15.75
Carr Ref	2021	79.16	114.59	88	221	260	172	18.07	23.08	15.54
Carr Imp1	2017	42.18	64.79	91	139	228	137	4.70	12.72	4.16
Carr Imp1	2018	39.95	49.47	61	148	220	159	4.76	11.83	1.85
Carr Imp1	2019	33.60	60.70	101	158	261	160	6.00	11.56	3.89
Carr Imp1	2020	26.72	43.58	97	104	192	95	2.41	4.24	0.26

Carr Imp1	2021	22.77	39.26	105	146	238	133	3.48	5.61	0.44
Carr Imp2	2020									
Carr Imp2	2021	5.05	6.91	100	146	197	97	0.27	0.69	0.03

Table S.3.8. Environmental Flows Components. Base flows (mm/s and days).

Basin	*Year*	*Annual Mean Daily Discharge*	*Annual Baseflow Volume*	*Annual Mean Baseflow*	*Annual Maximum Baseflow*	*Annual Minimum Baseflow*	*Mean Baseflow Index*	*25% Annual Baseflow*	*Baseflow Center of Volume*	*75% Annual Baseflow*	*25% - 75% Baseflow Duration*
CoyAlto Ref	2017	16.91	1.52	13.03	48.08	0.44	0.83	119	192	238	119
CoyAlto Ref	2018	14.64	2.68	10.55	85.06	0.30	0.82	211	241	255	44
CoyAlto Ref	2019	16.68	3.61	11.58	114.32	0.30	0.81	226	241	254	28
CoyAlto Ref	2020	13.27	2.42	9.46	76.75	0.23	0.81	222	240	252	30
CoyAlto Ref	2021	3.91	0.74	2.82	23.48	0.14	0.80	212	232	245	33
CoyAlto Imp1	2017	17.66	0.98	13.99	31.07	0.94	0.83	118	186	238	120
CoyAlto Imp1	2018	8.11	0.48	6.35	15.10	1.29	0.80	162	217	259	97
CoyAlto Imp1	2019	5.49	0.49	4.23	15.40	1.12	0.81	140	222	255	115
CoyAlto Imp1	2020	5.87	0.65	4.50	20.48	0.82	0.81	126	220	243	117
CoyAlto Imp1	2021	3.30	0.17	2.62	5.49	1.15	0.81	105	189	249	144
CoyAlto Imp2	2020	7.75	1.41	5.54	44.56	0.17	0.79	215	241	253	38
CoyAlto Imp2	2021	2.06	0.25	1.52	7.81	0.06	0.77	196	226	250	54
Trapa Ref	2017	18.32	2.58	12.46	81.95	0.35	0.83	108	205	232	124
Trapa Ref	2018	14.35	1.39	10.16	44.22	0.30	0.80	144	207	244	100
Trapa Ref	2019	9.38	1.28	6.88	40.67	0.27	0.82	161	218	242	81
Trapa Ref	2020	10.47	2.24	6.90	71.03	0.41	0.80	119	228	241	122
Trapa Ref	2021	6.62	1.33	4.41	42.28	0.15	0.82	129	194	224	95
Trapa Imp1	2017	19.14	1.98	14.78	62.66	0.29	0.83	158	205	234	76
Trapa Imp1	2018	7.53	0.99	5.20	31.24	0.27	0.77	146	193	207	61
Trapa Imp1	2019	4.69	0.45	3.69	14.18	0.27	0.82	174	219	247	73
Trapa Imp1	2020	5.02	0.64	3.87	20.31	0.00	0.81	178	229	247	69
Trapa Imp1	2021	2.48	0.15	1.91	4.80	0.00	0.78	150	201	241	91
Trapa Imp2	2020	6.01	1.04	4.21	33.12	0.81	0.79	140	216	243	103
Trapa Imp2	2021	2.47	0.20	1.90	6.32	0.53	0.80	122	183	242	120
Port Ref	2017	63.59	3.11	41.55	98.67	6.90	0.76	107	186	253	146

Port Ref	2018	71.19	3.66	46.16	116.08	0.07	0.75	86	190	240	154
Port Ref	2019	47.89	2.56	28.60	81.16	0.05	0.72	117	213	278	161
Port Ref	2020	52.74	4.27	30.98	135.55	0.13	0.71	74	125	248	174
Port Ref	2021	50.35	3.32	30.49	105.19	1.55	0.74	102	161	218	116
Port Imp1	2017	49.29	3.54	28.04	112.17	2.67	0.77	86	155	230	144
Port Imp1	2018	60.12	3.75	33.53	118.95	1.72	0.73	88	189	229	141
Port Imp1	2020	74.86	6.14	42.59	194.69	0.74	0.74	99	187	240	141
Port Imp1	2021	57.92	5.65	30.48	179.20	1.03	0.76	102	147	205	103
Port Imp2	2020	88.49	17.37	52.74	550.76	7.38	0.80	83	104	180	97
Port Imp2	2021	57.20	9.59	33.24	303.99	3.57	0.81	101	132	184	83
Carr Ref	2017	92.75	5.22	62.01	165.38	6.21	0.76	222	260	313	91
Carr Ref	2018	87.45	5.31	54.97	168.32	11.00	0.77	70	229	284	214
Carr Ref	2019	88.47	5.65	57.10	179.31	19.91	0.78	101	237	291	190
Carr Ref	2020	75.25	4.49	49.31	142.23	12.67	0.77	91	241	290	199
Carr Ref	2021	59.62	5.19	36.55	164.53	12.47	0.77	94	195	258	164
Carr Imp1	2017	30.99	2.47	22.77	78.18	2.48	0.84	75	122	225	150
Carr Imp1	2018	25.29	1.89	17.66	60.05	1.37	0.79	68	158	219	151
Carr Imp1	2019	28.72	3.08	18.54	97.57	1.88	0.79	104	161	260	156
Carr Imp1	2020	22.52	4.69	14.67	148.74	0.07	0.79	98	115	201	103
Carr Imp1	2021	21.04	2.64	13.36	83.82	0.19	0.80	118	156	236	118
Carr Imp2	2020										
Carr Imp2	2021	3.11	0.25	2.13	8.02	0.02	0.79	103	153	198	95

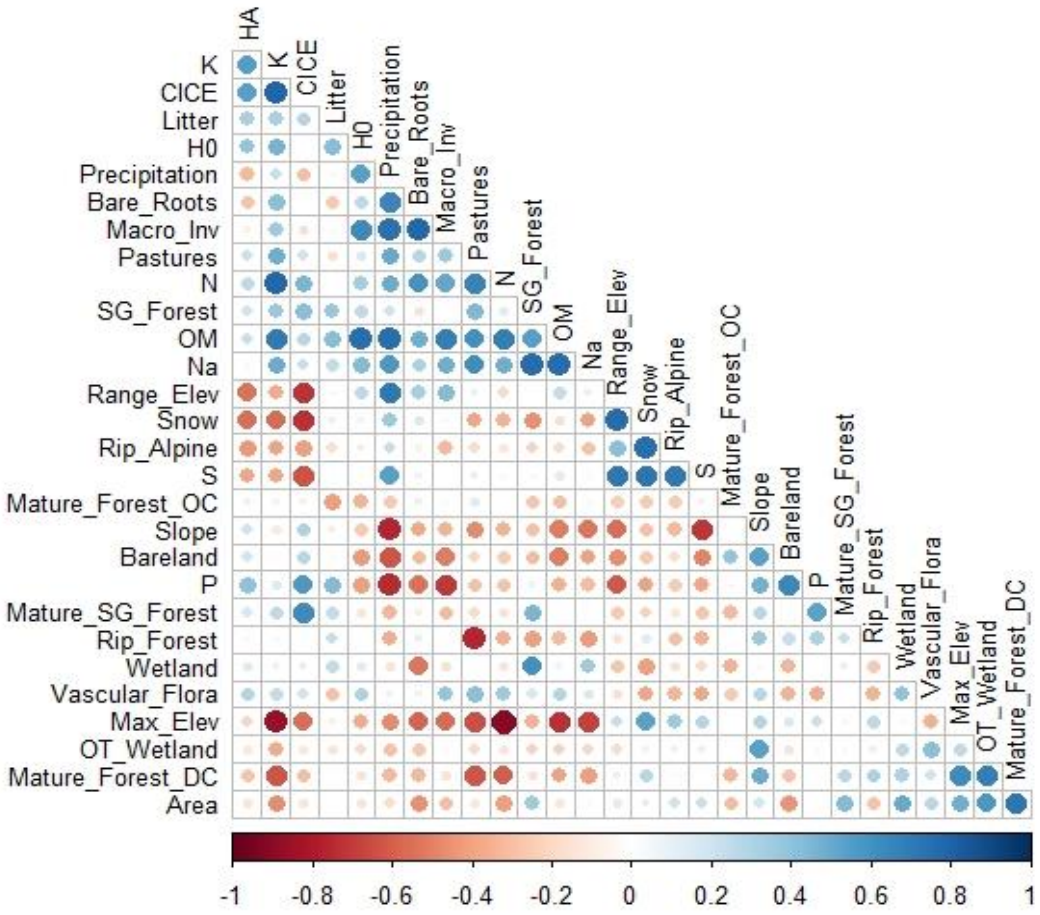

Figure S.3.1. *Pearson correlation of selected catchment attributes. Description and details in methods. Note: Abbreviations explained in table 5.2.*

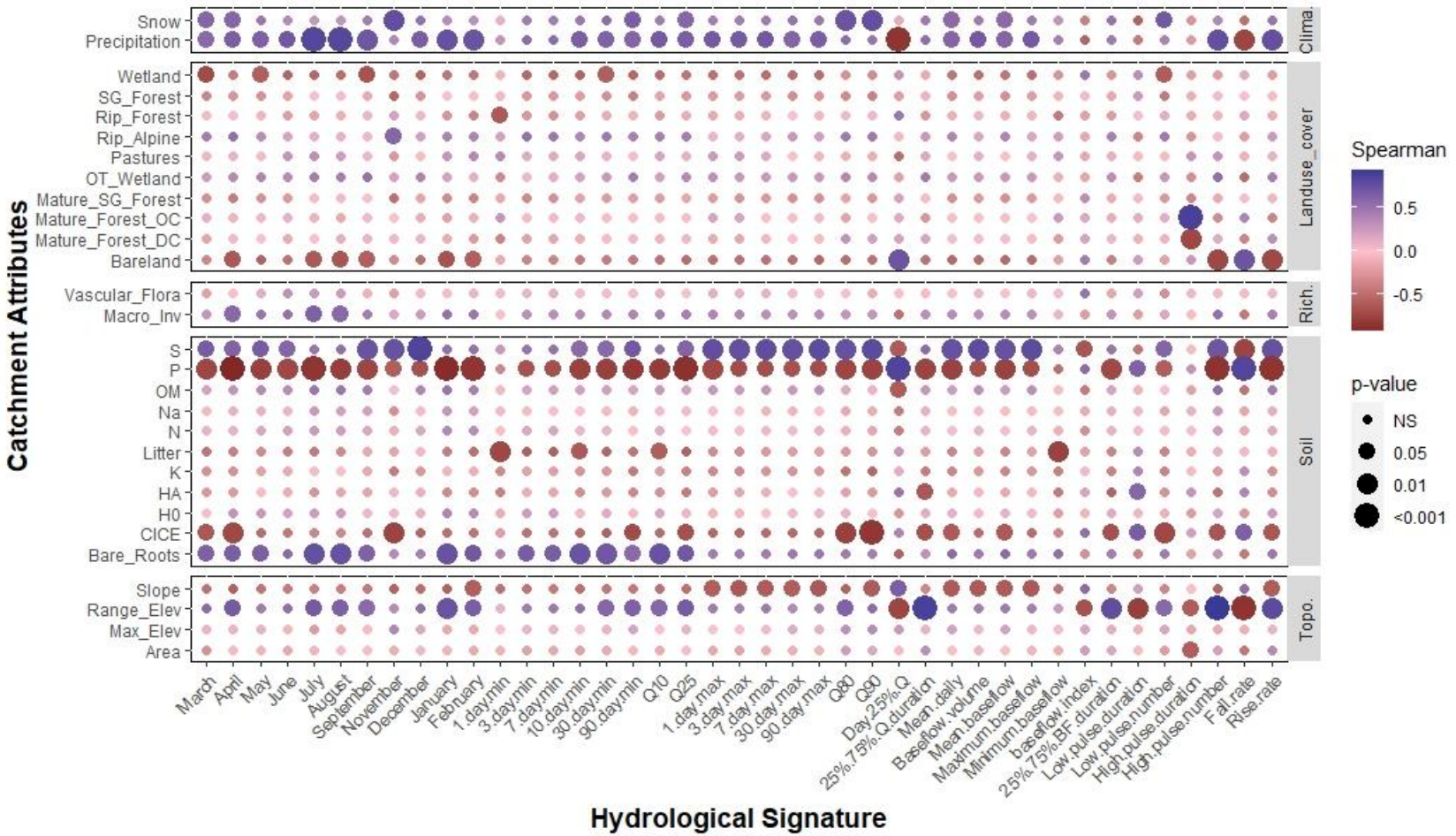

Figure S.3.2. *Spearman correlation between catchment attributes and hydrological signatures in the 12 catchments. More details about the variables are shown in the methods.*

FINAL REMARKS

The crucial role of coastal freshwater discharges in the ecosystems of inner seas, fjords, and channels is undoubted. These riverine forcings are critical for salinity, allochthonous/autochthonous nutrient cycling, water temperature, and light availability, among other processes, in estuarine and coastal systems essential for human well-being ecosystem services (Millenium Ecosystems Assessment, 2005). On the other hand, west-southern Patagonia has had the subsidence of the central valley and later erosive processes resulting from the glaciations (Castilla et al., 2021). These characteristics of west-southern Patagonia produce a system of channels and fjords with an extended coastline, one of the most relevant worldwide (Kelso & Patterson, 2010; Schneider et al., 2014). The present work addressed the need to interconnect different ecosystems, such as marine, freshwater, and terrestrial, where most of the time are studied as closed systems. For example, studies related to terrestrial and marine ecosystems are dispersed and without of integrate analysis producing inefficient conservation programs (Castilla et al., 2021). Everything happening in the terrestrial, here from a watershed perspective, affects the streams from headwater until coastal discharges, producing diverse consequences in fjords and channels of west-southern Patagonia. On the other hand, the two primary drivers of terrestrial landscapes are land use/cover changes (LUC) and variability in climate forcing (including climate change). Thus, a transversal objective in this study was identifying and understanding how LUC affects the streams and the coastal freshwater discharges.

Coastal freshwater discharges quantification and characterization

West-southern Patagonia, with its extensive coastline, inner seas, archipelagos, glaciers, lakes, fjords, and channels, is one of the most critical land/sea ecosystems on a global scale. For example, the particularity of this territory with a coastline corresponds to 34% of South America, or the

highest continental ice fields in the South Hemisphere, excluding Antarctica. In addition, the high rate of precipitation and the short distances of fluvial courses from the source to the sea generates a significant coastal discharge of freshwater runoff. The importance of these freshwater flows into marine ecosystems provokes the well-known vertical stratification of the water column. Our study estimates by modeled data (FLOW model from IFOP, http://chonos.ifop.cl/flow/) a coastal discharge close to the 2% global (692 km^3/year), with no other significant continental landmass comparable in these southern latitudes (below 30°S). The Baker/Pascua complex is the most considerable point input of freshwater discharges south of the Parana basin, with 53.6 km^3/year (Reid et al., 2021). Besides, Puelo, Yelcho, Palena, and Aysén basins are between the Chiles' ten most prominent rivers. A significant difference between the latter and the major rivers in the southeast Pacific is that the firsts discharge freshwater to interior seas rather than offshore coasts.

Land/sea zoning (seven zones) is presented in this study (Chapter 1), assimilating the work of Pickard and Staton (1980) but with a basin point of view, including differences between inner seas, channel zones, and offshore coasts. The interannual hydrologic variability is much more evident in zones with the most extensive continental basins (Zones 1,3,5), while coastal systems (Zones 2, 4) have the slightest variation across years. This would be expected to have consequences regarding freshwater influence and density stratification: inland marine areas linked to continental systems are potentially more susceptible to drought influences on both physical stratification and the water quality of inputs. Seasonal variability is also distinct across coastal vs. continental zones, with much less variability in coastal systems across seasons.

Additionality, west-southern Patagonia has a scarcity of observational flow data, even more if we focus on coastal rivers and the archipelago zone. Thus, the extrapolation of a hydrology model, such as FLOW, generates significant uncertainties. Nonetheless, the uncertainties of the FLOW

model were associated with shorter time scales, i.e., monthly and daily, due to the acceleration of snowpack melting process (Olivares, 2022). Conversely, the modeled data at an annual and seasonal level performs satisfactorily.

On the other hand, a considerable volume/chemistry variability in the seasonal and annual freshwater flows due to climate, geology, soils, dry conditions, and land use/cover was identified. The northern half of the region, dominated by volcanic andosols, is expected to have consistently higher levels of DSi in river export (Zones 1,3,5). Exceptions are due to the leeward side of the volcanic sources (Zones 2, 4) and dilution by other sources slow DSi, such as meltwater (Zone 4). Therefore, a maximum focused load of DSi might be expected for large continental basins in these zones, where high discharge coincides with moderate to high concentrations (Yelcho, Palena, and Puelo rivers). Arid zones with concentrated weathering products, including DSi (parts of Zone 7), might also be expected to have significant yet diffuse loadings. Conversely, iron loading may be more predominant in southern regions (Zones 5-7) due to increased glacial inputs and arid zone concentration. Suspended sediments are similarly expected to increase southward (Zones 5-7), except seasonal inputs during fall rains or spring snowmelt of more northern cordilleran basins.

The humid coastal region was characterized by extremely low weathering inputs yet significant temperate zone vegetation that has received low levels of intervention (Zones 2,4), with extremely low macronutrient inputs and moderate to high DOC inputs of relatively labile quality (leaching of forests litter). Meanwhile, colder humid regions dominated by peatlands (Zones 6-7) may have a variable to high DOC loads of a more refractory quality (e.g., humic substances sourced from Sphagnum bogs). Finally, in terms of macronutrients, inorganic N and P levels are expected to be naturally very low throughout; however, this baseline may be affected by urban and crops (Zones 1, 3).

A specific study (chapter 2 and appendix 2), associated with marine sampling stations on interior fjord waters transect from Magellan Strait until Madre de Dios Archipelago (south to north; 53.7-50.5°S) showed high variability in the freshwater quantification. The latter is because the transect was characterized by constrained inland marine waters in close contact with innumerable minor to medium point sources of continental runoff, areas of concentrated high-volume runoff where interior canals connect with large continental basins. Additionally, the freshwater inputs partitioning as direct precipitation into marine regions (trace solutes), glacial runoff from melting (high suspended load and low nutrient), and land-surface runoff (diverse and variable solute and suspended load), presented considerable importance in favor of the latter sources of discharges. Even direct precipitation volume resulted higher than income from melting, characterized by a precipitation gradient ranging from 2000 to 7000 mm/year.

Additionally, for improved flow modeling, integrating a regional precipitation raster, such as the Patagonia Met dataset (chapter 2), into a more intricate and hydrologically comprehensive model like VIC, as demonstrated in the FLOW study (chapter 1), presents notable advantages. Furthermore, placing a significant emphasis on refining the estimation of solid precipitation's impact on discharge is paramount, particularly in light of climate change projections indicating diminished snowfall and heightened rates of glacier melting. By incorporating these enhancements, the accuracy and reliability of flow modeling can be significantly improved, enabling a more comprehensive understanding of hydrological processes and their response to changing climatic conditions.

Finally, better information about coastal discharges in Patagonia will be possible with an intensive net of permanent flow sampling. Specifically, covering those isolated areas with no data, incorporating more chemical monitoring stations, and joining different monitoring initiatives in a

long-term strategy. The monitoring is even more necessary due to the high variability found in this study for west-southern Patagonia, either as flows, chemistry, temporal-scale (yearly/season/daily/sub-daily), etc. Moreover, the current variability will be more considerable with the future effects of the two primary drivers of terrestrial landscape: LUC and climate forcing (including climate change).

Identification of LUC on headstreams through hydrological signatures metrics

The importance of headstreams has been explained before, because their vulnerability and capacity of identification of environmental changes, as LUC and climate forcing, in the watersheds better than big rivers. However, one of the difficulties on watershed studies is the highly dynamic stream ecosystem, specifically hydrology and water chemistry, and the corresponding dependence on longer-term and/or high-frequency observations in order to characterize patterns and responses. This study analyzed 2-6 years of high-frequency discharge observations based on two time-scale systems of hydrologic indicators (daily and sub-daily), testing for their utility in discerning physical watersheds condition defined by vegetation, soils, and basin geomorphology in 12 basins in four groups along a strong climatic gradient (precipitation 700-2000 mm/year), each group consisting of three land use grades (intact, moderate and high level of intervention).

The event dynamics associated with sub-daily indicators presented a high predictive power to detect LUC in headwater catchments with short-time datasets. In detail, sub-daily indicators were crucial to mainly address flow changes due to evapotranspiration, being most critical in water-limited ecosystems. The amplitude was higher in intact watersheds, consistent with the interpretation that the diel flow amplitude is a measure of evapotranspiration, and these watersheds have more forest, which evapotranspire more than other land cover types. In detail, intact watersheds had higher transpiration and interception, as was mentioned before, but at the same

time, had a higher water storage rate. Instead, impacted catchments had more erosion with less volume soil, thus lower storage capacity. Impacted catchments had less vegetation implying less interception and transpiration. Hence, the only variable to reduce flow fluctuations in impacted catchments was evaporation provoked by the exposition of soils with no coverage due to anthropogenic impacts, such as forest fires, clear-cutting, and cattle breeding.

Flow duration curves (FDC) showed a similar interpretation about lower evaporation rates in those watersheds less affected by LUC. For example, the intact catchments flows were notorious higher in comparison to the impacted watersheds in Trapananda (deciduous forests; 800 mm/year) and Carrera (evergreen/deciduous forests; 2200 mm/year) sites and slightly higher in Portales (evergreen forest; 2500 mm/year). Specifically, impacted catchments have high percentages of second-growth forests, pastures, and bare land coverages. The similarity between FDCs of intact and impacted watershed flows in Portales must be because, in high-rainfall regions, evaporation represents a much smaller fraction of precipitation (Asbjornsen et al., 2011). On the contrary, in a water-limited ecosystem such as Coyhaique Alto (deciduous forests; 690 mm), the impacted catchment presented higher low flows 60% of the time but lowered magnitudes in high flows. One hypothesis is that in those months with enough rain or snow melting, higher evaporations were the causes of lower runoff in the impacted catchment. However, in summer, with more dry conditions, vegetation interception and transpiration were crucial factors that provoked the reference catchment, with more forest coverage, to have a lower water yield.

Contrary to the dynamics observed during specific events, daily hydrology indicators were found to be less effective in identifying the impacts of Land Use Change (LUC). According to McMillan (2021), climate descriptors demonstrated higher predictive power, while catchment attributes related to LUC offered limited predictive capabilities for hydrological patterns. Our own

study yielded similar findings, where precipitation and snow emerged as the most influential predictors in random forest models across various hydrology indicators utilizing daily datasets. However, certain LUC-related attributes displayed superior predictive power. These included the depth of mineral soil, percentage of pastures in the catchment, percentage of forest within the riparian zone, depth of bare roots, percentage of bare lands, and the extent of mature forests with open- and dense canopies. Notably, attributes like mineral soil depth, bare roots depth, and bare land percentage directly influence soil loss (erosion process) and subsequently affect water storage capacity. To further comprehend the magnitudes and directional effects of predictors on responses, specific hypotheses need to be formulated. Additionally, research efforts can be categorized based on time scales, such as annual, dry season, wet season, and event dynamics.

Finally, the connection between impacts and hydrology signatures must incorporate those catchment attributes that define a watershed as impacted. In other words, it is preferable to work with characteristics of the catchment than a categorization as impacted or reference (intact). The watershed characteristics bring specific information associated with possible impacts, but it also is possible to understand watershed processes. For example, one of the essential effects of land use transformation by human activities is the changes in evapotranspiration on watersheds affecting the flows. Thus, to see changes in streams with few monitoring years (five years in our study), sub-daily indicators were much more sensitive than daily indicators to detect the evapotranspiration effects.

Bioindicators for detecting impact of LUC and forest degradation

Watersheds integrate vegetation, soils, geology, hydrology, climate, and human activities. Watersheds as fundamental ecosystem units, as has been proposed, would in practice depend on questions of scale, context, and available resources for monitoring. Besides, in a vulnerability

context, headwater watersheds are the most sensitive area of a stream net where, e.g., LUC, contamination, and climate/global change watershed-scale drivers, are evident, underscoring the importance of headwaters streams to organisms and ecosystems downstream (Lowe & Likens, 2005; Máčka et al., 2023).

Appendix 3 addressed the identification of headwaters stream macroinvertebrate taxonomic and functional feeding group (FFG) composition in a bioclimatic and geomorphological gradient but also of human impacts, with the general idea of finding bioindicators for LUC monitoring. However, the main environmental driver of taxonomic and FFG's composition was forest cover (and inversely alpine zone) at the watershed scale. Additionally, the balance of forested vs. alpine zone cover indicates the effect of energy/food resources and stream productivity. The forest-alpine zone gradient may also be interpreted as a disturbance gradient. Higher alpine zone cover in the watershed was linked to harsher environmental conditions, such as faster current velocity and lower temperatures, which seemed to influence FFGs significantly. Besides, patterns of forest cover and stream productivity potentially differ in their effects on stream invertebrates between coastal evergreen forested watersheds and the cordilleran deciduous forested watersheds (i.e., across the wide bioclimatic and geomorphological gradient east to west of the region). No significant correlation with LUC was identified in the study, possibly because the intensity of land use transformation is still low with a recent human occupation of approximately 100 years old and mainly focused in valleys. Finally, the results suggest a vital role of the watershed level variables explaining macroinvertebrate taxonomic and FFG assemblages in the mountainous Patagonian region, specifically regarding the forest cover gradient affecting local physical conditions and autotrophic/allotrophic productivity dynamics within watersheds.

On the other hand, in appendix 4, bioindicators of degradation in evergreen forests were identified. Forest degradation in west-southern Patagonia is mainly caused by high grading, harvesting of fuelwood, and sub-canopy grazing by livestock. Some of these actions may emulate short-scale natural disturbances and therefore have a little spatial and temporal impact on forest watershed functioning, for example, soil infiltration capacity, evapotranspiration, hydrologic perturbances on wetlands into the forest, etc. Based on study results, a temperate evergreen rainforest is in an evident state of degradation if it contains less than 200 trees per hectare with a diameter at breast height (DBH) $\geq$ 10 cm. Other concomitant situations characterizing forest degradation that can be added to the list are 1) 5 or more exotic species per hectare of vascular flora with a DBH < 10 cm, 2) 12 or fewer native species per hectare of vascular flora with a DBH < 10 cm, and 3) a relatively neutral soil pH where more intact forests present more acid conditions. Finally, thanks to these results, managers or practitioners could carry out flora vascular inventories to declare if a forest is in a degraded status. Additionally, using remote sensing combined with forest inventories could also identify tree density-based forest degradation at the watershed scale. Finally, the spatial identification of degraded forest areas besides land use/cover transformation in a catchment could be an integral approach to better estimate runoff and chemical characteristics of coastal freshwater discharges.

Projections, threats and opportunities in west-southern Patagonia

Although both climate and land use drivers of water quality are expected to change, initial trends and rates are still unclear (Falvey & Garreaud, 2009). Global models predict a drying climate northward, more humid trends toward the south (Garreaud et al., 2013) although the rate and precise location of this transition, in the complex mountain geography of Patagonia, has not been evaluated adequately with regional climate modeling. A shift in runoff dominance from fall to

spring, a potential consequence of declining annual runoff, and seasonally declining fall rains together with only a somewhat less significant declining snowpack, has been observed for the Puelo basin (41°S). Here the potential decline in DOM input suggested by Leon-Munoz et al. (2021) may be offset by change in organic matter quality (unknown) nutrient and weathering inputs (potentially reduced load from declining discharge together with slightly reduced weathering rates). These potential trends, however based on a relatively more complete baseline, are still highly speculative.

The colonization process in Patagonia was severe in the landscape transformation, with extensive forest fires, wood harvesting, habilitation of new pastures for cattle breeding, exotic species invasion, and the incorporation of the salmon farming industry (Castilla et al., 2021). But at the same time, more than 50% of terrestrial Chilean Patagonia (Tacón et al., 2021) and 41% of marine areas are part of state national parks, state reserves, and other figures of conservation. Furthermore, it is concerning to see how human activities are transforming the land use and cover in Patagonia, according to the projections, for example, population increase, more intensive tourism, expansion toward lower latitudes of salmon farming, a more extensive network of roads with state programs for accessibility to new lands for small owners, a more aggressive mining industry due to current prospecting permits, increasing of speculative real estate business through subdivisions or buying large areas of land, among others (Castilla et al., 2021). An example of the vulnerability present in Patagonia, even with the vast area in conservation status, 49% (~33,000 km^2) of the intact forested watershed in Patagonia are with no protection (Astorga et al., 2021)

The possibility of an integrative management vision for terrestrial, freshwater, and marine ecosystems is an excellent opportunity to bring west-south Patagonia a new development model, avoiding extractive activities without state planning. Obviously, the base for conserving these

land/sea connections are the national parks and national reserves and other conservation figures in Chile and Argentina (trans-Andes basins). As was mentioned before, the extensive area with some conservation status is unusual worldwide. Still, at the same time, an enormous opportunity to have effective long-term conservation with holistic planning of watersheds, streams, and inner seas but also with public financial support that prevents a conservation just in maps. Additionally, the conservation must not be framed only in public lands but also in private areas, some still within near-reference conditions. Finally, the estate must impulse regional planning with practical applicability in the territory, not only with recommendations to the private sector.

LITERATURE CITED

Astorga, A., Reid, B., Moreno, P., & Rojas, P. (2021). Donde nacen los ríos: cuencas de bosques prístinos en la Patagonia occidental austral. In J. C. Castilla, J. J. Armesto, & M. J. Martínez-Harms (Eds.), Conservación en la Patagonia chilena: evaluación del conocimiento, oportunidades y desafíos. (pp. 167-198). Ediciones Universidad Católica.

Castilla, J. C., Armesto, J. J., & Martínez-Harms, M. J. (2021). Conservación en la Patagonia Chilena: Evaluación del conocimiento, oportunidades y desafíos. Ediciones UC.

Falvey, M., & Garreaud, R. D. (2009). Regional cooling in a warming world: Recent temperature trends in the southeast Pacific and along the west coast of subtropical South America (1979–2006). Journal of Geophysical Research: Atmospheres, 114(D4).

Garreaud, R., Lopez, P., Minvielle, M., & Rojas, M. (2013). Large-Scale Control on the Patagonian Climate. Journal of climate, 26(1), 215-230. https://doi.org/10.1175/JCLI-D-12-00001.1

Kelso, N. V., & Patterson, T. (2010). Introducing natural earth data-naturalearthdata. com. Geographia Technica, 5(82-89), 25.

León-Muñoz, J., Aguayo, R., Marcé, R., Catalán, N., Woelfl, S., Nimptsch, J., Arismendi, I., Contreras, C., Soto, D., & Miranda, A. (2021). Climate and Land Cover Trends Affecting Freshwater Inputs to a Fjord in Northwestern Patagonia. Frontiers in Marine Science, 8. https://doi.org/10.3389/fmars.2021.628454

Lowe, W. H., & Likens, G. E. (2005). Moving headwater streams to the head of the class. BioScience, 55(3), 196-197. https://doi.org/10.1641/0006-3568(2005)055[0196:MHSTTH]2.0.CO;2

Máčka, Z., Galia, T., Škarpich, V., Michalková, M. Š., & Krejčí, L. (2023). A method for assessment of sediment supply and transport hazard and risk in headwater catchments for management purposes. Environmental Earth Sciences, 82(1). https://doi.org/10.1007/s12665-022-10707-z

McMillan, H. K. (2021). A review of hydrologic signatures and their applications. WIREs Water, 8(1), e1499. https://doi.org/10.1002/wat2.1499

Olivares, J. (2022). Variabilidad e incerteza de la herramienta FLOW (IFOP): Ríos de la Patagonia modelados con VIC Universidad de Concepción]. Concepción, Chile.

Pickard, G. L., & Stanton, B. R. (1980). Pacific Fjords - A Review of Their Water Characteristics. In H. J. Freeland, D. M. Farmer, & C. D. Levings (Eds.), Fjord Oceanography (pp. 1-51). Springer US. https://doi.org/10.1007/978-1-4613-3105-6_1

Reid, B., Astorga, A., Madriz, I., & Correa, C. (2021). Estado del conocimiento y conservación de los ecosistemas dulceacuícolas de la Patagonia occidental austral. In J. C. Castilla, J. J. Armesto, & M. J. Martínez-Harms (Eds.), Conservación en la Patagonia chilena: evaluación del conocimiento, oportunidades y desafíos. Ediciones Universidad Católica.

Schneider, W., Pérez-Santos, I., Ross, L., Bravo, L., Seguel, R., & Hernández, F. (2014). On the hydrography of Puyuhuapi Channel, Chilean Patagonia. Progress in Oceanography, 129, 8-18. https://doi.org/10.1016/j.pocean.2014.03.007

Tacón, A., Tecklin, D., Farías, A., Peña, M. P., & García, M. (2021). Áreas Terrestres Protegidas por el Estado en la Patagonia chilena: Caracterización, Evolución Histórica y Estado de Gestión. In (pp. pp 129-166).

Appendix 1. List of publications

Palmas S, **Moreno P.C.**, Cropper W.P., Ortega A., Gezan S.A. 2020. Stand-Level Components of a Growth and Yield Model for *Nothofagus* Mixed Forests from Southern Chile. *Forests* 11:810. https://doi.org/10.3390/f11080810

Zamorano-Elgueta C., **Moreno P.C**. 2021. Restoration for Provision of Ecosystem Services in Patagonia-Aysén, Chile. In: Peri P.L., Martínez Pastur G., Nahuelhual L. (eds) *Ecosystem Services in Patagonia. Natural and Social Sciences of Patagonia*. Springer, Cham. https://doi.org/10.1007/978-3-030-69166-0_9

Gezan S.A., **Moreno P.C.**, Palmas S., and A. Ortega. 2021. NOTHOPACK: A Growth and Yield Simulator for Nothofagus Second Growth Forests. Version 1.0. Universidad Austral de Chile, Valdivia, Chile. https://github.com/sgezan

Astorga A., **Moreno P**., Rojas P., Reid B. 2021. Donde nacen los ríos: cuencas de bosques prístinos en la Patagonia occidental austral. En: Castilla, J. C., Armesto, J. J., y Martínez-Harms, M. J. (Eds.). *Conservación en la Patagonia chilena: evaluación del conocimiento, oportunidades y desafíos*. Santiago, Chile: Ediciones Universidad Católica, 600 pp.

Moreno-Meynard P., Palmas S., Gezan S.A. 2021. Prediction Comparison of Stand Parameters and Two Ecosystem Services through New Growth and Yield Model System for Mixed Nothofagus Forests in Southern Chile. *Forests 2021*, 12, 1236. https://doi.org/10.3390/f12091236

Fajardo, A., Llancabure, J.C. and **Moreno, P.C.** 2021. Assessing forest degradation using multivariate and machine learning methods in the Patagonian temperate rainforest. *Ecological applications 32*(2):e02495. https://doi.org/10.1002/eap.2495

Astorga Roine, A., Reid, B., Uribe, L., **Moreno-Meynard, P**., Fierro, P., Madriz, I., & Death, R. G. 2022. Macroinvertebrate community composition and richness along extreme gradients: The role of local, catchment, and climatic variables in Patagonian headwater streams. *Freshwater Biology*, *67*, 445-460. https://doi.org/10.1111/fwb.13853

Piper, F. I., **Moreno-Meynard, P.**, & Fajardo, A. 2022. Nonstructural carbohydrates predict survival in saplings of temperate trees under carbon stress. *Functional Ecology, 00*, 1–13. https://doi.org/10.1111/1365-2435.14158

Moreno-Meynard, P., Méndez C., Irarrázaval I. & Nuevo-Delaunay A. 2022. Past Human Mobility Corridors and Least-Cost Path Models South of General Carrera Lake, Central West Patagonia (46° S, South America). *Land 11*, no. 8: 1351. https://doi.org/10.3390/land11081351

Torres, R., Reid, B., Pizarro, G., Frangópulos, M., Alarcón, E., Márquez, M., Díaz, F., Menschel, E., González, H.E., **Moreno-Meynard, P**., Montero, P., Pacheco, H., Pinto-Torres, M., Alarcón, C., Ibañez, R., Hawkings, J. 2023. Iron and silicic acid addition effects on early Spring macronutrient drawdown and biogenic silica production of Patagonia estuarine waters, *Progress in Oceanography, 102982*, https://doi.org/10.1016/j.pocean.2023.102982

Fajardo, A., Gazol, A., **Moreno-Meynard, P**., Mayr, C., Martínez-Pastur, G.,Peri, P., Camarero, J. 2023. Climate change-related growth improvements in a wide-niche breadth tree species across contrasting environments. *Annals of Botany*, in press.

Appendix 2. Iron and silicic acid addition effects on early Spring macronutrient drawdown and biogenic silica production of Patagonia estuarine waters.

Rodrigo Torres, Brian Reid, Gemita Pizarro, Máximo Frangópulos, Emilio Alarcón, Magdalena Márquez, Francisco Díaz, Eduardo Menschel, Humberto E. González, Paulo Moreno-Meynard, Paulina Montero, Hernán Pacheco, Marco Pinto-Torres, Cesar Alarcón, Rodrigo Ibañez, Jon Hawkings.

Progress in Oceanography, 102982, doi: 10.1016/j.pocean.2023.102982

Abstract

The Patagonia archipelago interior sea (PAIS) of southern Chile is one of the largest fjord systems on earth. These coastal waters include remote and virtually pristine areas where extreme rainfall/runoff and glacial meltwaters intensify the land-ocean interaction impinging on the biological, physical, and chemical characteristics of oceanic subantarctic Surface Water (SAASW) that flood the archipelago basins. The SAASW mix with silicon- and iron-replete continental water and diatom growth would occur concomitantly with a rapid drawdown of SAASW macronutrients. Consequently, phytoplankton metabolism (e.g., macronutrient utilization for primary productivity) in estuaries of southern Patagonian has been previously assumed independent of iron availability (i.e., iron-replete conditions). Experimental results shown here suggest that the nitrate and phosphate drawdown in low salinity (29) water can be enhanced by a 5 nM dissolved iron enrichment (by 13% and 28%, respectively) during the developing phase of a diatom bloom. The simultaneous enrichment in iron (5 nM) and silicic acid (5 µM) in these estuarine waters resulted in a similar macronutrient uptake enhancement, a 119% increment of the production of biogenic silica and a 2-fold rise in the abundance of *Pseudo-nitzschia spp* (a diatom capable to produce the

neurotoxin domoic acid). We suggest that natural freshwater pulses of allochthonous bioavailable forms of iron and silicon to inner waters of the Patagonia archipelago during the onset of the productive season play a potentially significant role modulating macronutrient dynamics (input vs utilization) and influencing coastal phytoplankton assemblages.

Keywords: dissolved iron, silicic acid, fjord, domoic acid, sub-Antarctic surface water, Patagonia, Chile.

A2.1 INTRODUCTION

Iron (Fe) is an essential micronutrient for marine phytoplankton, and its availability limits primary production in 30-50 % of the surface ocean (Boyd et al., 2007; de Baar et al., 2005; Sunda & Huntsman, 2011)**.** Fe plays a key role in multiple microbial physiological pathways (Raven et al., 1999) including the capacity to utilize macronutrients (e.g., NO_3^-) and resources (e.g., light) (Falkowski & Raven, 1997). Iron limitation in the ocean is primarily associated with poor solubility of thermodynamically stable Fe(III) chemical species in well-oxygenated surface waters and distance from continental Fe sources (de Baar et al., 1999; Liu & Millero, 2002; Martin & Fitzwater, 1988). Coastal waters are proximal to Fe sources and are often characterized by elevated levels of iron, particularly in the form of particles and colloids (Batchelli et al., 2010; Fujii et al., 2008; Gobler et al., 2002; Kunde et al., 2019; Nishioka et al., 2001; Raiswell & Canfield, 2012; Raiswell et al., 2006; von der Heyden & Roychoudhury, 2015). The dissolved iron concentration is controlled by several processes and factors (Croot & Heller, 2012), including the availability of organic Fe-chelators that raise the solubility limit (Kuma et al., 1996; 1998; Liu & Millero, 2002) and the scavenging of iron on to particles (Seo et al., 2022; Tagliabue et al., 2019).

Low concentrations of trace-nutrients (e.g., Fe) and other resources (e.g., silicic acid, light) in macronutrient-rich waters promote the proliferation of smaller organisms and functional groups with adaptations for coping with environmental stressors (e.g., larger surface/area ratio, low or no Si requirement, vertical mobility, mixotrophic capacity; (Caron et al., 2017; Finkel et al., 2010; Lewis, 1976)). However, both smaller sized phytoplankton, as well as other functional groups, struggle to outcompete diatoms under resource replete conditions. The success of coastal diatoms as dominant phytoplankton groups in dynamic and nutrient-rich coastal waters partially rely on their capacity to acclimatize to rapid fluctuations in light availability and to rapidly use available macronutrients (e.g., NO_3^- and PO_4^{-3}). The ability to rapidly utilize macronutrients requires Fe-rich photosynthetic architecture (Strzepek & Harrison, 2004) and Fe-based enzymatic pathways for the reduction of thermodynamically stable forms of inorganic nitrogen (Schoffman et al., 2016). Diatoms have likely evolved to cope with Fe limitation (Lampe et al., 2018) implying that more recently evolved branches of diatoms (i.e., *Coscinodiscophytina, Coscinodiscophyceae*; (Medlin & Kaczmarska, 2004)) could be less sensitive to iron levels of the modern ocean. Genes for iron storage proteins such as Ferritin have been discovered in diatoms (Marchetti et al., 2009). It has been shown that Ferritin-containing pennate diatom *Pseudo-nitzschia granii*, native to iron-limited waters of the Northeast Pacific Ocean, exhibited an exceptionally large luxury iron storage capacity and increased ferritin gene expression at high iron concentrations (Cohen et al., 2018). However, in general, no systematic differences among Ferritin-containing and non-Ferritin containing diatom lineages in their ability to store iron in excess of that needed to support maximum growth rates (Cohen et al., 2018). Has been suggested that Ferritin may serve multiple functional roles that are independent of diatom phylogeny (Cohen et al., 2018).

Diatom growth requires silicic acid (DSi), but silicification of diatom frustules is highly plastic, allowing them to grow in a wide range of environments. Hence diatoms can significantly reduce their silicification levels under silicon-limited conditions (Ragueneau et al., 2000), however DSi concentration < 2µM often preclude diatoms to dominate the phytoplankton ensemble (Egge & Aksnes, 1992). Diatoms stressed by macro or micronutrients shortage (e.g., Fe, N) can continue silicification depending on the availability of DSi. Indeed, iron limitation in macronutrient and DSi rich waters induce high DSi/N uptake ratios (Hutchins & Bruland, 1998; Takeda, 1998), potentially leading to High Nutrient Low Silicate Low Chlorophyll (HNLSiLC) conditions. Although iron limitation effect on DSi/N uptake rates in diatoms can be fully reverted after iron enrichment (Brzezinski et al., 2002; Franck et al., 2003; M. Franck et al., 2000), the DSi deficient seawater relative to N will remain unless an allochthonous Si input occurs. Iron stimulated diatom division rate in low DSi but N and P-rich waters could result in thin frustules due the dependency in the extent of silicification on the growth rate (Martin-Jézéquel et al., 2000).

N and Si metabolism in diatoms is not closely tied since cellular energy for silicification and transport comes from aerobic respiration without any direct involvement of photosynthetic energy (Martin-Jézéquel et al., 2000). Therefore, it has been proposed that when both Si and Fe are depleted, Si uptake is limited by silicic acid concentration while N uptake and photosynthesis are limited by Fe (Ragueneau et al., 2000). The degree of silicification may in turn play a role in the diatom prey-predator dynamics, frustules recycling times, cell density and therefore with the potential to modulate the channeling of diatom biomass energy through both the water column and the trophic web (Assmy et al., 2013; Grønning & Kiørboe, 2020; Kemp et al., 2000; Ryderheim et al., 2022; Smetacek, 1998; 2012). While the inputs of bioavailable Fe to nitrate rich waters could be critical in setting the timing and intensity of new productivity during the productive season of high latitude

ecosystems, inputs of bioavailable Si may be pivotal in the fate of this new productivity (Martin et al., 2013). Diatom standing stock in surface waters can be controlled by mortality (e.g., grazing (Steinberg & Landry, 2017), parasitism (Tillmann et al., 1999)) and the formation of rapidly sinking aggregates (Logan et al., 1995; Mopper et al., 1995).

Bottle-incubation experiments using Subantarctic Front water at Crozet basin (Sedwick et al., 2002) showed that soon after (< 4.5 days) adding iron a macronutrient drawdown increased relative controls. Greater abundance of pennate diatom and biogenic silica (bSi) were also observed in bottles that were amended with both Fe and DSi, relative to controls and bottles that were amended exclusively with Fe (Hutchins et al., 2001; Sedwick et al., 2002). Similar experiments conducted in equatorial Pacific HNLCLSi surface waters demonstrated that the simultaneous addition of Fe and DSi enhanced rates of diatom organic matter accumulation and cell division (Marchetti et al., 2010). Larger diatom standing stock after the addition of both DSi and Fe could be attributed to large diatom growth rates and/or lower diatom mortality rates compared to controls.

Micro-zooplankton grazing is considered one of the largest loss factors of marine primary production (Calbet & Landry, 2004; Steinberg & Landry, 2017). Heterotrophic dinoflagellates can comprise 60–80% of microplankton grazer biomass during spring blooms at high latitudes (Menden-Deuer et al., 2018). In subantarctic waters dinoflagellates of the genus *Gymnodinium* and *Gyrodinium* have been reported to feed and grow on diatom blooms (Saito et al., 2006). Grazer activity is significantly modulated by the characteristic of the prey (e.g., size, shape, silicification degree, physiological state (Assmy et al., 2013; Liu et al., 2016; Lürling, 2021)) which in turn can be a function of the availability of nutrients and silicic acid, among other factors.

The natural enrichment of Fe and DSi in macronutrient-rich eastern Pacific subantarctic waters could be a key process driving the shift in phytoplankton assemblage from flagellates (e.g., *Prymnesiophytes*) dominating in open eastern Pacific subantarctic waters (Bouman et al., 2012; de Baar et al., 1999) to large diatoms dominating in the inner waters of PAIS during the productive growing season (Iriarte et al., 2001). The orographic effect of the Patagonian Andes intercepting the moist Westerlies (Smith & Evans, 2007) results in a major supply of terrestrial waters and associated solutes into the coastal ocean. Large volume of precipitation, run-off and continental ice melt result in a buoyant surface layer likely enriched in allochthonous "continental" nutrients (e.g., silicon and iron; Hopwood et al., 2019; Pryer et al., 2020 ; Torres et al., 2014) which are scarce in the subantarctic open waters (Sarmiento et al., 2004; Torres et al., 2014) that flow into the archipelago. However, the internal cycling of bioavailable forms iron in the water column (Tagliabue et al., 2019), the complex interaction between continent-ocean-atmosphere, and the estuarine metabolism (Bianchi, 2007; Bianchi et al., 2020) are expected to drive high spatio-temporal variability of the concentration of terrestrially derived bioactive elements (e.g., silicon and iron).

High nutrient low chlorophyll (HNLC) concentrations in the euphotic layer during austral spring has been reported in the southern western portion of the Patagonian archipelago (Iriarte et al., 2018). While the observation of "coastal HNLC" conditions during austral spring has been attributed to light (low stratification) and DSi deficit waters because of oceanic SAASW intrusion into the archipelago, events of high biological productivity and drastic drops in surface seawater pCO_2 are often associated to stratification forced primarily from freshwater discharge from the continent. Indeed, along Patagonia, surface waters of salinity lower than 28 are typically under saturated in pCO_2 during the productive season (Torres et al., 2011). Fe has been shown to be the

limiting nutrient in the productive continental shelves surrounding the Antarctic continent; however, no attempt to assess the levels of dissolved Fe or test its effects on phytoplankton has been reported for PAIS. The bioavailability of Fe in PAIS has been assumed to be replete for phytoplankton needs due the many and varied potential sources of Fe (e.g., large amount surface runoff (Dávila et al., 2002) and glacial meltwater inputs (Chen et al., 2007; Glasser et al., 2011; Hopwood et al., 2019; Willis et al., 2012). However, removal of dissolved iron at low salinities in estuaries can be significant due to flocculation, aggregation, and scavenging from the euphotic zone (Boyle et al., 1977; Hopwood et al., 2016; Schroth et al., 2014; Sholkovitz, 1976; Sholkovitz et al., 1978; Yeats & Bewers, 1976). Processes of bioavailable Fe removal could lead to suboptimal conditions for blooming phytoplankton in fjord waters (Öztürk et al., 2002). Currently, comprehensive datasets and integrated analysis of trace metals, nutrients and phytoplankton characteristics in the productive dynamic of this austral ecosystem are lacking.

We report an on-deck nutrient addition bottle incubation experiment as an initial attempt to explore the response of phytoplankton communities in southern PAIS waters to Fe and Fe+DSi amendments. We test the microbial consortia's capacity to use macronutrients (nitrate, phosphate, silicate, carbon) and phytoplankton (diatom and dinoflagellates) abundance, composition, allocation of photosynthetic pigments in different size ranges, cellular domoic acid (DA) production and biogenic silica concentration. Additionally, we describe the spatial variability of the majority of variables mentioned above for a latitudinal transect along the southern portion of the PAIS (53.5-50.5°S) with a spatial resolution of <15 km during austral spring. The discussion of survey results will explore the effect of continental freshwater discharge and associated solutes on the spatial-temporal variability of diatom blooms in southern Patagonia.

A2.2 METHODS

A2.2.1 Study area

Hyper humid subantarctic fjords and continental reservoirs of freshwater (including ice fields and peatlands) result in high levels of freshwater discharge year-round, particularly during the warm summer period associated with snow and glacier melting as is observed in the largest hydrographic basin of the study area (Rio Serrano basin, figure A2.1).

Freshwater discharge varied spatially depending on hydrographic basin configuration, latitudinal and longitudinal gradients in precipitation associated with westerlies, with maximum levels (up to 7-10 m y^{-1}) at the western boundary of the archipelago where hydrographic basins are small (e.g., near 50°S) contrasting with large hydrographic basin at the continental side. The continental inputs include different freshwater discharge sources (glacier runoff and non-glacier runoff fed by direct precipitation) that flow into coastal waters, likely influencing the dissolved and particulate material loads of freshwaters (Pryer et al., 2019 ; 2020).

The transect of marine interior fjord waters starts in the Magellan Strait, running from Peninsula Brunswick near the mouth of Otway sound (Sta. 1; 53.7°S) to the mouth of Xaultegua Gulf (Sta. 7; 53.1°S), where the transect is interrupted by western ocean exposure, resuming in interior waters near Isla Renourd (Sta. 8; 52.6°S) and continuing until Madre de Dios Archipelago (Sta. 29; 50.5°S). The transect is therefore characterized by constrained inland marine waters in close contact with innumerable small to medium point sources of continental runoff, areas of concentrated high-volume runoff where interior canals connect with the large Rio Serrano basin (Stations 12-13, near the western mouth of Union Channel), and areas of glacial input from the Darwin Range (Stations 1-2) and the Southern Patagonia Icefields (Stations 17-22). In addition to runoff generated from continental basins and glacial meltwater, direct precipitation is expected to

contribute a significant percentage of dilute freshwater input along the transect, which is characterized by a precipitation gradient ranging from 2.000 to 7.000 mm y^{-1}. Surface lithology along this transect is diverse (Torres et al., 2014), as is vegetation cover (Luebert & Pliscoff, 2006) and potentials soils (virtually uncharacterized, but likely ranging from volcanic Andosols, Entisols in recently deglaciated areas, and abundant Histosols corresponding with extensive wetlands). The corresponding quality of freshwater inputs, in terms of nutrients and other solutes is also expected to be diverse but remains poorly unknown. Partitioning of freshwater inputs is generalized here (figure A2.1B, A2.1C) as direct precipitation (trace solutes), glacial runoff (high suspended load and low nutrient), and land-surface runoff (diverse and variable solute and suspended load). The experimental location and surface water grab samples which constitute the experimental matrix were between stations 25 and 29 (figure A2.1, Concepción Channel), at the end of the fjord transect near the Madre de Dios Archipelago, representing transitions in surface runoff lithology from crystaline/granitic to sedimentary limestone, strong climatic gradient, and geographic transition from inner to outer fjords, with corresponding gradients in salinity and terrestrial subsidy (described in Torres et al. (2020)).

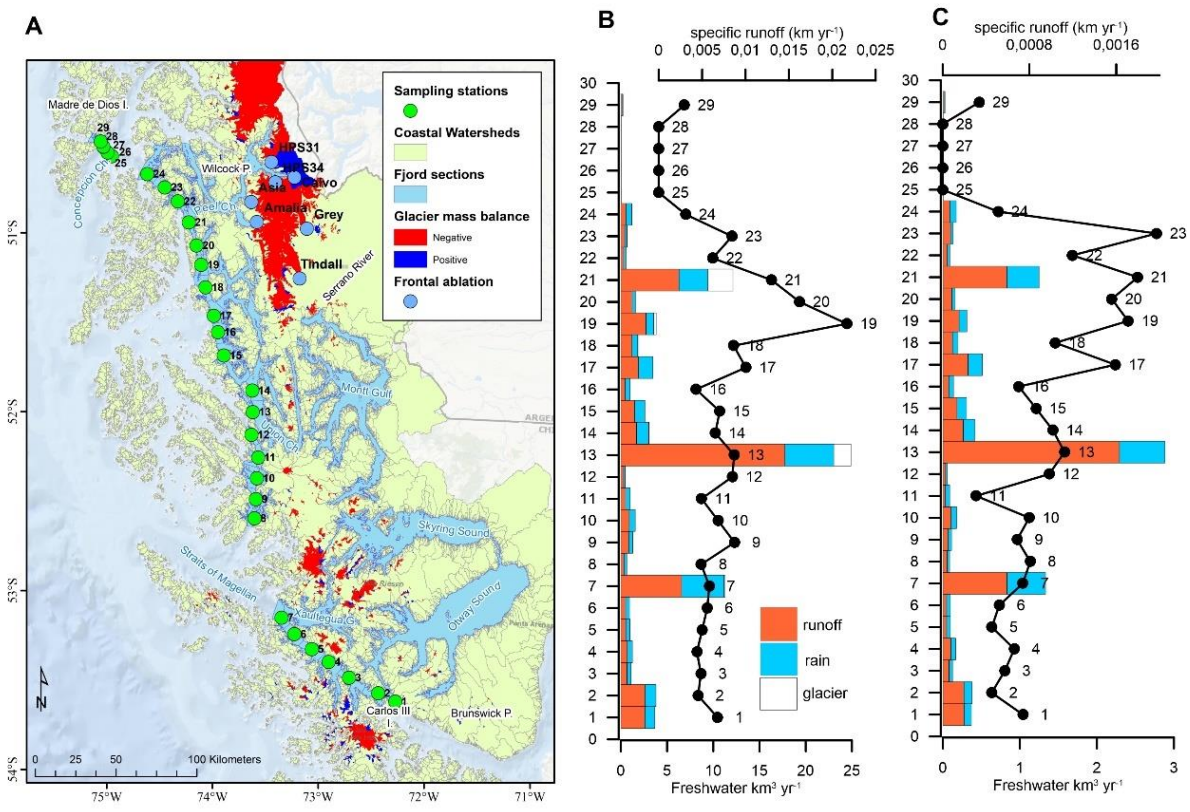

Figure A2.1. *Surface water sampling stations and estimation of freshwater inputs linked to transect stations. Left panel shows stations along the coastal transect of fjords and channels spanning 3 degrees. Also shown are coastal watersheds providing runoff from adjacent terrestrial sources, together with glacial inputs indicated by areas of receding glaciers, and net changes in ice field thickness. Central panel summarized mean annual freshwater volume input near sampling stations and respective sources along the transect, based on calculation shown in supl. table A.1. Right panel summarized freshwater input near the stations during August and September 2017 and respective sources along the transect, based on calculation shown in Supl.Mat A.*

A2.2.2 Underway sampling

Underway sampling of surface waters from 53.5°S to 50.5°S (figure A2.1) was carried out from 22-23 September 2017. Surface water was collected at ~1m depth and ~3m off the side of the vessel using a lab-made, metal free, tow “fish" connected through polyethylene tubes with two non-metallic ARO™ air operated diaphragm pumps. All surfaces that came into contact with the sample were acid cleaned. One sampling line outlet, was located inside a small ($1m^2$) flow laminar

bench to allow clean sampling (used exclusively to trace metal work), and the other sampling line outlet was connected to a small CTD (Idronaut 304) and used to collect discrete samples for determining pH, A_T, nitrate, phosphate, silicic acid (DSi), biogenic silica and size fractionated chlorophyll a (chl a). This underway system was used to collect 29 discrete seawater surface samples (Stations 1-29, figure A2.1A,B) at an approximate rate of one sample per hour while steaming (8-14 km h^{-1}) along the track shown in figure A2.1a.

A2.2.3 Incubation water

Unfiltered surface seawater for bottle incubation experiments was collected using the tow fish systems described above. Twelve acid cleaned (soaked in 10% trace metal grade HCl for 3 months), and carefully rinsed with 18.2 MΩ cm^{-1} milli-Q water within a laminar flow bench. 25 L polycarbonate carboys (Nalgene) were filled with surface seawater while steaming at low speed (<8 km h^{-1}) across Concepcion channel (CC), from St. 25 to St. 27 (figure A2.1). The carboys correspond to four groups (G1 to G4) of three 25 L incubations carboys (control, +Fe, and +Fe+Si; i.e., 12 carboys in total). Each group was filled virtually simultaneously immediately before station 25, between stations 25-26, 26-27, and immediately before station 27. Iron enrichments were spikes of an aqueous solution of $FeCl_3$ to a final concentration of 5 nM. Similarly, Fe and Si enrichments to a final solution of 5nM (Fe) and 5µM (Si) were achieved by the addition of aliquots of aqueous solutions of $FeCl_3$ and Na_2SiO_3. Environmental DSi variability ranged between 3-9 µM therefore it is likely that initial concentration of DSi in the Si enrichment treatments (i.e., +Fe+DSi) lay between 44% to 133% the initial DSi concentration in control and +Fe treatment (see discussion section A4). We measured total dissolved iron (DFe, see method section A2.2.7) at the end of each experiment, and it ranged from 4.9 nM to 11.4 nM. The average net increment in DFe in iron

enriched carboys (i.e., +Fe and +Fe+Si) relative to controls was ca. 1 nM (see section A2.3.2; figure A2.3).

The 12 carboys were incubated on deck for three days (the daylength was ~12 h) and immersed in an intermittently surface seawater running water bath to keep them near the ambient sea surface water temperature (ca. 8°C, see figure A2h). Immediately after the incubation period, pH was measured and subsamples were collected for size-fractionated chlorophyll a, macronutrients, biogenic silica, domoic acid, phytoplankton abundance and SEM identification, total alkalinity, and salinity.

A2.2.4 Salinity and carbonate system parameters

Discrete samples collected along the transect were analyzed for salinity with a salinometer (YSI Model Pro30; calibrated with IAPSO standard seawater) at a constant temperature of 25.0°C. Total alkalinity (A_T) was determined using an automatic potentiometric titration system (Haraldsson et al., 1997). A_T accuracy was verified with certified reference material (CRM) supplied by Andrew Dickson (Scripps Institution of Oceanography). Based on the analysis of blind A_T samples during the "2017 Inter-laboratory Comparison of CO_2 Measurements" (coordinated. Emily Bockmon and Andrew Dickson, unpublished data) we estimate deviations of approximately 0.1% from the reference value (uncertainties ca. 2 µmol kg^{-1}). Surface seawater pH was measured in discrete samples immediately after collection, at a constant temperature (25.0°C), following (DOE, 1994) using a Metrohm pH meter (model 780) and a glass-fixed ground-joint diaphragm electrode with an integrated platinum resistance thermometer (model Aquatrode Plus, Metrohm) calibrated every 12h with Tris buffer in synthetic seawater. Accuracy was previously verified using a certified Tris buffer supplied by Andrew Dickson Laboratory (Scripps Institution of Oceanography), and the overall uncertainty in the measured pH values was estimated by Torres et al. (1999) as 0.006 pH

units for marine surface waters. A previous at-sea comparison between pH measured by spectrophotometric (DOE, 1994) and pH measured by the potentiometric method described above, showed absolute mean differences of 0.01 pH units in the salinity range from 22 to 27 (E. Alarcón, unpublished data). Carbonate system speciation and the seawater saturation state with respect to calcium carbonate (Omega) were determined using CO2SYS software (Lewis & Wallace, 1998) set with K_1 and K_2 constants (Dickson & Millero, 1987) derived from a refit of Mehrbach solubility data (Mehrbach et al., 1973), using measured values of pH, A_T, temperature, salinity, silicic acid, and phosphate. Overall uncertainties in the calculated pCO_2 and C_T, including those derived from uncertainties in carbonate system measurements and uncertainties in constants (K_0, K_1, and K_3), were previously estimated to be approximately 9 µatm and 9 µmol kg^{-1}, respectively (Torres et al., 1999).

A2.2.5 Nutrients, fractionated chlorophyll a and biogenic Si

Nitrate, nitrite, phosphate and silicic acid (DSi) were analyzed colorimetrically following (Strickland & Parsons, 1968) manual method. The standard solutions were made from salts of KNO_3 (Riedel-de Haën Lot 6167A), $NaNO_2$ (Riedel-de Haën Lot 51010) and KH_2PO_4 (Riedel-de Haën Lot 53550), in the case of silicic acid, a Merck™ silicon standard solution (traceable to NIST Standard Reference Material) was used. Although no replicates or other assessment of precision was performed during the analysis of the samples, the attainable precision for the used methods is likely < 6% (Grasshoff et al., 1998). We use Whatman GF/F 0.7 µm glass microfiber filters, 0.45µm and 2µm polycarbonate membranes, in combination with 20 µm and 200 µm mesh nets to fractionate phytoplankton in three size fractions: 0.45-2 µm, 2-20 µm, 0.7-200 µm. The 0.45, 0.7 and 2 µm filters were kept in liquid nitrogen, until pigments were extract in 90% acetone solution to be analyzed for chlorophyll a (chl a) using a Trilogy Turner Designs fluorometer previously

calibrated with a *Anacystis nidulans* chl a standard (Strickland & Parsons, 1968). Each individual chla measurement was done without replicates. Size fractionated chl a was classified as pico-chl a (0.45-2 µm), nano-chl a (2-20 µm) and total-chl a (0.7-200 µm). The difference between the total chla and the sum of pico and nano chl a and was assumed equal to micro-chl a. This calculated micro-chl a (20-200 µm) value, however, could be slightly underestimated since total-chl a do not consider the fraction from 0.45 to 0.7 µm size as the pico-chl a fraction do. Indeed, in some stations calculated micro-chl a was slightly negative, in that case they were assumed equal to zero.

Biogenic silicate (bSi) of seston larger 2 µm (retained on 2 µm pore polycarbonate membrane) of one liter of sample was estimated from the digestion of particles in a 85°C Na_2CO_3 0.5 % solution for 2h (DeMaster, 2002). We assumed that although digestion could dissolve some lithogenic silicate (Ragueneau et al., 2005; Ragueneau & Tréguer, 1994), its effect would be minimal due the exclusion of clay (lithogenic silicate particles < 2 µm). Additionally, any relative effect would be canceled when net bSi production is calculated from the same seawater batch incubation.

A2.2.6 Domoic acid

Samples for domoic acid (DA) were processed by vacuum filtration of 1 liter seawater through a muffled 0.7µm Whatman GF/F filter and stored in liquid nitrogen before analysis at the Marine Toxins Laboratory, University of Chile (labtox.cl). At the laboratory the individual filters were transferred to a 100% methanol solution by homogenizing the filter in 1ml of solvent. The homogenized solution was centrifuged (14,000 rpm x 10 min), filtered through a 0.22 µm PVDF Millipore Millex-GV, and dried under nitrogen gas. The dried extract was resuspended and measured via liquid chromatography–tandem mass spectroscopy (LC-MS/MS) with a detection limit of ca. 0.025 µg DA/ml (López-Rivera et al., 2005)

A2.2.7 Phytoplankton

A2.2.7.1 Phytoplankton Abundance determined by optic microscopy

Samples for phytoplankton cell counts were preserved in Lugol´s solution. For samples along the transect (figure A2.1) a 50-mL sub-sample was placed in a sedimentation chamber and allowed to settle for 24 h (Utermohl, 1958) prior to identification under an inverted microscope (Carl Zeiss, Axio Observer A.1). Phytoplankton counting was done without replicates. For experimental samples, phytoplankton abundance was determined similarly (Utermohl, 1958) at the IFOP phytoplankton laboratory (IFOP-Punta Arenas).

A2.2.7.2 Phytoplankton Abundance determined by scanning electron microscopy

Scanning Electron Microscopy (SEM) imagery (Díaz et al., 2020) was used to facilitate phytoplankton identification, diatom volume and estimation of the abundance of *Minidiscus* spp. with apical axis smaller than 3.5 µm (see an example SEM imagery in Supplementary Material B). Intact frustules (single or in aggregates) were counted in 36 SEM images per sample, covering 1.8 mm^2 of the filter area corresponding to 1.5 mL of water analyzed. The *Minidiscus* spp. abundances were calculated using the same equation for coccolithophores given in Díaz et al. (2021).

A2.2.7.3. Diatom biovolume

Several geometric shapes were selected for determining biovolume of diatoms according mainly to (Naz et al., 2013; Olenina et al., 2006), and the website http://nordicmicroalgae.org. The linear dimensions were measured digitally, through scanning electronic photomicrographs using the Photoshop™ software. The volume of each cell was measured and computed in an excel worksheet by applying average dimensions for each species to its most closely geometrical shape (cylinder, sphere, ellipsoid, cone, etc.). For each treatment, at least 30 randomly selected cells for each

species were measured, and in the case of rare species, they were measured as they occurred. The mean biovolume was calculated from the mean value individual cell biovolumes.

A2.2.7.4 Diatom total volume

Total diatom volume was defined as the sum of total volume of each taxa, where the total volume of a particular taxa was equal to an average diatom-taxon biovolume multiplied by diatom-taxa abundance. Therefore, the relative differences in total biovolume of diatoms reported here (comparison between treatments) indicates a change on the diatom assemblage size structure. We assume that biovolume errors are primarily systematic (associated with the simplification of diatom shape to perform the volume calculations, see section A2.2.7.3) which tend to cancel out when analyzed in relative terms, and the non-systematic errors (which is a function primarily dependent on the number of measured individuals) are minimized in the most abundant taxa (were the biometric measurements were carried out in 30 organisms per specie, see section A2.2.7.3). However, we did not attempt to estimate the error of our estimation of total diatom biovolume (since diatom-taxa abundance was done without replicates) and therefore these estimates should be viewed with caution and analyzed in relative terms.

A2.2.7.5. Mean diatom cell volume

Defined as diatom total volume/ diatom abundance ratio. Mean diatom cell volume is therefore exclusively driven by changes in the size structure of the diatom community.

A2.2.8 Dissolved Iron measurements

Seawater samples were filtered through an acid cleaned 0.45 μm capsule filter (Whatman PolyCap GW) and subsequently through a 0.02 μm Anotop 25 syringe filter (pre-cleaned with 0.02 M ultra trace metal grade HCl as per Hawkings et al., 2020) inside a flow laminar bench into acid

cleaned LDPE bottles (cleaned as per GEOTRACES protocols; Cutter et al. (2017)). Samples were acidified with hydrochloric acid to pH~2 in a Class 100 clean room bench and let stand for a month before analysis for Fe, Mn and other metals (not shown here) after preconcentration and matrix removal using an ESI seaFAST pico system. Isotope dilution inductively coupled plasma mass spectrometry (on a sector field inductively coupled plasma mass spectrometer Thermo Element 2) was used to determine Fe concentrations as described in Forsch et al. (2021). Accuracy and precision for Fe were ± 3 %, as determined by repeat measurements of an in-house low Fe seawater reference standard. We use the naming convention of Raiswell et al. (2018) for <0.45 μm and <0.02 μm filtrate as dissolved Fe (DFe) and soluble Fe (sFe), respectively. The difference between DFe and sFe will be assumed to correspond to the colloidal Fe concentration.

A2.2.9 Interpolation, used parameters, analysis and inference limitation.

A2.2.9.1. Interpolation-extrapolation of initial values.

The initial condition for the four incubated groups (G1 to G4) of three treatments (control, +Fe and +Fe+Si) were interpolated/extrapolated assigning station 25 as t=0 of G1, the average value of Sts. 25-26 and Sts. 26-27 as t=0 for G2 and G3, respectively, and assigning station 27 values as t=0 for G4, the merits of this method of "running interpolation" can be seen in the agreement between dashed lines and black filled circles in figures 4, 6-8, 10 and 12.

A2.2.9.2. Parameters and data reduction rationality

We signal the difference of response variables nitrate, phosphate, DSi, pH subtracting the respective initial values (t=0 days) from corresponding end values (t=3 days) of each experimental bottle, shown as Δ. e.g., $\Delta NO_3^- = [NO_3^-{}_{(t=3)} - NO_3^-{}_{(t=0)}]$.

Response was expected to be dependent on initial conditions, which in turn may vary between experimental groups. We therefore define the accumulation parameter (Σ) as the coefficient

between the variation rate of the response variable (Δ response variable / 3 days) and the response variable at the corresponding t=0. e.g., Σ Chla = (ΔChla/3 days)/ Chla $_{(t=0)}$, with units (day^{-1}).

In the specific case of DFe (which was measured only at t=3) we utilize a unitless parameter (Σ_c) to show the magnitude DFe variation (between iron enriched treatment and control) relative to DFe at the control, e.g., Σ_c DFe = [DFe$_{(t=3;\ +Fe)}$ − DFe $_{(t=3,\ control)}$]/ DFe $_{(t=3,\ control).}$

A2.2.9.3. Experimental design: assumption/limitations and interpretation of results.

In order to prevent metal contamination from the vessel´s hull, the collection of seawater for experimentation was done while steaming using a single clean sampling device (see section A2.2.2). Although surface seawater sampling within each experimental group was virtually simultaneous, changes in the characteristics of surface water across Concepcion Channel (CC), discussed in section A2.4.2, preclude considering experimental groups (G1-G4) as replicates.

The accumulative effect (3-day experiment) of the spatial variability of seawater properties across CC has the potential to lead to large differences in standing stock response by means of top-down (e.g., grazing variability between experimental groups) and bottom-up processes (e.g., nutrient variability between experimental groups). The data analysis is therefore be based on the differences between treatments and corresponding controls between treatment and controls (i.e., when all four experimental groups, G1 to G4, show the same pattern) as an increment (+Δ) or a reduction (-Δ) of a response variable. Inconsistent differences between treatment and controls between experimental groups are also analyzed and discussed, searching for potential relationships between the differences between control and treatments of a given response variable with the chemical- biological peculiarities across the CC environmental gradient where surface water was collected (i.e., t=0 spatial gradients). This last analysis is based upon the statistical significance of

the correlation between the experimental response variables and environmental gradient descriptors.

A2.3 RESULTS

A2.3.1 Spatial variability of biogeochemical parameters in the southern portion of the PAIS (53.5-50.5°S) during austral spring 2017

Surface waters along the transect exhibited low salinity values (salinity 25-30, figure A2.2a) compared to fully oceanic SAASW off Patagonia during austral spring (salinity 33-34, (Palma & Silva, 2004)). The percentage of fresh water in surface water (FW) along the transect ranged between 9% and 24%, assuming a two-points dilution curve of terrestrial and marine waters with salinities of 0 and 33.5, respectively. Specific runoff during August and September 2017 near sampling stations (see Sup. Mat A methodology and figure A2.1 and A2.2a) was negatively correlated to salinity ($R=-0.4$; $p=0.03$) and nitrate ($R=-0.4$; $p=0.02$) and positively correlated to SST ($R=+0.6$; $p<0.01$) and the percentage of chl a allocated in micro-size range ($R=+0.5$; $p=0.04$).

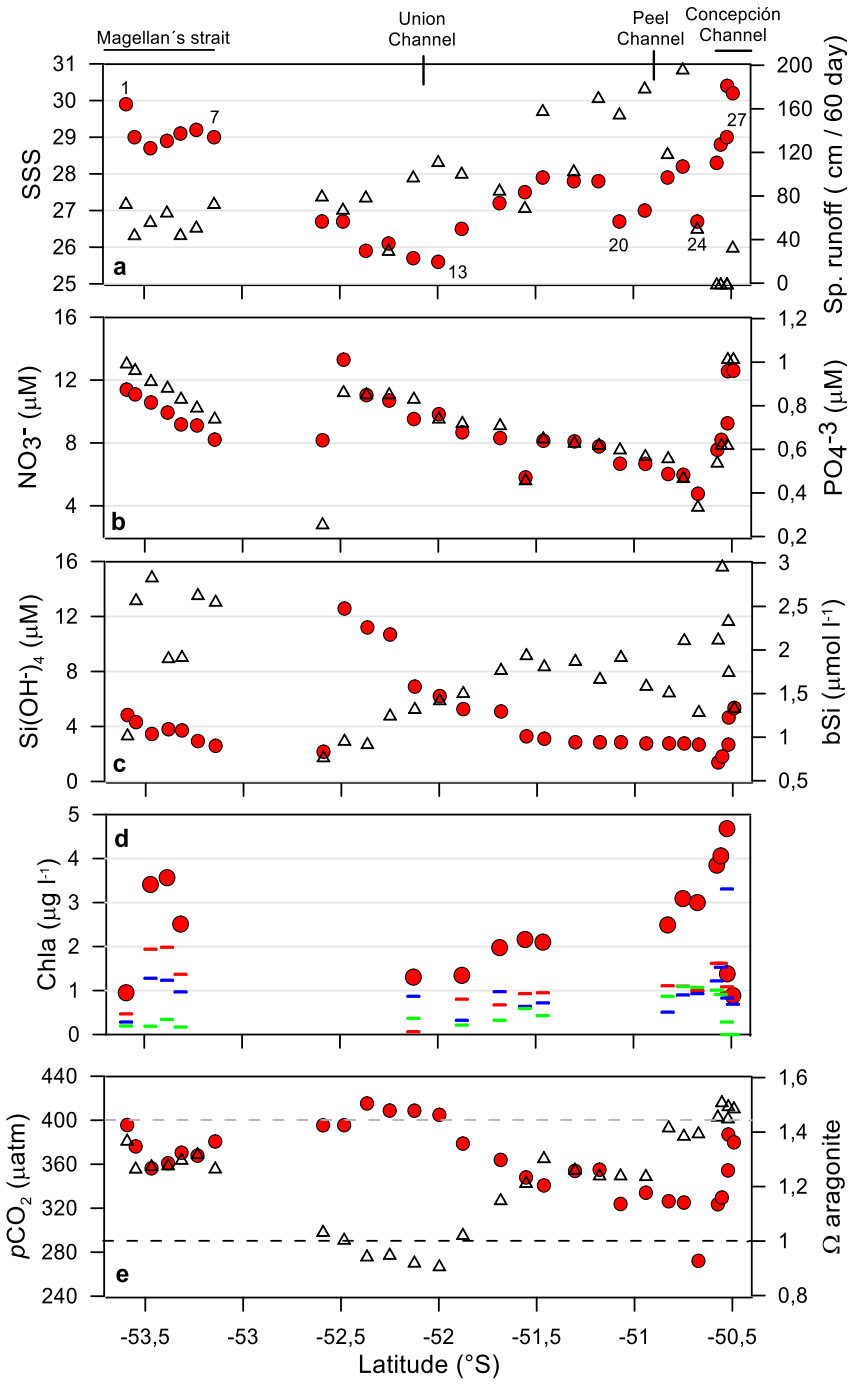

Figure A2.2. *Surface water properties and freshwater inputs along a transect during austral spring 2017. Dots and triangles correspond to the left and right axis respectively. (a) Sea Surface Salinity (SSS) and 60 days mean specific runoff (cm / 60 days) corresponding to august and september 2017 based on figure1c, (b) nitrate (NO3-) and phosphate (PO4-3), (c) dissolved silicate (DSi) and biogenic silicate (bSi), (d) Chlorophyll a (chl a) allocated in the pico, nano and micro size fraction are depicted by the red, blue and green horizontal line, respectively. The summa of all three fractions (total_chl a) is depicted by red dots. (e) Carbon dioxide partial pressure*

(pCO2) and Omega Aragonite (Ωaragonite), atmospheric pCO2 and calcium carbonate saturation with respect to seawater is depicted by upper and lower segmented lines, respectively.

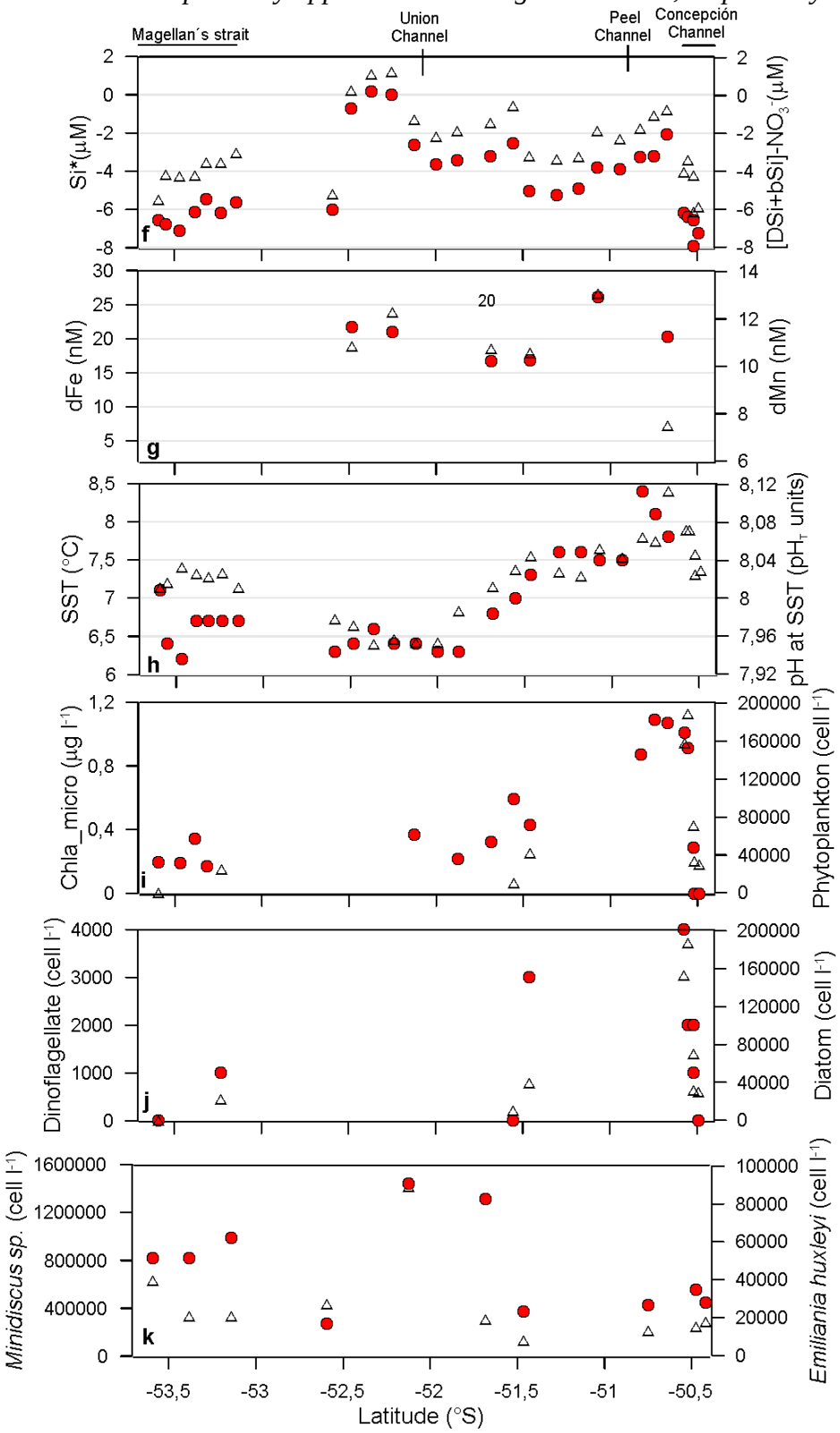

Figure A2.2 (Continuation). *Surface water properties and freshwater inputs along a transect during austral spring 2017. Dots and triangles correspond to the left and right axis, respectively. (f) Silica star (Si*) and the difference between total silicate and nitrate ([DSi+bSi]-NO_3^-). (g) dissolved iron (DFe) and dissolved manganese (DMn). (h) Sea Surface Temperature (SST) and Total-scale pH at in situ temperature. i) chlorophyll a allocated in the micro size fraction (micro-chl a) and micro-phytoplankton abundance. j) Dinoflagellate and diatom abundance. k) Abundances of* Minidiscus spp. *and* Emiliania huxleyi *estimated by SEM. Abundance estimations of* E. huxleyi *were taken from Díaz et al. (2021).*

The surface water with the lowest proportion of FW (i.e., Sts. 1, 28 and 29; salinity ca. 30, figure A2.2a) have the highest levels of nitrate and phosphate (12 ± 0.7 µM and 1.0 ± 0.0 µM respectively; figure A2.2b), and low to moderate levels of DSi (4.9 ± 0.4 µM; figure 2.2c) and biogenic silica (1.4 ± 0.4 µM; figure A2c) with particularly low (negative) Si* values (figure A2.2f) even when dissolved and biogenic silica were summated to estimate a proxy of the potential Si* (i.e., [DSi+bSi] -NO_3^-). Total-chl a concentration in high salinity surface waters (ca. 30) was 1.1 ± 0.3 µg l^{-1} (figure A2.2d), mostly contained in the pico and nano size fractions (figure A2.2d, also see figure A2.2i). pCO_2 of this high salinity water was slightly undersaturated (387±8 µatm; figure A2.2e) relative to atmospheric levels (likely near 403 ppm, see www.esrl.noaa.gov/gmd/ccgg/trends/) and saturated with respect calcium carbonate in the form of aragonite (Omega aragonite ranging from 1.4 to 1.5 approximately, figure A2.2e). Samples for DFe and DMn were not collected in waters with salinities larger than 28, however DFe and DMn were measured in surface waters of salinity 29.3 collected for the incubation experimentation blank in St.27 and were 6 nM DFe and 5 nM DMn (after 3 days of incubation). In stations 11 (salinity 26) and 15 (salinity 27) we analyzed DFe (12 and 17 nM, respectively) and sFe (5 and 3 nM, respectively), suggesting that most the DFe (59 and 79%, respectively) was in the colloidal size fraction (i.e., between 0.45 µm and 0.02 µm in size).

The pH (at temperature in situ) and SST of higher salinity surface water values (corresponding to station 1, 28 and 29) ranged from 8.01 to 8.03 pH units and from 7.1 to 8.0 °C, respectively

(figure A2.2h). These stations were also characterized by very low levels of micro-chl a (<0.4 µg l^{-1}, figure A2.2i) and micro-phytoplankton abundance (<4 x 10^{-3} cell l^{-1}, 2j).

The maximum contribution of FW (~22%) was observed ca. 52.0°S (see St.12-13, figure A2.1; Salinity <26, figure A2.2a) corresponding to the influence of Southern Patagonia Ice Field and the Rio Serrano the only major hydrographic basin that connect to the study area through Montt Gulf and Kirke channel (see figure A2.1). These brackish waters were also high in nitrate and phosphate (~10 µM nitrate, ~0.8 µM phosphate; figure A2.2b), with moderate levels of DSi (~6 µM; figure A2.2c), biogenic silicate of ~1.3 µM (figure A2.2c) and relatively low total-chl a levels (~1.3 µg l^{-1}; figure A2.2d) corresponding mainly to the nano size fractions (~0.9 µg l^{-1}; figure A2.2d). pCO_2 levels of this low salinity water were virtually in equilibrium with the atmosphere (405-409µatm; figure A2.2e) and characterized by the undersaturation of surface water with respect calcium carbonate in the form of Aragonite (Omega aragonite < 0.93; figure A2.2e) and by the highest Si* values (Si*~0 µM; figure A2.2e). This low salinity water (St.11) has DFe and DMn concentrations of 21 nM and 12 nM respectively (figure A2.2g). SST, pH at in situ SST and micro-chl a were relatively low (6.5°C, 7.96 pH units, ~0.4 µg l^{-1}, respectively. See figures A2.2h and A2.2i).

The largest concentrations of biogenic silicate (2.5 ± 0.4 µM; figure A2.2e) and total-chl a (3.5 ± 0.4 µg l^{-1}; figure A2.2f) were found at intermediate salinities (approximately between 27 and 29) adjacent to relatively salty water (>29). These large stock maximums coincided with lower concentrations of nitrate, phosphate, DSi, and pCO_2 (9 ± 2 µM nitrate, 0.7 ± 0.2 µM phosphate, 2.9 ± 1.1 µM dissolved silicate and 350 ± 24 µatm, respectively; figures. A2.2b-c and A2.2e).

In general, nitrate, phosphate and pCO_2 were negatively correlated to chl a in the micro size range (table A2.1). Macronutrients and the amount of chl a in pico and nano size range were not correlated (table A1) although the mean concentration of both pico-chl a (1.1±0.5 µgl^{-1}) and nano-

chl a (1.0±0.5 $\mu g l^{-1}$) were ~ 2 fold larger than micro-chl a (0.5±0.6 $\mu g l^{-1}$). Total-chl a was better correlated with DSi (negatively) and bSi (positively) than any particular size fraction of chl a.

Table A2.1. Pearson correlation coefficient between standing stock of chl a and environmental variables for the transect shown in figure A2.1. N=17. Marked correlations are significant at p < 0.050.

	T_Chla	Pico	Nano	Micro	%pico	%nano	%micro
Sal	0,0317	0,3372	0,164	-0,3895	0,5257	0,0222	-0,6337
	p=,904	p=,186	p=,529	p=,122	p=,030	p=,932	p=,006
Specific	-0,2806	-0,2923	-0,4638	0,2241	-0,0895	-0,3547	0,5039
runoff	p=,275	p=,255	p=,061	p=,387	p=,733	p=,162	p=,039
pH@25°C	0,5471	0,4096	0,2456	0,6937	0,0198	-0,3246	0,3433
	p=,023	p=,103	p=,342	p=,002	p=,940	p=,204	p=,177
AT	-0,0172	0,2341	0,1919	-0,4441	0,4425	0,1257	-0,6541
	p=,948	p=,366	p=,461	p=,074	p=,075	p=,631	p=,004
NO3-	-0,3796	-0,0636	0,0292	-0,8472	0,3211	0,4131	-0,8379
	p=,133	p=,808	p=,911	p=,000	p=,209	p=,099	p=,000
PO4-3	-0,4808	-0,0771	-0,1506	-0,8572	0,3765	0,2916	-0,7649
	p=,051	p=,769	p=,564	p=,000	p=,136	p=,256	p=,000
DSi	-0,7947	-0,6728	-0,3838	-0,6872	-0,0989	0,3735	-0,3069
	p=,000	p=,003	p=,128	p=,002	p=,706	p=,140	p=,231
bSi	0,7548	0,7195	0,577	0,1964	0,0646	0,0918	-0,1783
	p=,000	p=,001	p=,015	p=,450	p=,806	p=,726	p=,493
pCO2	-0,5937	-0,4211	-0,1571	-0,8292	0,0666	0,4287	-0,5609
	p=,012	p=,092	p=,547	p=,000	p=,799	p=,086	p=,019
Si*	-0,1383	-0,4226	-0,3187	0,4954	-0,4538	-0,2132	0,7659
	p=,596	p=,091	p=,212	p=,043	p=,067	p=,411	p=,000

Micro phytoplankton composition analyzed in stations 1, 6, 16, 17, 25-29 were largely dominated by diatoms, but with a large variability along the transect. Minimum abundances were found at St.1 (ca. $1x10^3$ cell l^{-1}) and maximum at St. 27 (ca. $5 x10^5$ cell l^{-1}), mostly corresponding to the class Mediophyceae (e.g., *Thalassiosira*, *Chaetoceros*, *Leptocylindrus*, and *Skeletonema* genus; data not shown). Dinoflagellates represented between 0.5-8 % of micro-phytoplankton abundance, with densities that did not exceed $4x10^3$ cell l^{-1} (data not shown). Scanning Electron Microscopy (SEM) imagery for stations 1, 4, 7, 8, 12, 15, 17, and 23 showed the presence of very small free centric diatoms of a mean diameter of 2-3.5 µm (*Minidiscus spp*. Rivera and Koch, 1984, see Supplementary material B) co-occurring with the coccolithophore *Emiliania huxleyi* with abundances ranging between 1.3×10^5-1.4×10^6 and 1.7×10^4- 9.1×10^5 cell l^{-1}, respectively

(figure A2.2k; *n* = 11 stations). The micro-phytoplankton were dominated by diatoms, however the biogenic silicate in particles > 2µm were not correlated to the content of micro-chl a but correlated with total-chl a, pico-chl a and nano-chl a (table A2.1).

The pCO_2 along the transect was positively correlated to nitrate, phosphate and dissolved silicate (R^2: 0.7, 0.6 and 0.7 respectively; p-value < 0.005) and negatively correlated with micro-chl a and total-chl a (table A2.1). pH and A_T in surface waters ranged from 7.95 to 8.11 pH units and from 1742 to 2068 µmol Kg^{-1} respectively (data not shown). A_T was strongly correlated to salinity (R^2=0.96). Surface waters with salinity lower than 26.5 were virtually in equilibrium with the atmosphere (pCO_2 = 409±4uatm, figure A2.2j) but undersaturated with respect to calcium carbonate in the form of Aragonite (figure A2.2l).

A2.3.2 DFe and DFe+DSi enrichment incubations

A2.3.2.1 Initial conditions

Sea surface water used in the iron enrichment experiment was collected over salinities from 28 to 29, characterized by high levels of total-chl a (3.9-4.7 µg chl a l^{-1}) and low chl a percentage (6%-26%) in the micro size-range. The diatom abundance ranged between $4x10^4$ and $5x10^5$ cell l^{-1}. Diatom mean volume, bSi, and DSi ranged from 400 -1600 μm^3 $cell^{-1}$, 2 - 3 µmol Si l^{-1} and 3 - 9 µM, respectively. The concentration of nitrate and phosphate ranged from 7.6 - 9.2 µM and 0.5 - 0.6 µM respectively. The pCO_2 calculated from pH-A_T pairs suggests that this water was undersaturated relative to the atmosphere, ranging between 324 µatm and 354 µatm. Salinity, total -chl a, nitrate, phosphate, and pCO_2 tended to increase westward from St.25 to St.27, but micro-chl a and diatom abundance tended to decrease (see dashed line in figure A2.6). Diatom mean volume, bSi and DSi reached a relative maximum at the middle station (i.e., St.26). Dissolved iron was only measured at the end of the experiment (t=3; figure A2.3). The final mean increments of

total dissolved iron (DFe) in +Fe enriched treatments relative controls was ca. 1 nM but highly variable between bottles, representing a moderate increment from the control levels (20 - 25 %) and only the 20 % of the intended Fe enrichment (i.e., 1 of 5 nM).

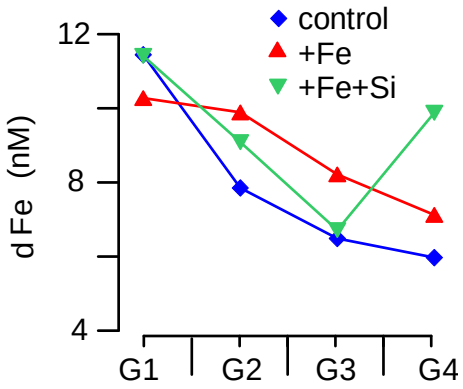

Figure A2.3. *Dissolved iron at t=3 days in control carboys (blue), enriched in Fe (red) and enriched in both Fe and Si (green). The values of figure A2.3 can be inspected in supplementary material D.*

A2.3.2.2 Macronutrients and DSi drawdown

The concentrations of nitrate and phosphate at the end of the incubation period (t=3) were low relative to t=0, reaching minimum levels in the iron enriched treatments (+ Fe and + Fe+Si treatments) compared to controls. DSi concentrations in t=0 and t=3 were highly variable, with the exception of +Fe treatment at t=3 where DSi levels were consistently close to 2µM.

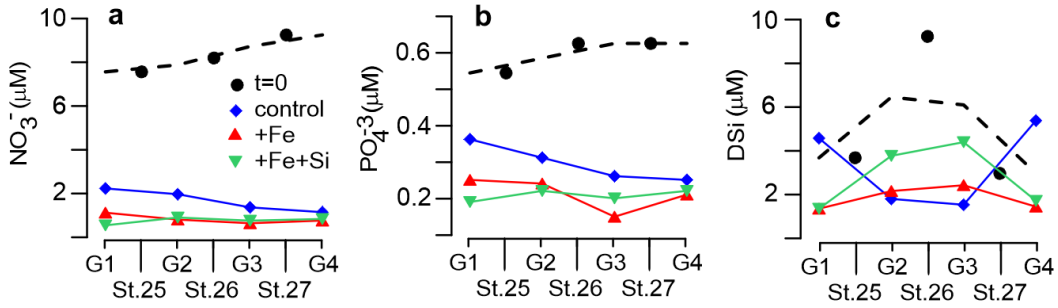

Figure A2.4. *Surface water nitrate, phosphate and DSi at the start (t = 0) and after three days of "on-deck" incubation (t = 3). Dots depict the surface water concentration of macronutrients and DSi within the East-West transect where experimental carboys (G1-G4) were filled. Coloured symbols depict the concentration of macronutrients and DSi (in controls and in Fe and Fe+Si treatments) after 3 days of "on-deck" incubation. Dashed line corresponds to the interpolated t=0 values that were used for the calculation of macronutrients drawdown for each group of carboys (G1-G4).*

Nitrate drawdown (ΔNO_3^-) at + Fe and + Fe+Si treatments was enhanced by 13% and 14% respectively relative to the control (figure A2.4a). Maximum ΔNO_3^- occurred at G4 (western side of CC transect), however, the maximum difference in ΔNO_3^- between controls and +Fe treatments seems to occur in G1-G2 (eastern side of the CC transect, figure A2.4a). A similar pattern followed phosphate drawdown in +Fe and +Fe+Si treatments, with drawdown enhanced by 28% and 30% respectively relative to the control (figure A2.4b).

In general, the nitrate drawdown and phosphate drawdown relationship was linear and positive ($\Delta NO_3^- = 11.9 \times \Delta PO_4^{-3} - 3$, $R^2=0.8$, n=12, $p<0.005$); the calculated slope (i.e., 11.9) was fully consistent with mean drawdown ratio reported for diatom-dominated Antarctic waters (Arrigo et al., 2002). Total inorganic carbon drawdown and phosphate drawdown were not correlated ($\Delta C_T = 99.2 \times \Delta PO_4^{-3} + 28$, $R^2=0.2$, n=12, p=0.17). Similarly, the nitrate drawdown and DSi drawdown were not correlated ($R^2=0.01$). The nitrate/ DSi drawdown ratio was 1.3±0.3 (n=4) at +Fe+Si treatments and 3-fold larger in +Fe treatments (3.0±1.7, n=4). Indeed, the ΔDSi drawdown reached a maximum in the +Fe+Si treatment (ca. 6 µM, assuming that the added DSi was not polymerized). DSi drawdown was similar in the +Fe and control incubations at G2 and G3, but significantly different at G1 and G4, where a small DSi increase in controls occurred relative t = 0 levels (ΔDSi ca. +2µM; figure A2.4c).

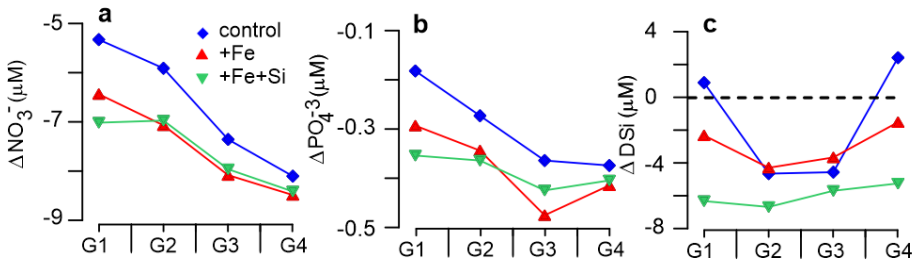

Figure A2.5. *Nitrate, phosphate, and DSi drawdown during the incubation period (3 days). Negative values indicate drawdown and positive values indicate gain.*

A2.3.2.3 Chlorophyll a

The mean concentrations of total chl a doubled after 3 days incubation, associated mainly with phytoplankton growth in the pico and micro size fractions. No consistent differences between treatment and control were observed, with the exception of relatively low total chl a levels in +Fe treatments relative to controls (figure A2.6a). Spatial patterns were evident for total chl a, e.g., it was relatively low in G1 and G2 compared to G3 and G4 at both t = 0 and t = 3 (figure A2.6a). Additionally, in t = 0 and controls (no nutrient enrichment), nano-chl a increased from G1 to G4 (figure A2.6c). Micro-chl a in Fe-enriched treatments was higher in G3 and G4 relative to G1 and G2, with the exception of the G1 control (figure A2.6d).

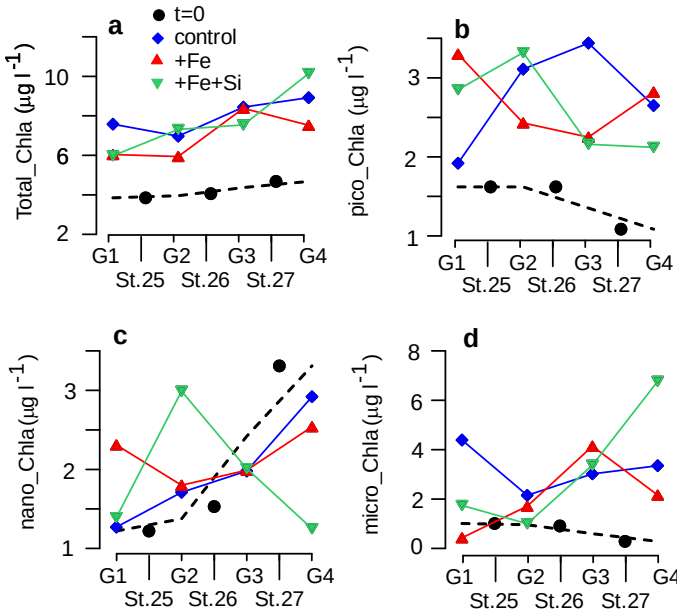

Figure A2.6. *Surface water total chlorophyll a in three size ranges (pico, nano, and micro) at t=0 and after three days of "on-deck" incubation. Dots depict the chl a within the East-West transect stations (Sts. 25-27) where experimental carboys (G1-G4) were filled. Colored symbols depict the concentration of chl a (in controls and in DFe and DFe+DSi treatments) after 3 days of "on-deck" incubation. The dashed line corresponds to the interpolated t = 0 values that were used for the calculation of the chl a accumulation for each group of carboys (G1-G4).*

A2.3.2.4. Biogenic silicate, diatom total volume

The bSi was higher in +Fe+Si than in +Fe and the control (figure A2.7a). The total diatom volume was variable but higher in the control and +Fe+Si treatments at t = 3 compared to t=0, (figure A2.7b). The diatom mean volume was variable but tended to be small and less variable in G1 and G2 compared to G3 and G4 (figure A2.7c), note that diatom mean volume tend to be smaller at t = 3 compared to t = 0, with the exception of +Fe+Si G3 and control G4 (figure A2.7c).

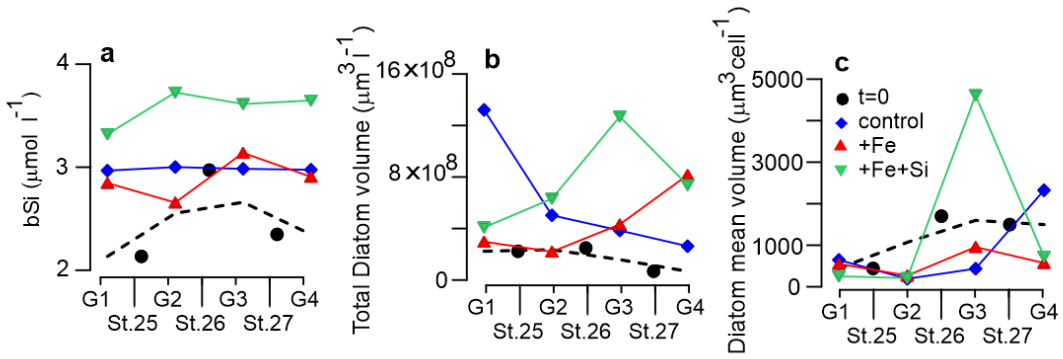

Figure A2.7. *Surface water bSi, total diatom volume, and diatom mean volume at t=0 and after three days of "on-deck" incubation. Dots depict the last variables within the East-West transect stations (Sts. 25-27) where experimental carboys (G1-G4) were filled. Colored symbols depict the variable levels (in controls and in Fe and Fe+Si treatments) at t=3 of "on-deck" incubation. The dashed line corresponds to the interpolated t=0 values that were used for the calculation of the accumulation parameter for those variables.*

Diatom abundance was highly variable and different between taxa (figure A2.8). No consistent differences were detected with the notable exception of *Pseudo-nitzschia*, as described in the section A2.3.2.5.

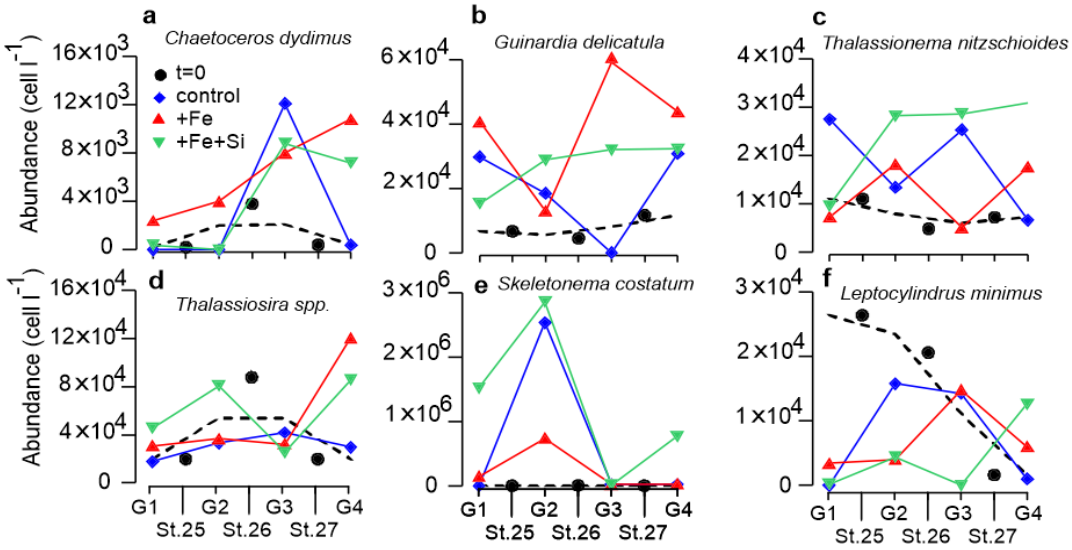

Figure A2.8. *Selected diatom taxas from surface water at t=0 and after three days of "on-deck" incubation. Dots depict the abundance of selected taxas within the East-West transect stations (Sts. 25-27) where experimental carboys (G1-G4) were filled. Colored symbols depict the taxon´s abundance (in controls and in Fe and Fe+Si treatments) after 3 days of "on-deck" incubation. The dashed line corresponds to the interpolated abundance of the shown diatom taxa at t=0.*

In general, the mean relative contribution of diatom classes to the total biovolume shown little variability, with the exception of +Si+Fe treatment, which seems to suggest increased contribution of Mediophyceae and reduced the influence of Coscinodiscophyceae (table A2.2). Bacillariophyceae contribution to diatom biovolume was low (ranging between 3% and 6%), but twice as large in +Fe+Si relative to control. The total diatom biovolume was variable, but for Mediophyceae and Bacillariophyceae was larger in +Fe+Si treatment compared to t=0 (figure A2.9).

Table A2.2. Relative contribution of diatom classes (Bacillariophyceae, Mediophyceae and Coscinodiscophyceae) to total diatom biovolume at t=0 and t=3 (control, +Fe and +Fe+Si).

	% Bacilliophyceae	**% Mediophyceae**	**% Coscinodiscophyceae**
t0	**5.2±2.3 (n=3)**	**75±12 (n=3)**	**19±13 (n=3)**
Control	**3.3±0.9 (n=4)**	**75±11 (n=4)**	**22±12 (n=4)**
+Fe	**4.7±4.7 (n=4)**	**76±7 (n=4)**	**20±20 (n=4)**
+Fe+Si	**6.2±4.8 (n=4)**	**88±8 (n=4)**	**11±7 (n=4)**

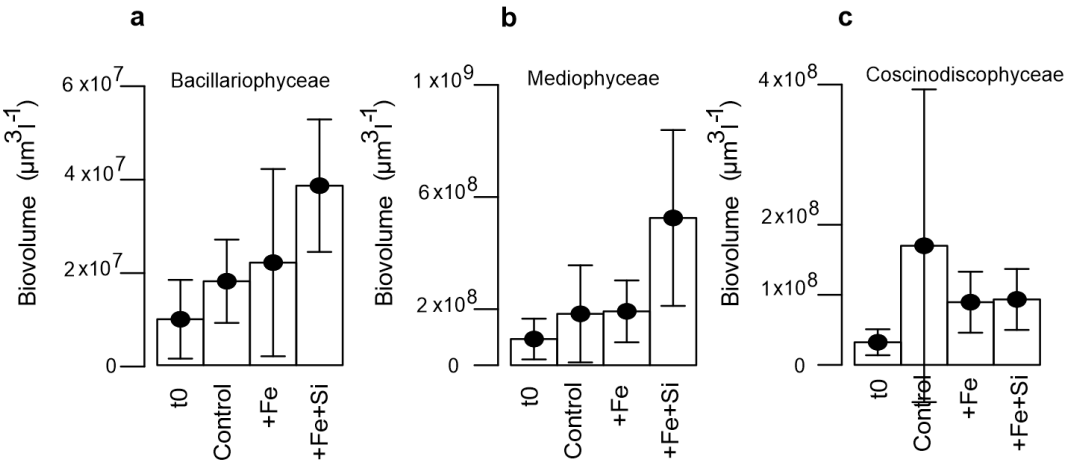

Figure A2.9. *Total diatom volume (biovolume) at t=0 and after three days (control, +Fe and +Fe+Si) of "on-deck" incubation. Bars indicate standard deviation.*

A2.3.2.5. Pseudo-nitzschia and cellular domoic acid.

Bacillariophyceae abundance was dominated by relatively small *Pseudo-nitzschia* var *seriata* and *delicatissima*, which show a sharp increase from t=0 to t=3 in control and +Fe+Si treatment but not +Fe treatment (figure A2.10). From all 22 diatom taxa identified, only *Pseudo-nitzschia var. dellicatissima* (Hasle et al., 1996) was consistently higher in +Fe+Si treatment relative to controls. *Pseudo-nitzschia var. dellicatissima* abundance at +Fe treatment was close to t=0 abundances.

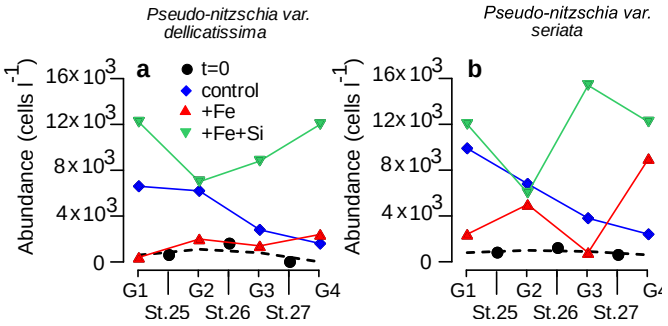

Figure A2.10*. Pseudo-nitzschia spp. at t=0 and after three days of "on-deck" incubation. Dots depict the abundance of* Pseudo-nitzschia spp. *within the CC East-West transect where experimental carboys (G1-G4) were filled. Colored symbols depict the abundance of* Pseudo-nitzschia spp *(in controls and in+Fe and +Fe+Si treatments) after 3 days of "on-deck" incubation. The dashed line corresponds to the interpolated abundance of the shown diatom taxa at t=0.*

Domoic acid (DA), a neurotoxin attributed to the diatom genus *Pseudo-nitzschia*, was highly variable and not correlated with *Pseudo-nitzschia* abundance. However, the DA per *Pseudo-nitzschia* cell was very low and constant in the +Fe+DSi treatment relative to both the control and +Fe treatment (figure A2.11).

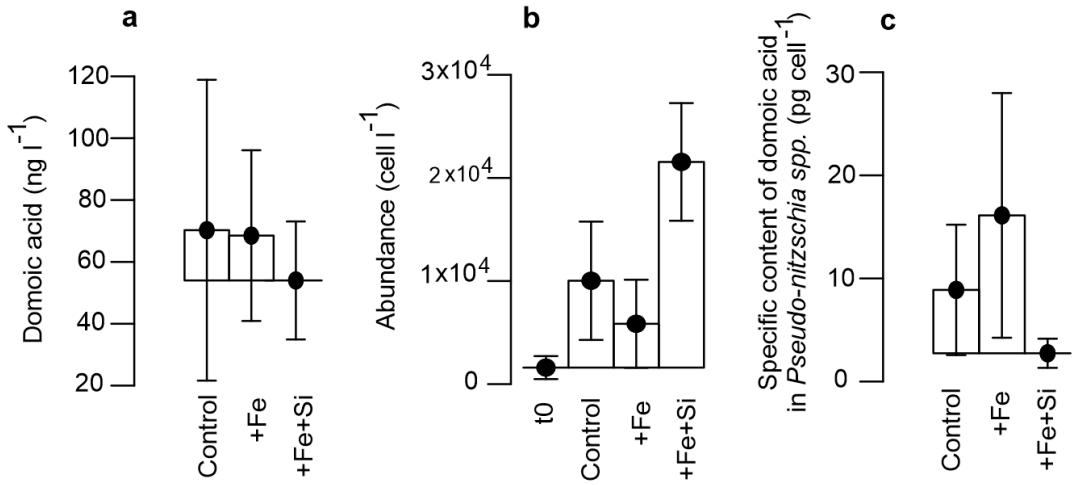

Figure A2.11. *Average values of cellular Domoic acid, Pseudo-nitzschia abundance and DA normalized by Pseudo-nitzschia abundance at t=0 and after three days (control, +Fe and +Fe+Si). Bars indicate standard deviation*

.

A2.3.2.6. Dinoflagellates

The abundance of dinoflagellates, their total volume and mean volume were variable, with positive and negative net changes with respect to t = 0 (figure A2.12a-c). Naked dinoflagellates, (*Gyrodinium* spp., *Gymnodinium* spp.; figure 2.12d-e) reduce their abundance in G2 and G3 relative t=0. The abundance of *Gyrodinium spp*. in Fe enriched treatments increased at G1 and G4 (figure A2.12d). The abundance of *Gyrodinum spp*. was consistently larger at +Fe+Si treatment relative to controls (figure A2.12d). The thecate dinoflagellate *Protoperidinum* only showed an increase in its abundance at G3 (+Fe+Si treatment) and at G4 (control) (figure A2.12f).

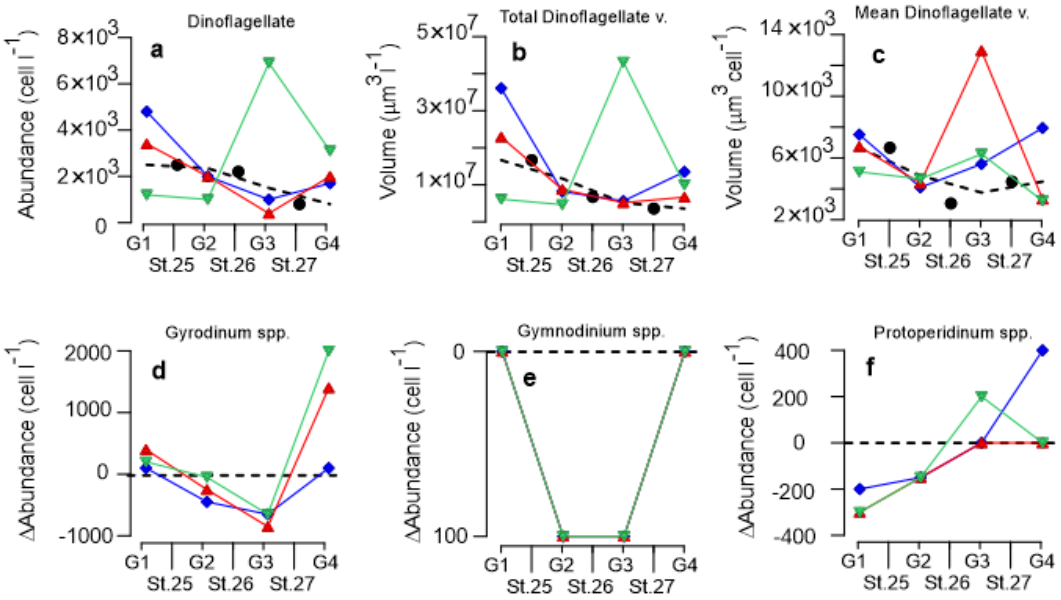

Figure A2.12. *Surface water dinoflagellate abundance (a), Total volume of dinoflagellates (b), Mean dinoflagellate volume (c) at t=0 and after three days of "on-deck" incubation. Variation (Δ=t3-t0) in the abundance of selected dinoflagellate taxon's (d-f).*

A2.3.2.7. Carbonate system parameters

pH measured at 25.0°C increased by ca. 0.22 pH units in both Fe enriched treatments and controls. The range of measured pH in control, +Fe and +Fe+Si bottles at t=3 were small (0.09, 0.05 and 0.07 pH units, respectively). The A_T normalized by salinity was higher in t_3 compared to t_0 (ΔA_T = 27, 14 and 16 µmol kg^{-1} in control, + Fe and + Fe + Si treatment, respectively). The ΔA_T corrected for nitrate consumption (i.e., $\Delta A_T + \Delta NO_3$) was 20, 6 and 9 µmol kg^{-1} in control, + Fe and +Fe+Si treatments, respectively.

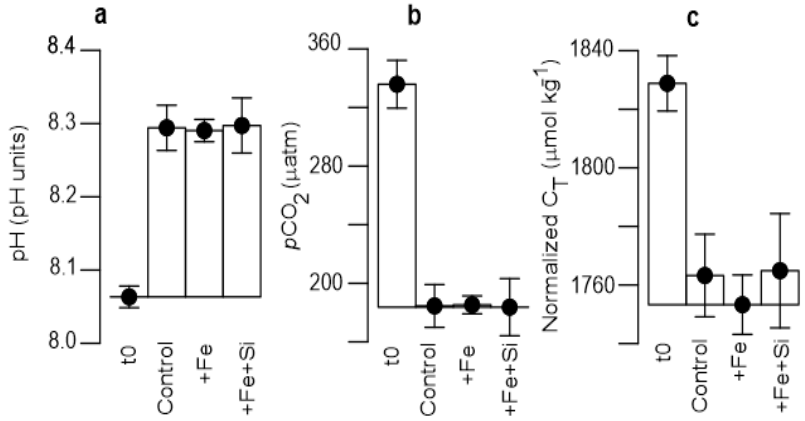

Figure A2.13. *pH at a temperature in situ, pCO2 and dissolved inorganic carbon standardized to salinity 28.8 at t=0 and after three days (control, +Fe and +Fe+Si) of "on-deck" incubation. Bars indicate standard deviation.*

A2.3.2.8. Relationship between response variables

Nitrate drawdown was negatively correlated to nitrate concentration at t = 0 in treatments and controls. Superimposed on this last general trend, the maximum nitrate drawdown levels take place in +Fe and +Fe+Si treatments (figure A2.14a). No correlation was found between the increase DFe and nitrate decline relative corresponding controls (figure A2.14b), however maximum DFe increase and a large reduction of nitrate relative to controls occurred at G4+Fe+Si treatment (figures A2.14b-c). The increase in micro-chla and DFe in iron enriched treatments relative to corresponding controls (see method section A2.2.9.2) were positively correlated (R^2=0.73, p=0.006, n=8; figure A2.14c). In general, nitrate drawdown was negatively correlated with micro-chl a accumulation (figure A2.14d), the accumulation of micro-chl a per mol of nitrate was particularly high in controls (figure A2.14d). The accumulation of nano-chl a only occurred when the accumulation of micro-chl a was low or null (figure A2.14e). Biogenic silica accumulation (in particles > 2µm) was positively correlated with diatom biovolume accumulation only in controls (figure A2.14f). In the +Fe and +Fe+Si treatments, the accumulation of biogenic silica was not

associated with the accumulation of diatom biovolume (figure A2.14f). The accumulation of bSi tended to be higher when the mean volume of the diatoms increased in +Fe and controls (figure A2.14g). However, in +Fe+Si treatment, the accumulation of bSi was high even when the mean volume of the diatoms decreased (figure A2.14g). The accumulation of Gyrodinium spp. cells and the accumulation of diatoms were highest in G4 in +Fe and +Fe+Si treatments. The accumulation of Gyrodinium spp was inversely correlated with the total accumulation of diatoms in controls (figure A2.14h). The ratio of accumulation between Gyrodinium spp and diatoms was maximum at +Fe G1 (figure A2.14i). This carboy (+Fe G1) was also characterized by loss of micro-chl a (figure A2.14d) and accumulation of nano-chl a (figure A2.14e).

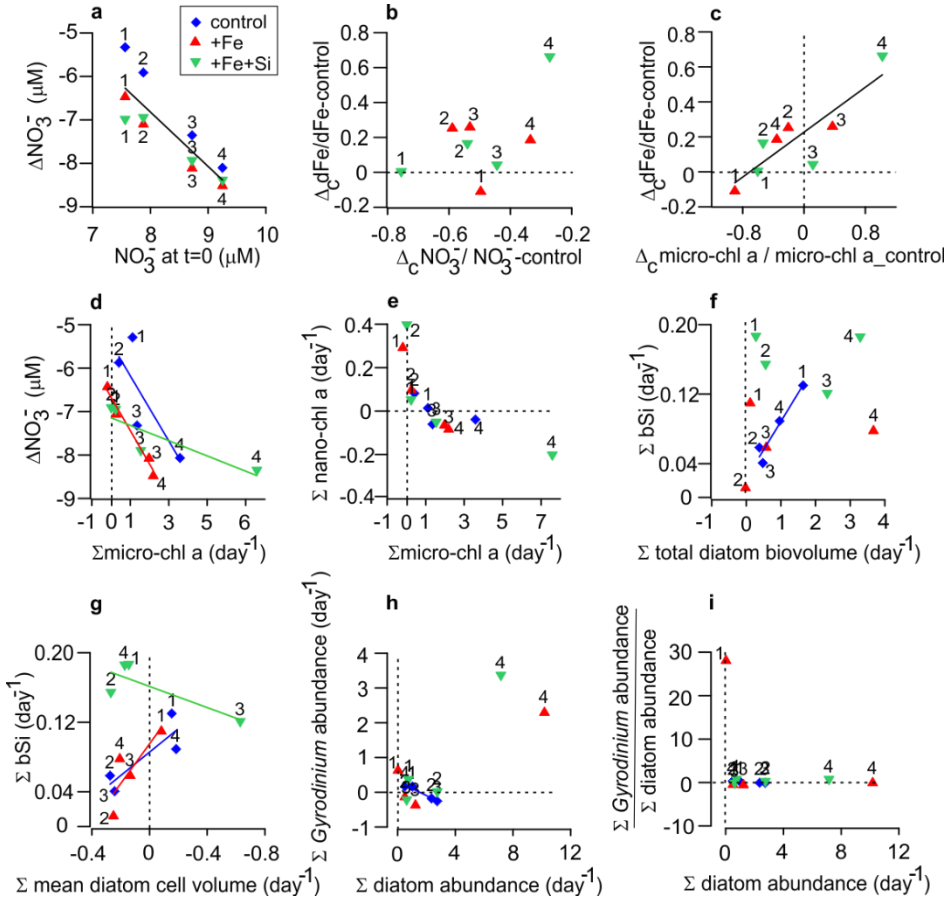

Figure A2.14. *Relationship between response variables, numbers indicate the experimental group. a) Nitrate drawdown vs. nitrate concentration at the beginning of the experiment. b) DFe* Σ_C *vs.*

Nitrate Σ_C c) DFe Σ_C vs. micro-chl a Σ_C, solid line depict a regression, d) Nitrate drawdown vs. micro-chl a accumulation. e) Nano-chl a accumulation vs. micro-chl a accumulation. f) biogenic silica accumulation vs. diatom abundance accumulation. g) biogenic silica accumulation vs. mean diatom cell volume accumulation. h) Gyrodinium spp *abundance accumulation vs. diatom abundance accumulation. i) ratio between* Gyrodinium spp *abundance accumulation and diatom abundance accumulation vs. diatom abundance accumulation.*

A2.4 DISCUSSION

A2.4.1. Iron-enhanced new productivity in estuarine waters of Southern Patagonia

The general rapid drop in macronutrient (nitrate, phosphate, and C_T) concentrations in both control and Fe-enriched treatments relative to initial conditions suggest that very high levels of new productivity were most likely associated with alleviation of any light limitation due the on-deck incubation that emulates an extreme stratification condition (see figure 2.1 in de Baar et al. (2005)), together with already high initial levels of chlorophyll of the surface water used for the experiment (total-chl a ~ 4 µg l^{-1}). The initial experimental conditions (undersaturated levels of CO_2, moderate levels of macronutrients) suggest a micro-phytoplankton bloom was in its developing phase at the sampling time, particularly near station 25, where relatively low salinity and macronutrients levels (figure A2.4a-b) and high micro-chl a levels (figure A2.6d) were recorded; The higher nitrate (and phosphate) drawdown in all Fe-enriched carboys relative to controls (figure A2.5a-b), suggest that the addition of unchelated Fe was the factor inducing higher macronutrients drawdown levels. Since nitrate: phosphate drawdown ratio (see section A2.3.2.2.) was consistent with what has been reported for high latitude diatom-dominated waters (Arrigo et al., 2002), we suggest that macronutrients drawdown reported here was mainly due to diatom new production. However, the DFe:nitrate ratio (mmol mol^{-1}) in estuarine surface waters varied between 0.4 and 4, several orders of magnitude higher than the expected phytoplankton cellular Fe:nitrate ratio for fjord waters (Kanna et al., 2020) suggesting no iron limitation. Therefore, we

conclude that only a fraction of the ambient DFe is bioavailable or readily bioavailable for phytoplankton. i.e., the amount of bioavailable Fe was higher in those treatments enriched with unchelated iron, enhancing new productivity and therefore causing a significative acceleration in the nitrate and phosphate drawdown.

The enhanced productivity in Patagonian estuarine waters after a 5 nM Fe enrichment was small compared to previous experiments carried out in HNLC coastal upwelling areas off central Chile during austral spring (Ampuero, 2007; Torres & Ampuero, 2009). This difference was likely a result of chl a-rich waters in our study (although most of it was allocated in the pico and nano size fraction) and not with HNLC coastal waters as determined in Torres and Ampuero (2009). We hypothesize that events of iron stress in coastal water are potentially more severe in recently upwelling waters of central Chile, which are typically low in chl a (<1 µg l^{-1}), high in nitrate and silicate, and low in DFe (ca. 1.4nM), compared to PAIS surface waters. We note that DFe concentration of PAIS surface waters were high (particularly at salinity < 29) but likely not readily available to fully meet potential maximum rates of macronutrient uptake / new productivity under blooming conditions.

A2.4.2. The role of initial conditions and grazing pressure on Fe enrichment experiments

The experimental groups (G1-G4) were collected over a salinity, macro-nutrient, micro-chl a, and DFe gradient that may represent a changing "age" or "maturity" of the diatom community along the CC E-W transect. While the early stage of the diatom bloom appears located in the salty water of the western CC portion (e.g., relative high nitrate, low micro-chl a and low DFe in G4), a more mature diatom community was observed at the CC east stations (e.g., relative low nitrate, high micro-chl a and high DFe in G1). Since an Fe pulse has the potential to increase the maximum potential uptake rate (V-max) of both DSi and nitrate (Franck et al., 2003) we expected that the

sudden relief of Fe stress in an already large "mature" diatom community (e.g., G1 at t = 0) resulted in early resource limitation relative to controls, which could explain the occurrence of low diatom stock in +Fe relative controls at eastern portion of the transect (i.e., G1 and G2). On other hand, the gain (positive accumulation) of micro-chl a and total diatom volume after an iron pulse at western portion of the CC transect (e.g., G4+Fe) suggest a diatom standing stock builtup (i.e., increase diatom production/diatom mortality ratios).

In general, we suggest that the impact of iron pulses on diatom stock in a given period of time could be dependent on the developing stage of the diatom bloom, this last dependency can explain the contrasting effect of iron addition on micro-chl a accumulation and total diatom volume at the two extremes of the transect (i.e., G1 vs. G4). Complementary, no differences between bSi accumulation in controls and +Fe treatment, suggest that new productivity enhanced by Fe addition was independent to diatom bSi accumulation. If new production was mostly driven by diatoms, the rise in diatom standing stock (e.g., G4) should correspond to small or thin diatom in +Fe relative controls. Indeed, blooming diatoms were typically small of the class Mediophyceae. Blooming of small/thin diatoms could be particularly vulnerable to protozoan grazers that select for diatoms with thin frustules (Zhang et al., 2017). Accumulation of micrograzers in G1 and G4 suggest that micrograzing pressure was intense in those experimental groups. Micrograzer pressure could be particularly intense in G1 where accumulation of *Gyrodinum spp.* (the dominant naked dinoflagellate group) was substantially larger compared to the accumulation of diatom biovolume (which indeed was null or negative in G1, see figure A2.7b). The accumulation of *Gyrodinum spp* in G1-control and G4-control coincide with a small increase in DSi (relative t=0; figure A2.5c).

A2.4.3. +Fe+Si enrichment experiment outputs: bSi, Pseudo-nitzchia and domoic acid

Silicic acid uptake by diatoms likely explains the rapid DSi shortage even in +Fe+Si treatments. bSi accumulation and *Pseudo-nitzschia var dellicatissima* abundance were consistently greater in +Fe+Si incubations relative to +Fe and controls. Since the "poorly silicified" *Pseudo-nitzchia sp. cf. dellicatissima.* represent less than 1% of the total diatom abundance and less than 0.2% of the total diatom biovolume, the increase in bSi was likely associated with the frustules of the Mediophyceae and Bacilliophycea rather than a small increase in abundance of one single taxa.

Even though we identify DSi as a factor controlling bSi and *Pseudo-nitzchia sp. cf. delicatissima,* our experimental design precludes discrimination between the role of DSi by itself and the role of its interaction with iron, particularly considering that previous iron addition experiments have shown that Fe levels are important in the promotion of *Pseudo-nitzschia* blooms in coastal waters (Hutchins et al., 1998).

One characteristic of *Pseudo-nitzschia* is its ability to produce DA. The level of cellular DA in the *Pseudo-nitzschia* community was particularly low in +Fe+Si experiments (figure A2.11c), supporting the generalized concept that DA is produced under nutrient (Davidson et al., 2012) and/or Si stress (Fehling et al., 2004; Pan et al., 1996; 1998). The generation of high specific levels of allelopathic substances in some diatom taxa (e.g., DA in *Pseudo-nitzschia*) could be a way to compensate for the vulnerability to grazing associated with lower diatom community silicification in low DSi environments. Our observations suggest that low and constant specific cellular DA concentration in *Pseudo-nitzschia* spp. is associated with high *Pseudo-nitzschia* abundance and high concentrations of bSi (i.e., +Fe+Si treatment), which agrees with the suggestion that DA production varies inversely with *Pseudo-nitzschia* growth rates (Maldonado et al., 2002). Our results imply that the specific DA cellular content of *Pseudo-nitzschia* could reach a maximum at

the western boundary of PAIS (particularly negative Si* waters) due a reduced allochthonous Si supply. This hypothesis needs to be tested in the future given the detrimental impact of DA in ecosystems.

PAIS is expected to have longitudinal gradients in the fluxes of iron and DSi to surface water due the mixing between oceanic water (west) with continental water (east). Eastward increases of DSi and DFe fluxes likely results in neither Fe or Si -stress near the continental sources. Along the E-W salinity gradient, however, the DFe and DSi relief may be uncoupled. for example, when continental subsidies are sufficient to relieve iron stress, but insufficient to relieve DSi stress. In the later conditions of higher new productivity together with high DSi stress, *Pseudo-nitzschia* cells could be particularly toxic. Consistent with this last hypothesis, high levels of DA in mussels have been only reported on the western side of the archipelago (Pizarro et al., 2017) in regions of low continental DSi supply (Torres et al., 2020). A similar rationale has been suggested for the northeast Pacific Ocean (Ribalet et al., 2010). Ribalet et al. (2010) identified the oceanic size of ecotones as optimum condition for blooming of small cell phytoplankton and DA production. We hypothesize that the ratio of bioavailable "continental elements" (e.g., Fe and Si) during the freshening of subantarctic waters (SAASW) could play a role in modifying predator-prey interaction though the degree of toxicity of specific phytoplankton taxon´s, as well as by the ability to produce and export bSi.

A2.4.4. The role of environmental DFe and the addition of unchelated DFe.

The internal cycle of iron in surface waters is constituted by a complex matrix of components and processes (Croot & Heller, 2012) and internal fluxes critically determine its bioavailability. In this experiment, the addition of unchelated iron to estuarine water likely caused an acute and transient increase in the concentration of bioavailable iron, follows by the formations of colloids

which become rapidly aggregated (Nowostawska et al., 2008) and removed from the dissolved pool. Indeed, ca. 80 % of added Fe did not remain in the <0.45µm size fraction. Based on our colloidal iron measurements (0.02-0.45 µm size fraction) we expect that DFe (<0.45µm) increase relative to controls were allocated in both colloidal fraction and ligand bond Fe complexes, where extension of the latter depends upon ligand availability. The G1-control, like all other experimental groups controls, showed low levels of nitrate drawdown compared to Fe-enriched treatments (i.e., G1+Fe and G1+Fe+Si). However, the DFe concentration in the G1-control was high (12 nM at t=3) and similar or larger than those measured in Fe-enriched treatments at t=3, suggesting that the ligand pool in this experimental group (G1) was close to being saturated for DFe, however this initial ligand-Fe complex pool was not entirely available to produce obviously "iron-replete conditions" for macronutrient drawdown, confirming that DFe pool is a poor indicator of what is bioavailable for phytoplankton assimilation (Gobler et al., 2002). Since additions of readily bioavailable iron can eventually trigger luxury iron storage (Cohen et al., 2018; Lampe et al., 2018) or faster iron assimilation in Fe-depleted diatoms compare to Fe-replete diatoms (Chen & Wang, 2008), the increase of nitrate drawdown in Fe-enriched treatments could be attribute to both an initial pulse of unchelated iron (forcing a rapid assimilation and storage of iron) and/or to an enhanced lability of newly formed ligand bond Fe complexes and colloids. Certainly, there are some evidences that phytoplankton can take up Fe derived from colloids and from ligand-bond Fe (Chen & Wang, 2008; Maldonado & Price, 1999; Maldonado et al., 2005) but the later may largely dependent on the specific phytoplankton and ligand group in question (Blain et al., 2004). Dissolved organic matter of terrestrial origin, a ubiquitous characteristic of estuarine water, contain a wide variety of ligands with varying binding strengths (e.g., Humic acids, HA). Fe^{3+} ions form strong but reversible bonds with hydroxyl and carboxyl groups of HA, allowing the transfer of iron to siderophore-type ligands released by microorganisms for its subsequent uptake (Chen & Wang,

2008) or/and could act as substrate (HA-Fe complexes) to photoreactions that produce highly soluble reduced iron (Croot & Heller, 2012) that can be directly incorporated through microorganism membrane channels. Therefore, is believed that HA play an important role transferring Fe to marine phytoplankton (Batchelli et al., 2010; Chen & Wang, 2008). Our experimental result may indicate that despite a presumably high Fe solubility in coastal waters (forced by marine and continental ligands) the rates of transfer to marine phytoplankton (which may be dependent on a broad range of direct and indirect factors as for example: UV light regimen, characteristics of terrestrial organic matter pool and the availability of siderophore-type ligands) could be insufficient to allow maximum potential productivity levels during a diatom bloom.

In general, the capacity of a unchelated iron addition to intensify macronutrient drawdown (figure A2.5a-b), the positive correlation between the increments in Σ_cDFe and $\Sigma_c$micro-chl a (figure A2.14c) and a nitrate: phosphate drawdown ratio typical of diatom dominated systems (see section A2.3.2.2.) seem consistent with the hypothesis that pulses of unchelated iron to estuarine water of Patagonia can accelerate diatom new productivity during the study period.

A2.4.5 Integration of the surface waters characteristics in austral spring and iron enrichment experiment results

The negative relationship of nitrate, phosphate and pCO_2 to micro-chl a in surface waters (table A2.1) along the latitudinal transect (figure A2.1) indicates that diatoms, which dominate micro-chl a size fraction, were the main driver of surface water new productivity in the study area during September 2017 (austral spring), consistently micro-phytoplankton represent the dominant fraction of phytoplankton community exported from upper layer to subpycnocline waters during the productive season in Patagonian waters (González et al., 2016).

Surface seawater salinity (SSS) and the specific runoff near each station was positively correlated with micro-chl a percentage, but only runoff was negatively correlated to nitrate (table A2.1). This pattern may suggest that the drop in nitrate concentration rather than a consequence of freshening per se (i.e., dilution), is a positive response of new productivity to continental solutes (e.g., Fe, Si, Fe+Si).

At the most brackish extreme (i.e., salinity 26) chl a was mostly present in the small size fractions. Our finding of small phytoplankton in the most brackish waters is consistent with previous reports suggesting that brackish waters in southern Patagonia are characterized by small-cell photosynthetic organisms (Díaz-Rosas et al., 2021; Torres et al., 2011). This surface water salinity minimum located at 52°S (i.e., salinity 26 at St.13) could be associated the influence of glaciated hydrographic basins in southern Patagonia (e.g., Serrano River basin and Estero las Montañas). Although we did not assess any optically active constituents, we hypothesize that optically active particles and solutes from continental origin could produce intense light attenuation (e.g., silt-rich brackish waters associated to subglacial discharges and/or CDOM leached out of the periglacial peatlands, as reported for others fjord systems (Paredes & Montecino, 2011; Mascarenhas et al., 2017)) selecting for small-cell photosynthetic organisms (Chisholm, 1992). However, the effect of CDOM on phytoplankton metabolism may be broader than just its effect on PAR attenuation, for example, UV photoreduction of CDOM ligand-Fe complexes (Croot & Heller, 2012) could provide highly soluble reduced iron, which eventually may help phytoplankton to adapt to low PAR environments. Alternatively, the extreme stratification of brackish waters could favor the persistence of small photosynthetic flagellates (due to their ability to swim to locate themselves in a better PAR regime) compared to large diatoms that require turbulence to avoid sedimentation (Kiørboe, 1993).

At the highest salinities (SSS ~ 30; St. 1, 28 and 29) where the lowest water column stability was expected, the chemical characteristics of surface waters (low in total-chl a particularly in micro-chl a size range, rich in nitrate with moderate levels Si and pCO_2 levels near equilibrium with the atmosphere) were consistent with a pre-bloom condition in a poorly stratified surface layer, as previously reported for Pacific extreme of Strait of Magellan during Austral spring 1989 (Cabrini & Fonda-Umani, 1991; Saggiomo et al., 1994; 2011) and for Concepción Channel (near station 28-29) during austral spring 2009 (Iriarte et al., 2018). Direct measurements of Gross Primary Productivity (GPP) and community respiration (CR) reported by Iriarte et al. (2018) suggest very low levels of "net productivity" (GPP-CR) in surface waters (e.g., 10 µg C l^{-1} d^{-1}) which contrast with the high levels of productivity (Saggiomo et al., 2011) and biomass reported for the fresher easter portion of the Strait of Magellan. We hypothesize that the reduced haline stratification of the upper water column at the western boundary of the archipelago may delay spring diatom productivity due to light limitation but also due to suboptimal levels of bioavailable Fe as our bottle experiments suggest. Nonetheless, the typical negative Si* values (ca. -6) of salty surface waters (>30) are expected to lead to rapid Si stress as diatom development progresses. If an intense diatom proliferation is triggered in these saltier and moderately DSi rich waters (e.g., due a high irradiance in combination with a pulse of iron bioavailability), the onset of Si stress could lead to the activation of physiological adaptation and selection mechanisms to cope with DSi scarcity (e.g., lower Si:NO_3^- diatom uptake ratio and a reduction of silicification). Indeed, the occurrence of physiological adaptation and/or selection mechanisms to Si stress could explain high Si:NO_3^- drawdown ratios (near 1) in +Fe+Si treatments compared to controls and +Fe treatments (where no DSi was added, see section A2.3.2.2).

Favorable conditions for augmenting micro chl a and bSi standing stocks, and consequently the drawdown of macronutrients during early spring, seem to occur at intermediate salinity levels. These optimal growth conditions are likely linked to the combined effect of reduced turbulent mixing due to haline stratification, and a complementary mix of marine (N and P) and terrestrial nutrients (Si and micronutrients like Fe). However, our experimental results suggest that even in frontal waters with high diatom productivity, a pulse of highly bioavailable sFe (over a relatively high DFe baseline) could accelerate the nitrate uptake likely due to the particularly high biological demand for Fe and reduction of sFe in these high productivity and high pH levels waters.

During early spring, bioavailable Fe and DSi supply from the continent likely allows for maximum rates of new productivity in surface waters. Consistently, field observations suggested that runoff and surface water nitrate were negatively correlated during the study period (table 2.1). Conversely, at higher SSS (e.g., SSS >30 typically associated with nitrate concentration greater than DSi concentration, see Torres et al. (2014)), suboptimal Fe and/or Si supply could favor the growth of thinner/small diatom community (Leynaert et al., 2004; Marchetti & Cassar, 2009), as well as, small-sized non-silicic functional groups. While the former groups likely base its growth on regenerated nutrients and therefore with limited abilities to produce high rates of new productivity (Eppley et al., 1969), higher new productivity levels of thinner/small diatoms may result in low diatom stocks due an efficient control by micrograzing compared to thicker/large diatom with higher Si needs. A Fe-Si colimitation scenario, may be particularly true under low light regime (Falkowski & Raven, 1997; Raven et al., 1999; Strzepek & Price, 2000), in the study area we expect low light regime at western boundary of Patagonian archipelago (well exposed to open ocean and to Westerlies) associated to a deeper turbulent layer caused by the interaction between low haline stratification and higher wind speeds, and signaled by high surface salinity

levels. We hypothesize that a Fe-Si-light colimitation dynamic could better explain reports that salty surface waters are often not depleted in nitrate even at the height of the productive season (A time series showing high salinity high nitrate low silicate conditions near Faro San Isidro at Strait of Magellan is shown in Supplementary Material C).

In summary, this first experimental response of phytoplankton communities in southern PAIS waters to Fe and Fe+DSi amendments, identifies both factors (Fe and Fe+DSi) as capable of modulating aspects of spring diatom bloom dynamics (e.g., community composition and abundance, nutrient drawdown rate, biogenic silica production). The intensity of this modulation is likely sensitive to the location and flux of continental water discharge and the oceanographic characteristics that set the fluxes of marine and continental complementary nutrients. It is also likely to be strongly variable temporally (mainly on seasonal basis), depending on the diatom bloom development stage when continental runoff nutrients pulses do occur. It seems evident that timing of Fe (DSi) fertilization pulses should be a key variable to take in account when assessing the effect of iron, DSi or both on coastal waters phytoplankton stocks. Therefore, care must be taken in extrapolating these first experimental results to other periods and places. Certainly, more focused research is required to better understand the role of continental solutes, their geographic and temporal variability in response to climatic events and local watershed-scale variability, in different aspects of spring bloom characteristics and dynamics at Patagonian waters.

A2.5 CONCLUDING REMARKS

1.- Optimum conditions for diatom new productivity and diatom stock accumulation take place within the salinity gradient in inner surface waters of Southern Patagonia Archipelago during austral spring 2017.

2.- Environmental variability in both macronutrient and CO_2 was driven by micro phytoplankton in early austral spring 2017, although most of chl a was located in smaller size fractions.

3.- Nano-diatoms (e.g., *Minidiscus sp*) were abundant, likely constituting a significant fraction of phytoplankton biomass during early austral spring 2017.

4.- Nominal 5nM unchelated Fe-enrichment of estuarine waters (salinity 28-29) of Concepcion Channel (Southern PAIS) enhance nitrate and phosphate drawdown during an experimentally triggered diatom bloom, even when environmental levels of DFe were relatively high.

5.- Early spring diatom bloom characteristics in the Patagonia archipelago, mainly caused by increments light regimen, is likely modulated by the bioavailability of iron and DSi.

6.- DSi or DSi+Fe stress relief can enhance standing stocks of *Pseudo-nitzschia* and biogenic silicate, but tends to reduce the specific content of domoic acid in *Pseudo-nitzschia.*

7.- Rapid iron-forced depletion of macronutrients probably led to early decay of diatom stocks in experiments with low DSi levels (i.e., +Fe treatments).

A2.6. ACKNOWLEDGMENTS

We thank the members of the 2017 field Punta Arenas – Madre de Dios campaign. A special thanks to Steve Beldham for his help with the sampling instrumentation. We thank the Toxin Laboratory of the University of Chile for the analysis of domoic acid, Captain and crew of M/B Forrest for its assistance at sea and Osvaldo Artal at IFOP for its help handling data from the CHONOS-Flow platform (http://chonos.ifop.cl/). This research was primarily funded by FONDECYT 1140385, additional support was granted by IDEAL (FONDAP-IDEAL Grant 15150003), IFOP and PATSER (ANID R20F0002) program.

A2.7. REFERENCES

Alejandra Paredes, M., & Montecino, V. (2011). Size diversity as an expression of phytoplankton community structure and the identification of its patterns on the scale of fjords and

channels. *Continental Shelf Research*, 31(3), 272-281. https://doi.org/10.1016/j.csr.2010.07.012

Ampuero, P. (2007). Efectos del Fe disuelto sobre la productividad primaria y estructura fitoplanctonica en el centro de surgencias de Coquimbo (30°S) [Tesis de grado Biologo Marino, Universidad de Concepción]. Concepción.

Arrigo, K. R., Dunbar, R. B., Lizotte, M. P., & Robinson, D. H. (2002). Taxon-specific differences in C/P and N/P drawdown for phytoplankton in the Ross Sea, Antarctica. Geophysical Research Letters, 29(19), 44-41-44-44. https://doi.org/10.1029/2002GL015277

Assmy, P., Smetacek, V., Montresor, M., Klaas, C., Henjes, J., Strass, V. H., Arrieta, J. M., Bathmann, U., Berg, G. M., Breitbarth, E., Cisewski, B., Friedrichs, L., Fuchs, N., Herndl, G. J., Jansen, S., Krägefsky, S., Latasa, M., Peeken, I., Röttgers, R., . . . Wolf-Gladrow, D. (2013). Thick-shelled, grazer-protected diatoms decouple ocean carbon and silicon cycles in the iron-limited Antarctic Circumpolar Current. *Proceedings of the National Academy of Sciences*, *110*(51), 20633-20638. https://doi.org/10.1073/pnas.1309345110

Batchelli, S., Muller, F. L. L., Chang, K.-C., & Lee, C.-L. (2010). Evidence for Strong but Dynamic Iron−Humic Colloidal Associations in Humic-Rich Coastal Waters. *Environmental Science & Technology*, *44*(22), 8485-8490. https://doi.org/10.1021/es101081c

Bianchi, T. S. (2007). Biogeochemistry of Estuaries. Oxford University Press.

Bianchi, T. S., Arndt, S., Austin, W. E. N., Benn, D. I., Bertrand, S., Cui, X., Faust, J. C., Koziorowska-Makuch, K., Moy, C. M., Savage, C., Smeaton, C., Smith, R. W., & Syvitski, J. (2020). Fjords as Aquatic Critical Zones (ACZs). *Earth-Science Reviews*, *203*, 103145. https://doi.org/10.1016/j.earscirev.2020.103145

Blain, S., Guieu, C., Claustre, H., Leblanc, K., Moutin, T., Quèguiner, B., Ras, J., & Sarthou, G. (2004). Availability of iron and major nutrients for phytoplankton in the northeast Atlantic Ocean. *Limnology and Oceanography*, *49*(6), 2095-2104. https://doi.org/10.4319/lo.2004.49.6.2095

Bouman, H. A., Lepère, C., Scanlan, D. J., & Ulloa, O. (2012). Phytoplankton community structure in a high-nutrient, low-chlorophyll region of the eastern Pacific Subantarctic region during winter-mixed and summer-stratified conditions. Deep Sea Research Part I: *Oceanographic Research Papers*, *69*(0), 1-11. http://dx.doi.org/10.1016/j.dsr.2012.04.008

Boyd, P. W., Jickells, T., Law, C. S., Blain, S., Boyle, E. A., Buesseler, K. O., Coale, K. H., Cullen, J. J., de Baar, H. J. W., Follows, M., Harvey, M., Lancelot, C., Levasseur, M., Owens, N. P. J., Pollard, R., Rivkin, R. B., Sarmiento, J., Schoemann, V., Smetacek, V., . . . Watson, A. J. (2007). Mesoscale Iron Enrichment Experiments 1993-2005: Synthesis and Future Directions. *Science*, *315*(5812), 612-617. https://doi.org/10.1126/science.1131669

Boyle, E. A., Edmond, J. M., & Sholkovitz, E. R. (1977). The mechanism of iron removal in estuaries. *Geochimica et Cosmochimica Acta*, *41*(9), 1313-1324. https://doi.org/10.1016/0016-7037(77)90075-8

Brzezinski, M. A., Pride, C. J., Franck, V. M., Sigman, D. M., Sarmiento, J. L., Matsumoto, K., Gruber, N., Rau, G. H., & Coale, K. H. (2002). A switch from Si(OH)4 to NO3− depletion in the glacial Southern Ocean. *Geophysical Research Letters*, *29*(12), 5-1-5-4. https://doi.org/10.1029/2001GL014349

Cabrini, M., & Fonda-Umani, S. (1991). Phytoplankton populations in the Strait of Magellan. *Bolletino di Oceanologia Teorica ed Applicata*, 9(2-3), 137-144.

Calbet, A., & Landry, M. R. (2004). Phytoplankton growth, microzooplankton grazing, and carbon cycling in marine systems. *Limnology and Oceanography, 49*(1), 51-57. https://doi.org/10.4319/lo.2004.49.1.0051

Caron, D. A., Alexander, H., Allen, A. E., Archibald, J. M., Armbrust, E. V., Bachy, C., Bell, C. J., Bharti, A., Dyhrman, S. T., Guida, S. M., Heidelberg, K. B., Kaye, J. Z., Metzner, J., Smith, S. R., & Worden, A. Z. (2017). Probing the evolution, ecology and physiology of marine protists using transcriptomics. *Nature Reviews Microbiology, 15*(1), 6-20. https://doi.org/10.1038/nrmicro.2016.160

Chen, J. L., Wilson, C. R., Tapley, B. D., Blankenship, D. D., & Ivins, E. R. (2007). Patagonia Icefield melting observed by Gravity Recovery and Climate Experiment (GRACE). *Geophysical Research Letters, 34*(22). https://doi.org/10.1029/2007gl031871

Chen, M., & Wang, W. X. (2008). Accelerated uptake by phytoplankton of iron bound to humic acids. *Aquatic Biology, 3*(2), 155-166. https://www.int-res.com/abstracts/ab/v3/n2/p155-166/

Chisholm, S. W. (1992). Phytoplankton Size. In P. G. Falkowski, A. D. Woodhead, & K. Vivirito (Eds.), Primary Productivity and Biogeochemical Cycles in the Sea (pp. 213-237). Springer US. https://doi.org/10.1007/978-1-4899-0762-2_12

Cohen, N. R., Mann, E., Stemple, B., Moreno, C. M., Rauschenberg, S., Jacquot, J. E., Sunda, W. G., Twining, B. S., & Marchetti, A. (2018). Iron storage capacities and associated ferritin gene expression among marine diatoms. *Limnology and Oceanography, 63*(4), 1677-1691. https://doi.org/10.1002/lno.10800

Croot, P., & Heller, M. (2012). The Importance of Kinetics and Redox in the Biogeochemical Cycling of Iron in the Surface Ocean [Original Research]. *Frontiers in Microbiology, 3*. https://doi.org/10.3389/fmicb.2012.00219

Cutter, G., Casciotti, K., Croot, P. L., Geibert, W., Haimbürger, L.-E., Lohan, M. C., Planquette, H., & van de Flierdt, T. (2017). Sampling and Sample-handeling Protocols for GEOTRACES Cruises. G. S. a. I. Committe.

Davidson, K., Gowen, R. J., Tett, P., Bresnan, E., Harrison, P. J., McKinney, A., Milligan, S., Mills, D. K., Silke, J., & Crooks, A.-M. (2012). Harmful algal blooms: How strong is the evidence that nutrient ratios and forms influence their occurrence? *Estuarine, Coastal and Shelf Science, 115*, 399-413. https://doi.org/10.1016/j.ecss.2012.09.019

Dávila, P. M., Figueroa, D., & Müller, E. (2002). Freshwater input into the coastal ocean and its relation with the salinity distribution off austral Chile (35-55°S). *Continental Shelf Research, 22*(3), 521-534. http://dx.doi.org/10.1016/S0278-4343(01)00072-3

de Baar, H. J. W., Boyd, P. W., Coale, K. H., Landry, M. R., Tsuda, A., Assmy, P., Bakker, D. C. E., Bozec, Y., Barber, R. T., Brzezinski, M. A., Buesseler, K. O., Boyé, M., Croot, P. L., Gervais, F., Gorbunov, M. Y., Harrison, P. J., Hiscock, W. T., Laan, P., Lancelot, C., . . . Wong, C.-S. (2005). Synthesis of iron fertilization experiments: From the Iron Age in the Age of Enlightenment. *Journal of Geophysical Research: Oceans, 110*(C9). https://doi.org/10.1029/2004JC002601

de Baar, H. J. W., de Jong, J. T. M., Nolting, R. F., Timmermans, K. R., van Leeuwe, M. A., Bathmann, U., Rutgers van der Loeff, M., & Sildam, J. (1999). Low dissolved Fe and the absence of diatom blooms in remote Pacific waters of the Southern Ocean. *Marine Chemistry, 66*(1), 1-34. https://doi.org/10.1016/S0304-4203(99)00022-5

DeMaster, D. J. (2002). The accumulation and cycling of biogenic silica in the Southern Ocean: revisiting the marine silica budget. Deep Sea Research Part II: Topical *Studies in Oceanography, 49*(16), 3155-3167.

http://www.sciencedirect.com/science/article/B6VGC-45C1N5M-2/2/8c4d473241bf23d35e56c962d52f8b8e

Díaz-Rosas, F., Alves-de-Souza, C., Alarcón, E., Menschel, E., González, H. E., Torres, R., & von Dassow, P. (2021). Abundances and morphotypes of the coccolithophore Emiliania huxleyi in southern Patagonia compared to neighboring oceans and northern-hemisphere fjords. *Biogeosciences Discuss.*, 2021, 1-34. https://doi.org/10.5194/bg-2020-449

Dickson, A. G., & Millero, F. J. (1987). A comparison of the equilibrium constants for the dissociation of carbonic acid in seawater media. *Deep Sea Research, 34*(10A), 1733-1743. http://www.sciencedirect.com/science/article/pii/0198025488924600

DOE. (1994). Handbook of methods for the analysis of the various parameters of the carbon dioxide system in sea water; version 2.1 (A. G. Dickson & C. Goyet, Eds.). U. S. Department of Energy. http://cdiac.ornl.gov/oceans/DOE_94.pdf

Egge, J. K., & Aksnes, D. L. (1992). Silicate as regulating nutrient in phytoplankton competition. *Marine Ecology Progress Series*, *83*, 281-289.

Falkowski, P. G., & Raven, J. A. (1997). Aquatic photosynthesis. Blackwell Science.

Fehling, J., Green, D. H., Davidson, K., Bolch, C. J., & Bates, S. S. (2004). Domoic acid production by Pseufo-Nitzschia seriata (Bacillariophyceae) in scottish waters. *Journal of Phycology*, *40*(4), 622-630. https://doi.org/10.1111/j.1529-8817.2004.03200.x

Finkel, Z. V., Beardall, J., Flynn, K. J., Quigg, A., Rees, T. A. V., & Raven, J. A. (2010). Phytoplankton in a changing world: cell size and elemental stoichiometry. *Journal of Plankton Research, 32*(1), 119-137. https://doi.org/10.1093/plankt/fbp098

Forsch, K. O., Hahn-Woernle, L., Sherrell, R. M., Roccanova, V. J., Bu, K., Burdige, D., Vernet, M., & Barbeau, K. A. (2021). Seasonal dispersal of fjord meltwaters as an important source of iron and manganese to coastal Antarctic phytoplankton. *Biogeosciences, 18*(23), 6349-6375. https://doi.org/10.5194/bg-18-6349-2021

Franck, V. M., Bruland, K. W., Hutchins, D. A., & Brzezinski, M. A. (2003). Iron and zinc effects on silicic acid and nitrate uptake kinetics in three high-nutrient, low-chlorophyll (HNLC) regions. *Marine Ecology Progress Series*, *252*, 15-33. http://www.jstor.org/stable/24866578

Fujii, M., Ito, H., Rose, A. L., Waite, T. D., & Omura, T. (2008). Transformation dynamics and reactivity of dissolved and colloidal iron in coastal waters. *Marine Chemistry*, *110*(3), 165-175. https://doi.org/10.1016/j.marchem.2008.04.005

Glasser, N. F., Harrison, S., Jansson, K. N., Anderson, K., & Cowley, A. (2011). Global sea-level contribution from the Patagonian Icefields since the Little Ice Age maximum. *Nature Geoscience, 4*(5), 303-307. http://dx.doi.org/10.1038/ngeo1122

Gobler, C. J., Donat, J. R., Consolvo, J. A., & Sañudo-Wilhelmy, S. A. (2002). Physicochemical speciation of iron during coastal algal blooms. *Marine Chemistry, 77*(1), 71-89. https://doi.org/10.1016/S0304-4203(01)00076-7

González, H. E., Graeve, M., Kattner, G., Silva, N., Castro, L., Iriarte, J. L., Osmán, L., Daneri, G., & Vargas, C. A. (2016). Carbon flow through the pelagic food web in southern Chilean Patagonia: relevance of Euphausia vallentini as a key species. *Marine Ecology Progress Series, 557*, 91-110. https://www.int-res.com/abstracts/meps/v557/p91-110/

Grønning, J., & Kiørboe, T. (2020). Diatom defence: Grazer induction and cost of shell-thickening. *Functional Ecology, 34*(9), 1790-1801. https://doi.org/10.1111/1365-2435.13635

Haraldsson, C., Anderson, L. G., Hassellöv, M., Hulth, S., & Olsson, K. (1997). Rapid, high-precision potentiometric titration of alkalinity in ocean and sediment pore waters. *Deep Sea*

Research Part I, 44(12), 2031-2044. http://www.sciencedirect.com/science/article/pii/S0967063797000885

Hasle, G. R., Lange, C. B., & Syvertsen, E. E. (1996). A review ofPseudo-nitzschia, with special reference to the Skagerrak, North Atlantic, and adjacent waters. *Helgoländer Meeresuntersuchungen, 50*(2), 131-175. https://doi.org/10.1007/BF02367149

Hopwood, M. J., Carroll, D., Höfer, J., Achterberg, E. P., Meire, L., Le Moigne, F. A. C., Bach, L. T., Eich, C., Sutherland, D. A., & González, H. E. (2019). Highly variable iron content modulates iceberg-ocean fertilisation and potential carbon export. *Nature Communications, 10*(1), 5261. https://doi.org/10.1038/s41467-019-13231-0

Hopwood, M. J., Connelly, D. P., Arendt, K. E., Juul-Pedersen, T., Stinchcombe, M. C., Meire, L., Esposito, M., & Krishna, R. (2016). Seasonal Changes in Fe along a Glaciated Greenlandic Fjord. *Frontiers in Earth Science, 4*(15). https://doi.org/10.3389/feart.2016.00015

Hutchins, D. A., & Bruland, K. W. (1998). Iron-limited diatom growth and Si:N uptake ratios in a coastal upwelling regime. *Nature, 393*(6685), 561-564. http://dx.doi.org/10.1038/31203

Hutchins, D. A., DiTullio, G. R., Zhang, Y., & Bruland, K. W. (1998). An iron limitation mosaic in the California upwelling regime. *Limnology and Oceanography, 43*(6), 1037-1054. https://doi.org/10.4319/lo.1998.43.6.1037

Hutchins, D. A., Sedwick, P. N., DiTullio, G. R., Boyd, P. W., Quéguiner, B., Griffiths, F. B., & Crossley, C. (2001). Control of phytoplankton growth by iron and silicic acid availability in the subantarctic Southern Ocean: Experimental results from the SAZ Project. *Journal of Geophysical Research, 106*(C12), 2156-2202. https://doi.org/ 10.1029/2000JC000333

Iriarte, J. L., Cuevas, L. A., Cornejo, F., Silva, N., González, H. E., Castro, L., Montero, P., Vargas, C. A., & Daneri, G. (2018). Low spring primary production and microplankton carbon biomass in Sub-Antarctic Patagonian channels and fjords (50–53°S). *Arctic, Antarctic, and Alpine Research, 50*(1), e1525186. https://doi.org/10.1080/15230430.2018.1525186

Iriarte, J. L., Kusch, A., Osses, J., Ruiz, M., & Iriarte, J. L. (2001). Phytoplankton biomass in the sub-Antarctic area of the Straits of Magellan (53°S), Chile during spring-summer 1997/1998. *Polar Biology, 24*(3), 154-162. https://doi.org/10.1007/s003000000189

Kanna, N., Sugiyama, S., Fukamachi, Y., Nomura, D., & Nishioka, J. (2020). Iron Supply by Subglacial Discharge Into a Fjord Near the Front of a Marine-Terminating Glacier in Northwestern Greenland. *Global Biogeochemical Cycles, 34*(10), e2020GB006567. https://doi.org/10.1029/2020GB006567

Kemp, A. E. S., Pike, J., Pearce, R. B., & Lange, C. B. (2000). The "Fall dump" — a new perspective on the role of a "shade flora" in the annual cycle of diatom production and export flux. Deep Sea Research Part II: Topical Studies in Oceanography, 47(9), 2129-2154. https://doi.org/10.1016/S0967-0645(00)00019-9

Kiørboe, T. (1993). Turbulence, Phytoplankton Cell Size, and the Structure of Pelagic Food Webs. In J. H. S. Blaxter & A. J. Southward (Eds.), Advances in Marine Biology (Vol. 29, pp. 1-72). Academic Press. https://doi.org/10.1016/S0065-2881(08)60129-7

Kuma, K., Katsumoto, A., Nishioka, J., & Matsunaga, K. (1998). Size-fractionated Iron Concentrations and Fe(III) Hydroxide Solubilities in Various Coastal Waters. *Estuarine, Coastal and Shelf Science, 47*(3), 275-283. https://doi.org/10.1006/ecss.1998.0355

Kuma, K., Nishioka, J., & Matsunaga, K. (1996). Controls on iron(III) hydroxide solubility in seawater: The influence of pH and natural organic chelators. *Limnology and Oceanography, 41*(3), 396-407. https://doi.org/10.4319/lo.1996.41.3.0396

Kunde, K., Wyatt, N., González-Santana, D., Tagliabue, A., Mahaffey, C., & Lohan, M. (2019). Iron distribution in the subtropical North Atlantic: The pivotal role of colloidal iron. *Global Biogeochemical Cycles, 33*(12), 1532-1547.

Lampe, R. H., Mann, E. L., Cohen, N. R., Till, C. P., Thamatrakoln, K., Brzezinski, M. A., Bruland, K. W., Twining, B. S., & Marchetti, A. (2018). Different iron storage strategies among bloom-forming diatoms. *Proceedings of the National Academy of Sciences*, 115(52), E12275-E12284. https://doi.org/10.1073/pnas.1805243115

Lewis, E., & Wallace, D. (1998). Program developed for CO2 system calculations. Carbon Dioxide Information Analysis Center. http://cdiac.ornl.gov/oceans/co2rprt.html

Lewis, W. M. (1976). Surface/Volume Ratio: Implications for Phytoplankton Morphology. *Science, 192*(4242), 885-887. https://doi.org/10.1126/science.192.4242.885

Leynaert, A., Bucciarelli, E., Claquin, P., Dugdale, R., Martin-Jézéquel, V., Pondaven, P., & Ragueneau, O. (2004). Effect of iron deficiency on diatom cell size and silicic acid uptake kinetics. *Limnology and Oceanography, 49*(4), 1134-1143.

Liu, H., Chen, M., Zhu, F., & Harrison, P. J. (2016). Effect of Diatom Silica Content on Copepod Grazing, Growth and Reproduction. *Frontiers in Marine Science*, 3(89). https://doi.org/10.3389/fmars.2016.00089

Liu, X., & Millero, F. J. (2002). The solubility of iron in seawater. *Marine Chemistry, 77*(1), 43-54. https://doi.org/10.1016/S0304-4203(01)00074-3

Logan, B. E., Passow, U., Alldredge, A. L., Grossartt, H.-P., & Simont, M. (1995). Rapid formation and sedimentation of large aggregates is predictable from coagulation rates (half-lives) of transparent exopolymer particles (TEP). *Deep Sea Research Part II: Topical Studies in Oceanography, 42*(1), 203-214. https://doi.org/10.1016/0967-0645(95)00012-F

López-Rivera, A., Suarez-Isla, B. A., Eilers, P., Beaudry, C., Hall, S., Amandi, M., Furey, A., & James, K. (2005). Improved high-performance liquid chromatographic method for the determination of domoic acid and analogues in shellfish: Effect of pH. *Analytical and bioanalytical chemistry, 381*, 1540-1545. https://doi.org/10.1007/s00216-005-3109-4

Luebert, F., & Pliscoff, P. (2006). Sinopsis bioclimática y vegetacional de Chile. Editorial Universitaria.

Lürling, M. (2021). Grazing resistance in phytoplankton. *Hydrobiologia, 848*(1), 237-249. https://doi.org/10.1007/s10750-020-04370-3

M. Franck, V., Brzezinski, M. A., Coale, K. H., & Nelson, D. M. (2000). Iron and silicic acid concentrations regulate Si uptake north and south of the Polar Frontal Zone in the Pacific Sector of the Southern Ocean. *Deep Sea Research Part II: Topical Studies in Oceanography, 47*(15), 3315-3338. https://doi.org/10.1016/S0967-0645(00)00070-9

Maldonado, M., Hughes, M., Rue, E., & Wells, M. (2002). The effect of Fe and Cu on growth and domoic acid production by Pseudo-nitzschia multiseries and Pseudo-nitzschia australis. *Limnology and Oceanography, 47*, 515-526. https://doi.org/10.4319/lo.2002.47.2.0515

Maldonado, M., & Price, N. (1999). Utilization of iron bound to strong organic ligands by plankton communities in the subarctic Pacific Ocean. *Deep Sea Research Part II: Topical Studies in Oceanography, 46*(11), 2447-2473. https://doi.org/10.1016/S0967-0645(99)00071-5

Maldonado, M. T., Strzepek, R. F., Sander, S., & Boyd, P. W. (2005). Acquisition of iron bound to strong organic complexes, with different Fe binding groups and photochemical reactivities, by plankton communities in Fe-limited subantarctic waters. *Global Biogeochemical Cycles, 19*(4). https://doi.org/10.1029/2005GB002481

Marchetti, A., & Cassar, N. (2009). Diatom elemental and morphological changes in response to iron limitation: a brief review with potential paleoceanographic applications. *Geobiology, 7*(4), 419-431. https://doi.org/10.1111/j.1472-4669.2009.00207.x

Marchetti, A., Parker, M. S., Moccia, L. P., Lin, E. O., Arrieta, A. L., Ribalet, F., Murphy, M. E. P., Maldonado, M. T., & Armbrust, E. V. (2009). Ferritin is used for iron storage in bloom-forming marine pennate diatoms. *Nature, 457*(7228), 467-470. https://doi.org/10.1038/nature07539

Marchetti, A., Varela, D. E., Lance, V. P., Lance, V. P., Palmucci, M., Giordano, M., & Virginia Armbrust, E. (2010). Iron and silicic acid effects on phytoplankton productivity, diversity, and chemical composition in the central equatorial Pacific Ocean. *Limnology and Oceanography, 55*(1), 11-29. https://doi.org/10.4319/lo.2010.55.1.0011

Martin-Jézéquel, V., Hildebrand, M., & Brzezinski, M. A. (2000). Silicon metabolism in diatoms: implications for growth. *Journal of Phycology, 36*, 821-840. https://doi.org/10.1046/j.1529-8817.2000.00019.x

Martin, J. H., & Fitzwater, S. E. (1988). Iron deficiency limits phytoplankton growth in the north-east Pacific subarctic. *Nature, 331*(6154), 341-343. http://dx.doi.org/10.1038/331341a0

Martin, P., van der Loeff, M. R., Cassar, N., Vandromme, P., d'Ovidio, F., Stemmann, L., Rengarajan, R., Soares, M., González, H. E., Ebersbach, F., Lampitt, R. S., Sanders, R., Barnett, B. A., Smetacek, V., & Naqvi, S. W. A. (2013). Iron fertilization enhanced net community production but not downward particle flux during the Southern Ocean iron fertilization experiment LOHAFEX. *Global Biogeochemical Cycles*, n/a-n/a. https://doi.org/10.1002/gbc.20077

Mascarenhas, V. J., Voß, D., Wollschlaeger, J., & Zielinski, O. (2017). Fjord light regime: Bio-optical variability, absorption budget, and hyperspectral light availability in Sognefjord and Trondheimsfjord, Norway. *Journal of Geophysical Research: Oceans, 122*(5), 3828-3847. https://doi.org/10.1002/2016JC012610

Medlin, L. K., & Kaczmarska, I. (2004). Evolution of the diatoms: V. Morphological and cytological support for the major clades and a taxonomic revision. *Phycologia, 43*(3), 245-270. https://doi.org/10.2216/i0031-8884-43-3-245.1

Mehrbach, C., Culberson, C. H., Hawley, J. E., & Pytkowicz, R. N. (1973). Measurement of the apparent dissociation constants of carbonic acid in seawater at atmospheric pressure. *Limnology and Oceanography, 18*, 897-907.

Menden-Deuer, S., Lawrence, C., & Franzè, G. (2018). Herbivorous protist growth and grazing rates at in situ and artificially elevated temperatures during an Arctic phytoplankton spring bloom. *PeerJ, 6*, e5264. https://doi.org/10.7717/peerj.5264

Mopper, K., zhou, J., Sri Ramana, K., passow, U., dam, H. G., & Drapeau, D. T. (1995). The role of surface-active carbohydrates in the flocculation of a diatom bloom in a mesocosm. *Deep Sea Research Part II: Topical Studies in Oceanography, 42*(1), 47-73. https://doi.org/10.1016/0967-0645(95)00004-A

Naz, T., Burhan, Z., Munir, S., & Siddiqui, P. J. A. (2013). Biovolume and biomass of common diatom species from the coastal waters of Karachi, Pakistan. Pak. *J. Bot, 45*(1), 325-328.

Nishioka, J., Takeda, S., Wong, C. S., & Johnson, W. K. (2001). Size-fractionated iron concentrations in the northeast Pacific Ocean: distribution of soluble and small colloidal iron. *Marine Chemistry, 74*(2), 157-179. https://doi.org/10.1016/S0304-4203(01)00013-5

Nowostawska, U., Kim, J., & Hunter, K. (2008). Aggregation of riverine colloidal iron in estuaries: A new kinetic study using stopped-flow mixing. *Marine Chemistry, 110*, 205-210. https://doi.org/10.1016/j.marchem.2008.03.001

Olenina, I., Hajdu, S., Edler, L., Andersson, A., Wasmund, N., Busch, S., Göbel, J., Gromisz, S., Huseby, S., Huttunen, M., Jaanus, A., Kokkonen, P., Jurgensone, I., & Niemkiewicz, E. (2006). Biovolumes and size-classes of phytoplankton in the Baltic Sea. HELCOM Balt. *Sea Environmental Proceedings*, 106.

Öztürk, M., Steinnes, E., & Sakshaug, E. (2002). Iron Speciation in the Trondheim Fjord from the Perspective of Iron Limitation for Phytoplankton. *Estuarine, Coastal and Shelf Science*, 55(2), 197-212. https://doi.org/10.1006/ecss.2001.0897

Palma, S., & Silva, N. (2004). Distribution of siphonophores, chaetognaths, euphausiids and oceanographic conditions in the fjords and channels of southern Chile. *Deep Sea Research Part II: Topical Studies in Oceanography, 51*(6-9), 513-535. http://dx.doi.org/10.1016/j.dsr2.2004.05.001

Pan, Y., Bates, S. S., & Cembella, A. D. (1998). Environmental stress and domoic acid production by Pseudo-nitzschia: a physiological perspective. *Natural Toxins, 6*(3-4), 127-135. https://doi.org/10.1002/(SICI)1522-7189(199805/08)6:3/4<127::AID-NT9>3.0.CO;2-2

Pan, Y., Rao, D. V. S., Mann, K. H., Li, W. K. W., & Harrison, W. G. (1996). Effects of silicate limitation on production of domoic acid, a neurotoxin, by the diatom Pseudo-nitzschia multiseries. II. Continuous culture studies. *Marine Ecology Progress Series, 131*(1/3), 235-243. http://www.jstor.org/stable/24855792

Pizarro, G., Frangópulos, M., Krock, B., Zamora, C., Pacheco, H., Alarcón, C., Toro, C., Pinto, M., Torres, R., & Guzmán , L. (2017). Watch out for ASP in the Chilean Subantarctic region. Marine and Fresh-Water Harmful Algae. Proceedings of the 17th International Conference on Harmful Algae, Florianópolis, Brazil.

Pryer, H., J. Hawkins, JL. Wadham, LF. Robinson, KR. Hendry, JE. Hatton, B. Gill Olivas, A. Kellerman, M. Marshall, G. Daneri, S. Bertrand, V. Haussermann, & Brooker., R. (2020). Glacial cover affect silicon and iron exports from rivers. . submitted to *Global Biogeochemical cycles.*

Pryer, H., Wadham, J. L., Hawkings, J. R., Robinson, L. F., Hendry, K. R., Marshall, M., Yates, C., & Hatton, J. E. (2019, 13-23 August). Glacial cover affects nutrient fluxes from rivers in Chilean Patagonia. Goldshmidt, Barcelona.

Ragueneau, O., Savoye, N., Del Amo, Y., Cotten, J., Tardiveau, B., & Leynaert, A. (2005). A new method for the measurement of biogenic silica in suspended matter of coastal waters: Using Si:Al ratios to correct for the mineral interference. *Continental Shelf Research, 25*, 697-710. https://doi.org/10.1016/j.csr.2004.09.017

Ragueneau, O., & Tréguer, P. (1994). Determination of biogenic silica in coastal waters: applicability and limits of the alkaline digestion method. *Marine Chemistry, 45*(1-2), 43-51. http://www.sciencedirect.com/science/article/pii/0304420394900906

Ragueneau, O., Tréguer, P., Leynaert, A., Anderson, R. F., Brzezinski, M. A., DeMaster, D. J., Dugdale, R. C., Dymond, J., Fischer, G., François, R., Heinze, C., Maier-Reimer, E., Martin-Jézéquel, V., Nelson, D. M., & Quéguiner, B. (2000). A review of the Si cycle in the modern ocean: recent progress and missing gaps in the application of biogenic opal as a paleoproductivity proxy. *Global and Planetary Change, 26*(4), 317-365. http://www.sciencedirect.com/science/article/B6VF0-41V33VT-1/2/9807079da965def4f6a4650fdec22daf

Raiswell, R., & Canfield, R. E. (2012). The Iron Biogeochemical Cycle Past and Present. *Geochemical Perspective, 1*(1), 1. https://doi.org/10.7185/geochempersp.1.1

Raiswell, R., Hawkings, J., Elsenousy, A., Death, R., Tranter, M., & Wadham, J. (2018). Iron in Glacial Systems: Speciation, Reactivity, Freezing Behavior, and Alteration During Transport. *Frontiers in Earth Science*, 6. https://doi.org/10.3389/feart.2018.00222

Raiswell, R., Tranter, M., Benning, L. G., Siegert, M., De'ath, R., Huybrechts, P., & Payne, T. (2006). Contributions from glacially derived sediment to the global iron (oxyhydr)oxide cycle: Implications for iron delivery to the oceans. *Geochimica et Cosmochimica Acta*, *70*(11), 2765-2780. https://doi.org/10.1016/j.gca.2005.12.027

Raven, J. A., Evans, M. C. W., & Korb, R. E. (1999). The role of trace metals in photosynthetic electron transport in O2-evolving organisms. *Photosynthesis Research, 60*(2), 111-150. https://doi.org/10.1023/A:1006282714942

Ribalet, F., Marchetti, A., Hubbard, K. A., Brown, K., Durkin, C. A., Morales, R., Robert, M., Swalwell, J. E., Tortell, P. D., & Armbrust, E. V. (2010). Unveiling a phytoplankton hotspot at a narrow boundary between coastal and offshore waters. *Proceedings of the National Academy of Sciences*, *107*(38), 16571-16576. https://doi.org/10.1073/pnas.1005638107

Ryderheim, F., Grønning, J., & Kiørboe, T. (2022). Thicker shells reduce copepod grazing on diatoms. *Limnology and Oceanography Letters,* n/a(n/a). https://doi.org/10.1002/lol2.10243

Saggiomo, V., Goffart, A., Carrada, G. C., & Hecq, J. H. (1994). Spatial patterns of phytoplanktonic pigments and primary production in a semi-enclosed periantarctic ecosystem: the Strait of Magellan. *Journal of Marine Systems*, *5*(2), 119-142. https://doi.org/10.1016/0924-7963(94)90027-2

Saggiomo, V., Santarpia, I., Saggiomo, M., Margiotta, F., & Mangoni, O. (2011). Primary production processes and photosynthetic performance of a unique periantarctic ecosystem: The Strait of Magellan (Vol. 34). https://doi.org/10.1007/s00300-011-1038-6

Saito, H., Ota, T., Suzuki, K., Nishioka, J., & Tsuda, A. (2006). Role of heterotrophic dinoflagellate Gyrodinium sp. in the fate of an iron induced diatom bloom. *Geophysical Research Letters, 33*(9). https://doi.org/10.1029/2005GL025366

Sarmiento, J. L., Gruber, N., Brzezinski, M. A., & Dunne, J. P. (2004). High-latitude controls of thermocline nutrients and low latitude biological productivity. *Nature, 427*(6969), 56-60. http://dx.doi.org/10.1038/nature02127

Schoffman, H., Lis, H., Shaked, Y., & Keren, N. (2016). Iron–Nutrient Interactions within Phytoplankton. *Frontiers in Plant Science, 7*(1223). https://doi.org/10.3389/fpls.2016.01223

Schroth, A. W., Crusius, J., Hoyer, I., & Campbell, R. (2014). Estuarine removal of glacial iron and implications for iron fluxes to the ocean. *Geophysical Research Letters, 41*(11), 3951-3958. https://doi.org/10.1002/2014GL060199

Sedwick, P. N., Blain, S., Quéguiner, B., Griffiths, F. B., Fiala, M., Bucciarelli, E., & Denis, M. (2002). Resource limitation of phytoplankton growth in the Crozet Basin, Subantarctic Southern Ocean. *Deep Sea Research Part II: Topical Studies in Oceanography, 49*(16), 3327-3349. http://www.sciencedirect.com/science/article/B6VGC-45CVX2K-2/2/b7c8308d112f5cd17e6df7c235c12a05

Seo, H., Kim, G., Kim, T., Kim, I., Ra, K., & Jeong, H. (2022). Trace elements (Fe, Mn, Co, Cu, Cd, and Ni) in the East Sea (Japan Sea): Distributions, boundary inputs, and scavenging processes. *Marine Chemistry, 239*, 104070. https://doi.org/10.1016/j.marchem.2021.104070

Sholkovitz, E. R. (1976). Flocculation of dissolved organic and inorganic matter during the mixing of river water and seawater. *Geochimica et Cosmochimica Acta, 40*(7), 831-845. http://dx.doi.org/10.1016/0016-7037(76)90035-1

Sholkovitz, E. R., Boyle, E. A., & Price, N. B. (1978). The removal of dissolved humic acids and iron during estuarine mixing. *Earth and Planetary Science Letters, 40*(1), 130-136. https://doi.org/10.1016/0012-821X(78)90082-1

Smetacek, V. (1998). Biological oceanography: Diatoms and the silicate factor. *Nature, 391*, 224-225.

Smetacek, V., Klaas, C., Strass, V. H., Assmy, P., Montresor, M., Cisewski, B., Savoye, N., Webb, A., d/'Ovidio, F., Arrieta, J. M., Bathmann, U., Bellerby, R., Berg, G. M., Croot, P., Gonzalez, S., Henjes, J., Herndl, G. J., Hoffmann, L. J., Leach, H., . . . Wolf-Gladrow, D. (2012). Deep carbon export from a Southern Ocean iron-fertilized diatom bloom [10.1038/nature11229]. *Nature, 487*(7407), 313-319. https://doi.org/http://www.nature.com/nature/journal/v487/n7407/abs/nature11229.html#supplementary-information

Smith, R. B., & Evans, J. P. (2007). Orographic precipitation and water vapor fractionation over the Southern Andes. *Journal of Hydrometeorology, 8*(1), 3-19.

Steinberg, D. K., & Landry, M. R. (2017). Zooplankton and the Ocean Carbon Cycle. *Annual Review of Marine Science, 9*(1), 413-444. https://doi.org/10.1146/annurev-marine-010814-015924

Strickland, J. D. H., & Parsons, T. R. (Eds.). (1968). A practical handbook of seawater analysis. (Vol. 167).

Strzepek, R. F., & Harrison, P. J. (2004). Photosynthetic architecture differs in coastal and oceanic diatoms. *Nature, 431*, 689. https://doi.org/10.1038/nature02954

Strzepek, R. F., & Price, N. M. (2000). Influence of irradiance and temperature on the iron content of the marine diatom Thalassiosira weissflogii (Bacillariophyceae). *Marine Ecology Progress Series, 206*, 107-117. https://www.int-res.com/abstracts/meps/v206/p107-117/

Sunda, W. G., & Huntsman, S. A. (2011). Interactive effects of light and temperature on iron limitation in a marine diatom: Implications for marine productivity and carbon cycling. *Limnology and Oceanography*, *56*(4), 1475-1488. https://doi.org/10.4319/lo.2011.56.4.1475

Tagliabue, A., Bowie, A. R., DeVries, T., Ellwood, M. J., Landing, W. M., Milne, A., Ohnemus, D. C., Twining, B. S., & Boyd, P. W. (2019). The interplay between regeneration and scavenging fluxes drives ocean iron cycling. *Nature Communications, 10*(1), 4960. https://doi.org/10.1038/s41467-019-12775-5

Takeda, S. (1998). Influence of iron availability on nutrient consumption ratio of diatoms in oceanic waters. *Nature, 393*(6687), 774-777. http://dx.doi.org/10.1038/31674

Tillmann, U., Hesse, K.-J., & Tillmann, A. (1999). Large-scale parasitic infection of diatoms in the Northfrisian Wadden Sea. *Journal of Sea Research, 42*(3), 255-261. https://doi.org/10.1016/S1385-1101(99)00029-5

Torres, R., & Ampuero, P. (2009). Strong CO2 outgassing from high nutrient low chlorophyll coastal waters off central Chile (30°S): The role of dissolved iron. *Estuarine, Coastal and Shelf Science, 83*(2), 126-132. http://www.sciencedirect.com/science/article/pii/S0272771409001012

Torres, R., Frangopulos, M., Hamamé, M., Montecino, V., Maureira, C., Pizarro, G., Reid, B., Valle-Levinson, A., & Luis Blanco, J. (2011). Nitrate to silicate ratio variability and the composition of micro-phytoplankton blooms in the inner-fjord of Seno Ballena (Strait of

Magellan, 54°S). *Continental Shelf Research, 31*(3-4), 244-253. http://www.sciencedirect.com/science/article/pii/S0278434310002451

Torres, R., Pantoja, S., Harada, N., González, H. E., Daneri, G., Frangopulos, M., Rutllant, J. A., Duarte, C. M., Rúiz-Halpern, S., Mayol, E., & Fukasawa, M. (2011). Air-sea CO2 fluxes along the coast of Chile: From CO2 outgassing in central northern upwelling waters to CO2 uptake in southern Patagonian fjords. *Journal of Geophysical Research*, *116*(C9), C09006. https://doi.org/10.1029/2010jc006344

Torres, R., Reid, B., Frangópulos, M., Alarcón, E., Márquez, M., Häussermann, V., Försterra, G., Pizarro, G., Iriarte, J. L., & González, H. E. (2020). Freshwater runoff effects on the production of biogenic silicate and chlorophyll-a in western Patagonia archipelago (50–51°S). *Estuarine, Coastal and Shelf Science, 241*, 106597. https://doi.org/10.1016/j.ecss.2020.106597

Torres, R., Silva, N., Reid, B., & Frangopulos, M. (2014). Silicic acid enrichment of subantarctic surface water from continental inputs along the Patagonian archipelago interior sea (41–56°S). *Progress In Oceanography, 129*, Part A, 50-61. http://dx.doi.org/10.1016/j.pocean.2014.09.008

Torres, R., Turner, D., Silva, N., & Ruttlant, J. (1999). High short-term variability of CO2 fluxes during an upwelling event off the Chilean coast at 30S. *Deep Sea Research Part I., 46*, 1161-1179.

Utermohl, H. (1958). Zur Ver vollkommung der quantitativen phytoplankton-methodik. , , . Mitteilung Internationale Vereinigung Fuer Theoretische unde Amgewandte Limnologie, 9, 39 p.

von der Heyden, B. P., & Roychoudhury, A. N. (2015). A review of colloidal iron partitioning and distribution in the open ocean. *Marine Chemistry, 177*, 9-19. https://doi.org/10.1016/j.marchem.2015.05.010

Willis, M. J., Melkonian, A. K., Pritchard, M. E., & Ramage, J. M. (2012). Ice loss rates at the Northern Patagonian Icefield derived using a decade of satellite remote sensing. *Remote Sensing of Environment, 117*, 184–198.

Yeats, P. A., & Bewers, J. M. (1976). Trace metals in the waters of the Saguenay fjord. Canadian *Journal of Earth Sciences, 13*(9), 1319-1327. https://doi.org/10.1139/e76-133

Zhang, S., Liu, H., Ke, Y., & Li, B. (2017). Effect of the Silica Content of Diatoms on Protozoan Grazing. *Frontiers in Marine Science, 4*. https://doi.org/10.3389/fmars.2017.00202

SUPPORTING INFORMATION

Additional supporting information may be found online at: https://www.sciencedirect.com/science/article/abs/pii/S0079661123000253?CMX_ID=&SIS_ID=&dgcid=STMJ_AUTH_SERV_PUBLISHED&utm_acid=268535156&utm_campaign=STMJ_AUTH_SERV_PUBLISHED&utm_in=DM352260&utm_medium=email&utm_source=AC_

Appendix 3: Macroinvertebrate community composition and richness along extreme gradients: the role of local, catchment and climatic variables in Patagonian headwater streams

Anna Astorga, Brian Reid, Luis Uribe, Paulo Moreno-Meynard, Pablo Fierro, Isaí Madriz, Russell G. Death

Freshwater Biology, 2022;67:445-460, doi: 10.1111/fwb.13853

Abstract

1. We investigated how interacting multi-scale environmental variables affect taxonomic composition and functional feeding groups (FFG) of macroinvertebrates in headwater streams of western Patagonia in southern Chile (45-47°S), a region characterized by extreme climatic gradients, intact forested catchments and recent intense land use change. The opportunity of establishing biological/functional diversity patterns for near-reference conditions of headwaters streams is paramount.
2. We used Multi-Dimensional Scaling (MDS) ordination and Boosted Regression Tree (BRT) analysis of macroinvertebrate communities to evaluate the link between reach, catchment, spatial and regional climatic variables and community structure.
3. The high diversity of predators in low productivity streams, together with genera previously unreported for this latitudinal range underscore the unique characteristics and very limited understanding of Patagonian freshwater stream communities.
4. Two main groups of environmental variables were linked to both taxonomic and FFG diversity. The strongly associated variables were related to forest cover (and inversely alpine zone) at the catchment scale, together with stream velocity at the local scale. The

second group reflected local indicators of productivity and weathering inputs, associated with the regional east-west precipitation gradient.

5. We present a conceptual model for the catchment scale effects on invertebrate functional groups in forested headwater streams. While the results highlight potentially singular characteristics of the study region, they also suggest a macro-ecological generalization of how global change variables, operating on mountain catchments, may differentially affect stream ecosystems as a consequence of the variations in the forest/alpine gradient, across both deciduous and evergreen temperate biomes.

Keywords: freshwater, invertebrates, Chilean Patagonia, functional feeding group, forested catchment.

A3.1 INTRODUCTION

Compared to terrestrial and marine systems, the limited spatial coverage of freshwater ecosystems belies both their higher biological diversity and greater proportion of species of conservation concern (Dudgeon et al., 2006). Freshwater ecosystems are also uniquely structured at the landscape level (Johnson & Gage, 1997; Allan, 2004), the hydrologic networks of freshwaters are directional and hierarchical, a critical element of their vulnerability. At the origins of these networks, headwaters are perhaps the catchment's most vulnerable point. Small streams are closely connected to land use change (especially forest cover), and climate/global change catchment-scale variables, underscoring the importance of headwaters streams to organisms and ecosystems downstream (Lowe & Likens 2005, Abell et al., 2007).

Multiscale approaches to understanding the relationship between diversity of freshwater macroinvertebrates and their environment has long been recognized in stream ecology (Hynes, 1970; Vannote et al., 1980; Poff, 1997; Lake, 2000). Local in-stream or stream-side riparian

variables often play a key role in structuring stream communities (Sandin & Johnson, 2004; Death & Joy, 2004; Lecraw & Mackereth, 2010; Astorga et al. 2014). A given stream reach will also be defined by its contributing catchment (Hynes, 1970), and local variables will in turn be determined by processes acting at the watershed scale (Kärnä et al., 2019). Catchment scale variables such as geomorphology and land cover affect flow regimes, productivity/energy inputs, water chemistry, substrate composition and dispersal opportunities (Allan et al., 1997; Soininen, 2015; Kärnä et al., 2019). Catchments are also nested within a regional climate, where spatial patterns in precipitation, solar radiation, wind and temperature act on both the watershed and reach scale to shape local stream ecosystems (Dodds et al., 2015; Clarke 2017). All three scales, local/reach, catchment and climatic, are linked hierarchically; larger scale variables affecting smaller scale characteristics (Frissell et al., 1986; Poff, 1997).

This nested hierarchy is responsible for the large and interconnected suite of potentially important variables, and the correspondingly high heterogeneity of stream habitat, related to macroinvertebrate community structure, and fundamentally challenging any broad generalizations about stream ecosystems. This variability may be better constrained by broadening the response variables to include both taxonomic and functional diversity of stream organisms, the complementary information from each providing more chance of finding explanation at different scales (Hoeinghaus et al., 2007, Heino et al., 2007). At smaller spatial scales, such as stream communities within one drainage network, will likely be associated with a single regional species pool, thus taxonomic and functional trait structure may vary similarly across the same environmental gradients (Finn & Poff, 2005; Heino et al., 2007). At larger spatial scales, such as areas that span greater bioclimatic variability, higher species turnover is expected, with stronger relationships between taxonomic structure and large scale environmental or spatial drivers.

Meanwhile functional traits should closely follow the local environment, also providing a way of identifying mechanism behind the patterns in community structure (Johnson et al., 2004).

Mountain regions such as the southern Patagonian Andes may represent an extreme in terms of spatial heterogeneity and temporal variability of streams and their multiscale drivers (e.g., local, catchment, or climatic). Strong east-west climatic gradients (<500 to 5,000+ mm/y precipitation range over a few 100s of kilometers) correspond with vegetation shifts representing four biomes (evergreen temperate rainforest, deciduous forest, cold-steppe grassland and alpine glaciers/tundra). Steep elevational gradients result in dramatic shifts in stream habitat and river geomorphology over short distances and transit times. The origins of streams also vary across glacial meltwater, seasonal snowmelt, peatland, deciduous or evergreen forest, or lowland coastal plains, all within close geographic proximity. These marked topographic and climatic gradients, together with geomorphic processes such as glaciation and basin capture (Valdovinos et al., 2010), isolation and Gondwana origin also contributes a unique biodiversity of terrestrial vertebrates, invertebrates, and plants with a high degree of endemism (Armesto et al., 1998; Rozzi et al., 2012).

Despite the generally disproportionate threats to, and biodiversity value of freshwater systems, patterns for aquatic biodiversity and its relationship to environmental characteristics has received limited attention in much of Patagonia. While work on freshwater macroinvertebrate diversity of eastern pre-cordilleran Patagonia systems is noteworthy (Argentina: 40°-48°S; Miserendino & Masi, 2010; Miserendino et al., 2018), these systems represent a fraction of the trans-Andean environmental gradients. Limited studies have represented fragments of the extreme climatic and geomorphologic gradients of western Patagonia (Oyadenel et al., 2008;Valdovinos et al., 2010; Contador et al., 2015; Rendoll Cárcamo et al., 2019), while others are marked by the belated

impacts of invasive species (Anderson& Rosemond, 2007; Contador et al., 2012; Anderson et al., 2014).

In western Patagonia, the Aysén region (Southern Chile 44-47°S) represents an ideal scenario for evaluating the influence of multi-scale environmental variables on stream ecosystems (Oyadenel et al., 2008) over complex bioclimatic and geographic gradients. Impacts to aquatic ecosystems are minimal, as contemporary human colonization is relatively recent (see Astorga et al., 2018). The most significant impacts have been from fires set by humans to clear land for cattle and sheep ranching (peaking generally in the 1940-60s). While lower elevations experienced either reforestation (regrowth) or conversion to pasture (Astorga et al., 2018), higher elevation headwaters have been relatively unaffected by wildfires. This a useful scenario for studying freshwater biodiversity across a significant bioclimatic range of reference conditions, together with local comparison to areas of recent land use changes.

The objective of this study was to determine stream macroinvertebrate taxonomic and functional feeding group (FFG) composition in 53 forested headwater streams along two major continental basins in western Patagonia: Aysén and upper Baker River (45-47°S). We restricted our sampling and field observations to forested reaches, although respective catchments included a wide range of non-forested area (e.g., alpine zone). Although the study area is within a limited geographic extent (<250 km range) the climatic gradient is significant (500-2200 mm precipitation, 4-9°C mean annual temperature). We addressed two main questions, related to hierarchical environmental effects and also taxonomic vs. functional responses: 1) What are the main environmental variables explaining taxonomic and FFG composition?, and 2) Does the relative contribution of local, catchment, climatic and spatial environmental variables differ between taxonomic and FFG composition?

We expected that species traits such as FFG should be under strong control by the local riparian forest and stream reach environment (e.g., factors affecting local trophic sources such as light penetration, nutrients, and retention of allocthonous materials) with primarily allochthonous organic and detritus-based communities. Meanwhile, taxonomic composition and richness might be affected by local environmental conditions, but also larger scale processes at the catchment scale, biogeography and bioclimatic zone (Hoegnius et al. 2007, Heino et al. 2007, Tolonen et al. 2017). We also expected that catchment and climatic effects on taxonomic composition and richness would vary by forest type (evergreen vs. deciduous leaf inputs).

A3.2 METHODS

A3.2.1 Study sites

Two of the principal continental basins of the Patagonian southern Andes (Aysén River and upper Baker River, 45.1°-46.5°S and 71.6°-72.9°W; figure 3.1) were selected to represent nearly the full climatic gradient. The strong precipitation gradient and corresponding forest cover transitions range from cold steppe transition (*Nothofagus antartica*) with ca. 500 mm/year of rain, deciduous temperate forests (*N. pumilio* and *N. antartica*) up to 1000 mm/year, transitioning evergreen temperate forests at around 1800 mm/year (dominated by *N. nitida and Drimys winteri*) and reaching 3000-4000 mm/year (grading to more diverse vegetation with *N. dombeyi, N. betuloides, Laureliopsis philippiana, Pilgerodendron uviferum and Tepualia stipularis*). Elevation of the cordillera in these basins approaches 1200-1500m, hence many first order streams originate in alpine zone (>1200 m a.s.l.).

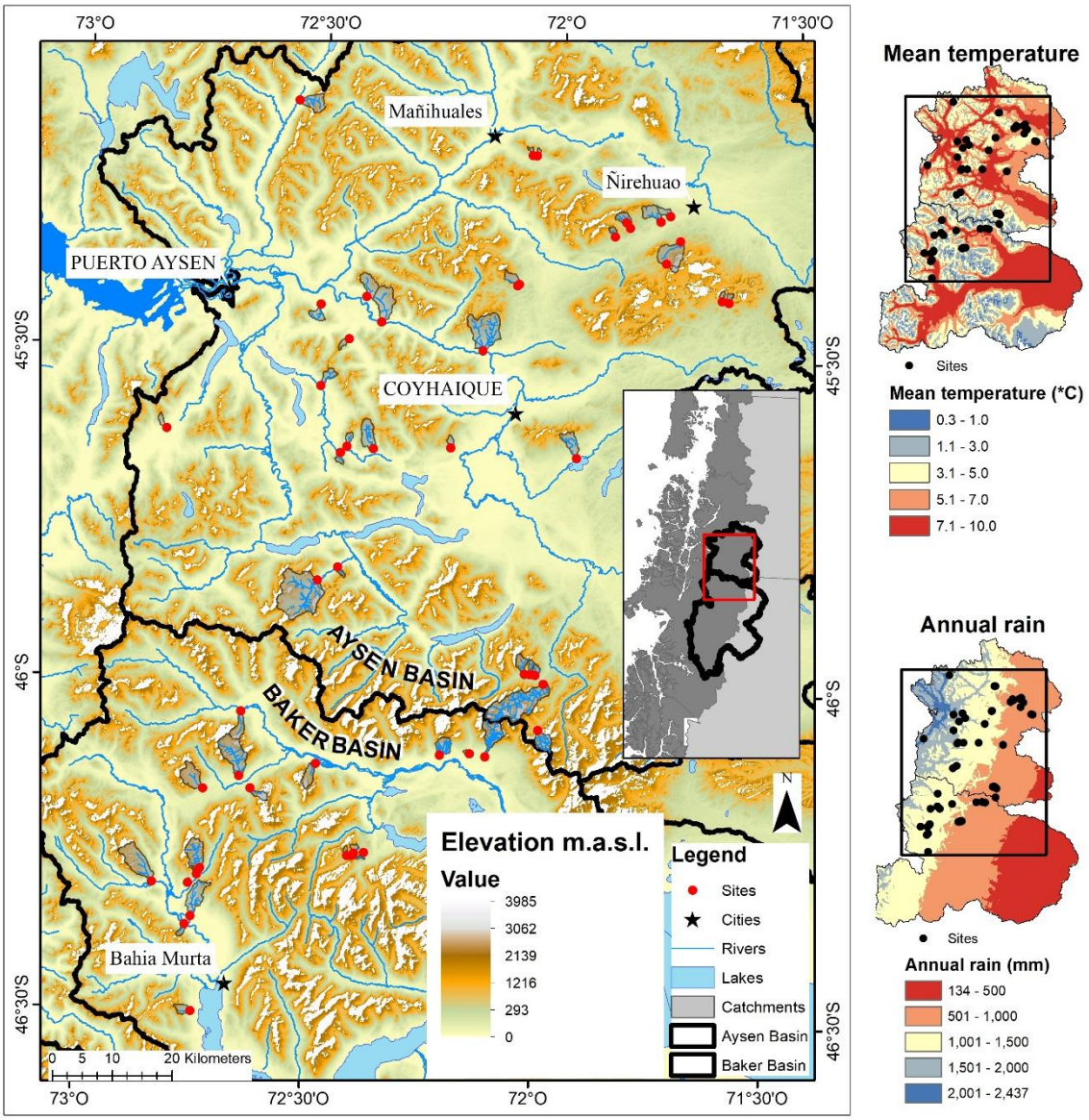

Figure A3.1. *Map of the study sites in the Aysén and Baker basin catchments, in Chilean Patagonia. Shown are local sites and contributing catchments, and bioclimatic patterns in temperature, precipitation and elevation.*

A3.2.2 Macroinvertebrate sampling

We sampled riffle habitat in 53 streams within forested reaches (0-3 Strahler order) during the austral spring, October – November 2015. Sampling locations were identified following preliminary mapping of intact forested catchments (0.5-1km^2 micro-catchment mapping unit;

ArcGIS v. 10.6 with ArcHydro 10. 2 extensions; Astorga et al., 2018) and selected based on feasibility of access and representation across the regional climatic gradient. Sampling sites were upstream of vehicular road access, representing near-reference condition stream segments within old-growth forested catchments. Additional sites with evidence of anthropogenic impacts in the catchment (e.g., fire, wood harvest, roads, and cattle ranching) were also selected. The strongest anthropogenic impacts of fire and low intensity ranching predominate at lower elevations, while higher elevations were near pristine, the general condition of headwater streams in the Aysén region (Astorga et al., 2018).

In each stream, we sampled biological and environmental variables over 30m transects within the riffles of pool-riffle reaches. Four-minute kick-net samples (mesh size 0.3 mm), consisting of eight 30-s subsamples across different microhabitats, were subsequently pooled. Macroinvertebrate samples were preserved in 70% ethanol in the field with a second change into clean 70% ethanol in the lab. Samples were sorted from debris (unaided and 10x stereomicroscope) and individuals were enumerated and identified to the lowest feasible taxonomic level (usually genus for insects and crustaceans), based on continental scale taxonomic references (Courtney & Merritt, 2008; Stark et al., 2009; Domínguez & Fernandez, 2009; Thorp et al. 2019) or regional literature for respective taxonomic groups (Edwards, 1929; Mackerras & Fuller, 1942; Brundin, 1966; Teskey, 1970; Elgueta &Arriagada 1989; Cranston & Edward 1992; Rojas 2006; Coscarón & Coscarón Arias, 2007;Woodley, 2007; Borkent & Rotheray, 2010; Llanos et al., 2015; Madriz & Courtney, 2016). In a few cases taxa were determined to subfamily, family, or order. Reference material for all determinations is maintained at the Centro CIEP laboratory in Coyhaique, Chile.

For assigning FFG for each taxon, we conducted a synthesis of macroinvertebrate FFG assignments for the Aysén region (table S1, Supplementary Information). Sources included: 1)

Original work based on a combination of morphological, stomach content and/or behavioral characteristics. 2) Works that only used morphological characteristics. For discrepancies, we assigned FFG based on Brand & Miserendino (2015), and Miserendino & Pizzolon (2004). When literature was not available, we assigned an FFG based on morphological character analysis of the mouth parts (7 taxa) or omitted from the analysis of diversity (2 taxa).

A3.2.3 Environmental variables

Water samples collected simultaneously upstream of benthic sampling were stored on ice and then refrigerated (alkalinity, major ions) or frozen (nutrients) for laboratory analysis. Field measurement of water temperature, pH, dissolved oxygen and specific conductivity were recorded with hand-held instruments (ProDSS, YSI Inc.). Alkalinity was analyzed by titration to colorimetric endpoint using a Metrohm Inc. Dosimat with bromcresol green-methyl red indicator, and reported as mg/l carbonate (APHA 2005). Total nitrogen (TN) and total phosphorus (TP) were analyzed following digestion with potassium persulfate, followed by colorimetric analysis using cadmium reduction or ascorbic acid methods, respectively (APHA 2005). Inorganic nitrogen (NOx) and soluble reactive phosphorous were also analyzed from filtered samples, however since nearly half of the sites were below detection limits for dissolved inorganic species (e.g., < 2.5 ug N/L), values reported here are for site characterization only. Dissolved silica was analyzed using a modified molybdo-silicate method with metol-sulfide as the reducing agent (Strickland & Parsons, 1968). Major ions (Na^+, K^+, $Mg^{2+,}$ Ca^{2+}) were analyzed by ion chromatography (Dionex™ ICS-5000 with eluent generation).

Local physical stream and riparian zone variables were based on cross-channel transects spaced evenly along the 30 m longitudinal transects. Canopy cover by riparian trees was estimated at 20 locations per site along equidistant cross-channel transects. Stream depth and current velocity (at

0.4 m depth, Swoffer 3000 Current Velocity Meter-Flowmeter, Sumner, WA, USA) at 20 bank to bank points within transects. Stream width was recorded in 5 equidistant cross channel transects in each reach, and channel slope was measured with an Abney level over 10-20 m, depending on channel steepness. Substrate composition was determined by Wolman pebble count, 100 particles selected at 1m intervals along a path at 45° to each stream bank and assigned to one of 13 size classes (bedrock, >300 mm, 300–128, 128–90.5, 90.5–64, 64–45.3, 45.3–32, 32–22.6, 22.6–16, 16–11.3, 11.3–8 8–5, <5 mm; (Wolman, 1954). A single substrate size index (SI) was calculated by summing the mid-point values of the size classes weighted by the number of stones in each size class (bedrock was assigned a nominal size of 400 mm; (Quinn & Hickey, 1990).

Six stones were randomly selected along the reach (generally 5–20 cm diameter) and removed for Chlorophyll-a analysis. Entire surfaces were repeatedly brushed and washed, the pooled biofilm was collected on glass fiber filters, which were wrapped in foil, transported on ice, and frozen in the lab. Surface area was estimated following Biggs & Kilroy (2000). Analysis of Chlorophyll-a, and accessory carotenoid pigments was performed within 2-3 weeks using 90% buffered acetone extraction (Hauer & Lamberti, 2016), spectrophotometric analysis and calculations based on APHA (2005).

Environmental variables at the catchment scale, or regional climatic variables based on catchment location, were calculated from global gridded datasets applied to respective site (figure A3.1), processed in ArcGIS 10.6 (ESRI 2018) and Arc Hydro 10.2 for ArcGIS (ESRI 2011). Variables related to catchment geomorphology and watershed boundaries were calculated from a SRTM 90 m digital elevation model (DEM; CGIAR-CSI version 4.1; Jarvis et al., 2017; Astorga et al., 2018). Sampling catchments were then overlaid with the Chilean national land use inventory maps (CONAF 2011) to calculate the percentages of each land cover variable in each catchment

(table A3.1). Percentage of alpine zone was calculated based on the sum of three land cover categories: i) areas above tree line, ii) bare rocks and iii) snow cover (CONAF 2011), the latter two also above tree line. Percentage of total forest cover was based on the sum of all forest types (evergreen, mixed and deciduous) as a proportion of the total area of contributing catchment. Percentage of deciduous or evergreen forest was based on the proportion of total forest cover (not catchment area). Percentage of forested riparian zone for the entire upstream network was calculated based on forest cover to tree line within a buffer of 50 m from the center of the stream. The percentage of the catchment with no impact from roads, fires or forest harvest (i.e., the upstream catchment area with no evidence of alteration to land cover) was calculated based on previously mapped limits of intact forested catchments (Astorga et al., 2018). Catchment slope was obtained using the digital elevation model and ArcGIS Spatial Analyst. We calculated mean annual precipitation and mean annual temperature each catchment based on downscaled gridded climate data (WorldClim Version 2, Fick & Hijmans, 2017) (table 3.1).

Table A3.1. List of the environmental variables pertaining to each category (stream, catchment, spatial and climatic), and their mean, standard deviation (SD), minimum values (Min) and maximum values (Max). See methods for more detail on calculations. * Alpine zone cover (%) and dissolved oxygen are reported for site characterization only and were excluded from Boosted Regression Tree analysis (see text).

Variable	Mean	SD	Min	Max
Stream				
Canopy cover (%)	54.0	27.8	1.5	97.5
Stream width (m)	5.6	3.8	1.6	17.2
Stream depth (cm)	19.1	7.7	5.2	38.7
Current velocity (m/s)	0.47	0.18	0.09	0.88
Stream slope (degrees)	6.9	4.7	1.1	20
Substrate index (unitless)	13.84	4.47	2.06	23.89
Stream segment elevation (m a.s.l.)	610	314	61	1086
Temperature (°C)	5.0	2.2	0.5	10.4
Specific conductivity (μS cm^{-2})	38.2	23.2	12	112
pH	7.51	0.37	5.89	8.37

**Dissolved oxygen (%)*	*99.9*	*1.71*	*95.2*	*103*
Chlorophyll-a (mg m^{-2})	0.53	0.48	0.002	2.19
Carotenoid/Chl-a ratio (mSPU/mg)	1.71	0.75	0.41	4.21
Alkalinity (mg L^{-1})	16.8	10.8	4.7	51.3
Total nitrogen (µg N L^{-1})	72.4	67.3	9.6	300
Total phosphorus (µg P L^{-1})	12.5	15.4	2.2	77.5
Chloride (mg L^{-1})	1.32	2.32	0.24	12.7
Sulfate (mg L^{-1})	2.14	2.11	0.12	8.85
Sodium (mg L^{-1})	1.74	1.28	0.52	7.26
Potassium (mg L^{-1})	0.34	0.22	0.07	1.40
Magnesium (mg L^{-1})	0.67	0.81	0.17	5.39
Calcium (mg L^{-1})	5.10	3.26	1.57	14.45
Dissolved silica (µmol L^{-1})	246	211	11	855
Catchment				
Catchment area (km^2)	6.2	8.7	0.14	45.2
Catchment slope (%)	17.4	5.7	5.6	28.1
**Alpine zone cover (%)*	*35.4*	*27.4*	*0*	*88.1*
Forest cover (%)	61.2	26.4	11.9	100
Riparian forest cover (%)	81.2	21.9	12.8	100
Deciduous forest cover (%)	53.8	26.1	11.9	100
Evergreen forest cover (%)	7.4	11.8	0	46.5
Intact forest cover (%)	38.6	26.0	0	100
Spatial				
Longitude (UTM WGS84)	710214	27921	666844	763494
Latitude (UTM WGS84)	4924352	44477	4847541	4999848
Climatic				
Mean precipitation (mm/year)	1190	387	598	2110
Mean annual temperature (°C)	6.3	1.3	3.5	8.6

A3.2.4 Statistical analysis

Complementary exploratory and predictive approaches were used to respond our main questions, each explained under the following subtitles.

A3.2.4.1 Exploratory analysis

Metric multidimensional scaling (MDS) ordination was applied to reduce the dimensionality of our macroinvertebrate composition data. MDS analysis was based on a dissimilarity matrix using the Bray-Curtis index (Oksanen et al., 2016), and 52 dimensions to represent the data (k=52) (Everitt & Hothorn, 2011). The resulting ordination was combined with the *envfit* function from the vegan package (R program, Oksanen et al., 2016) to identify the most significant environmental variables ($p < 0.001$) correlated with the first two ordination axes explaining most of the variation. Second, Pearson correlation coefficient was used to examine correlations between the original list of 40 environmental variables.

A3.2.4.2 Predictive analysis

We used Boosted Regression Tree analysis (BRT, James et al., 2013) to explain the variation in taxonomic and FFG diversity, using the first two axes of each MDS analysis as the response variables (Gansfort & Traunspurger, 2019, Xu et al., 2019), and the reduced list of environmental variables as model predictors (James et al., 2013). Additionally, for including another diversity metric, we also included taxonomic richness as a response variable, but not in the case of FFG given the small number of groups to calculate richness (n=5).

BRT is a non-parametric, machine learning method that can be understood as an advanced form of regression (Elith et al. 2008). It uses the technique of boosting to combine large numbers of relatively simple tree models adaptively, to optimize predictive performance. Using gbm.step function allowed us to calibrate the models regarding tree complexity, learning rate and bag fraction. The tree complexity (tc) controls whether interactions are fitted: a tc of 1 fits an additive model, a tc of two fits a model with up to two-way interactions, and so on (Elith et al. 2008). The learning rate, also known as the shrinkage parameter, determines the contribution of each tree to the growing model, and the bag fraction separates the input data to calibration and evaluation data

(Elith et al. 2008). Given the relatively small number of sites (e.g., less than 100), we used a tc of 2 (Gansfort & Traunspurger, 2019). As we reduced the length of the trees, we included a slower learning rate (0.001) to reach at least 1000 trees. A bag fraction of 0.75 used 75% of the data for fitting and 25% for prediction (Kärnä et al. 2019).We used a Gaussian family of relationships and 10-fold cross-validation. BRT models were also simplified by eliminating those less-informative predictors that may degrade performance (Elith et al., 2008). The identification of interactions between predictors was calculated following the Elith et al. (2008). To understand the relative contribution of local, catchment, climatic and spatial variables we summed up the relative influence of each selected predictor of each category to taxonomic richness, composition, and FFG composition. The relative influence is estimated by the model and is based on the number of times a variable is selected for splitting, weighted by the squared improvement to the model as a result of each split and averaged over all trees (Elith et al. 2008). Finally, the efficiency of the models was evaluated using the percent of the explained deviance [(mean total deviance – mean residual deviance)/mean total deviance] and the cross-validation correlation coefficients (Kärnä et al., 2019).

We visualized the fitted functions of the BRT model by using partial dependence functions that show the effect of a variable on the response after accounting for the average effects of all other variables in the model (Elith et al. 2008). These partial dependence plots describe the effect of the variable on the whole community, thus to be able to further interpret the effects of each predictor on taxonomic and FFG diversity, we plotted the critical thresholds (values of thresholds based on the partial dependence function) of the most influential variables against abundance and richness of Ephemeroptera (Mayflies), Plecoptera (Stoneflies), Trichoptera (Caddisflies), Coleoptera, and Diptera, and FFG abundance (shredders, predators, collector-gatherers, collector-filterers,

scrappers). All statistical analyses were performed using R v.3.4.1 statistical software (R Core Team 2017), specifically packages Stats (R Core Team 2017), vegan (Oksanen et al., 2016), and gbm (Ridgeway, 2013, Elith et al., 2008).

A3.3 RESULTS

Seventy-seven macroinvertebrate taxa were collected across the 53 sampled streams, the majority identified to genus (54 taxa), the rest to subfamily or family (see table S1 Suppl. Inf. for complete list of taxonomic resolution and FFG assignments). The most diverse macroinvertebrate orders were Trichoptera (18 taxa), Plecoptera (18 taxa), Diptera (12 taxa), Ephemeroptera (9 taxa) and Coleoptera (8 taxa) (table S1, Suppl. Inf.). The predator FFG was the most diverse (24 taxa), with collector-gatherers, shredders and scrapers equally diverse with 17 taxa each, while only two taxa were identified as collector-filterers (table S1 Suppl. Inf.). Our taxonomic list includes new distributional records for the Aysén region (44-48°S); *Luchoelmis* (Coleoptera: Elmidae); *Aphroteniella* (Diptera: Chironomidae); *Pelecorhynchus* (Diptera: Pelecorhynchidae); and *Oecetis* (Trichoptera: Leptoceridae) (table S1 Suppl. Inf.). Also, 12 Trichoptera and 10 Coleoptera have not been previously reported from streams in the Aysén region (Oyadenel et al., 2008 or Valdovinos et al., 2010), including a first record for the Neotropics (table S1 Supp. Inf.). However, most of these genera and families have been previously reported somewhat northward (41-43°S) in Argentina (Miserendino & Pizzolon, 2000; Misenrendino & Pizzolon, 2004; Mauad et al., 2015).

Site characterization and habitat varied widely for local, catchment and bioclimatic/regional scale variables (table A3.1). Local riparian forest cover ranged from full canopy cover to none, together with an order of magnitude range in stream width, depth, velocity, and a 20-fold range in local stream slope. Water chemistry also varied widely: average pH was circumneutral yet ranging

almost 2.5 log units, together with a 10-fold range in conductivity and alkalinity, and a 20–100x range in dissolved and total nitrogen and phosphorus. Streams were in general highly aerated, slightly sub-saturated to supersaturated dissolved oxygen indicating potential variation in stream productivity or heterotrophy. Chlorophyll-a concentration was generally very low (<0.5 mg/m^2) but ranged three orders of magnitude, and was associated with a high concentration of carotenoid accessory pigments (mean 0.83 mg/m^2). At the catchment scale, sites varied from having 88% of alpine zone cover to none (only 5 sites), and an average of 66% of forest cover at the catchment scale. Several environmental variables were significantly correlated (Fig. S1 Suppl. Inf.), thus the initial list of 40 variables was reduced to 33 by excluding the highly correlated variables (Pearson's r ≥0.9) for the multivariate and predictive analysis (table A3.1). For example, forest cover was negatively correlated with alpine zone cover (Pearson= -0.96, p<0.0001), a relationship not associated with land use change, but a reflection of natural vegetation breaks (hence a reduction in forest cover equates to an increase in alpine zone, the two usually summing to >95% cover).

The most prominent environmental variables correlated with the community ordination (MDS) were generally similar for taxonomic and functional composition. The MDS ordination axis-1 for taxonomic and FFG composition was strongly correlated with forest/alpine zone cover and current velocity (figure A3.2). Taxonomic composition axis-2 was associated with stream width and temperature, while for the FFG assemblage it was correlated with magnesium and potassium concentrations. For the taxonomic ordination (figure A3.2a), the first and second axis explained 22% and 15% of the variation in the data, respectively. For the FFG composition the first and second axis explained 40% and 17% of the variation in the data, respectively (figure A3.2b).

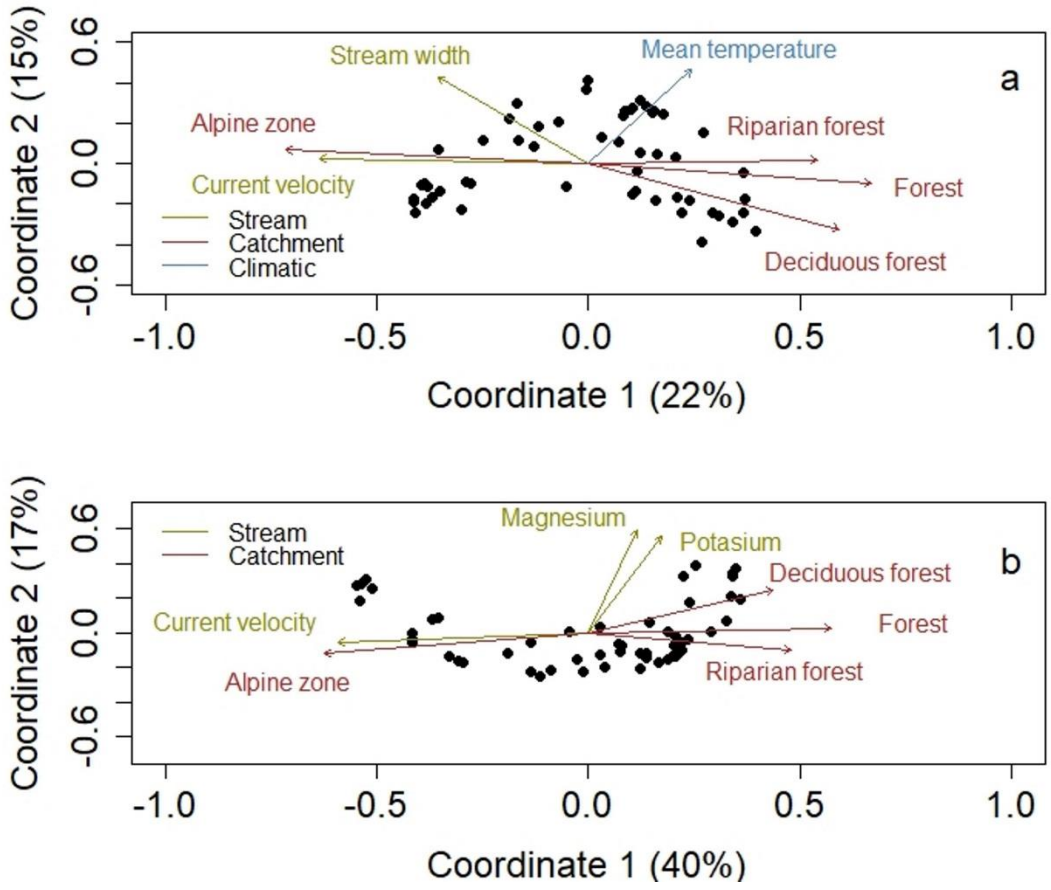

Figure A3.2. *Plot of sites along the first two axes of multidimensional scaling of (a) taxonomic, and (b) functional feeding group assemblages. Catchment scale (bold) and local scale (gray) environmental variables correlated with ordination axes are plotted as arrows. See text and table A3.1 for description of variables.*

The predictive BRT models explained 92% (cv. corr. coeff. = 0.78) and 72% (cv. corr. coeff. = 0.58) of axis-1 and axis-2 from the taxonomic MDS respectively (figures A3.3a-b). BRT models of FFG composition explained 82% (cv. corr. coeff. = 0.77) and 76% (cv. corr. coeff, = 0.60) of axis-1 and axis-2, respectively (figures A3.3c-d), while it explained 81% (cv. Corr. coeff = 0.7) of taxonomic richness (figure A3.3e). The relative contribution of catchment scale variables was highest for taxonomic composition and richness, with catchment forest cover having by far the highest individual relative importance (25% and 50% respectively, figures A3.3a&e). The

strongest contribution of spatial variables was observed for taxonomic richness, latitude being the third most important predictor (figure A3.3e). Local stream variables were somewhat more important for FFG composition (figure A3.3c), with local current velocity the strongest predictor of MDS axis-1 (27%), but closely followed by catchment-scale forest cover (25.5%, figure A3.3c). MDS axis-2 for the taxonomic and FFG composition was predicted by mostly local stream variables (figures A3.3b&d): sodium ion concentration, elevation, magnesium, total phosphorus and pH being the most important predictors of taxonomic composition (figure A3.3b), while chlorophyll-a and carotenoid/Chl pigment ratio had a much higher relative importance for FFGs compared to other predictors (~30% each, figure A3.3d).

Plotting the BRT-predicted thresholds (partial dependency plots, right panels in figures A3.4, A3.5 & 3A.6) against changes in abundance and richness, showed that streams with higher forest cover in their contributing catchments (>60%) had higher abundance of all the main orders (figure A3.4a). The contrary was observed with current velocity: higher current velocities (>0.42m/s) resulted in a general decrease in abundance for all orders (figure A3.4b). Higher concentrations of sodium (>1.4 mg/L) corresponded with a significant increase in abundance for Trichoptera and Diptera, while Ephemeroptera, Plecoptera and Coleoptera showed little change (figures A3.4c&d). Finally, an increase in elevation (>600 and >830 m a.s.l.) was generally marked by a decrease in abundances, although these changes were only significant for Ephemeroptera and Plecoptera (figures A3.4c&d).

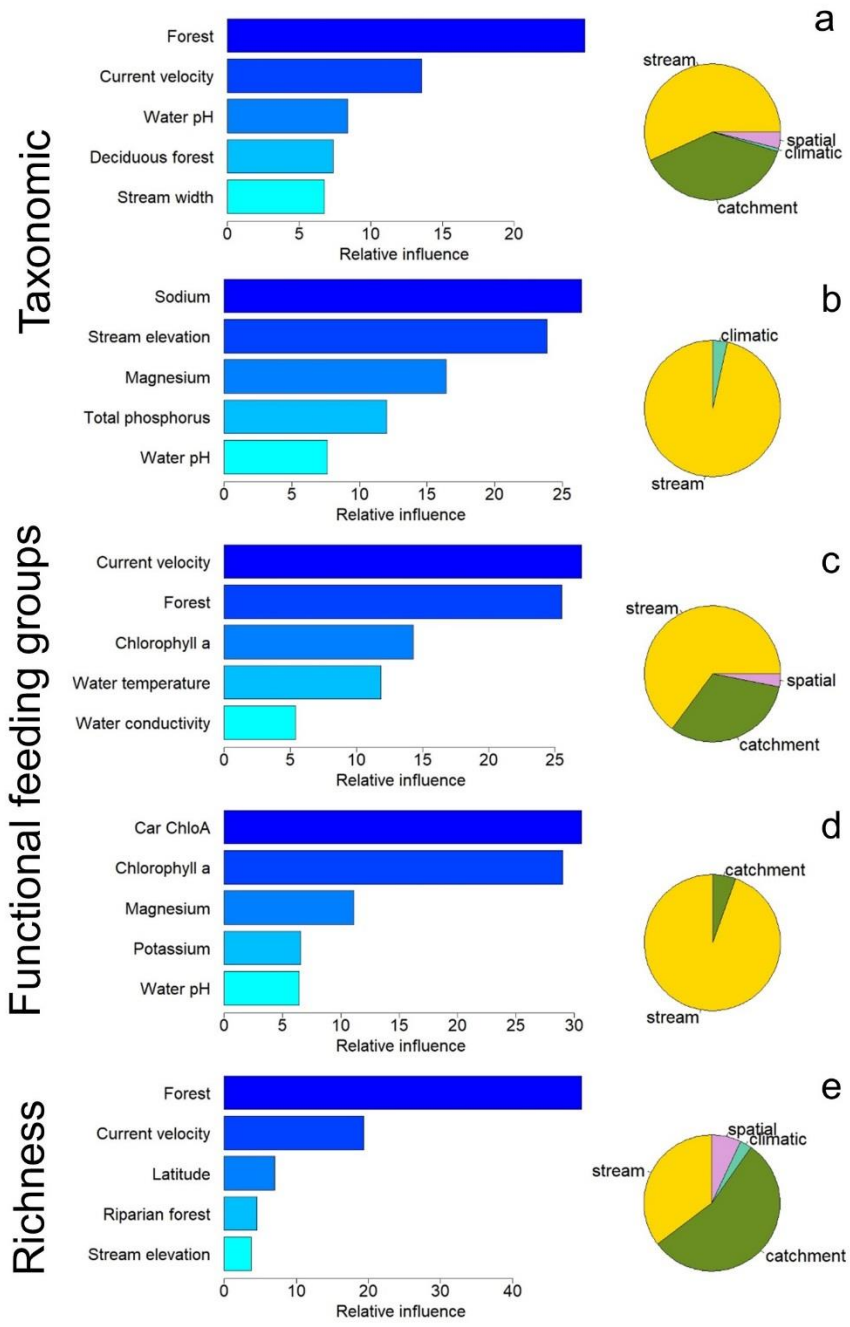

Figure A3.3. *Relative influence of five most important predictor variables for macroinvertebrate taxonomic composition MDS axis-1 (a), and axis-2 (b); FFG composition MDS axis-1 (c) and axis-2 (d); and taxonomic richness (e) in Boosted Regression Tree analysis. The pie chart besides each plot shows the total contribution of each predictor category: stream, catchment, climatic and spatial variables.*

Similar responses were observed for richness, which increased with higher percentage of forest cover in the catchment, and decreased with higher stream current velocities (figures A3.5a&b). The latitudinal threshold (~46°S) coincided with the north-south transition between the Aysén and Baker basins (figure A3.1), with the Baker river basin showing significantly higher richness for most orders (figure A3.5c). FFGs behaved in a similar way, with most groups increasing with higher forest cover, and decreasing with higher current velocity (figures A3.6a&b), although scrapers and predators showed the least change and the effects were non-significant (figure A3.6b). Increases in the Carotenoid/Chlorophyll-a pigment ratio corresponded with a slight decline in abundance, or no change (figure A3.6c). Meanwhile, increased Chlorophyll-a concentrations corresponded with a general increase in abundance of all FFGs, although the effect was significant only for scrapers (figure A3.6d).

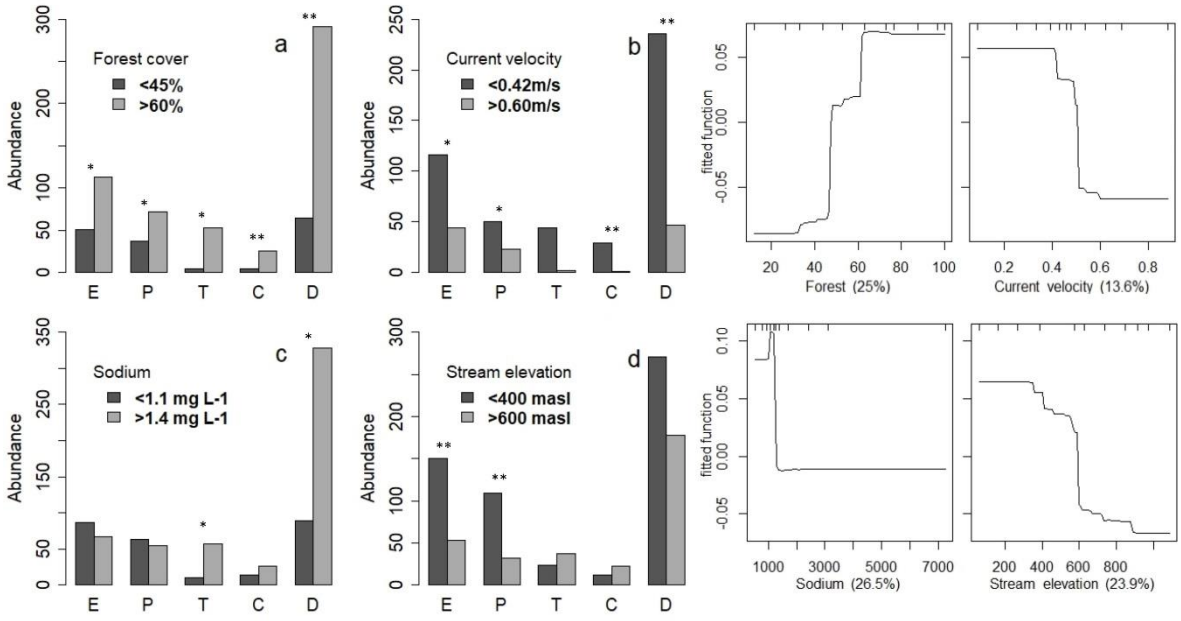

Figure A3.4. *Comparative abundance across main predictor thresholds for main taxonomic orders (a-e). E: Ephemeroptera, P: Plecoptera, T: Trichoptera, C: Coleoptera, D: Diptera. Asterisks indicate significance level: *<0.05, **<0.001 ***<0.0001. On the right side partial dependence plots are shown for the 4 most influential predictors (for axis 1 and 2 of MDS) showing the effect of each predictor (x-axis) variable in taxonomic abundance (y-axis).*

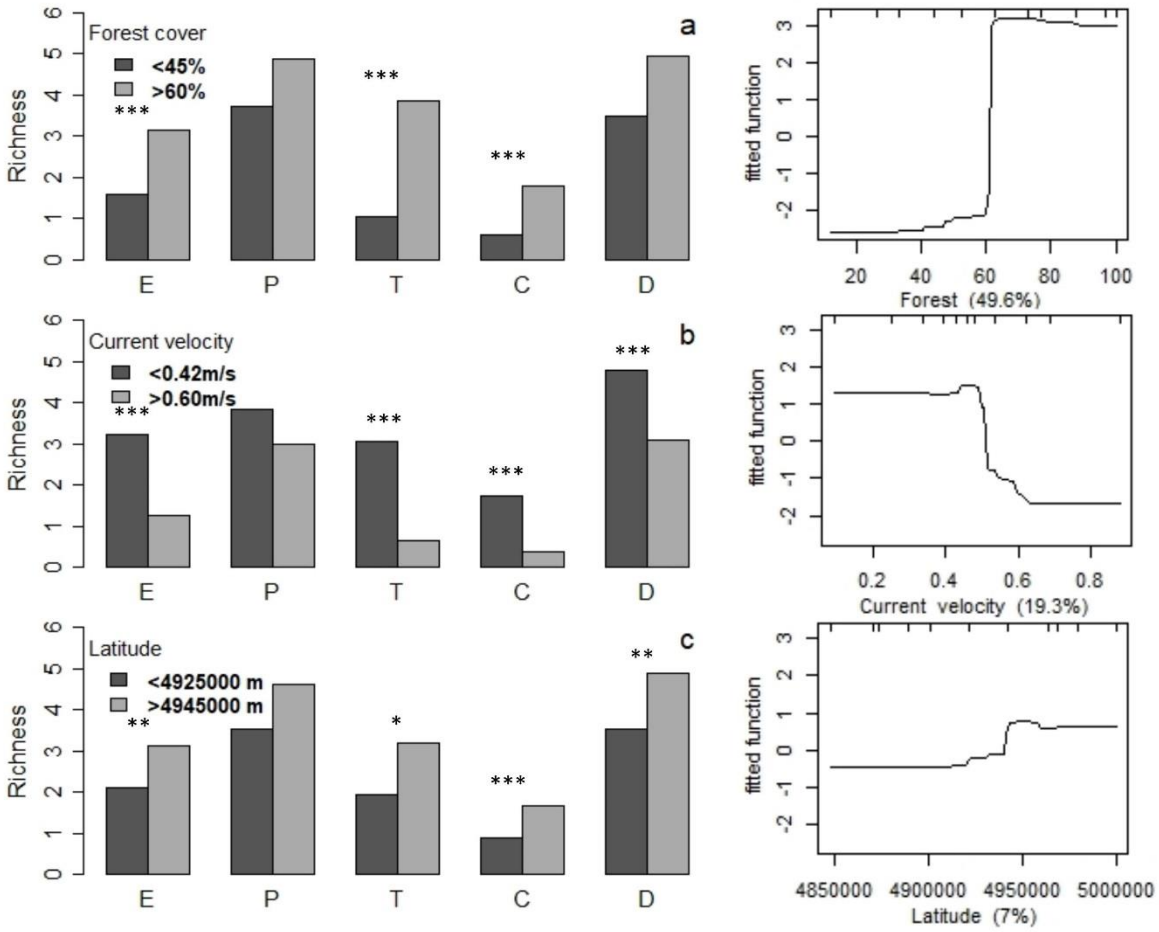

Figure A3.5. *Comparative richness across main predictor thresholds for main taxonomic orders (a-e). E: Ephemeroptera, P: Plecoptera, T: Trichoptera, C: Coleoptera, D: Diptera. Asterisks indicate significance level: *<0.05, **<0.001 ***<0.0001. Partial dependence plots are shown for the 3 most influential predictors of taxonomic richness, showing the effect of each predictor (x-axis) variable in richness (y-axis).*

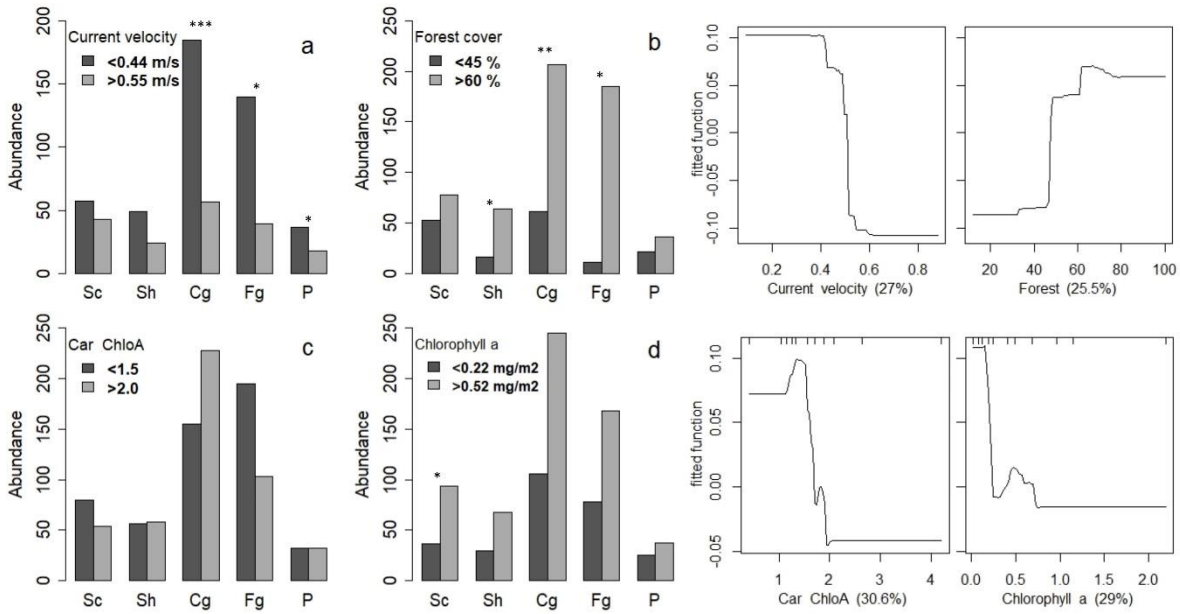

Figure A3.6. *Comparative abundance across main predictor thresholds for FFGs (a-e). Sc: Scrapers, Sh: Shredders, Cg: Collector-gatherers, Fg: Filter gatherers, P: Predators. Asterisks indicate significance level: *<0.05, **<0.001 ***<0.0001. Partial dependence plots are shown for the 4 most influential predictors (for axis 1 and 2 of MDS), showing the effect of each predictor (x-axis) variable in FFG abundance (y-axis).*

A3.4 DISCUSSION

A3.4.1 General composition and traits of stream invertebrates

This is the first study to investigate the ecological characteristics of the wide range of headwater streams in southwestern Patagonia, with simultaneous consideration of taxonomic (richness and composition) and FFGs of stream macroinvertebrates. Collector-gatherers and filter-gatherers were the most numerically abundant feeding traits, corresponding with our expectations for forested reaches, allochthonous energy sources and detritus-based communities. Despite the dominant filter-gatherer trait, they were represented by only two taxa: *Gigantodax* (Diptera: Simuliidae) and *Smicridea* (Trichoptera: Hydropsychidae). Meanwhile, predators were the most diverse feeding group (24 taxa) almost exclusively represented by aquatic insects (23 taxa). High predator diversity is usually associated with productive systems and high periphyton biomass

(Dinh & Death, 2018), making for an unusual result, given the oligotrophic streams studied here with limited visible periphyton biomass (Chlorophyll and dissolved reactive nutrients below the range reported for New Zealand streams; Biggs and Kilroy 2004). Invertebrate predator trait richness has also been associated with unimpaired systems in southern South America (Fierro et al., 2018), a higher proportion of native forest in Argentinean Patagonia (Miserendino & Masi, 2010), or the absence of introduced salmonids in New Zealand (Winterbourne 2004). Barquin and Death 2006 argue that insect predators in New Zealand springbrooks may regulate each other, relieving predation pressure on prey populations and enhancing total invertebrate diversity compared to amphipod dominated springbrooks in the Northern Hemisphere (Barquin and Death 2006). High predator diversity amongst the main insect orders may therefore be a general characteristic of southern South American or temperate southern hemisphere streams, in our case especially within the *Hydrobiosidae* family (Trichoptera). We note that interpretation of FFG results should also be taken with caution: the majority FFG determinations sourced here assign only one category of FFG for each taxa, meanwhile feeding habits may vary by habitat, time of the year, food is availability and life stage (Winterbourne 2004).

A3.4.2 Environmental variables influencing taxonomic richness, composition, and FFG's

The environmental variable most associated with taxonomic and FFG's composition was forest cover at the catchment scale, however the potential mechanisms are probably also related to other variables. The balance of forested vs. alpine zone cover is on one hand indicative of the effect of energy/food resources and/or productivity in our systems. A greater proportion of forest cover in the catchment will translate into higher allochthonous organic inputs, especially in the reaches with greater deciduous forest cover where pulsed detrital input are significant (Anderson & Rosemond, 2010). This is supported by our results showing abundance and richness of all orders increasing

significantly with higher forest cover in the contributing catchment, together with increased shredders, collector-filterers and collector-gatherer FFGs.

The relative contribution of forest vs. alpine cover, being almost inversely proportional across all sites (usually supping to >95% cover), may also be interpreted as a natural disturbance gradient. Higher alpine zone cover in the catchment was linked to harsher local environmental conditions, such as faster current velocity and lower temperatures, in turn influencing FFGs: abundance of collector-gatherers, filter gatherers and predators were significantly lower in streams with catchments with higher current velocity. Dinh & Death (2018) showed that deposit feeders and filter feeders in New Zealand streams decreased with increasing natural flow disturbance, providing support for our findings (note that our study did not include a direct measure of flow disturbance). Their results also showed that the interaction coefficients between traits and periphyton were stronger than for flow disturbance, implying that mechanisms based on food loss may outweigh physical stress to organisms.

Collectively, the main environmental variables related to taxonomic richness, composition and FFGs show a strong separation between coastal evergreen forested catchments and the cordilleran deciduous forested catchments. Since vegetation transitions occur in ways that defy classification (e.g., mixed or transition forest), this "separation" based on forest types is perhaps more realistically a gradient, moreover one that is simultaneous reflected in forest type, climate drivers of forest type, and climate-driven weathering processes in the catchment. Eastern sites in deciduous forest also have lower and more seasonal rainfall, higher evapotranspiration, and higher weathering inputs contributing to major dissolved ions, specific conductivity and pH. Together with an inverse gradient in periphyton biomass, which was higher in the warmer lower-elevation evergreen sites,

autocthonous productivity underlies the regional patterns of macroinvertebrate diversity (MDS axis-2 of both taxonomic and FFG composition).

A3.4.3 A conceptual model of macroinvertebrate functional diversity in the Southern Andes

Perhaps one of the singular characteristics of southern Patagonian Andes catchments is the dominance of a single tree genus *Nothofagus* across a full elevational gradient (0-1200 m), and the transition from evergreen to deciduous species with higher elevation (c. 800 m), something that lacks comparison in the global context. While all our sampled reaches were forested, most of their contributing catchments have at least some alpine zone cover, another defining characteristic of the steep elevational gradients for the main Andes Cordillera and some corresponding coastal regions. Figure A3.7 presents a conceptual model based on local Patagonian geography: based on the generalized southern Patagonian forest-alpine zone gradient, separated by deciduous and evergreen biomes, the general patterns in stream invertebrate functional feeding groups are superimposed, together with the threshold for catchment scale forest cover. Figure A3.7 is intended to represent the forested headwater position within a broader continuum (representing the upper stream continuum *sensu* Vannote et al., 1980), focusing on the zone of catchment-scale influence of the forest/alpine transition. Aside from general expectations of light limitation and productivity along the elevational gradient (the original stream continuum model), additional shifts in macroinvertebrate communities, across coastal vs. cordilleran streams, and as a function of catchment forest cover, are proposed here. Scraper total abundance increased with higher alpine zone cover in evergreen forested catchments, while not as much change was observed for cordilleran deciduous forested catchments. This could be related to the strong light limitation in the lower elevation reaches along the evergreen forested catchments. Meanwhile, the transition from evergreen forests to deciduous forests at higher elevation reaches in the coastal evergreen

streams produced an increase in shredders. Complementary patterns were reported by Contador et al. (2015), were scrapers and predators where the traits least affected by elevation in temperate forested streams in Patagonia. More specifically, figure A3.7 indicates that the FFG composition is dependent both on local forest type and also catchment scale effect of alpine zone/forest cover. This runs contrary to the idea of a generalized stream continuum model, since forest/alpine zone cover was not related to reach elevation or catchment size. Conversely, the catchment scale effect of alpine zone, extending downstream into forested reaches, does in fact suggest consistencies with river continuum concepts, namely: the products of upstream interactions and processes become the reactants for downstream systems.

The complex gradients and responses suggest several lines of reasonable next steps in terms of understanding the diversity of energy/food resources and/or productivity vs. natural disturbance related variables along the elevational gradient (figure A3.7). A complementary longitudinal design (Finn & Poff, 2005; Contador et al. 2015) would have the advantage of reflecting base line conditions and potential future response to land use stress encroaching from lower elevations, and climate change stress operating from higher elevations.

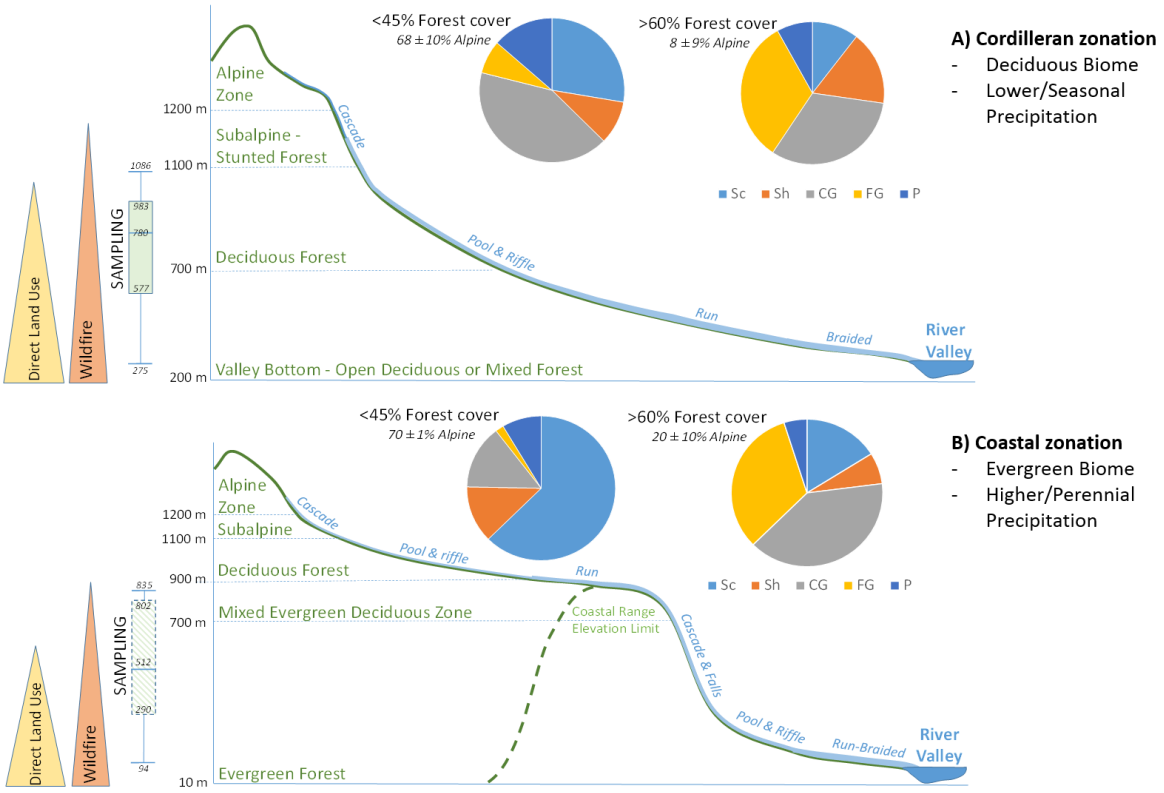

Figure A3.7. *Conceptual model of stream ecosystem zonation and upper continuum for the Subantarctic Ecoregion, for cordilleran and coastal regions. The Y-axis elevational range indicates generalized human impact zones, and range of sampling elevations. Pie charts show generalized relative abundances of FFG at streams (redrawn from figure A3.6; Sc: Scrapers, Sh: Shredders, CG: Collector-gatherers, FG: Filter gatherers, P: Predators) as two general types partitioned by catchment forest cover threshold (<45% and >60%; figure 3.6). Example from deciduous temperate forest (a) represents the main cordilleran central valley, with stream generation in the alpine or deciduous subalpine forest, and transitioning to lower elevation open deciduous forest. Land use impacts (ranching, roads and forest management) are less limited by topography and extend to relatively higher elevations, while historic wildfire impacts may occasionally reach alpine zones. Example from the evergreen temperate forest and coast range (b) reflect typical U-shaped glacial valleys, with stream generation in the alpine or deciduous subalpine forest, and transitioning to evergreen forest. Topographic constraints may limit land use impacts to the lower valleys.*

A3.4.4 Relative contribution of local, catchment and climatic variables for taxonomic vs. FFG

Generally, our results suggest a strong role of the catchment scale variables explaining macroinvertebrate taxonomic and FFG assemblages, however slightly different responses were obtained for these community characterizations, supporting the idea of complementary glimpses

of the overall variability of stream invertebrate communities (Hoeinghaus et al., 2007). Taxonomic richness and composition were predicted by a larger number of variables at different scales, while local stream variables showed an overall stronger role explaining FFG composition (figure A3.3), corresponding to our initial prediction. This was especially true for taxonomic richness, where catchment scale variables had a major contribution (more than 50% of the relative importance), while spatial patterns (latitude) corresponding with a major basin transition (~46°S) was another main predictor. These results for taxonomic structure correspond with Townsend et al. (2003), who showed a major role of catchment scale variables, together with geographic location along the river system accounting for invertebrate assemblages. Heino et al. (2007) also found some support for this; spatial variables were more important for taxonomic than for functional structure, and local environmental factors were more important for functional than taxonomic structure. Nonetheless Heino et al. (2007) support for this was relatively weak and they generally concluded that taxonomic and functional structure were rather similar descriptors of stream macroinvertebrate communities across several ecoregions in Finland, corresponding also to smaller scale studies with similar findings such as Finn and Poff (2005).

A3.4.5 Global change implications for conservation of freshwater ecosystems

To return to one of the principal motivations for this research effort, our study sites represent the intact character of headwaters in the region (Astorga et al., 2018). Catchment forest cover (deciduous and evergreen, regardless of condition) indeed appeared to be among the top two most influential environmental variables associated with stream invertebrate community composition, richness and FFGs. However, total forest cover overshadowed characterization of land use change (e.g., riparian zone cover, or intact forest cover). Meanwhile, other catchment-to-reach scale variables appeared more relevant in terms of patterns in taxonomic or FFGs diversity. Elsewhere,

macroinvertebrate communities and FFGs have shown a stronger response to human land use change, including central Chile and Argentine Patagonia (Fierro et al., 2017; Miserendino & Pizzolon, 2004). The distinct results from the Aysén region may be attributed to the very recent intensive human occupation (at most 100 years), low intensity of land use transformation (e.g., exotic tree plantations are not dominant), meanwhile the impacts of the pre-settlement forest fires were concentrated in the lower valleys (shown conceptually in Fig. A3.7). Most small headwaters in the region are still at near-reference condition in terms of biological integrity, with variations in biological diversity and function being associated with naturally high spatial heterogeneity, and intact longitudinal connectivity (no dams and limited road networks). Under these conditions, temporal asynchrony of populations may be a significant factor in diversity pattern observed here, based on the high heterogeneity of physical conditions across the bioclimatic gradient and sources of rivers (McCluney et al. 2014). As a potential consequence, natural resistance and resilience, two important properties of riverine macrosystems (McCluney et al. 2014), may still be conserved at the large basin scale. This latter inference may be particularly relevant on a global scale, since forested headwater streams in Patagonia are exceptional in terms of minimal anthropogenic atmospheric impacts (Dentener et al., 2006; Perakis & Hedin, 2002) and heretofore limited climate change stressors (Falvey & Garreaud, 2009).

Despite the apparently limited effects of recent land use on headwaters streams (Astorga et al., 2018) and their aquatic communities (this study), increasing encroachment is inevitable and showing little sign of abatement. At the same time, given the importance of the catchment scale variables in determining stream invertebrate communities, climate change may present disproportionate effects on downstream macroinvertebrate communities via changes in higher elevation processes (i.e., stream temperature and diel temperature cycling, snowmelt timing and

intensity, precipitation intensity). Catchments with higher alpine zone cover may be more sensitive to climate change pressures on catchment hydrology, a possibility that would require increased emphasis on elevational gradient studies (e.g., Hauer et al., 2000; Jacobsen, 2003; Contador et al., 2015). Any climate-alpine zone effect would also be expected to be dichotomous across western Patagonia, as implied by the evergreen forested coastal ranges and deciduous forested headwaters (figure A3.7).

A3.5 CONCLUSIONS

Our observations suggest a strong role of the catchment level variables explaining macroinvertebrate taxonomic and FFG assemblages in the mountainous Patagonian region, specifically regarding the forest cover gradient affecting local physical conditions and autotrophic/allotrophic productivity dynamics within catchments. Strong regional precipitation gradients were reflected by readily measurable weathering inputs, as potential proxy for nutrient state or productivity, and observed at the local scale. We highlight the need to further establishing biological and functional diversity patterns along elevational and land-use/global change gradients. This is simultaneously viewed as an opportunity for understanding the near-reference conditions in these extensive headwater streams, despite the added challenges given the strong bioclimatic gradients, diverse geomorphology, and distinct forest transitions.

A3.6 ACKNOWLEDGEMENTS

We acknowledge Sara Montiel and Omar Mansilla for their assistance in collection of data in the field. Britney Clark for assistance in the field and laboratory with macroinvertebrate sorting. This research was funded by FONDECYT 11140495, Laboratorio Ecoclimatico Conicyt (R17A10002) and PATSER (R-20F0002).

A3.7 REFERENCES

Abell, R., Allan, J., & Lehner, B. (2007). Unlocking the potential of protected areas for freshwaters. *Biological Conservation*, 34, 48-63.

Allan, J.D., Erickson, D.L., & Fray, J. (1997). The influence of catchment land use on stream integrity across multiple spatial scales. *Freshwater Biology*, 37, 149-162.

Allan, J.D. (2004). Landscapes and Riverscapes: The influence of land use on stream ecosystems. *Annual Review of Ecology Evolution and Systematics*, 35(1), 257-84. https://doi.org/10.1146/annurev.ecolsys.35.120202.110122

Anderson, C., & Rosemond, A. (2007). Ecosystem engineering by invasive exotic beavers reduces in-stream diversity and enhances ecosystem function in Cape Horn, Chile. *Oecologia*, 154, 141-153.

Anderson, C., Lencinas, M., Wallem, P., Valenzuela, A., Simanonock, M., &Pastur, G. (2014). Engineering by an invasive species alters landscape-level ecosystem function, but does not affect biodiversity infreshwater systems. *Diversity Distributions*, 20, 214-222.

Anderson, C., & Rosemond, A. (2010). Beaver invasion alters terrestrial subsidies to subantarctic stream food webs. *Hydrobiologia*, 652, 349-361.

APHA (2005). Standard methods for the examination of water and wastewater, 21st ed. American Public Health Association, Washington DC.

Armesto, J., Rozzi, R., Smith-Ramirez, C., &Arroyo, M.T.K. (1998). Effective conservation targets in South American temperate forests. *Science*, 282, 1271-1272. https://doi.org/10.1126/science.282.5392.1271

Astorga, A., Moreno, P., & Reid, B. (2018). Watersheds and trees fall together: An analysis of intact forested watersheds in southern Patagonia (41–56 S). *Forests*, 9, 385. https://doi.org/10.3390/f9070385

Astorga, A., Death, R.G., Death, F., Paavola, R., Chakraborty, M., & Muotka, T. (2014). Habitat heterogeneity drives the geographical distribution of beta diversity: the case of New Zealand stream invertebrates. *Ecology and Evolution*, 4(13), 2693–2702.

Barquín, J. & Death, R.G. (2006). Spatial patterns of macroinvertebrate diversity in New Zealand springbrooks and rhithral streams. *Journal of the North American Benthological Society*, 25 (4), 768–786.

Biggs, B.J.F. &Kilroy, C. (2000). Stream periphyton monitoring manual. New Zealand Institute Water and Atmosphere for Ministry for the Environment, Christchurch, New Zealand.

Biggs, B.J.F., & Kilroy, C. (2004) Periphyton. Chapter 15. In: Freshwaters of New Zealand (Eds: Harding, J.S., Mosley, M.P., Peason, C.P., Sorrell, B.K.). New Zealand Hydrological Society Inc. and New Zealand Limnological Society Inc., Christchurch, New Zealand.

Borkent, A., & Rotheray, G. (2010) Larvae. Chapter 7. In: Manual of Central American Diptera Vol. 2. (Eds: Brown, B.V., Borkent, A., Cumming, J.M. Wood, D.M., Woodley, N.E. &Zumbado, M.A.). NRC Research Press, Ottawa.

Brand, C., & Miserendino, M.L. (2015). Testing the performance of macroinvertebrate metrics as indicators of changes in biodiversity after pasture conversion in Patagonian mountain streams. *Water Air Soil Pollution*, 226, 370.

Brundin, L. (1966). Transantartic relationships and their significance, as evidenced by chironomid midges. With a monograph of the subfamilies Podonominae and Aphroteniinae and the austral Heptagyiae. *Kongliga Svenska Vetenskaps Academiens Handlingar* 11, 1–472.

Clarke, A. (2017). Principles of thermal ecology: Temperature, energy, and life. Oxford University Press.

CONAF (2011). Catastro de los recursos vegetacionales nativos de Chile. Monitoreo de cambios y actualizaciones. Periodo 1997–2011; Ministerio de Agricultura: Santiago, Chile.

Contador, T.A., Kennedy, J.H., & Rozzi, R. (2012). The conservation status of South American aquatic insects in the literature. *Biodiversty Conservation*, 21, 2095–2107. https://doi.org/10.1007/s10531-012-0299-x

Contador, T.A., Kennedy, J.H., Rozzi, R., &Ojeda Villarroel, J. (2015) Sharp altitudinal gradients in Magellanic Sub-Antarctic streams: patterns along a fluvial system in the Cape Horn Biosphere Reserve (55S). *Polar Biology*, 38(11), 429–437. https://doi.org/10.1007/s00300-015-1746-4

Coscarón, S. & Coscarón Arias, C. (2007). Neotropical Simuliidae (Diptera: Insecta). In: Aquatic Biodiversity of Latin America (ABLA Series), Volume 3. Pensoft Publishers, Sofia-Moscow.

Courtney, G.W. & Merritt, R.W. (2008) Aquatic Diptera. Part one. Larvae of aquatic Diptera. Chapter 22. In: An introduction to the aquatic insects of North America, 4th edition. (Eds: R.W. Merritt, K.W. Cummins & M.B. Berg). Kendall / Hunt Publishing Company, Iowa, USA.

Cranston, P.S. & Edward, D.H.D. (1992). A systematic reappraisal of the Australian Aphroteniinae (Diptera: Chironomidae) with dating from vicariance biogeography. *Systematic Entomology*, 17, 41–54.

Death, R. G., &Joy, M. K. (2004). Invertebrate community structure in streams of the Manawatu-Wanganui region, New Zealand: the roles of catchment versus reach scale influences. *Freshwater Biology*, 49, 982–997.

Dentener, F., Drevet, J., Lamarque, J.F., Bey, I., Eickhout, B., Fiore, A.M.,...Wild, O. (2006). Nitrogen and sulfur deposition on regional and global scales: A multimodel evaluation. *Global Biogeochemical Cycles*, 20 (4).

Dinh, Y.T.H., & Death, R.G. (2018). Do disturbance and periphyton productivity affect stream invertebrate traits? *Freshwater Science*, 37 (2). https://doi.org/10.1086/697924

Dodds, W. K., Gido, K., Whiles, M.R., Daniels, M.D., & Grudzinski, B.P.(2015). The Stream Biome Gradient Concept: factors controlling lotic systems across broad biogeographic scales. *Freshwater Science*, 34, 1-19.

Domínguez, E., & Fernández, H. (Eds.). (2009). Macroinvertebrados bentónicos Sudamericanos: Sistemática y biología. Primera Edición. Fundación Miguel Lillo. San Miguel de Tucumán, Argentina.

Dudgeon, D., Arthington, A., Gessner, M., Kawabata, Z-I., Knowler, D., Leveque, C., Naiman, R., Prieur-Richard, A-H., Soto, D., Stiassny, M., y Sullivan, C. (2006). Freshwater biodiversity: importance, threats, status and conservation challenges. *Biological Reviews*, 81, 163-182.

Edwards, F.W. (1929) Fascicle II.–Blephariceridae. In: Diptera of Patagonia and south Chile, Part 2. (Ed: F.W. Edwards). British Museum (Natural History), London.

Elgueta, M., & Arriagada, G. (1989). Estado actual del conocimiento de los coleopteros de Chile (Insecta: Coleoptera). *Revista Chilena de Entomologia*, 17, 5-60.

Elith, J.,Leathwick, J. R., &Hastie, T. (2008) A working guide to boosted regression trees. *Journal of Animal Ecology*, 77, 802–813. https://doi.org/10.1111/j.1365-2656.2008.01390.x

ESRI 2011. Arc Hydro Tools Overview; ESRI Water Resources Team, Environmental Systems Research Institute: Redlands, CA, USA.

Everitt, B., & Hothorn, T. (2011). An introduction to applied multivariate analysis with R. Springer-Verlag New York. https://doi.org/10.1007/978-1-4419-9650-3

Falvey, M., & Garreaud, R.D. (2009). Regional cooling in a warming world: Recent temperature trends in the southeast pacific and along the west coast of subtropical South America (1979–2006). *Journal of Geophysical Research: Atmospheres*, 114, D04102. https://doi.org/10.1029/2008JD010519

Fick, S.E. & Hijmans, R.J. (2017). WorldClim 2: New 1-km spatial resolution climate surfaces for global land areas. *International Journal of Climatology*. https://doi.org/10.1002/joc.5086

Fierro, P., Bertrána, C., Tapia, J., Hauenstein, E., Peña-Cortés, F.,Vergara, C., Cerna, C., Vargas-Chacoff, L. (2017). Effects of local land-use on riparian vegetation, water quality, and the functional organization of macroinvertebrate assemblages. *Science of the Total Environment*, 609, 724–734.

Fierro, P., Arismendi, I., Hughes, R. M., Valdovinos, C., &Jara-Flores, A. (2018). A benthic macroinvertebrate multimetric index for Chilean Mediterranean streams. *Ecological indicators*, 91, 13-23.

Finn, D. S. and Poff, N. L. (2005). Variability and convergence in benthic communities along the longitudinal gradients of four physically similar Rocky Mountain streams. *Freshwater Biology*, 50: 243–261.

Frissell, C.A., Liss, W.J., Warren, C.E., & Hurley, M.D. (1986).A hierarchical framework for stream habitat classification: Viewing streams in a watershed context. *Environmental Management* 10(2), 199-214. https://doi.org/10.1007/BF01867358

Gansfort, B., & Traunspurger, W. (2019). Environmental factors and river network position allow prediction of benthic community assemblies: A model of nematode metacommunities. *Scientific Reports*, 9, 14716.

Hauer, F.R., Stanford, J.A., Giersch, J., & Lowe, W.H. (2000) Distribution and abundance patterns of macroinvertebrates in a mountain stream: an analysis along multiple environmental gradients. *Verh. Internat.Verein. Limnol*., 27, 1485-1488.

Hauer, F.R. & Lamberti, G. (2016). Methods in Stream Ecology, Second Edition, Academic Press.

Heino, J., Mykrä, H., Kotanen, J., Muota, T. (2007). Ecological filters and variability in stream macroinvertebrate communities: do taxonomic and functional structure follow the same path? *Ecography*, 30: 217–230.

Hoeinghaus, D. J., Winemiller, K. O., & Birnbaum, J.S. (2007). Local and regional determinants of stream fish assemblage structure: inferences based on taxonomic vs. functional groups. *Journal of Biogeography*, 34: 324–338.

Hynes, H. B. N. (1970). The ecology of running waters. University of Toronto Press.

Jakobsen, D. (2003). Altitudinal changes in diversity of macroinvertebrates from small streams in the Ecuadorian Andes. *Archiv für Hydrobiologie*, 158(2), 145–167.

James, G., Witten, D., Hastie, T., & Tibshirani, R. (2013). Tree-Based Methods. In: An Introduction to Statistical Learning. Springer, New York, NY. https://doi.org/10.1007/978-1-4614-7138-7_8

Jarvis, A., Reuter, H.I., Nelson, A., & Guevara, E. (2017) Hole-Filled Srtm for the Globe Version 4 Available from the CGIAR-CSI SRTM 90m Database. Available online: http://srtm.csi.cgiar.org (accessed on 16 October 2018).

Johnson, L.B.,&Gage, S.H.(1997). Landscape approaches to the analysis of aquatic ecosystems. *Freshwater Biology*, 37, 113–132.

Johnson, R. K. et al. (2004). Spatial scale and ecological relationships between the macroinvertebrate communities of stony habitats of streams and lakes. *Freshwater Biology*, 49: 1179–1194.

Kärnä, O-M., Heino, J., Laamanen, T., Jyrkankallio-Mikkola, J., Pajunen, V., Soininen, J., ...Hjort, J. (2019) Does catchment geodiversity foster stream biodiversity? *Landscape Ecology*, 34, 2469–2485.

Lake, S. (2000). Disturbance, Patchiness, and Diversity in Streams. *Journal of the North American Benthological Society*, 19(4), x-x. https://doi.org/10.2307/146818

Llanos, L., González, C.R., & Saldarriaga-Córdoba, M. (2015) Revision of the new world species of the genus *Pelecorhynchus* Macquart, 1850 (diptera: pelecorhynchidae). *Zootaxa*, 3955 (2), 188–210.

LeCraw, R. & Mackereth, R. (2010). Sources of small-scale variation in the invertebrate communities of headwater streams. *Freshwater Biology*, 55, 1219-1233.

Lowe, W.H., & Likens, G.E. (2005) Moving headwater streams to the head of the class. *BioScience* 55, 196–197.

Mackerras, I.M. & Fuller, M.E. (1942) Thegenus *Pelecorhynchus* (Diptera: Tabanoidea). *Proceedings of the Linnean Society of New South Wales*, 67, 9–77.

Madriz, R.I., & Courtney, G.W. (2016). The Neotropical Tanyderid*Araucoderusgloriosus* (Alexander) (Diptera, Tanyderidae), with description of the egg, larva and pupa, redescription of adults, and notes on natural history. *Zootaxa*, 4158, 325–351.

Mauad, M., Miserendino, M.L., Risso, M.A., & Massaferro, J. (2015). Assessing the performance of macroinvertebrate metrics in the Challhuaco-Ñireco System (Northern Patagonia, Argentina). *Iheringia Série Zoologia*, 105(3). DOI: https://doi.org/10.1590/167847662015105334858

McCluney, K.E., Poff, L.R.N., Palmer, M.A., Thorp, J.H., Poole, G.C., Williams, B.S., Williams, M.R. & Baron, J.S. (2014). Riverine macrosystems ecology: sensitivity, resistance and resilience of whole river basins with human alterations. *Frontiers in Ecology and the Environment*, 12 (1), 48-58. https://doi.org/10.1890/120367

Miserendino, M.L., & Pizzolon, L.A. (2004). Interactive effects of basin features and land-use change on macroinvertebrate communities of headwater streams in the Patagonian Andes. *River Research and Applications*, 20 (3), 967-983. https://doi.org/10.1002/rra.798

Miserendino, M.L., & Pizzolon, L.A. (2000). Macroinvertebrates of a fluvial system in Patagonia: altitudinal zonation and functional structure. *Archiv für Hydrobiologie*, 150, 55-83.

Miserendino, M.L. & Masi, C.I. (2010). The effects of land use on environmental features and functional organization of macroinvertebrate communities in Patagonian low order streams. *Ecological Indicators*, 10, 311-319.

Miserendino, M.L., Brand, C., Epele, L.B., Di Prinzio, C.Y., Omad, G.H., Archangelsky, M., …Kutschker, A.M. (2018). Biotic diversity of benthic macroinvertebrates at contrasting glacier-fed systems in Patagonia Mountains: The role of environmental heterogeneity facing global warming. *Science of the Total Environment*, 622-623, 152-163.

Oksanen, J., Blanchet, F.G., Friendly, M., Kindt, R., Legendre, P., McGlinn, D., …Wagner, H. (2016). vegan: Community Ecology Package. R package version 2.4-1. URL: https://CRAN.R-project.org/package=vegan.

Oyanedel, A., Valdovinos, C., Azocar, M., Moya, C., Mancilla, G., Pedreros, P., & Figueroa, R. (2008). Patrones de distribución espacial de los macroinvertebrados bentónicos de la cuenca del río Aysén (Patagonia chilena). *Gayana*, 72, 241-257.

Perakis, S. & Hedin, L.O. (2002). Nitrogen loss from unpolluted South American forests mainly via dissolved organic compounds. *Nature*, 415, 416-419.

Poff, N. L. (1997). Landscape filters and species traits: towards mechanistic understanding and prediction in stream ecology. *Journal of the North American Benthological Society*, 16, 391-409.

Quinn, J.M. & Hickey, C.W. (1990). Magnitude of effects of substrate particle size, recent flooding, and catchment development on benthic invertebrates in 88 New Zealand rivers. *New Zealand Journal of Marine and Freshwater Research*, 24 (3), 411-427. https://doi.org/10.1080/00288330.1990.9516433

Rojas, F. (2006). Current state of knowledge of Trichoptera of Chile. *Gayana*, 70(1), 65-71.

Rozzi R., Armesto, J.J., Gutiérrez, J., Anderson, C.B., Massardo, F., Likens, G., …Kalin M.T. (2012). Integrating ecology and environmental ethics: earth stewardship in the southern end of the Americas. *Bioscience*, 628, 1226–1236. https://doi.org/10.1525/bio.2012.62.3.4

Sandin, L. & Johnson, R.K. (2004). Local, landscape and regional factors structuring benthic macroinvertebrate assemblages in Swedish streams. *Landscape Ecology*, 19, 501–514.

Soininen, J. (2015). Are catchment properties useful proxies for freshwater biodiversity? In: Advances in environmental research, vol 38. (Ed: Daniels, J.A.). Nova Science Publishers, New York.

Rendoll Cárcamo, J., Contador, T., Gañan, M., Pérez Troncoso, C., Maldonado Márquez, A., Convey, P., …Rozzi, R. (2019). Altitudinal gradients in Magellanic sub-Antartic lagoons: the effect of elevation on freshwater macroinvertebrate diversity and distribution. *PeerJ*,7, e7128.

Ridgeway, G. (2013). gbm: Generalized Boosted Regression Models. R Package Version 2.1. https://cran.r-project.org/web/packages/gbm/gbm.pdf

Stark, B.P., Froehlich, C.G., & Zúñiga, M.C. (2009). South American Stoneflies (Plecoptera).Pensoft, Sofia-Moscow.

Strickland, J.D.H., & Parsons, T.R., (1968). A practical handbook of seawater analysis. Bulletin 167. Fisheries Research Board of Canada, Ottawa. Bulletin 167, 1968.

Teskey, H.J. (1970). The immature stages and phyletic position of *Glutopsrossi* (Diptera: Pelecorhynchidae). *Canadian Entomologist*, 102, 1130–1135.

Thorp, J.H. (2019). Keys to Neotropical Hexapoda. In: Thorp and Covich's Freshwater Invertebrates, Volume Three, Fourth Edition. (Eds: Hamada, N., Thorp, J.H., & Rogers, C.) Elsevier Inc. https://doi.org/10.1016/C2015-0-01626-4

Tolonen, K.E., Leinonen, K., Marttila, H., Erkinaro, J., & Heino, J. (2017). Environmental predictability of taxonomic and functional community composition in high-latitude streams. *Freshwater Biology*, 6 (1), 1-16. https://doi.org/10.1111/fwb.12832

Townsend, C. R. et al. (2003). The influence of scale and geography on relationships between stream community composition and landscape variables: description and prediction. *Freshwater Biology*, 48: 768-785.

Valdovinos, C., Kiessling, A., Mardones, M., Moya, C., Oyanedel, A, Salvo, J.,… Parra, O. (2010). Distribución de macroinvertebrados (Plecoptera y Aeglidae) en ecosistemas fluviales de la Patagonia chilena: ¿Muestran señales biológicas de la evolución geomorfológica post glacial? *Revista Chilena de Historia Natural* 83, 267-287. https://doi.org/10.4067/S0716-078X2010000200008

Vannote R.L., Minshall G., Cummins K.W., Sedell J.R. & Cushing C.E. (1980). The river continuum concept. *Canadian Journal of Fisheries and Aquatic Sciences*, 37, 130–137.

Winterbourn, M. (2004) Stream communities and ecosystem processes. Chapter 13. In: Freshwaters of New Zealand (Eds: Harding, J.S., Mosley, M.P., Peason, C.P., Sorrell,

B.K.). New Zealand Hydrological Society Inc. and New Zealand Limnological Society Inc., Christchurch, New Zealand.
Wolman, M.G. (1954). A method of sampling coarse river-bed material. Eos, Transactions American Geophysical Union, 35 (6), 951-956. https://doi.org/10.1029/TR035i006p00951
Woodley, N. E. (2007). Notes on South American *Dasyomma*, with the description of a remarkable new species from Chile (Diptera: Athericidae). *Zootaxa*, 1443, 29-35. DOI: https://doi.org/10.11646/zootaxa.1443.1.3
Xu, F., S. Harvolk-Schöning, P. J. Horchler, K. Ludewig, & Otte. A. (2019). Factors determining the distribution pattern of floodplain vegetation remnants along the Danube River between Straubing and Vilshofen. *Tuexenia*, 39, 75-100.

SUPPORTING INFORMATION
Additional supporting information may be found online at:

https://onlinelibrary.wiley.com/doi/full/10.1111/fwb.13853

Appendix 4: Assessing forest degradation using multivariate and machine learning methods in the Patagonian temperate rainforest

Alex Fajardo, Juan C. Llancabure and Paulo C. Moreno

Ecological Applications, 32(2), 2022, e02495, doi: 10.1002/eap.2495

Abstract

The process of forest degradation, along with deforestation, is the second greatest producer of global greenhouse gas emissions. A key challenge that remains unresolved is how to quantify the critical threshold that distinguishes a degraded from a non-degraded forest. We determined the critical threshold of forest degradation in mature stands belonging to the temperate evergreen rainforest of southern Chile by quantifying key forest stand factors characterizing the forest degradation status. Forest degradation in this area is mainly caused by high grading, harvesting of fuelwood, and sub-canopy grazing by livestock. We established 160 500-m^2 plots in forest stands that represented varied degrees of alteration (from pristine conditions to obvious forest degradation), and measured several variables related to the structure and composition of the forest stands, including exotic and native species richness, soil nutrient levels, and other landscape-scale variables. In order to identify a classes of forest degradation, we applied multivariate and machine learning analyses. We found that richness of exotic species (including invasive species) with a diameter at breast height (DBH) < 10 cm and tree density (N, DBH > 10 cm) were the two composition and structural variables that best explained the forest degradation status, e.g., forest stands with 5 or more exotic species were consistently found more associated with degraded forest and stands with N < 200 trees ha^{-1} represented degraded forests, while N > 1000 trees ha^{-1} represent pristine forests. We introduced an analytical methodology, mainly based on machine learning, that successfully identified the forest degradation status that can be replicated in other

scenarios. In conclusion, here by providing an extensive dataset quantifying forest and site attributes, the results of this study are undoubtedly useful for managers and decision-makers in classifying and mapping forests suffering various degrees of degradation.

Keywords: boosting regression trees; Chile; forest structure; non-metric multidimensional scaling; soil nutrients; species richness.

A4.1 INTRODUCTION

Natural disturbances occurring at various spatial and temporal scales (e.g., fires, landslides, wind) commonly knock down the forest structure and significantly alter the composition, function and development of the forest, rendering completely different plant communities (Pickett & White, 1985). And although forests are able to recover their pre-disturbance states, in some cases, where the frequency or intensity of disturbances are too high, or disturbances are too novel, the forest system may not be able to recover and alternate stable states (different trajectories) appear as the most likely outcomes through, for example, the establishment of a different cover type (Scheffer, 2009), which ultimately increases the vulnerability of the forest to degradation (J. Ghazoul et al., 2015; Seidl et al., 2016). Several attempts to define forest degradation have been proposed (e.g. FAO, 2002, 2011), but we concur with the recent definition offered by Ghazoul et al.' (2015), as a "human-induced loss of resilience which prevents natural recovery to the pre-disturbance state". It is worth mentioning that when a forest is degraded not only are forest carbon stocks and CO_2–absorption (i.e., mitigation of climate change) diminished, but the process of forest degradation also contributes significantly to the devalue of ecosystem services: e.g., increase of greenhouse gas emissions, which places plant and animal diversity at risk, decrease in the provision of productive goods like timber, non-woody forest products and other commodities (Pearson et al., 2017; Thompson et al., 2013). The process of forest degradation can perfectly flip forests from

carbon sinks to sources, i.e., the carbon released to the atmosphere by, for example, burning outweighs the carbon taken from the atmosphere as trees grow. In addition, these changes in forest structure and composition ultimately may alter soil properties and processes (Hudson & Alcántara-Ayala, 2006), and may deplete water sources, all of which can result in a reduction of forest ecosystem functioning as a whole (Chazdon, 2008) or end in an ecosystem collapse (Bergstrom et al., 2021). In fact, the process of forest degradation, along with deforestation, is the second greatest producer of greenhouse gas emissions, just behind the burning of fossil fuels (van der Werf et al., 2009). And yet, in practice, forest degradation has been difficult to quantify, mainly because forest resilience and ecological thresholds must be quantitatively determined (Hirota et al., 2011; Scheffer, 2009). It is easy to affirm that a forest is degraded when its structure, composition and function have unequivocally surpassed a critical threshold (Chazdon, 2008; Vásquez-Grandón et al., 2018), but quantitatively defining that threshold is more difficult. Although challenging, identifying a specific forest type degradation represents an important management tool that is urgently needed to halt forest degradation and improve forest recovery.

The principal human-induced factors of degradation are forest conversion to agriculture and other uses, fires, high grading logging, the introduction of livestock, and the spread of invasive species and pests, among others (e.g., Asner et al., 2008; Vásquez-Grandón et al., 2018; Zamorano-Elgueta et al., 2012). Some of these actions may emulate short-scale natural disturbances and therefore have little spatial and temporal impact on forest functioning, whereas others, like the use of fire to clear land for livestock or agriculture will inevitably modify functions and processes leading to alternate stable states or even to ecosystem collapsing (Bergstrom et al., 2021), thus making the recovery of the forest to its initial stable state unlikely. The identification of degraded forests needs to be a quantifiable measure less subject to qualitative ambiguities and idiosyncrasies. This is important since not all areas classified as forests are necessarily healthy or effective carbon

sinks. Thus, identifying when a forest is degraded is not only important in ecological terms or to increase our capacity to predict the main drivers responsible for ecosystem structure and functioning (Schwinning et al., 2004), but it is also important for forest management and legislation purposes. There is, for example, a clear difference between subsidizing the recovery or restoration of a forest and subsidizing the land for agricultural objectives. The proper identification of a degraded forest represents the starting point to the posterior application of silvicultural techniques intended to restore forest functioning (Vásquez-Grandón et al., 2018). Given that forest degradation is related not only to the loss of resilience, but to the loss of forest properties, functioning and processes, when attempting to quantify forest degradation we need to use a holistic approach that contains both as many variables as possible and also the use of multiple analytical tools.

In this study, we identified forest degradation in mature stands belonging to the temperate evergreen rainforest of southern Chile by the quantification of one or several key factors that characterize the critical transition between forest states link to both a resilient, non-degraded forest and a degraded forest. To achieve our main objective, we used a data analysis approach that combines multivariate and machine learning methods. First, by using a non-metric multidimensional scaling (NMDS) method, we aimed to discover general relationships among the several variables involved in forest degradation that would help us attain a preliminary understanding about the main drivers responsible for the degradation process of the temperate evergreen rainforest under study. Although the use of an NMDS, as an unsupervised (i.e., it allows us to learn the inherent structure of our data) method (Everitt & Hothorn, 2011), is very useful for exploratory analysis, in order to predict forest degradation it was necessary to further fit a statistical model able to incorporate several data types along with their singularities, such as nonlinearities and interactions. Thus, we decided to use machine learning (ML) techniques, in particular boosting

regression trees (BRT), that have proved to be an excellent supervised approach for ecological process predictions (e.g., Elith et al., 2008; G. James et al., 2013). The BRT is a method that combines regression trees (i.e., models that relate a response variable to their predictors by recursive binary splits) and boosting (an adaptive method for combining many simple models to provide an improved predictive performance); it helped us to identify the best predictors of forest degradation through the combination of several simple models (Elith et al., 2008; G. James et al., 2013). By following a threshold-based concept for forest degradation along with using a multivariate and machine learning combined methodology, our ultimate aim was to provide a framework that will allow forest managers and stakeholders to distinguish degraded from non-degraded forests based on a holistic perspective that is overall easy to implement, repeatable, cost-effective and of ecologically significance. We used this data analysis approach to identify the threshold of forest degradation in the temperate evergreen rainforest of the Aysén Region, southern Chile. As most temperate rainforests worldwide, this evergreen forest is complex in structure and diverse in composition, with multiple layers that can hold a great amount of biomass and species (including many epiphytes). The temperate evergreen rainforest of the Aysén Region is mainly degraded through either unsustainable (and illegal) selective logging, high grading, harvesting of fuelwood, or sub canopy grazing by livestock, or all of the above (Bahamondez & Thompson, 2016; Zamorano-Elgueta et al., 2012) (fig. A4.1). The relative importance of these drivers in the degree of forest degradation is completely unknown, thus the identification and particularly the magnitude of these drivers of forest degradation is imperative.

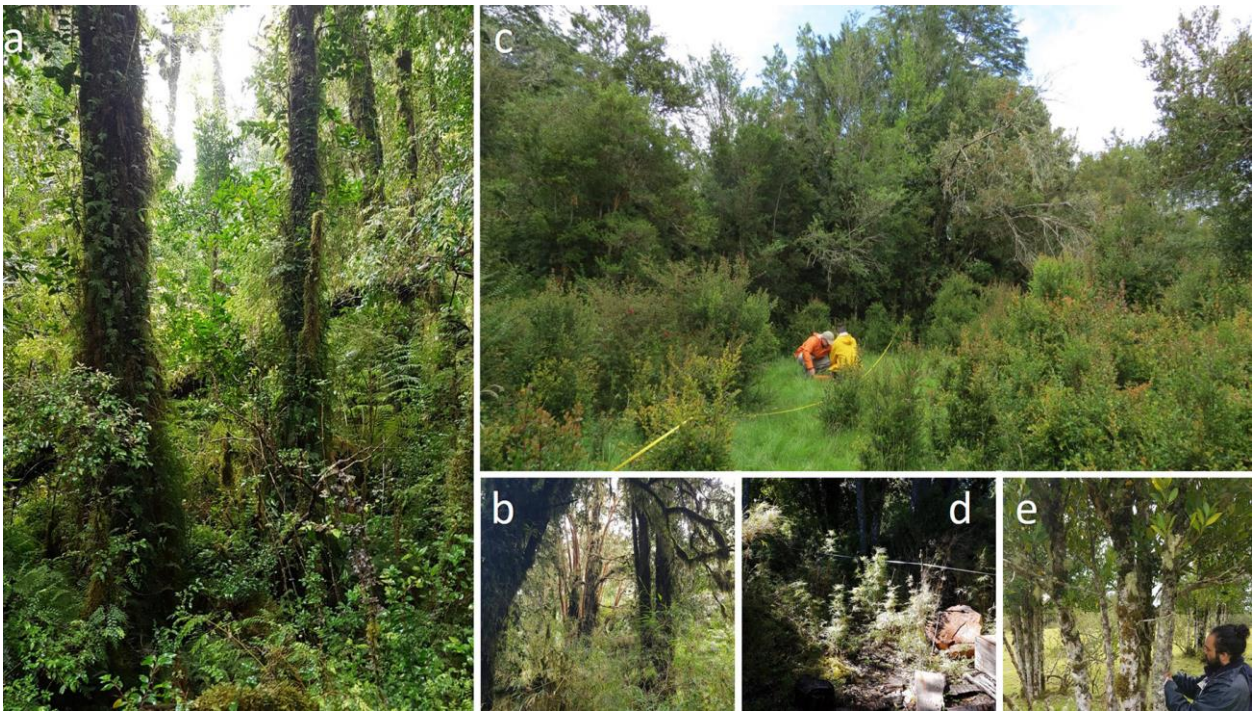

Figure A4.1. *The temperate evergreen rainforest of southern Chile is a multi-layered forest with a dense understory that includes the presence of bamboos (*Chusquea spp.*), ferns and a) many vascular epiphyte species. Dominant tree species are primarily evergreen angiosperms (e.g.,* Drimys winteri, Winteraceae, Laureliopsis philippiana, Atherospermataceae, Nothofagus nitida, Nothofagaceae, Weinmannia trichosperma, Cunoniaceae*) and conifers (e.g.,* Podocarpus nubigenus, Podocarpaceae*); b) Myrtacea species such as* Luma apiculata *(reddish stem) are also common. The temperate evergreen rainforest of southern Chile is mainly degraded through either c) sub-canopy grazing by livestock that keeps vegetation short, d) unsustainable selective logging, high grading, and harvesting of fuelwood, which e) considerably reduces tree density.*

A4.2 MATERIALS AND METHODS

A4.2.1 Study area

The temperate evergreen rainforests in Chile are mostly located in areas facing the Pacific Ocean and in the western aspect of the Andes, extending across 17 degrees of latitude (38°–55°). We worked in temperate evergreen rainforest sites located between 43° and 48° S in the Aysén Region of southern Chile, where these forests cover an area of ca. 1,900,000 hectares (CONAF, 2011) (fig. A4.2). Here, due to the predominant western winds and the Andes mountain range, precipitation ranges from 2,500 – 5,000 mm year–1. Precipitation is roughly evenly distributed throughout the year. In these moist locations, the temperate evergreen rainforests are characterized

by a dense understory that includes bamboos (Chusquea spp.), ferns and many vascular epiphyte species; these forests are in general dominated by evergreen angiosperms and conifers. The most common tree species of the mature phase of the temperate evergreen rainforest in the Aysén Region are: *Laureliopsis philippiana* (Atherospermataceae), *Podocarpus nubigenus* and *Saxegothea conspicua* (Podocarpaceae), *Weinmannia trichosperma* (Cunoniaceae) and some emergent individuals of *Nothofagus betuloides* and *N. nitida* (Nothofagaceae); *Drimys winteri* (Winteraceae), *Caldcluvia paniculata* (Cunoniaceae) dominate the intermediate positions of the canopy, whereas *Amomyrtus luma*, *Myrceugenia planiples*, *Luma apiculata*, and *Tepualia stipularis* (Myrtaceae) are all common species of the understory (Bannister & Donoso, 2013; Gutiérrez et al., 2008). Regarding the land use history in this region, it is one of the last temperate zones to be colonized in the world (ca. 100 years) (Martinic, 2005), which means that human impacts should still be evident since mature forested communities are much older than the human influence in the area.

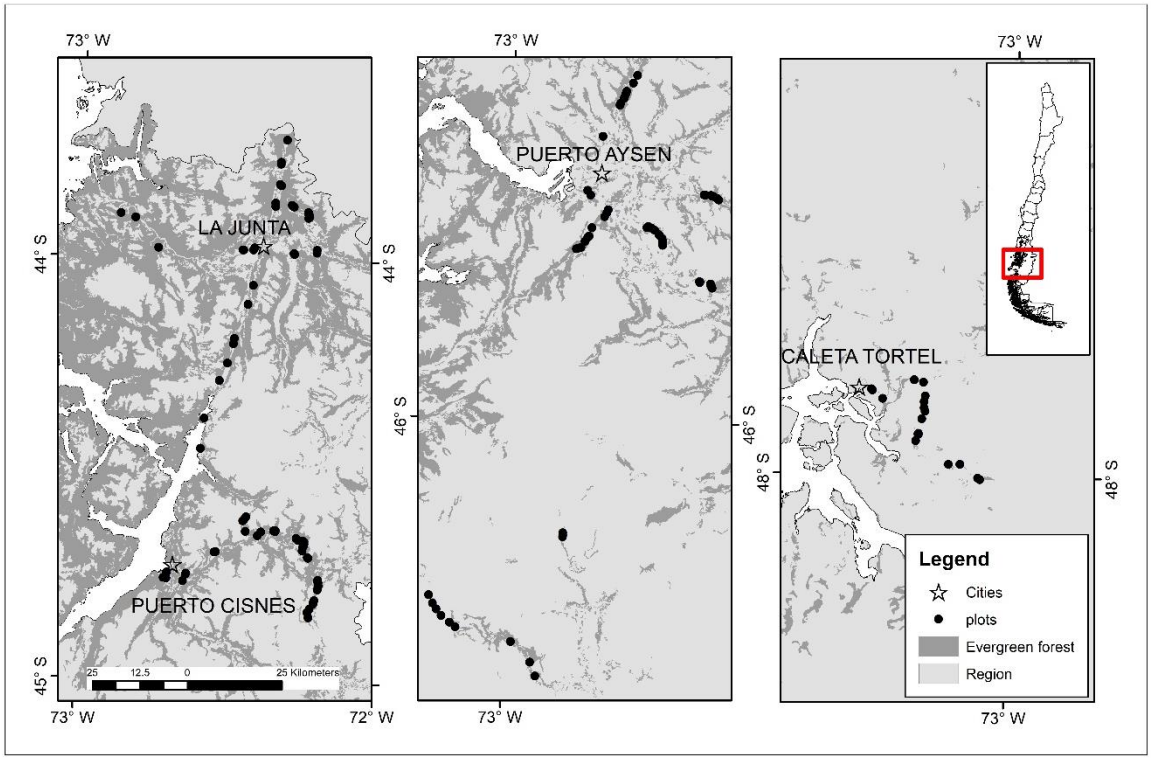

Figure A4.2. *Map depicting the three main areas and the sampling plots in the temperate evergreen rainforest of the Aysén Region of southern Chile.*

A4.2.2 Sampling and data collection

We gathered information about ownership location and the preliminary degree of forest degradation in three urban centers (La Junta [43°58'S, 72°24'S, 52 m a.s.l.], Puerto Aysén [45°24'S, 72°42'S, 9 m a.s.l.], and Cochrane [47°15'S, 72°34'S, 146 m a.s.l.]) with employees of the Chilean Forest Service (Corporación Nacional Forestal, CONAF) (figure A4.2). We also used Google Earth as a preliminary filter for avoiding swamps and rocky areas and to provide ways of accessibility to the forest as well as for general stand density and maturity levels of the forests roughly based on texture of images (forest structure). We then visited a non-exhaustive list of forest properties, talked to the owners and carried out a preliminary inspection of the forest stands in these properties. Previously forested areas that were completely converted to agriculture or pasture were discarded. For simplicity and representativeness, we also decided to work with mature

and old-growth evergreen forests and discarded second-growth forests or temperate rainforests dominated by *Pilgerodendron uviferum* or *D. winteri* that constitute variants of the temperate rainforest type in southern Chile (Bannister & Donoso, 2013; Donoso, 1981). Based on literature, and on the opinions of CONAF employees, forest owners, and academics, as well as the Google Earth primary filter, we elaborated a preliminary categorization of what we all understood as degradation in this particular type of forests. We considered several (mostly) qualitative and categorical aspects, including canopy openness, and the presence of exotic and invasive species (e.g., pasture), tree regeneration, cattle or recent cattle dung, stumps, etc. We ended up with 5 degradation levels: 1, well-conserved, pristine (PRIS, closed canopy, no stumps, no exotic species, and presence of tree regeneration); 2, not degraded, in good condition (GOOD, closed canopy, occasional presence of stumps, absence of exotic species, and presence of tree regeneration); 3, low degradation (LOW, no cattle, presence of stumps, occasional presence of invasive species, few tree regeneration); 4, degraded (MEDI, relatively low tree density but no evident pasture, presence of invasive species, some cattle dung, no tree regeneration other than sprouts); and 5, severely degraded (SEVE, presence of cattle, pasture, low tree density, invasive species, not tree regeneration at all). We coordinated several visits to the forest stands to validate our categorization of degraded forest until we reached consensus. Thus, we finalized with a three-way comparison to determine forest degradation that was the combination of pre-field understanding of degradation, the use of images (Google Earth), and general field observations plus intensive plot-based observations (i.e., we set pre-sampling plots to train ourselves with sampling methods). The general idea of this *a priori* exercise was to verify our capacity to detect forest degradation with the analytical, threshold-based approach used later on (see below).

We established a total of 160 500-m^2 rectangular (50 * 10 m, the largest side being perpendicular to the slope) plots that were distributed across the Aysén Region, covering 5 degrees of latitude (ca. 600 kms, fig. A4.2). The proportion for each degradation category was of 30, 21, 16, 18, and 14% for PRIS, GOOD, LOW, MEDI, and SEVE, respectively. Once at the selected property, we detoured from roads and established the plot at least 200 m away from the road. At each plot, we tallied all of the trees with a diameter at breast height (DBH, 1.35 m) greater or equal than 10 cm (DBH ≥ 10 cm), where we identified the species and measured their DBH using a diameter tape. We determined the total height from a subsample of 12 trees that were randomly selected from the overstory, for which we used a clinometer. Within each plot, trees < 10 cm DBH and regeneration (saplings < 1 m high), along with herbs, forbs and ferns were counted in 6 1-m^2 squared plots (regeneration plots) that were established every 10 m along the central longest transect crossing the plot starting at one edge. We followed the botanical nomenclature of Rodríguez et al. (2018) and for exotic and invasive species we followed Fuentes et al. (2013). For each plot, we determined the coordinates with a multiple averaged global positioning system (GPS, Garmin). Near three different regeneration plots, we removed 1 10-cm deep soil cores using a 12.4 cm diameter PVC soil-corer with a stainless-steel serrated edge (volume = 1,207. 627 cm^3). Soil was sampled to derive a measure of a consequence of degradation and also in order to control for potential underlying edaphic conditions that might explain some forest attributes independently of the degree of degradation. Before collecting each core, we removed all recognizable litter from the soil surface (O_i horizon), which was often very deep. After collection, each soil core was placed in a labeled resealable plastic storage bag that was immediately sealed and maintained in a cooler under fresh conditions (< 10°C air temperature) for ca. 2–3 h to minimize nutrient mineralization, then we placed them in a refrigerator (3°C).

A4.2.3 Soil chemical analyses

Soil samples were shipped to a soil testing laboratory (Universidad de Concepción, Chillán, Chile), where a portion of each sample was oven dried, and analyzed for moisture content and soil organic matter (SOM) content (% of soil dry weight basis, d.w.). The remaining portion of moist soil was analyzed for nitrate (NO_3^-, mg Kg^{-1} soil d.w.), ammonium (NH_4^+, mg Kg^{-1} soil d.w.), pH, and Olsen–P (a standard protocol to measure available P). The organic matter content was estimated by the rapid dichromate oxidation method (Walkley & Black, 1934). Mineral N (i.e. NH_4^+ and NO_3^-) was extracted using a 5:1 proportion of K_2SO_4 solution:soil, after which the extracts were analyzed for NH_4^+ and NO_3^- using standard colorimetric methods (Robarge et al., 1983). Olsen–P was extracted using a 20:1 proportion of pH 8.5 $NaHCO_3$ solution:soil, as described in Steubing and others (2002).

A4.2.4 Data preparation

First, all tree species with a DBH ≥ 10 cm were represented as an abundance matrix, whereas all species with a DBH smaller than 10 cm were represented in a presence/absence matrix. The latter were further separated into native and exotic species (there were no exotic tree species with a DBH larger than 10 cm). The number of trees (N, density) with a DBH ≥ 10 cm along with their basal areas (BA) per plot were scaled up to hectare and categorized for each tree species in order to incorporate more details regarding species distributions to the forest degradation analysis (see below). Climate variables such as annual precipitation, annual mean temperature, and the driest month's precipitation were incorporated into the modeling using an interpolation from WorldClim version 2, spatially downscaled gridded climate data based on the years 1970–2000 (S.E. Fick & R.J. Hijmans, 2017). Plot elevation and aspect were obtained from a digital elevation model (SRTM 90 m) (Jarvis et al., 2018). Latitude and longitude were also identified for each plot using

a WGS84 UTM 18S projection. Summary statistics of the above attributes are presented in table A4.1.

A4.2.5 Data analyses

We followed a threshold-based concept to determine forest degradation of the temperate evergreen rainforest using a two-step approach mixing non-metrical multidimensional scaling (NMDS)–a multivariate statistics analysis–and machine learning (ML). Besides the identification of one or several variables that were significantly correlated with conditions of forest degradation, our ultimate goal was the determination of certain thresholds in these variables that would differentiate degraded from non-degraded forest.

Table A4.1. Mean and standard deviation (SD) of the main structural, compositional and stand variables across the three areas sampled in the temperate evergreen rainforest of the Aysén Region.

	North		Central		South	
variable	mean	SD	mean	SD	mean	SD
N	614.5	367	515.2	291.2	877.8	293.3
BA	51.5	37.7	46	29.7	53.6	21.6
QD	34.1	16.6	35.3	15.6	27.8	5.5
H	15.1	5.6	13.5	4.3	13.7	1.9
R>10	3.6	1.9	3.4	1.9	4.4	1
R<10	20.1	5.1	21.4	4.7	18.1	3.5
NR<10	16.6	4.6	17.1	4.1	18.1	3.4
ER<10	3.5	3.8	4.3	3.9	0.1	0.2
pH	5.3	0.4	5.5	0.4	4.9	0.6
OM	19	11	16.2	7.8	6.2	5
Nitrate	9.5	13.7	8	9.5	3.4	3
Ammonium	78.3	58.4	57.4	37.5	17.4	15.6
Phosphate	14.2	18.3	14	17.3	5.3	2.8
Temperature	9.2	0.9	8.2	0.6	7.8	0.8
Precipitation	1998.2	247.2	1841.9	285.3	1617	159.4
Elevation	173.5	121.9	149.3	103.4	146.8	155.1
Aspect	197.7	90.3	204	89.1	223.4	105.6

Note: N = tree density per hectare; BA = basal area in m^2 per hectare; QD = stand quadratic diameter in cm; H = tree height in m; R>10, species richness with diameter at breast height (DBH) > 10 cm; R<10, species richness with diameter at breast height (DBH) < 10 cm; NR<10, native species richness with diameter at breast height (DBH) < 10 cm; ER<10, exotic species richness with diameter at breast height (DBH) < 10 cm; OM = organic matter in %.

In detail, we first used NMDS to describe and explore the community-level information coming from the plots network as a multivariate statistical analysis. The focus of this unsupervised method

was to find relevant relationships among several variables that could help us to have a preliminary understanding of the process of forest degradation. A Jaccard dissimilarity matrix was created using community-level composition above and below 10 cm of DBH. We used the most common reduction dimensionality (K=2) with 1,000 iterations, running several times with random starts and using previous solutions in order to avoid a local optima solution (Moreno et al., 2018; Oksanen et al., 2016), and we fit the stand, soil, plant species richness, and environmental vectors onto the new ordination based on a maximum correlation with a p-value < 0.001, and default options for other parameters. In order to test the hypothesis of no differences between the *a priori*, field-based degradation categorization we used the Nonparametric method PerMANOVA with 10,000 permutations.

NMDS as an unsupervised method is useful for preliminary exploratory analyses, but for the purpose of predicting forest degradation we had to fit a statistical model capable of incorporating several data types along with their singularities, such as nonlinearities and interactions. Within the last two decades, machine learning (ML) techniques have proved to be an excellent supervised approach to predict ecological processes (G. James et al., 2013). A powerful ML technique is boosting regression trees (BRT), a method that combines regression *trees* and boosting (a meta-algorithm intended to reduce bias and variance). Therefore, the model *is able* to identify the best predictors by recursive splits, improving its prediction performance through the combination of several simple models, *learning* from previously grown *trees* (Elith et al., 2008; G. James et al., 2013). In other words, BRT acts as an additive regression model that uses simple *trees* and includes complex nonlinear relationships and interactions among predictors; BRT has no need for prior data transformation or the elimination of outliers (Elith et al., 2008). By using BRT, one also avoids starting with a predefined model. Other benefits of using BRT are that it involves a stagewise

procedure, any type of predictive variable can be used, the overfitting is controlled, it effectively selects relevant predictive variables, fits accurate functions and automatically identifies and models interactions. It consequently has substantial predictive advantages over other methods, such as general linear models (GLM) or general additive models (GAM) (Elith et al., 2008). We also chose BRT as a predictor model because ecological processes, such as forest degradation, are inherently complex and, mostly involve unknown processes in nature, where the BRT method tries to determine the dependent variable by observing the inputs and finding dominant patterns without assuming inputs from a previous data model. This method also allows extrapolation to new scenarios by the use of the main results as *a priori* information for new modelling (Death et al., 2017; Elith et al., 2008). To determine the optimal number of *trees* used in the BRT, we used a *k*-fold cross-validation method that minimizes the hold-out residual deviance (Hastie et al., 2016). When fitting the BRT models, we followed Elith et al. (2008) indications, including: a Gaussian family of relationships, a random *seed* of 7, a *tree* depth or complexity of 2 given the relatively small number of plots (Gansfort & Traunspurger, 2019), a learning rate of 0.001 to reach at least 1000 trees in each model, 10-fold for cross-validation with a bagging rate of 2/3 to avoid overfitting, an initial number of *trees* to fit of 50, a maximum number of *trees* to fit of 10,000, where the other parameters were used as defaults following the custom code written by Leathwick and Elith based on the *gbm* package in *R* (Elith et al., 2008). Interactions between predictors were revised using the methodology developed by Elith et al. (2008) (including the code mentioned earlier). The prediction ability was determined by a cross-validated proportion of the total deviance explained (D^2), which was calculated as:

D^2 = (ratio of the total deviance – the cross-validated residual deviance) / total deviance

In general, we followed the methodology presented by Leathwick et al. (2006) for understanding the performance of the prediction metric of each BRT model using "unseen" data that were excluded during the training due to the cross-validation process. This cross-validation estimate of the prediction error is close to the prediction error on independent data (Elith et al., 2008).

The response variable, as expected, was the degree of degradation; however, we expanded this analysis and ran two BRTs. In the first BRT (BRT_1), we used the field-based degradation category whereas in the second BRT, we used the dimension obtained from the NMDS analysis that best explained the degradation. Thus, by incorporating the second BRT (BRT_2) we most likely avoided any bias that could have been originated from the data collection or by our *expert*, field-based categorization of forest degradation. The predictors for BRT_1 are stand parameters such as: N and BA per hectare, quadratic stand diameter, mean total height, N and BA per species, BA of stumps, soil variables (see table A4.1), and the presence/absence matrix of species with DBH less than 10 cm. The predictors for BRT_2 are similar to the ones used for BRT_1 without the community-level composition variables to avoid circularity in the prediction. Contributions through the reduction of squared errors and the critical threshold for each predictor were calculated and partial plots were obtained to identify patterns from those more important covariates, for which we used the first six predictors with higher relative influence (RI). We visualized the fitted functions of the BRT models for finding thresholds by using partial dependence plots that show the effect of a predictor on the response after accounting for the average effects of other predictors in the model. Besides, we contrast the null hypothesis of no effect of these thresholds on the a priori field-based degradation categorization by using Fisher's exact test for count data.

Database management and statistical analyses were performed using the statistical software R version 3.6.0 (R-Development-Core-Team, 2019). The R/VEGAN package was used for NMDS analysis (Oksanen et al., 2016), the R/GBM package for BRT analyses (Greenwell et al., 2019), and the custom code written by Elith et al. (2008). Spatial raster and vector information was processed in ArcGIS 10.6 (ESRI, 2018).

A4.3 RESULTS

A4.3.1 The forest degradation gradient

The forest stands sampled in this study did not change considerably in structure (density and basal area) across latitude (table 4.1, table S1) but they obviously did with the forest degradation level (see below). The PerMANOVA results showed significant differences between field-based degradation categories ($P < 0.001$).

Non-metrical multidimensional scaling (NMDS) results showed a convergent solution with a stress goodness-of-fit value of 0.18, a non-metric fit R^2 of 0.97, and a linear fit R^2 of 0.846, reflecting a fair enough representation of the original dissimilarity matrix composed by community-level composition variables. The representation of the ordination obtained showed a continuous order, from pristine plots (blue ellipse) to highly degraded plots (red ellipse) (from right to left in figure 4.3). The vector representing the category of degradation mirrors this pattern, i.e., the first axis of ordination was then interpreted as a forest degradation dimension. All those sites (or plots) with higher tree density (N) and species richness (R > 10) were, as expected, associated with less degraded forest conditions. On the contrary, higher degrees of degradation were related to less acidic soils (relatively higher pH), and a higher number of exotic species with a DBH < 10 cm (ER < 10). The second axis of ordination was not as easy to interpret as axis 1, and yet we identified it with site conditions more associated with plant community variation. For

example, forest stands with relative dominance of the tree species *L. philippiana* (Atherospermaceae) appeared to markedly differ from forests dominated by other evergreen species (e.g., *N. betuloides*, *P. nubigenus*, *D. winteri*). To our surprise, we found that in general soil nutrient levels were not associated with forest degradation but with plant community dimensions. The exception was NO_3^-; high concentrations of it were associated with more forest degraded conditions.

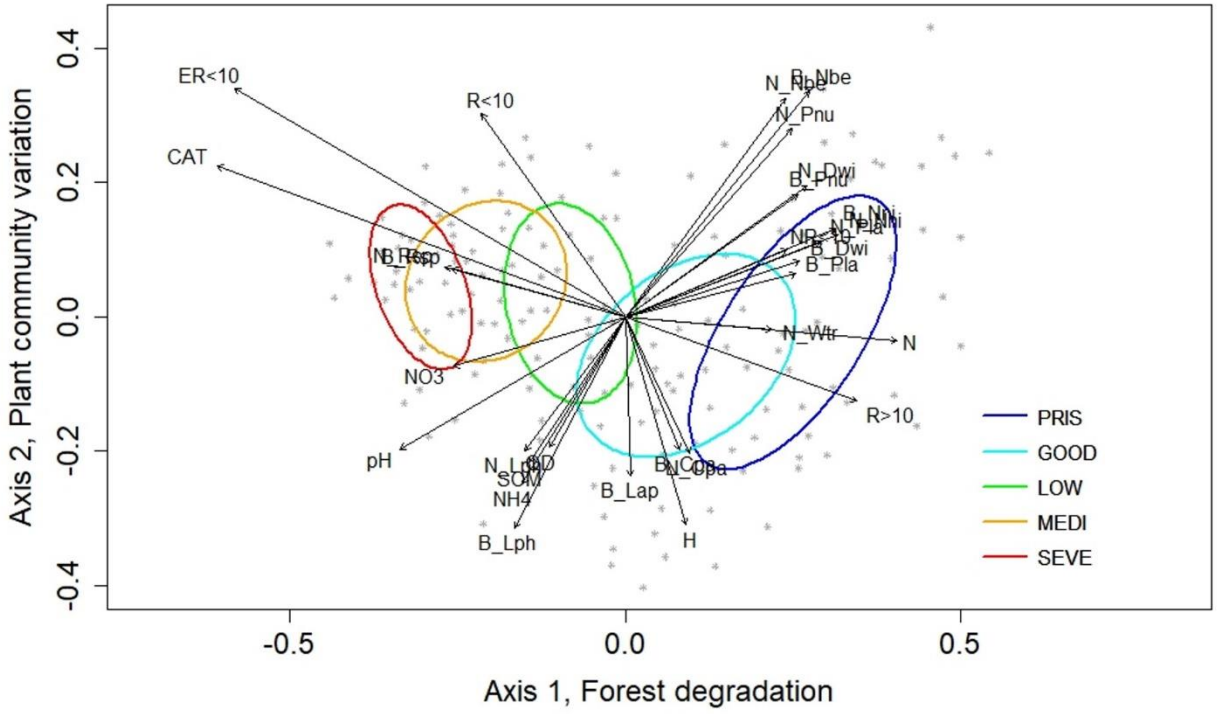

Figure A4.3. *Non-metric Multidimensional Scaling (NMDS) analysis outcomes for the forest degradation gradient of the temperate evergreen rainforest of the Aysén Region, southern Chile, for which we used the community-level composition (table S2).*

Once we identified the forest degradation dimension, this was compared with environmental and topographic variables, such as latitude, longitude, annual mean temperature, annual precipitation, the driest month's precipitation (ppdriestm), elevation and aspect. These

environmental and topographic variables appeared to be idiosyncratic and were related to the site and plant communities rather than the forest degradation dimension; however, a high precipitation in summer showed a significant correlation with more pristine forests (fig. S1). Stands with a relative dominance of *L. philippiana* were also significantly associated with high temperature and precipitation in summer (northernmost sampled locations).

Species richness of individuals with a DBH < 10 cm had a significant correlation with both axes of ordination, although the patterns were different for native and exotic species. Native species were associated with both dimensions, i.e., forest degradation and plant community variation, while exotic species, as expected, were markedly associated with only the first dimension of forest degradation. On the one hand, forest stands with a high presence of the native tree species *N. nitida* (Nothofagaceae), the vines *Asteranthera ovata* and *Mitraria coccinea* (Gesneriaceae), and the ferns *Asplenium dareoides* (Aspleniaceae) and *Hymenophyllum pectinatum* (Hymenophyllaceae) were associated with pristine or non-degraded forests. In contrast, a high presence of shade-intolerant species, mostly native species, such as *Acaena ovalifolia* (Rosaceae), *Fuchsia magellanica* (Onagraceae), *Berberis microphylla* and *B. darwinii* (Berberidaceae), *Juncus effusus* (Juncaceae), the tree species *Aristotelia chilensis* (Elaeocarpaceae) and *Rhaphitamnus spinosus* (Verbenaceae) were related to different stages of forest degradation (figure A4.4a). On the other hand, the presence of exotic (some of them invasive) species was always associated with degraded forests (figure A4.4b). Special attention should be paid to those species with longer vector lengths, such as *Trifolium repens* (Fabaceae), *Prunella vulgaris* (Lamiaceae), *Holcus lanatus* (Poaceae), *Ranunculus repens* (Ranunculaceae), *Plantago lanceolate* and *P. major* (Plantaginaceae), all of which are both exotic and invasive species (Fuentes et al., 2013) and could

be key for easily identifying degraded forest stands. The tabular outputs of environmental fit in the ordination are presented in table S2.

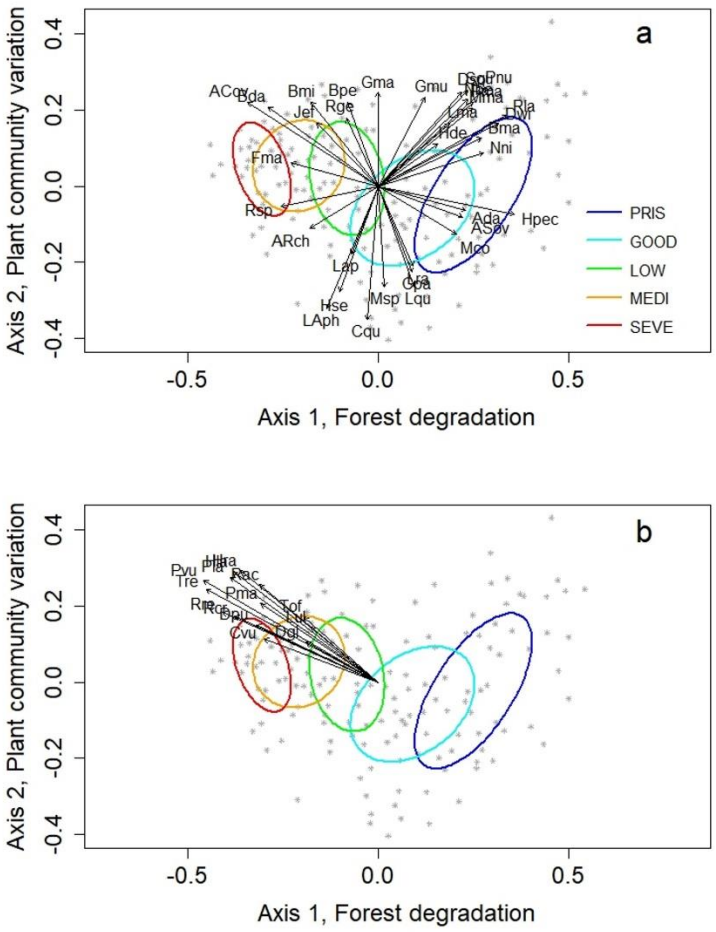

Figure A4.4. *Non-metric Multidimensional Scaling (NMDS) analysis outcomes for the forest degradation gradient of the temperate evergreen rainforest of the Aysén Region, southern Chile, for which we used species richness of individuals with a DBH < 10 cm vectors of native (a) and exotic (b) species (see Species richness, and Presence of species in Appendix S1: table S2).*

A4.3.2 Boosting regression tree models

Once the dimensions of forest degradation were analyzed in detail, the next step was to build the models capable of predicting forest degradation. The boosting regression tree (BRT) using the *a priori*, field-based forest degradation categories (BRT_1) had an optimal number of *trees* of 6,100, with a D^2 of 0.77, which overall represented a good performance in prediction. In this BRT, the

richness of exotic species with DBH < 10 cm (ER < 10) was the main predictor of forest degradation, with a relative importance of 61.50%, which is the number of times the predictor was selected for splitting the *tree*, weighted by the squared improvement to the model prediction error as a result of each split (the most important predictors' contribution to the model are presented in table A4.2). The richness of native species with DBH < 10 cm (NR < 10) also had a significant relative importance of 6.14%. The behavior of these two predictors showed evident thresholds (figure A4.5a, b; table A4.2). In particular, this BRT model predicted that anytime a forest stand has 5 or more exotic species with DBH < 10 cm and less than 12 native species with DBH < 10 cm, the stand is well correlated with a severely degraded forest (table A4.2). Both predictors showed some interaction that was identified and modelled by the BRT_1 model (Appendix S1: figure S2). In addition, stands with the presence of *A. ovalifolia* and *T. repens*, along with a mean annual temperature higher than 9.5 °C and a mean tree height lower than 10 m were also associated with degradation (table A4.2, fig. A4.5c-f). In contrast, the model predicted that a stand with no exotic species with DBH < 10 cm and >20 native species with DBH < 10 cm is well correlated with a pristine, non-degraded forest stand.

When we used the first dimension of NMDS as the response variable in the BRT_2 model, we found that its behavior was slightly different than in the BRT_1 model, as a new significant predictor was selected, tree density (N), where the relative importance of the main predictor was of 19.94%. The cross-validated proportion of the total deviance explained (D^2) was similar than that of the BRT_1 (D^2 = 0.73), identifying 8,300 *trees* run as an optimal. With this second BRT model we were able to predict that forest stands with N < 200 are completely degraded, whereas forest stands with N > 1,000 correspond to intact, pristine forests (table A4.2, fig. A4.6a). Besides N, longitude showed a relative importance of 11.47%, where the easternmost stands presented a

higher probability of degradation. Other predictors such as, *D. winteri* (N_Dwi) density, mean total tree height (H), soil pH, and NH_4^+ were also important to define more degraded forests. No significant interactions were detected in the BRT_2 model.

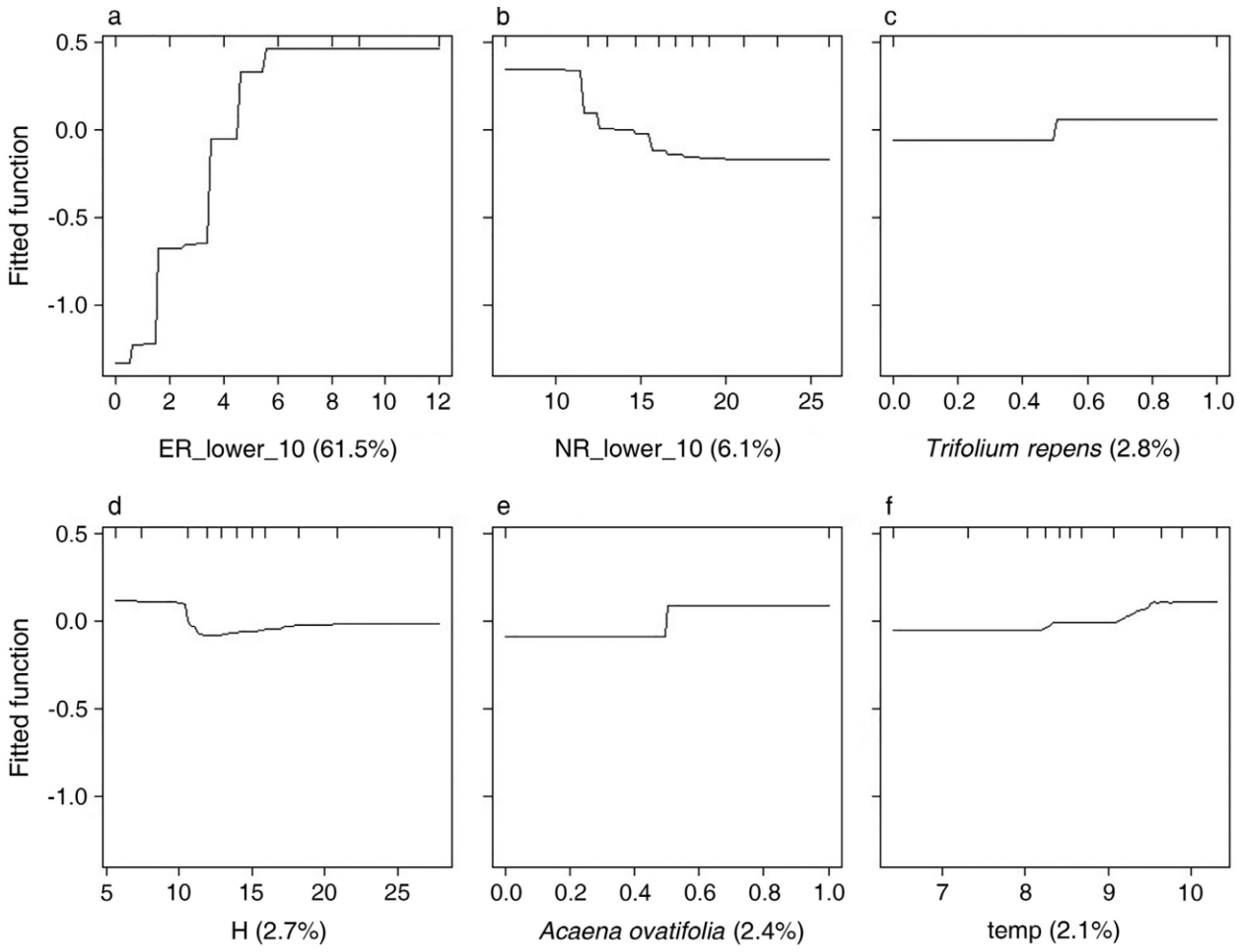

Figure A4.5. *Partial dependence plots of Boosting Regression Tree (BRT) model BRT_1 showing the shift between degraded (above zero) and non-degraded (below zero) temperate evergreen rainforest stands in the Aysén Region, southern Chile.*

A4.4 DISCUSSION

A4.4.1 Degradation thresholds in the temperate evergreen rainforests

The key factors we identified as characterizing the ecological threshold that defines the transition between a resilient and a degraded forest were species richness of individuals with a DBH < 10 cm and tree density. The BRT model 1, which was based on the field-based designation

of forest degradation and corroborated by the NDMS method, identified exotic species richness of individuals with a DBH < 10 cm as the key variables distinguishing degraded from non-degraded forests; forest stands with 5 or more exotic species were consistently found more associated with degraded forest. Although with significant less power of prediction than the richness of exotic species, native species richness was also identified by the model as a forest degradation predictor variable, where stands with more than 20 native species were more associated with non-degraded forests. In particular, the BRT model 2, which was not based on the *a priori*, field-based designation of forest degradation, unequivocally showed a shift in ecosystem state whenever tree density was heavily altered. Forest stands with densities of less than 200 trees ha^{-1} accrued values of variables related to degradation, while forest stands with densities greater than 1,000 trees ha^{-1} accrued values of variables related to pristine, well-conserved forests (table A4.2, fig. A4.6). In both cases, we were not only able to provide variables that proved to be significant in identifying shifts in ecosystem states, we were also able to provide figures that represent critical thresholds of forest degradation. Ultimately, the results provided by the unsupervised NDMS analysis were 1) mostly confirmatory in that tree density and exotic species richness were the key variables explaining forest degradation, and 2) they demonstrated that variable assemblages were mainly arrayed along a degradation gradient ranging from highly degraded to pristine forests. From this analysis, we would also like to point out the importance of soil pH and NO_3^-; the former tended to increase in value (more neutral) under degraded forest conditions, while the latter also increased in value with degradation. Soils in these temperate evergreen rainforests are relatively acidic (Huygens et al., 2008) and the openness of the canopy along with the decomposition of a higher amount of plant biomass (leaves and branches) left by logging may release a pulse of base cations, elevating the pH (Stevenson & Cole, 1999); a change in forest canopy cover, from mature

deciduous *Nothofagus* forests to pine plantations and grassland also led to an increase of pH in the soil in the Aysén Region (Fajardo & Gundale, 2015).

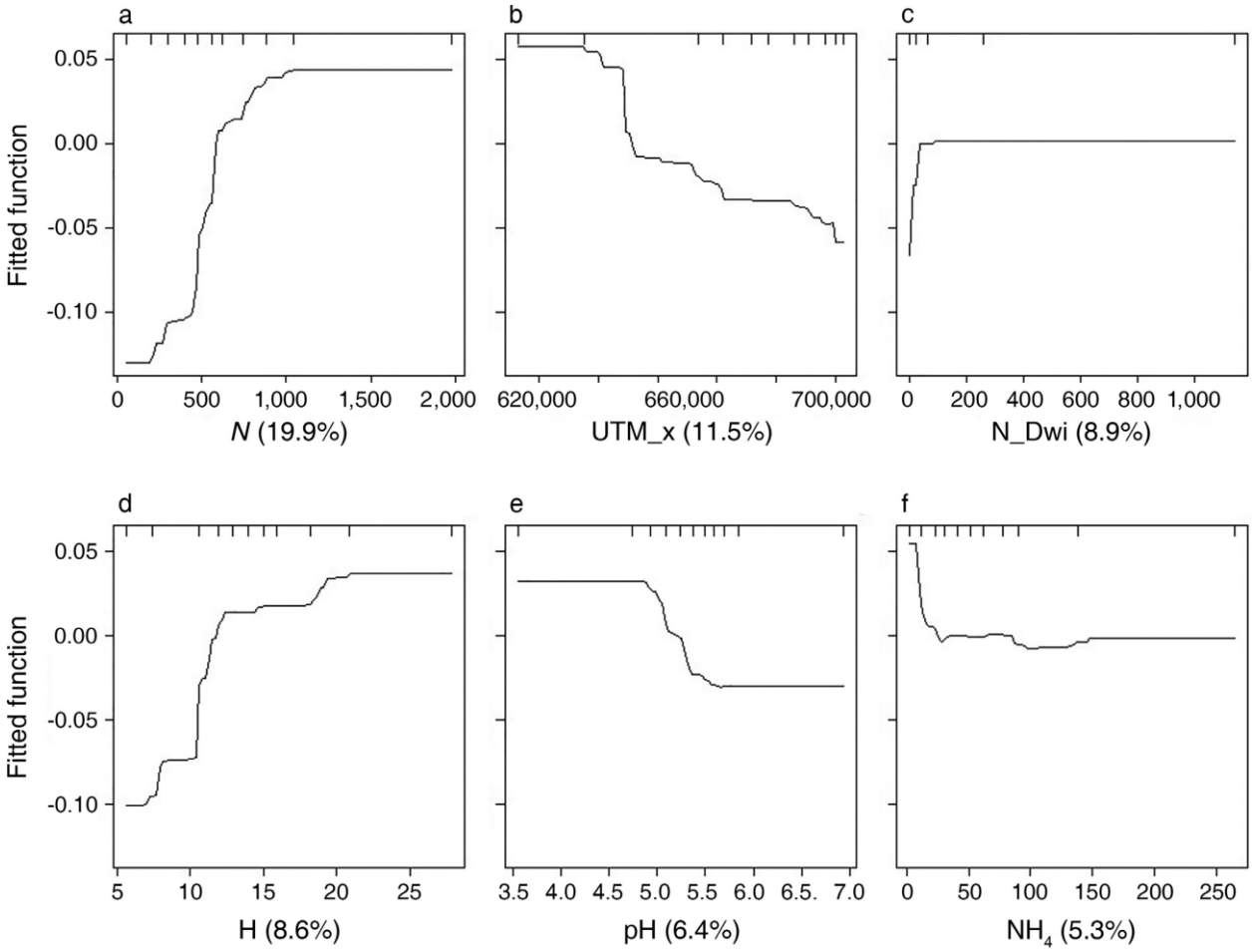

Figure A4.6. *Partial dependence plots of Boosting Regression Tree (BRT) model BRT_2 showing the shift between non-degraded (above zero) and degraded (below zero) temperate evergreen rainforest stands in the Aysén Region, southern Chile, for (b) tree density (N, tree ha^{-1}).*

Table A4.2. Relative influence of each predictor in the boosting regression tree (BRT) models and their relationship with an *a priori* categorization.

				Percentage in each a priori category				
model	**variable**	**RI** $^{+}$	**CT**	**1**	**2**	**3**	**4**	**5**
BRT_1	ER<10cm	61.50***	>5	0	3	35	76	87
BRT_1	NR<10cm	6.14***	<12	2	0	0	14	48
BRT_1	Tre	2.77***	1	0	9	54	86	91
BRT_1	H	2.74***	<10	2	3	15	34	57
BRT_1	ACov	2.44***	1	4	35	65	86	83
BRT_1	temp	2.05	>9.5	13	21	35	28	30
BRT_2	N	19.94***	<200	0	6	4	38	17
BRT_2	UTM_x	11.47***	>680,000	46	76	81	93	96
BRT_2	N_Dwi	8.94*	<80	71	79	81	93	100
BRT_2	H	8.60***	<10	2	3	15	34	57
BRT_2	pH	6.37**	>5.5	21	32	38	66	57
BRT_2	NH_4^+	5.26	>25	65	79	81	79	91

Note: only for the best six predictors with the highest relative influence (RI); RI = reduction of squared error attributable to each variable; CT = critical threshold for severe degradation; NE = not explicit. ER<10, exotic species richness with DBH < 10 cm; NR<10, native species richness with DBH < 10 cm; H, average total height (m); Tre, presence of *Trifolium repens*; ACov, presence of *Acaena ovalifolia*; temp, annual mean temperature (˚C); UTM_x, longitude WGS84/UTM18S (m); N, tree density (trees ha^{-1}); N_Dwi, tree density of Drimys winteri (trees ha^{-1}); NH_4^+ ammonium concentration (mg Kg^{-1}). + p-value using the Fisher's exact test for count data.

Our approach illustrates once more how over-harvesting, through the unsustainable reduction of tree density, can degrade the long-term forest functioning of a forest stand; e.g., reduction of carbon stocks, CO_2 absorption (Pearson et al., 2017; Thompson et al., 2013), deterioration of soil properties and processes leading to the depletion of water provision (Chazdon, 2008; Hudson & Alcántara-Ayala, 2006). According to the BRT_2 result, the drastic reduction in tree density appears to be the crucial factor that breaks the resilience of the forest. Other studies have found similar results (Bahamondez & Thompson, 2016; Hosonuma et al., 2012). For example, Bahamondez and Thompson (2016) used a productive-based perspective in second-growth temperate *Nothofagus*-mixed forests in central-south Chile and found that harvesting trees below a specific basal area was detrimental and led to forest degradation. Other factors responsible for forest degradation become important only when the forest has been logged, e.g., sub-canopy

grazing by livestock. In the temperate evergreen rainforest of southern Chile, logging of high-dimension trees (high grading) occurs for timber and fuelwood extraction; just after this, proprietors bring livestock (mainly cattle, *Bos taurus*) in, which feed on the regeneration or exotic grass species that have purportedly been sown (Zamorano-Elgueta et al., 2012). Cattle's instant deleterious effects on forest functioning are related to a reduction in native species regeneration by direct browsing, soil compaction via continuous transiting, the alteration of soil nutrition through the accumulation of manure, and the propagation of exotic species such as *T. repens*. It is not a surprise that a drastic and continuous reduction in a forest's tree density can have chain-reaction effects that may even interact with one another. According to regional forest managers, over-harvesting and cattle grazing in the forest are two inseparable processes that go purportedly together.

A4.4.2 Challenges

Elith and others (2008) proposed boosting regression *trees* (BRT) as a solution to understanding and fitting hidden ecological processes and states in exclusive function to the data without a pre-conceived or biased model (supervised). Above all, an excellent and pertinent advantage of BRT methods is that they provide the possibility of identifying thresholds for the most important predictors in the model. The main disadvantage of using the BRT method is that it is commonly not possible to identify a unique decision *tree* that explains the relationships between predictors and response variables because the model is composed of several *trees*. Several studies have gone further and incorporated ordination methods as exploratory analyses to the use of BRT as prediction model in order to have a more holistic understanding about the system under study (e.g., Canning, 2018; Compton et al., 2013; Death et al., 2017; Feng et al., 2018; le Roux & Luoto, 2014; Li et al., 2020; Mainali et al., 2015; Xu, 2019). For example, Xu and others (2019) and Gansfort

and Traunspurger (2019) used the NMDS axes as the response variable for the BRT models, exactly as we did. Indeed, we followed this approach and thus combined the advantages of both methods, incorporating significant variables provided by our first NDMS axis, also called "degradation", and the goodness-of-fit of the BRT. Furthermore, we ultimately analyzed the data using the predictive BRT model with and without the *a priori*, field-based categorization of forest degradation, which is both useful and important for forest managers and the employees of the Chilean Forest Service (CONAF).

Our results are mostly confined to mature, old-growth temperate evergreen rainforests, which could make it difficult to translate our results for second-growth forests, especially because we found that tree density is the key factor predicting forest degradation. Technically, we think that even though second-growth temperate evergreen rainforests represent an early stage in the development of a stand, tree density alone may still be an appropriate predictor of degradation, although figures expressing thresholds should change. We are sure, however, that our methodology could be easily applied to different forests in different regions.

The process of forest degradation is most probably being altered by climate change fluctuations, especially since these fluctuations are getting more extreme. We do not know, however, how the combined effects of climate change and anthropogenic unsustainable logging will manifest themselves in the temperate evergreen rainforest of southern Chile. We think that a larger-scale modelling approach would be necessary to endeavor this objective. In particular, we anticipate that the inclusion of global-scale drivers, such as climate change, will lead to the existence of non-linear thresholds encompassing patterns of cascading shifts in multiple ecosystem variables, as it is the case of drylands (see Berdugo et al., 2020).

A4.4.3 Guidelines for management

Based on our methodology and results, we consider a temperate evergreen rainforest stand to be in an evident state of degradation if it contains less than 200 trees of DBH ≥ 10 cm per hectare. Other concomitant situations characterizing forest degradation that can be added to the list are: 1) 5 or more exotic species with a DBH < 10 cm per hectare, 2) 12 or less native species with a DBH < 10 cm per hectare, and 3) a relatively neutral soil pH. We anticipate that forest managers and employees of CONAF can make use of these straightforward guidelines in order to first determine whether the forest is degraded, and secondly to take effective measures that work towards solving the restoration and conservation challenges we face today. Practitioners could, for example, carry out rapid species composition surveys to declare if a forest is in a degraded state. Our results could also be applied with remote sensing, which may be a very powerful approach to assessing tree density-based forest degradation at the landscape scale; this approach implies rapid evaluations and a higher chance of halting degradation.

A4.5 CONCLUSIONS

In this study, we were able to identify a critical resilience threshold of forest degradation that constitutes an ecological-based tool for management and conservation purposes that can be used by practitioners and authorities dealing with the administration and management of the temperate evergreen rainforest of the Aysén Region. Thus, practitioners and forest owners can make use of our forest degradation categorization based on simple observations of forest structure and composition. The identification of a critical threshold can support efforts aimed towards the halt of forest degradation and thus the promotion of forest recovery. Finally, we are sure that the methodology we used (particularly, machine learning) can be replicated as a strategy to respond

to similar objectives in different forest types and in different regions, which enlarges the impact of our study.

A4.6 ACKNOWLEDGEMENTS

This work was supported by the Chilean Fondo de Investigación del Bosque Nativo (FIBN) project 003/2016 to A. Fajardo and J.C. Llancabure. P.C. Moreno thanks the financial support of Programa Regional CONICYT R17A10002 Laboratorio Ecoclimático. The assistance in the field of J.P. Mora, T. Fuenzalida, and M. Peña is highly appreciated. The authors also thank L. Moraga and F. Silva for fruitful discussions about the topic in the Región de Aysén. Finally, the authors would like to thank R. Death, B. Reid, C. Zamorano-Elgueta and T. Veblen for their insightful comments that have overall enhanced the quality of the manuscript. The authors declare that they have no conflicts of interest of any kind regarding this study.

A4.7 LITERATURE CITED

Asner, G. P., Hughes, R. F., Vitousek, P. M., Knapp, D. E., Kennedy-Bowdoin, T., Boardman, J., Martin, R. E., Eatwood, M., & Green, R. O. (2008). Invasive plants transform the three-dimensional structure of rain forests. *Proceedings of the National Academy of Sciences USA*, *105*(11), 4519-4523.

Bahamondez, C., & Thompson, I. D. (2016). Determining forest degradation, ecosystem state and resilience using a standard stand stocking measurement diagram: theory into practice. *Forestry*, *89*, 290-300.

Bannister, J. R., & Donoso, P. J. (2013). Forest typification to characterize the structure and composition of old-growth evergreen forests on Chiloé Island, North Patagonia (Chile). *Forests*, *4*, 1087-1105.

Berdugo, M., Delgado-Barquerizo, M., Soliveres, S., Hernández-Clemente, R., Zhao, Y., Gaitán, J. J., Gross, N., Saiz, H., Maire, V., Lehman, A., Rillig, M. C., Solé, R. V., & Maestre, F. T. (2020). Global ecosystem thresholds driven by aridity. *Science*, *367*, 787-790.

Bergstrom, D. M., Wienecke, B. C., van den Hoff, J., Hughes, L., Lindenmayer, D. B., Ainsworth, T. D., Baker, C. M., Bland, L., Bowman, D. M. J. S., Brooks, S. T., Canadell, J. G., Constable, A. J., Dafforn, K. A., Depledge, M. H., Dickson, C. R., Duke, N. C., Helmstedt, K. J., Holz, A., Johnson, C. R., . . . Shaw, J. D. (2021). Combating ecosystem collapse from the tropics to the Antarctica. *Global Change Biology*, *27*(9), 1692-1703.

Canning, A. D. (2018). Predicting New Zealand riverine fish reference assemblages. *PeerJ, 6*, e4890.

Chazdon, R. L. (2008). Beyond deforestation: restoring forests and ecosystem services on degraded lands. *Science*, *320*, 1458-1460.

Compton, T. J., Bowden, D. A., Pitcher, C. R., Hewitt, J. E., & Ellis, N. (2013). Biophysical patterns in benthic assemblage composition across contrasting continental margins off New Zealand. *Journal of Biogeography*, *40*(1), 75-89.

CONAF. (2011). *Catastro de uso de suelo y vegetación*. Corporación Nacional Forestal, available online: http://www.ide.cl/descarga/capas/item/catastros-de-uso-de-suelo-y-vegetacion.html.

Death, R. G., Collier, K. J., Hudson, M., Canning, A., Niessen, M., David, B., Catlin, A., Hamer, M., & Pingram, M. (2017). *Does artificial intelligence modelling have anything to offer traditional management of freshwater food resources?* Environmental Research Institute, report no. 17, The University of Waikato, Hamilton, New Zealand.

Donoso, C. (1981). *Tipos forestales de los bosques nativos de Chile*. Documento de Trabajo No 38. Investigación y Desarrollo Forestal (CONAF-PNUD-FAO).

Elith, J., Leathwick, J. R., & Hastie, T. (2008). A working guide to boosted regression trees. *Journal of Animal Ecology*, *77*(4), 802-813.

ESRI. (2018). *ArcGIS Version 10. Environmental Systems Research Institute, Inc., Redlands, CA, USA.*

Everitt, B. S., & Hothorn, T. (2011). *An introduction to applied multivariate analysis with R*. Springer Science.

Fajardo, A., & Gundale, M. J. (2015). Combined effects of anthropogenic fires and land–use change on soil properties and processes in Patagonia, Chile. *Forest Ecology and Management*, *357*(1), 60-67.

FAO. (2002). *Proceedings: Second expert meeting on harmonizing forest-related definitions for use by various stakeholders*. Food and Agriculture Organization of the United Nations, Rome, Italy.

FAO. (2011). *Assessment and monitoring of forest degradation. Towards the development of globally applicable guidelines. Forest resource assessment working paper 177*. Food and agriculture organization of the United Nations, Rome, Italy.

Feng, M., Pusch, M., & Venohr, M. (2018). Estimating water residence time distribution in river networks by boosted regression trees (BRT) model. *Hydrology and Earth System Sciences Discussions*, *1*, 1-27.

Fick, S. E., & Hijmans, R. J. (2017). WorldClim 2: new 1-km spatial resolution climate surfaces for global land areas. *International Journal of Climatology*, *37*(12), 4302-4315.

Fuentes, N., Pauchard, A., Sánchez, P., Esquivel, J., & Marticorena, A. (2013). A new comprehensive database of alien plant species in Chile based on herbarium records. *Biological Invasions*, *15*(4), 847-858. https://doi.org/10.1007/s10530-012-0334-6

Gansfort, B., & Traunspurger, W. (2019). Environmental factors and river network position allow prediction of benthic community assemblies: A model of nematode metacommunities. *Scientific Reports*, *9*, 14716.

Ghazoul, J., Burivalova, Z., Garcia-Ulloa, J., & King, L. A. (2015). Conceptualizing forest degradation. *Trends in Ecology and Evolution*, *30*(10), 622-632.

Greenwell, B., Boehmke, B., & Cunningham, J. (2019). *gbm: Generalized Boosted Regression Models*. R package version 2.1.5. URL: https://github.com/gbm-developers/gbm.

Gutiérrez, A. G., Aravena, J. C., Carrasco-Farías, N. V., Christie, D. A., Fuentes, M., & Armesto, J. J. (2008). Gap-phase dynamics and coexistence of a long-lived pioneer and shade-tolerant tree species in the canopy of an old-grow coastal temperate rain forest of Chiloé Island, Chile. *Journal of Biogeography*, *35*, 1674-1687.

Hastie, T., Tibshirani, R., & Friedman, J. (2016). *The elements of statistical learning. Data mining, inference, and prediction*. Springer, 2nd edition.

Hirota, M., Holmgren, M., Van Nes, E. H., & Scheffer, M. (2011). Global resilience of tropical forest and savanna to critical transitions. *Science*, *334*, 232-235.

Hosonuma, N., Herold, M., De Sy, V., De Fries, R. S., Brockhaus, M., Verchot, L., Angelsen, A., & Romijn, E. (2012). An assessment of deforestation and forest degradation drivers in developing countries. *Environmental Research Letters*, *7*, 044009.

Hudson, P. F., & Alcántara-Ayala, I. (2006). Ancient and modern perspectives on land degradation. *Catena*, *65*(1), 102-106.

Huygens, D., Boeckx, P., Templer, P., Paulino, L., van Cleemput, O., Oyarzún, C., Müller, C., & Godoy, R. (2008). Mechanisms for retention of bioavailable nitrogen in volcanic rainforest soils. *Nature Geoscience*, *1*(5), 543-548.

James, G., Witten, D., Hastie, T., & Tibshirani, R. (2013). *An introduction to statistical learning with application in R*. Springer.

Jarvis, A., Reuter, H. I., Nelson, A., & Guevara, E. (2018). *Hole-filled Srtm for the globe, version 4 avaiable from the CGIAR-CSI SRTM 90m database*. Available online: http://srtm.csi.cgiar.org.

le Roux, P. C., & Luoto, M. (2014). Earth surface processes drive the richness, composition and occurrence of plant species in an arctic–alpine environment. *Journal of Vegetation Science*, *25*(1), 45-54.

Leathwick, J. R., Elith, J., Francis, M. P., Hastie, T., & Taylor, P. (2006). Variation in demersal fish species richness in the oceans surrounding New Zealand: an analysis using boosted regression trees. *Marine Ecology Progress Series*, *321*, 267-281.

Li, S., Huang, X., Lang, X., Xu, F., Li, H., Zheng, M., & Su, J. (2020). Effect of selective logging on soil microbial communities in a *Pinus yunnanensis* forest. *Land Degradation and Development*, *31*(16), 2268-2280.

Mainali, K. P., Warren, D. L., Dhileepan, K., McConnachie, A., Strathie, L., Hassan, G., Karki, D., Shrestha, B. B., & Parmesan, C. (2015). Projecting future expansion of invasive species: comparing and improving methodologies for species distribution modeling. *Global Change Biology*, *21*(12), 4464-4480.

Martinic, M. (2005). *De la Trapananda al Aysén*. Pehuén Editores, Santiago, Chile.

Moreno, P. C., Gezan, S. A., Palmas, S., Escobedo, F. J., & Cropper, W. P. (2018). Exploring stand and tree variability in mixed *Nothofagus* second-growth forests through multivariate analysis. *Bosque*, *39*(3), 397-410.

Oksanen, J., Blanchet, F. G., Friendly, M., Kindt, R., Legendre, P., McGlinn, D., Minchin, P. R., O'Hara, R. B., Simpson, G. L., Solymos, P., Stevens, M. H. H., Szoecs, E., & Wagner, H. (2016). *vegan: Community Ecology Package. R package version 2.4-1. URL: https://CRAN.R-project.org/package=vegan*.

Pearson, T. R. H., Brown, S., Murray, L., & Sidman, G. (2017). Greenhouse gas emissions from tropical forest degradation: an underestimated source. *Carbon Balance and Management*, *12*, 3.

Pickett, S. T. A., & White, P. S. (Eds.). (1985). *The ecology of natural disturbances and patch dynamics*. Academic Press.

R-Development-Core-Team. (2019). *R: A language and environment for statistical computing. Version,3.6.0. R Foundation for Statistical Computing, Vienna. ISBN 3-900051-07-0, http://www.R-project.org*.

Robarge, W., Edwards, A., & Johnson, B. (1983). Water and waste water analysis for nitrate via nitration of salicylic acid. *Communications in Soil Science and Plant Analysis*, *14*(12), 1207-1215.

Rodríguez, R., Marticorena, C., Alarcón, D., Baeza, C., Cavieres, L., Finot, V. L., Fuentes, N., Kiessling, A., Mihoc, M., Pauchard, A., Ruiz, E., Sánchez, P., & Marticorena, A. (2018). Catálogo de las plantas vasculares de Chile. *Gayana Botanica*, *75*(1), 1-430.

Scheffer, M. (2009). *Critical transitions in nature and society*. Princeton University Press.

Schwinning, S., Sala, O. E., Loik, M. E., & Ehleringer, J. R. (2004). Thresholds, memory, and seasonality: understanding pulse dynamics in arid/semi-arid ecosystems. *Oecologia*, *141*, 191-193.

Seidl, R., Spies, T. A., Peterson, D. L., Stephens, S. L., & Hicke, J. A. (2016). Searching for resilience: addressing the impacts of changing disturbance regimes on forest ecosystem services. *Journal of Applied Ecology*, *53*(1), 120-129.

Steubing, L., Godoy, R., & Alberdi, M. (2002). *Métodos de ecología vegetal*. Editorial Universitaria, Santiago, Chile.

Stevenson, F. J., & Cole, M. A. (1999). *Cycles of soil: Carbon, nitrogen, phosphorus, sulfur, macronutrients* (2nd ed.). Wiley.

Thompson, I. D., Guariguata, M., Okabe, K., Bahamondez, A., Heymell, V., Nasi, R., & Sabogal, C. (2013). An operational framework for defining and monitoring forest degradation. *Ecology and Society*, *18*(2), 20.

van der Werf, G. R., Morton, D. C., DeFries, R. S., Olivier, J. G. J., Kasibhatla, P. S., Jackson, R. B., Collatz, G. J., & Randerson, J. T. (2009). CO2 emissions from forest loss. *Nature Geoscience*, *2*, 737-738.

Vásquez-Grandón, A., Donoso, P. J., & Gerding, V. (2018). Forest degradation: when is a forest degraded? *Forests*, *9*, 726.

Walkley, A., & Black, I. A. (1934). An examination of the degtjareff method for determining soil organic matter, and a proposed modification of the chromic acid titration method. *Soil Science*, *37*, 29-38.

Xu, B. (2019). *Understanding the temporal dynamics of regional lakes: from temporal coherence analysis to model predictions* The University of Auckland].

Xu, F., Harvolk-Schöning, S., Horchler, P. J., Ludewig, K., & Otte, A. (2019). Factors determining the distribution pattern of floodplain vegetation remnants along the Danube River between Straubing and Vilshofen. *Tuexenia*, *39*, 75-100.

Zamorano-Elgueta, C., Cayuela, L., González-Espinosa, M., Lara, A., & Parra-Vázquez, M. R. (2012). Impacts of cattle on the South American temperate forests: Challenges for the conservation of the endangered monkey puzzle tree (*Araucaria araucana*) in Chile. *Biological Conservation*, *152*(1), 110-118.

SUPPORTING INFORMATION

Additional supporting information may be found online at: http://onlinelibrary.wiley.com/doi/10.1002/eap.2495/full

OPEN RESEARCH

Data upon which this study is based are available through the Figshare Digital Repository: https://doi.org/10.6084/m9.figshare.15000669 (Fajardo 2021).